Forum Geometricorum
Volume 15 (2015) 1–4.

FORUM GEOM
ISSN 1534-1178

Generalized Tucker Circles

Nikolaos Dergiades

Abstract. It is known that if we cut the sides of the angles of a triangle, with six consecutive alternating antipallel and parallel segments to the sides of the triangle then we get a closed hexagram that is inscribed in a circle, the Tucker circle. Since the above hexagram has sides parallel to the sides of the pedal triangles of O and H that are isogonal conjugate points, we generalize the Tucker circles by considering two isogonal conjugate points on the McCay cubic.

Given a reference triangle ABC, a Tucker hexagon $A_bA_cB_cB_aC_aC_b$ has vertices, two on each sideline (see Figur 1), such that B_cC_b, C_aA_c, A_bB_a are parallel to the sidelines BC, CA, AB respectively, whereas B_aC_a, C_bA_b, A_cB_c are antiparallel to these sidelines. It is well known that these six vertices all lie on a circle whose center is a point on the Brocard axis.

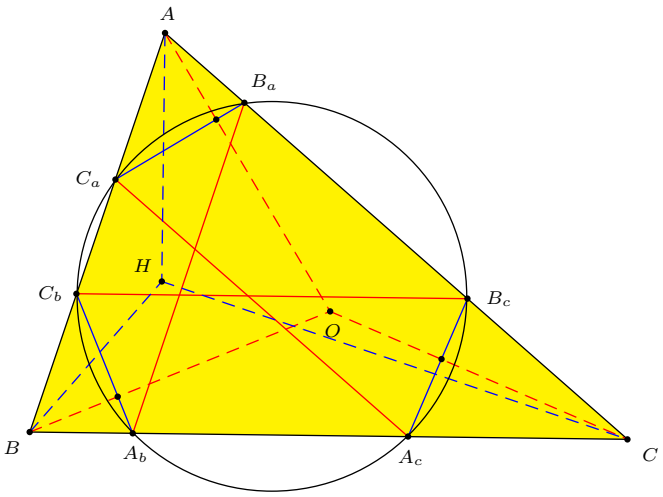

Figure 1.

The segments B_aC_a, C_bA_b, A_cB_c are parallel to the sides of the orthocenter H of triangle ABC, and the segments B_cC_b, C_aA_c, A_bB_a are parallel to the sides of the pedal triangle of the circumcenter O. Since O, H are isogonal conjugates, the segments B_aC_a, C_bA_b, A_cB_c are perpendicular to OA, OB, OC respectively, and the segments B_cC_b, C_aA_c, A_bB_a are perpendicular to HA, HB, HC respectively. From this aspect we shall generalize the Tucker hexagons and circles by requiring

Publication Date: January 12, 2015. Communicating Editor: Paul Yiu.

the sides B_aC_a, C_bA_b, A_cB_c of a hexagon $A_bA_cB_cB_aC_aC_b$ to be perpendicular to AP, BP, CP, and the sides B_cC_b, C_aA_c, A_bB_a perpendicular to AQ, BQ, CQ for a pair of isogonal conjugates P and Q. In Theorem 2 below we shall establish the necessary and sufficient that the line containing P and Q must pass through the circumcenter O. In other words, P and Q are points on the McCay cubic which has barycentric equation

$$\sum_{\text{cyclic}} a^2 S_A \mathbb{X}(c^2\mathbb{Y}^2 - b^2\mathbb{Z}^2) = 0. \tag{1}$$

We shall make use of the notion of directed angle of two lines. For two lines L_1, L_2, denote by $(L_1,\ L_2)$ the directed angle from L_1 to L_2. The basic properties of directed angles can be found in Johnson [2, §§16–19]. Here is a characterization of the points on the McCay cubic in terms of directed angles.

Lemma 1 ([1])**.** *The point P lies on the McCay cubic if and only if*

$$(BC,\ AP) + (CA, BP) + (AB,\ CP) = \frac{\pi}{2} \pmod{\pi}.$$

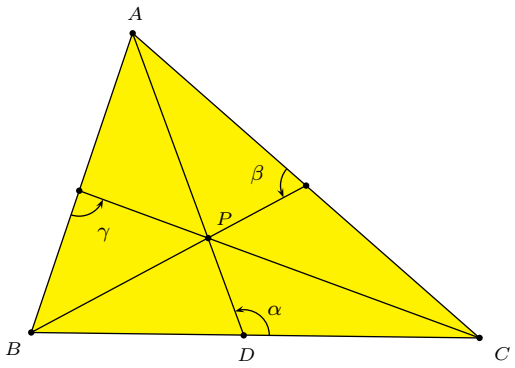

Figure 2.

Proof. Let $\alpha = (BC,\ AP)$, $\beta = (CA,\ BP)$, and $\gamma = (AB,\ CP)$ be the directed angles, and $x = \cot\alpha$, $y = \cot\beta$, $z = \cot\gamma$. It is known that

$$\alpha + \beta + \gamma = \frac{\pi}{2} \pmod{\pi} \quad \text{if and only if} \quad x + y + z = xyz. \tag{2}$$

If D is the trace of AP on BC (see Figure 2), then the law of sines in triangle ADC gives

$$\frac{\sin(\alpha + C)}{\sin\alpha} = \frac{DC}{AC} \implies \cot\alpha + \cot C = \frac{DC}{2R\sin B\sin C}. \tag{3}$$

Similarly, from triangle ABD we have

$$\frac{\sin(\pi - \alpha + B)}{\sin(\pi - \alpha)} = \frac{BD}{AB} \implies -\cot\alpha + \cot B = \frac{BD}{2R\sin B\sin C}. \tag{4}$$

From (3) and (4) we get

$$\frac{x+\frac{S_C}{S}}{-x+\frac{S_B}{S}}=\frac{DC}{BD}=\frac{v}{w}\implies x=\frac{S_Bv-S_Cw}{(v+w)S}.$$

Similarly we have $y=\frac{S_Cw-S_Au}{(w+u)S}$ and $z=\frac{S_Au-S_Bv}{(u+v)S}$. By substitution into (2), we get

$$\sum_{\text{cyclic}}a^2S_Au(c^2v^2-b^2w^2)=0.$$

Comparison with (1) shows that P is a point on the McCay cubic. □

Theorem 2. *Let P be a point on the plane of triangle ABC with cevians not perpendicular to the sides of ABC at their vertices, and Q be its isogonal conjugate. Beginning with an arbitrary point B_a on CA, construct points C_a on AB, A_c on BC, B_c on CA, C_b on AB, A_b on BC such that $B_aC_a\perp AP$, $C_aA_c\perp BQ$, $A_cB_c\perp CP$, $B_cC_b\perp AQ$, $C_bA_b\perp BP$. The following statements are equivalent.*
(a) *The perpendicular from A_b to CQ passes through the initial point B_a.*
(b) *The six points B_a, C_a, A_c, B_c, C_b, A_b are concyclic.*
(c) *The points P and Q lie on the McCay cubic.*

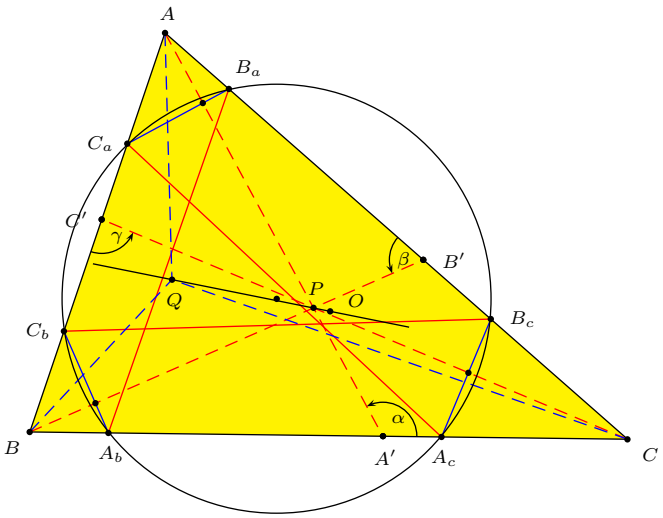

Figure 3.

Proof. Let $A'B'C'$ be the cevian triangle of P and $\alpha=(BC,\ AP)$, $\beta=(CA,\ BP)$, $\gamma=(AB,\ CP)$ the directed angles (see Figure 3).

(a) ⇒ (b) If the perpendicular from A_b to CQ passes through the initial point B_a, then since the segments B_aC_a, B_cC_b are perpendicular to the isogonal lines PA, QA relative to AB, AC, they are antiparallels relative to AB, AC and the points B_c, B_a, C_a, C_b are on a circle $\mathscr{C}_a$. Similarly the points C_a, C_b, A_b, A_c are on a circle $\mathscr{C}_b$, and the points A_b, A_c, B_c, B_a are on a circle $\mathscr{C}_c$. The three

circles coincide if any two of them do. Now, if they are distinct, then pairwise, they have a sideline of triangle ABC for radical axes, and the three radical axes are nonconcurrent, an impossibility. Therefore, the six points are concyclic.

(b) $\Rightarrow$ (a) If the circumcircle of triangle $B_aC_aA_c$ passes through B_c, then obviously it also passes through C_b and A_b. The lines A_cB_c, A_bB_a are antiparallels relative to CA, CB, and the lines CP, CQ are isogonal relative to CA, CB. Since $A_cB_c \perp PC$, we conclude that $A_bB_a \perp CQ$.

(b) $\Leftrightarrow$ (c) It is easy to see the equivalence of the following statements.
(b) The six points B_a, C_a, A_c, B_c, C_b, A_b are concyclic.
(b1) B_a, C_a, A_c, B_c are concyclic.
(c1) $(B_cB_a,\ B_aC_a) = (B_cA_c,\ A_cC_a)$.
(c2) $(BC, A_cB_c) + (B_cB_a,\ B_aC_a) + (A_cC_a, BC) = 0$.

Now, referring to Figure 3, we have

$$\begin{aligned}
(BC,\ A_cB_c) &= (BC,\ AB) + (AB,\ CP) + (CP,\ A_cB_c) = B + \gamma + \frac{\pi}{2},\\
(B_cB_a,\ B_aC_a) &= (CA,\ BC) + (BC,\ AP) + (AP,\ B_aC_a) = C + \alpha + \frac{\pi}{2},\\
(A_cC_a,\ BC) &= (A_cC_a,\ BQ) + (BQ,\ BC)\\
&= \frac{\pi}{2} + (AB,\ BP)\\
&= \frac{\pi}{2} + (AB,\ AC) + (AC,\ BP) = \frac{\pi}{2} + A + \beta.
\end{aligned}$$

From this,

$$\begin{aligned}
0 &= (BC,\ A_cB_c) + (B_cB_a,\ B_aC_a) + (A_cC_a,\ BC)\\
&= (A + B + C) + (\alpha + \beta + \gamma) + \frac{3\pi}{2}\\
&= \alpha + \beta + \gamma - \frac{\pi}{2} \pmod{\pi}.
\end{aligned}$$

It follows that (c1) and (c2) are equivalent to $\alpha+\beta+\gamma = \frac{\pi}{2} \pmod{\pi}$. By Lemma 1, this is equivalent to (c). This completes the proof of the theorem. □

For $P = O$, the above circles are the known Tucker circles. For $P = I$, the incenter, these circles are all concentric at I. For a fixed $P \neq I$ on the McCay cubic, the centers of the circles lie on a line through the Lemoine point. We leave it to the reader to find clever barycentric coordinates for the initial point B_a to obtain elegant cyclic formulas for the barycentric coordinates of the other vertices of the hexagon, and to expose interesting properties of these generalized Tucker circles.

References

[1] B. Gibert, *Cubics in the Triangle Plane*, McCay cubic, Prorerty 4; http://bernard.gibert.pagesperso-orange.fr/Exemples/k003.html
[2] R. A. Johnson, *Advanced Euclidean Geometry*, Dover reprint, 2007.

Nikolaos Dergiades: I. Zanna 27, Thessaloniki 54643, Greece
E-mail address: ndergiades@yahoo.gr

Forum Geometricorum
Volume 15 (2015) 5–12.

FORUM GEOM
ISSN 1534-1178

Heronian Triangles of Class K: Congruent Incircles Cevian Perspective

Frank M. Jackson and Stalislav Takhaev

Abstract. We relate the properties of a cevian that divides a reference triangle into two sub-triangles with congruent incircles to the system of inner and outer Soddy circles of the same reference triangle. We show that if constraints are placed on the reference triangle then relationships exist between the Soddy circles, the incircle of the reference triangle and the congruent incircles of the sub-triangles. In particular, we show that a class of Heronian triangles exists with inradius equal to integer multiples of their inner and outer Soddy circle radii.

1. Congruent incircles cevian

It has been shown by Yiu [4, pp.127–132] that if a triangle ABC (with side-lengths a, b, c) is divided by a cevian through A into two subtriangles with congruent incircles of radius ρ, then the length of the congruent incircles cevian AD is $\sqrt{s(s-a)}$, and

$$\rho = \frac{r}{1+\sqrt{t_b t_c}} = \frac{r}{a}(s - \sqrt{s(s-a)}), \tag{1}$$

where s is the semiperimeter and r the inradius of triangle ABC, and $t_a = \tan\frac{A}{2} = \frac{r}{s-a}$, $t_b = \tan\frac{B}{2} = \frac{r}{s-b}$, $t_c = \tan\frac{C}{2} = \frac{r}{s-c}$ are the tangents of the half angles of the triangle (see Figure 1). These numbers satisfy the basic relation

$$t_a t_b + t_b t_c + t_c t_a = 1. \tag{2}$$

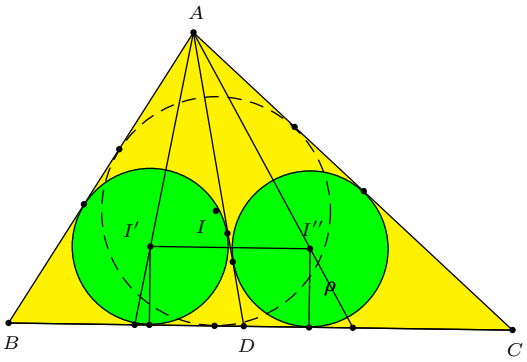

Figure 1.

Publication Date: January 21, 2015. Communicating Editor: Paul Yiu.

Proposition 1. *If θ denotes angle ADB for the congruent incircle cevian AD, then*

$$\cos\theta = \frac{t_b - t_c}{t_b + t_c} = \frac{b-c}{a}, \tag{3}$$

$$\sin\theta = \frac{2\sqrt{t_b t_c}}{t_b + t_c} = \frac{2\sqrt{(s-b)(s-c)}}{a}. \tag{4}$$

Proof. This follows from the formula $\tan\frac{\theta}{2} = \sqrt{\frac{t_c}{t_b}}$ in [4, p.131], and the identities $\cos\theta = \frac{1-t^2}{1+t^2}$ and $\sin\theta = \frac{2t}{1+t^2}$ where $t = \tan\frac{\theta}{2}$. □

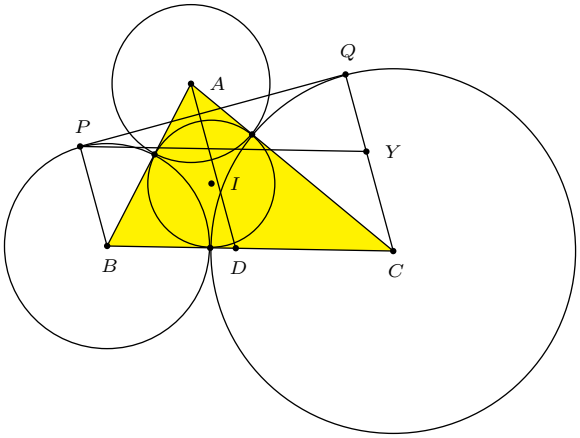

Figure 2.

Now consider the triad of mutually tangent circles with centers at the vertices A, B, C. These have radii $s-a$, $s-b$, $s-c$ respectively. Without loss of generality we may assume $b \geq c$. If the external common tangent of the B- and C- circles on the same side of A touches these circles at P and Q respectively, then $\cos PYQ = \frac{(s-c)-(s-b)}{(s-c)+(s-b)} = \frac{b-c}{a}$ (see Figure 2). It follows from (3) that PQ is perpendicular to the congruent incircle cevian AD. This leads to a simple ruler and compass construction of the congruent incircles cevian.

Theorem 2. *The congruent incircle cevian AD is the perpendicular through A to external common tangent of the B- and C- circles* (of the triad of mutually tangent circles with centers at the vertices) *on the same side of BC as vertex A.*

2. Radii of Soddy circles

The standard configuration for the Soddy circles of a reference triangle is shown in Figure 3. It has been shown by Dergiades [3] that the radii of $S(r_{\rm i})$ and $S'(r_{\rm o})$ are given by the formulas:

$$r_{\rm i} = \frac{\Delta}{4R + r + 2s} \quad \text{and} \quad r_{\rm o} = \frac{\Delta}{4R + r - 2s}. \tag{5}$$

where Δ is the area of the reference triangle, R its circumradius and r its inradius.

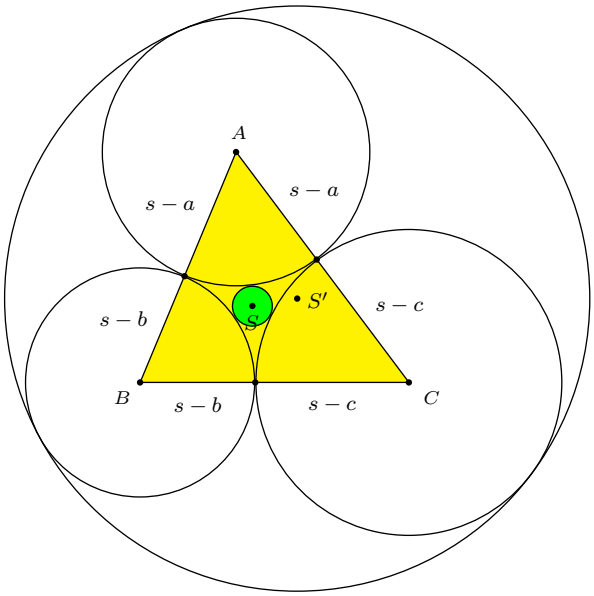

Figure 3.

Here are two well-known identities associated with the radii of the Soddy circles:

$$\frac{1}{s-a}+\frac{1}{s-b}+\frac{1}{s-c}+\frac{2}{r}=\frac{1}{r_{\mathrm{i}}}, \tag{6}$$

$$\frac{1}{s-a}+\frac{1}{s-b}+\frac{1}{s-c}-\frac{2}{r}=\frac{1}{r_{\mathrm{o}}}. \tag{7}$$

If we write $K := t_a + t_b + t_c$, these can be put in the form

$$\frac{r}{r_{\mathrm{i}}}=K+2, \qquad \frac{r}{r_{\mathrm{o}}}=K-2.$$

From these,

$$\frac{r_{\mathrm{o}}}{r_{\mathrm{i}}}=\frac{K+2}{K-2}. \tag{8}$$

3. Soddyian triangles

The case $K = 2$ has been considered by Jackson [2]. In this case, the outer Soddy circle has degenerated into a straight line, and the triangle is called *Soddyian*. It has the property that if the sides are $a \geq b \geq c$, then

$$\frac{1}{\sqrt{s-a}}=\frac{1}{\sqrt{s-b}}+\frac{1}{\sqrt{s-c}}.$$

By multiply through by $\sqrt{r}$ and converting to tangent half angles we get:

$$t_a = 1 + \sqrt{t_b t_c}.$$

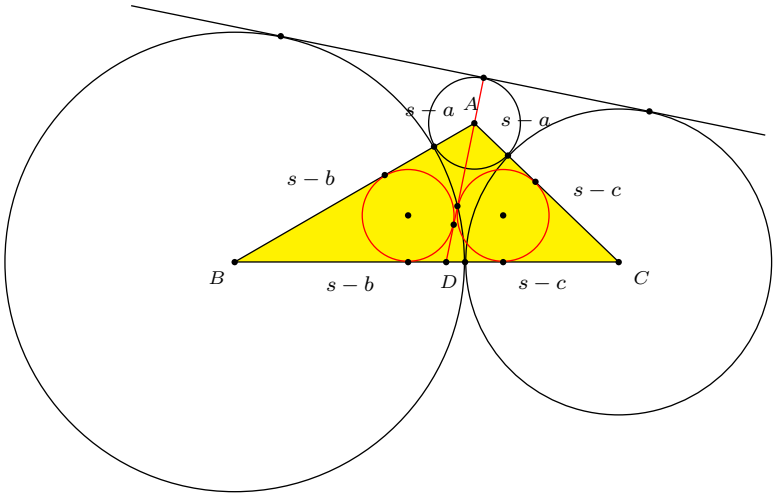

Figure 4.

Comparing this with the radius of the congruent incircles in (1), we obtain the following theorem.

Theorem 3. *In the triad of mutually tangent circles with centers at the vertices of a Soddyian triangle, the smallest circle is congruent to the incircles of the sub-triangles divided by the congruent incircle cevian through its center* (see Figure 4).

We prove another interesting property of the congruent incircles cevian triangle of a Soddyian triangle.

Theorem 4. *In a Soddyian triangle ABC with $a \geq b \geq c$, the congruent incircle cevian AD is parallel to the Soddy line* (joining the incenter to the Gergonne point); see Figure 5.

Proof. Set up a rectangular coordinate system with B as the origin, and positive x-axis along the line BC, so the the coordinates of the vertices and the incenter are

$$A = (c\cos B,\, c\sin B), \quad B = (0,\, 0), \quad C = (a,\, 0), \quad I = (s{-}b,\, r) = \left(\frac{r}{t_b},\, r\right).$$

The Gergonne point has homogeneous barycentric coordinates

$$G_{\mathrm{e}} = \left(\frac{1}{s-a} : \frac{1}{s-b} : \frac{1}{s-c}\right) = (t_a : t_b : t_c).$$

Since $t_a + t_b + t_c = 2$, this has Cartesian coordinates

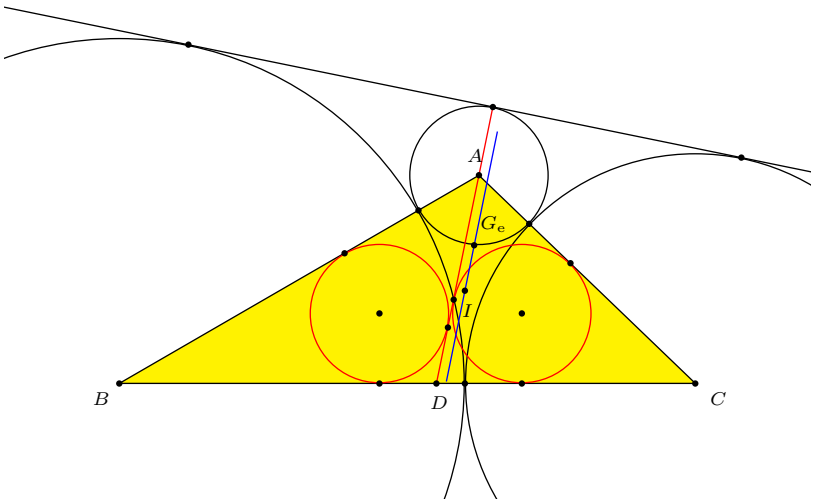

Figure 5.

$$
\begin{aligned}
G_{\mathrm{e}} &= \frac{1}{2}(t_a \cdot A + t_b \cdot B + t_c \cdot C) = \left(\frac{t_a c \cos B + t_c a}{2}, \frac{t_a c \sin B}{2} \right) \\
&= \left(\frac{t_a \left(\frac{r}{t_a} + \frac{r}{t_b} \right) \cdot \frac{1-t_b^2}{1+t_b^2} + t_c \left(\frac{r}{t_b} + \frac{r}{t_c} \right)}{2}, \frac{t_a \left(\frac{r}{t_a} + \frac{r}{t_b} \right) \cdot \frac{2t_b}{1+t_b^2}}{2} \right) \\
&= \left(r \cdot \frac{(t_a + t_b)(1 - t_b^2) + (t_b + t_c)(1 + t_b^2)}{2t_b(1 + t_b^2)}, \; r \cdot \frac{t_a + t_b}{1 + t_b^2} \right) \\
&= \left(r \left(\frac{1 - t_b^2}{2t_b(t_b + t_c)} + \frac{t_b + t_c}{2t_b} \right), \; \frac{r}{t_b + t_c} \right).
\end{aligned}
$$

Let ψ be the angle between the Soddy line and the base line BC.

$$
\begin{aligned}
\tan \psi &= -\frac{\frac{r}{t_b + t_c} - r}{r \left(\frac{1-t_b^2}{2t_b(t_b+t_c)} + \frac{t_b+t_c}{2t_b} \right) - \frac{r}{t_b}} \\
&= \frac{2t_b(t_b + t_c - 1)}{(1 - t_b^2) + (t_b + t_c)(t_b + t_c - 2)} \\
&= \frac{2t_b(t_b + t_c - 1)}{(1 - t_b^2) - t_a(t_b + t_c)} \\
&= \frac{2t_b(t_b + t_c - 1)}{(1 - t_b^2) - (1 - t_b t_c)} \\
&= \frac{2(1 - t_a)}{t_c - t_b} = \frac{2(t_a - 1)}{t_b - t_c}.
\end{aligned}
$$

However, from Proposition 1, we have

$$\tan\theta = \frac{2\sqrt{t_b t_c}}{t_b - t_c} = \frac{2(t_a - 1)}{t_b - t_c}.$$

This shows that the Soddy line is parallel to the congruent incircles cevian. □

4. Heron triangles from Soddy circles

Soddyian triangles with integer sides are always Heronian [2, §4].

We shall say that a triangle has class K if the sum of the tangents of its half angles is equal to K. Thus, Soddyian triangles have class 2. Heronian triangles of class 2 are constructed in [2]. Let K be a positive integer. An integer triangle of class K is Heronian if and only if the tangents of its half angles are rational. Let θ be the angle ADB for the congruent incircle cevian AD. We have $t_b - t_c = (t_b + t_c)\cos\theta$. Together with $t_a + t_b + t_c = K$ and the basic relation (2), we have

$$\begin{aligned} t_a &= \frac{K(1+\cos^2\theta) + 2\varepsilon\sqrt{K^2 - 3 - \cos^2\theta}}{3 + \cos^2\theta}, \\ t_b &= \frac{(1+\cos\theta)(K - \varepsilon\sqrt{K^2 - 3 - \cos^2\theta})}{3 + \cos^2\theta}, \\ t_c &= \frac{(1-\cos\theta)(K - \varepsilon\sqrt{K^2 - 3 - \cos^2\theta})}{3 + \cos^2\theta} \end{aligned} \tag{9}$$

for $\varepsilon = \pm 1$. Clearly, t_a, t_b, t_c are rational if and only if $K^2 - 3 - \cos^2\theta = v^2$ for a rational number v, i.e., $K^2 - 3$ is a sum of two squares of rational numbers. Equivalently, $K^2 - 3$ is a sum of squares of two integers.

Lemma 5. *An integer is a sum of two squares of rational numbers if and only if it is a sum of squares of two integers.*

Proof. We need only prove the necessity part, for square-free integers. Let $n = u^2 + v^2$ for two rational numbers. Writing $u = \frac{h}{q}$ and $v = \frac{k}{q}$ for integers h, k, q, we have $nq^2 = h^2 + k^2$ for integers h, k, q. Here, h and k must be relatively prime, since any common divisor must be prime to q, and so its square must divide n, contrary to the assumption that n is square-free. Let p be a prime divisor of n. Modulo p, $h^2 + k^2 \equiv 0$. Since at least one of h and k, say, k, is nonzero modulo p, we have -1 is a quadratic residue modulo p, and $p \equiv 1 \pmod 4$. Thus, p is a sum of two squares of integers. This being true for every prime divisor of n, the number n is itself a sum of two squares of integers. □

Theorem 6. *Let $K > 1$ be a positive integer. Heronian triangles of class K exists if and only if $K^2 - 3$ is a sum of two squares of integers.*

The necessity part follows from Lemma 5 above. We shall construct Heronian triangles of class 4 in the next section. The construction clearly applies to class K with $K^2 - 3$ equal to a sum of two squares of integers.

5. Heronian triangles of class 4

The ratio of the radii of the Soddy circles of a triangle is given by (8). For integer values of $K := t_a + t_b + t_c$, this ratio is an integer only when $K = 3, 4, 6$, and is equal to 5, 3, 2 respectively. By Theorem 6 above, there is no Heronian triangle of class $K = 3, 6$.

We construct Heronian triangles with $K = 4$. Without loss of generality, assume $a \geq b \geq c$. The parameters t_a, t_b, t_c are given in (9) with $K = 4$. Here, $K^2 - 3 = 13$, and we require $\cos\theta$ and $v := \sqrt{13 - \cos^2\theta}$ to be rational numbers. Since $13 = 3^2 + 2^2$, we rewrite $v^2 = 13 - \cos^2\theta$ as

$$(3 - \cos\theta)(3 + \cos\theta) = (v - 2)(v + 2).$$

Since all factors involved are rational, we assume $3 - \cos\theta = w(v + 2)$ for a rational number w. It follows that $w(3 + \cos\theta) = v - 2$. Solving these for $\cos\theta$ and v, we have

$$\cos\theta = \frac{3 - 4w - 3w^2}{1 + w^2}, \qquad v = \frac{2 + 6w - 2w^2}{1 + w^2}. \tag{10}$$

Note that $t_b = t_c$ if and only if $\cos\theta = 0$. In this case, w cannot be rational. We shall assume $b > c$, so that θ is an acute angle, and $0 < \cos\theta < 1$. For this, $\frac{\sqrt{3}-1}{2} < w < \frac{\sqrt{13}-2}{3}$. Substitution of $\cos\theta$ and $v = \sqrt{13 - \cos^2\theta}$ given in (10) into (9) (with $K = 4$), we obtain, for $\varepsilon = 1$,

$$t_a = \frac{3w^2 + 12w + 11}{w^2 + 3w + 3}, \qquad t_b = \frac{-w^2 - 2w + 2}{w^2 + 3w + 3}, \qquad t_c = \frac{2w^2 + 2w - 1}{w^2 + 3w + 3}, \tag{11}$$

and, for $\varepsilon = -1$,

$$t_a = \frac{11w^2 - 12w + 3}{3w^2 - 3w + 1}, \qquad t_b = \frac{-w^2 - 2w + 2}{3w^2 - 3w + 1}, \qquad t_c = \frac{2w^2 + 2w - 1}{3w^2 - 3w + 1}. \tag{12}$$

In the latter case, t_a cannot be greater than both t_b and t_c for $w \in \left(\frac{\sqrt{3}-1}{2}, \frac{\sqrt{13}-2}{3}\right)$. Therefore, Heronian triangles of class 4 are given by (11). Writing $w = \frac{m}{n}$ for relatively prime integers m and n, and using $s - a : s - b : s - c = \frac{1}{t_a} : \frac{1}{t_b} : \frac{1}{t_c}$, we may take

$$\begin{aligned} s - a &= (2m^2 + 2mn - n^2)(-m^2 - 2mn + 2n^2), \\ s - b &= (2m^2 + 2mn - n^2)(3m^2 + 12mn + 11n^2), \\ s - c &= (-m^2 - 2mn + 2n^2)(3m^2 + 12mn + 11n^2). \end{aligned}$$

This gives

$$\begin{aligned} a &= (m^2 + n^2)(3m^2 + 12mn + 11n^2), \\ b &= (-m^2 - 2mn + 2n^2)(5m^2 + 14mn + 10n^2), \\ c &= (2m^2 + 2mn - n^2)(2m^2 + 10mn + 13n^2). \end{aligned}$$

For integers $m, n \leq 15$ giving w in the range, we obtain *primitive* Heronian triangles of class 4 by dividing a, b, c by their greatest common denominator, as presented in the table below. An example is shown in Figure 6.

m	n	a	b	c	s	Δ	r	R
1	2	355	219	148	361	8094	$\frac{426}{19}$	$\frac{13505}{38}$
2	5	11803	10660	1299	11881	3460314	$\frac{31746}{109}$	$\frac{2574185}{218}$
3	7	47444	38963	9515	47961	92616414	$\frac{422906}{219}$	$\frac{20795465}{438}$
3	8	74387	72491	2180	74529	39502554	$\frac{144698}{273}$	$\frac{40620485}{546}$
4	9	132987	103156	33235	134689	856373214	$\frac{2333442}{367}$	$\frac{97695005}{734}$
5	11	301636	225235	84747	305809	4767644154	$\frac{8621418}{553}$	$\frac{333914045}{1106}$
5	12	2379	2035	388	2401	197274	$\frac{4026}{49}$	$\frac{233285}{98}$
5	13	526516	498675	31867	528529	3971806014	$\frac{5463282}{727}$	$\frac{765749525}{1454}$
6	13	595115	432452	179891	603729	19430005434	$\frac{25006442}{777}$	$\frac{925691645}{1554}$
7	15	1063668	757315	338059	1079521	63941458494	$\frac{61541346}{1039}$	$\frac{2212473965}{2078}$
8	15	1186923	620500	608179	1207801	94234794654	$\frac{85745946}{1099}$	$\frac{2611873625}{2198}$

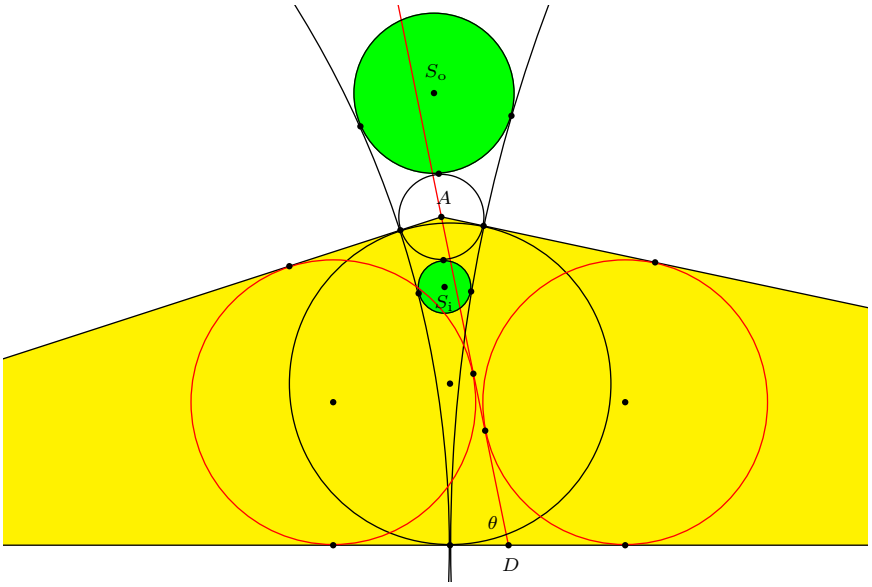

Figure 6.

References

[1] N. Dergiades, The Soddy circles, *Forum Geom.*, 7 (2007) 191–197.
[2] F. M. Jackson, Soddyian triangles, *Forum Geom.*, 13 (2013) 1–6.
[3] C. Kimberling, *Encyclopedia of Triangle Centers*, available at `http://faculty.evansville.edu/ck6/encyclopedia/ETC.html`.
[4] P. Yiu, *Notes on Euclidean Geometry*, Florida Atlantic University, 1998; available at `http://math.fau.edu/Yiu/Geometry.html`

Frank M. Jackson: Aldebaran, Mixbury, Northamptonshire NN13 5RR United Kingdom
E-mail address: `fjackson@matrix-logic.co.uk`

Stalislav Takhaev: Prybrezhnay Street, 4 KV.313, 192076 Saint-Petersburg, Russia
E-mail address: `stalislavt@mail.ru`

Forum Geometricorum
Volume 15 (2015) 13–44.

FORUM GEOM
ISSN 1534-1178

Volumes of Solids Swept Tangentially Around Cylinders

Tom M. Apostol and Mamikon A. Mnatsakanian

Abstract. In earlier work ([1]-[5]) the authors used the method of sweeping tangents to calculate area and arclength related to certain planar regions. This paper extends the method to determine volumes of solids. Specifically, take a region S in the upper half of the xy plane and allow the plane to sweep tangentially around a general cylinder with the x axis lying on the cylinder. The solid swept by S is called a *solid tangent sweep*. Its *solid tangent cluster* is the solid swept by S when the cylinder shrinks to the x axis. Theorem 1: *The volume of the solid tangent sweep does not depend on the profile of the cylinder, so it is equal to the volume of the solid tangent cluster.* The proof uses Mamikon's sweeping-tangent theorem: *The area of a tangent sweep to a plane curve is equal to the area of its tangent cluster*, together with a classical slicing principle: *Two solids have equal volumes if their horizontal cross sections taken at any height have equal areas*. Interesting families of tangentially swept solids of equal volume are constructed by varying the cylinder. For most families in this paper the solid tangent cluster is a classical solid of revolution whose volume is equal to that of each member of the family. We treat forty different examples including familiar solids such as pseudosphere, ellipsoid, paraboloid, hyperboloid, persoids, catenoid, and cardioid and strophoid of revolution, all of whose volumes are obtained with the extended method of sweeping tangents. Part II treats sweeping around more general surfaces.

1. FAMILIES OF BRACELETS OF EQUAL VOLUME

In Figure 1a, a circular cylindrical hole is drilled through the center of a sphere, leaving a solid we call a *bracelet*. Figure 1b shows bracelets obtained by drilling cylindrical holes *of a given height* through spheres of different radii. A classical calculus problem asks to show that all these bracelets have equal volume, which is that of the limiting sphere obtained when the radius of the hole shrinks to zero.

It comes as a surprise to learn that the volume of each bracelet depends only on the height of the cylindrical hole and not on its radius or the radius of the drilled sphere! This phenomenon can be explained (and generalized) without resorting to calculus by referring to Figure 2.

In Figure 2a, a typical bracelet and the limiting sphere are cut by a horizontal plane parallel to the base of the cylinder. The cross section of the bracelet is a circular annulus swept by a segment of constant length, tangent to the cutting cylinder. The corresponding cross section of the limiting sphere is a circular disk whose radius is easily shown (see Figure 3) to be the length of the tangent segment to the annulus. Thus, each circular disk is a tangent cluster of the annulus which, by Mamikon's sweeping-tangent theorem, has the same area as the annulus. (See

Publication Date: January 27, 2015. Communicating Editor: Paul Yiu.

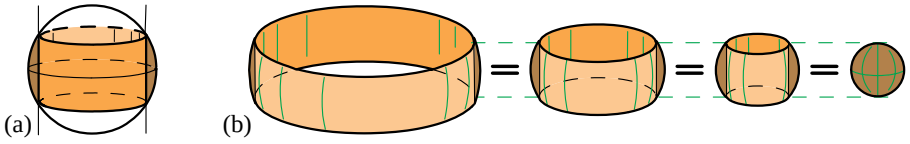

Figure 1. (a) Bracelet formed by drilling a cylindrical hole through a sphere. (b) The volume of each bracelet is the volume of a sphere whose diameter is the height of the hole.

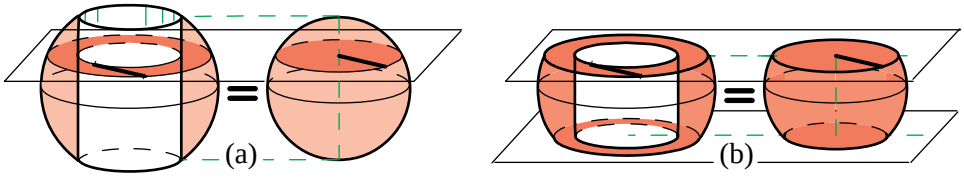

Figure 2. (a) Corresponding horizontal cross sections of bracelet and sphere have equal areas. (b) Solid slices cut by two parallel planes have equal volumes.

[2; Ch. 1], or [3].) Consequently, if the bracelet and sphere are sliced by two parallel planes as in Figure 2b, the slices have equal volumes because of the following *slicing principle*, also known as Cavalieri's principle:

Slicing principle. *Two solids have equal volumes if their horizontal cross sections taken at any height have equal areas.*

Thus, the equal volume property holds not only for all bracelets in Figure 1b, which are symmetric about the equatorial plane, but also *for any family of horizontal slices of given thickness.*

Generating bracelets by sweeping a plane region tangentially around a cylinder. Another way to generate the bracelets in Figure 1 is depicted in Figure 3a. A vertical section of the sphere cut by a plane tangent to the cylindrical hole is a circular disk whose diameter is the height of the hole. When half this disk, shown with horizontal chords, is rotated tangentially around the cylinder it sweeps out a bracelet as in Figure 3a. The tangent segment to the annulus in Figure 2a is a chord of such a semicircle, so the circular disk in Figure 2a is the planar tangent cluster of the corresponding annulus, hence *the annulus and disk have equal areas*. By the slicing principle, the bracelet and sphere in Figure 3a have equal volumes, as do arbitrary corresponding slices in 3b. We refer to each swept solid as a *solid tangent sweep* and to the corresponding portion of the limiting sphere as its *solid tangent cluster*.

Ellipsoidal bracelets. Figure 4 shows ellipsoidal bracelets swept by a given semielliptical disk rotating tangentially around circular cylinders of equal height but of different radii. The same bracelets can also be produced by drilling circular holes of given height through similar ellipsoids of revolution. The reasoning used above for spherical bracelets shows that each ellipsoiodal bracelet has the same volume as the limiting case, an ellipsoid of revolution. Moreover, *horizontal slices of these bracelets of given thickness also have equal volume*.

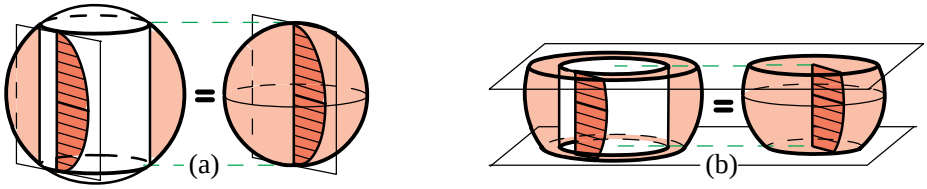

Figure 3. (a) Vertical section of sphere cut by a plane tangent to the cylindrical hole is a circular disk whose diameter is the height of the hole. (b) Arbitrary horizontal slice of (a).

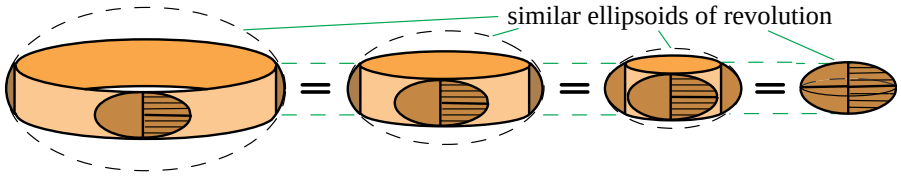

Figure 4. Ellipsoidal bracelets of equal height have the same volume as the limiting ellipsoid.

Paraboloidal bracelets. In Figure 5a a paraboloid of revolution is cut by a vertical plane, and half the parabolic cross section of height H is rotated tangentially around a circular cylinder of altitude H to sweep out a paraboloidal bracelet as indicated. The volume of this bracelet is equal to that of its solid tangent cluster, a paraboloid of revolution of altitude H. Figure 5b shows a family of paraboloidal bracelets, all of height H, cut from a given paraboloid of revolution by parallel equidistant planes. The bracelets have different radii, but each has the volume of the leftmost paraboloid of revolution of altitude H because it is easily shown that all the sweeping parabolic segments are congruent.

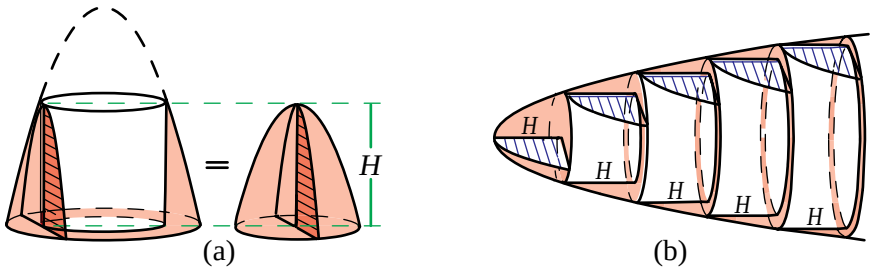

Figure 5. (a) Paraboloidal bracelet has the volume of the solid tangent cluster. (b) Family of paraboloidal bracelets of equal height and equal volume.

Hyperboloidal bracelets. Figure 6 shows a new family of bracelets, formed by drilling a cylindrical hole of given height through the center of a solid *hyperboloid of one sheet* (twisted cylinder). The generator of each hyperboloid makes the same angle with the vertical generator of the cylinder. The cylinder is tangent to the hyperboloid at its smallest circular cross section. The bracelets in Figure 6 have equal

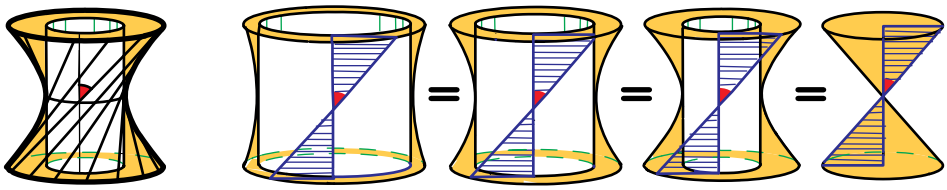

(a) twisted cylinder (b) similar hyperboloids, swept by double triangle

Figure 6. (a) Bracelet formed by drilling a solid hyperboloid of one sheet. (b) The volume of each bracelet equals the volume of the limiting cone of the same altitude.

volume, that of the limiting cone. The same bracelets can be obtained by tangential sweeping. In Figure 6b, a vertical section of the hyperboloid tangent to that cylinder is a symmetric double triangle, shown shaded. When this double triangle is rotated tangentially around the cylinder, the solid tangent sweep is a bracelet as in Figure 6b, and the limiting cone is its solid tangent cluster.

Figure 7 shows other hyperboloidal bracelets produced by tangential sweeping, but the type of bracelet depends on the relation between the radius r of the cylindrical hole and the length b of semitransverse axis of the hyperbola. In Figure 7a, $r > b$, and the outer surface of the bracelet is a hyperboloid of one sheet somewhat

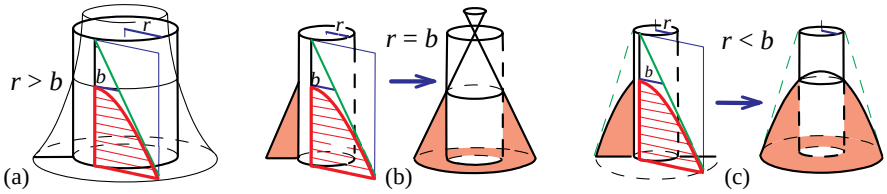

Figure 7. (a) Hyperboloidal bracelet with $r > b$. (b) Hyperboloidal bracelet with $r = b$ is a cone. (c) Hyperboloidal bracelet with $r < b$.

like those in Figure 6, except that the drilling cylinder is not tangent to the hyperboloid as in Figure 6, but intersects it. In Figure 7b, $r = b$, and the outer surface is that of a cone (a degenerate hyperboloid). In Figure 7c, $r < b$ and the outer surface is a *hyperboloid of two sheets* (only one sheet is shown). All hyperbolas in Figure 7 have the same asymptotes.

Figure 8 shows families of hyperboloidal bracelets of equal volume. Those in (a) are of one sheet; those in (b) are of two sheets (with only one sheet shown).

General oval bracelets. Figure 9a shows a bracelet swept by a semicircular disk moving tangentially around a general oval cylinder. Figure 9b shows a typical horizontal cross section of the bracelet, an oval ring swept by tangent segments of constant length. Such a ring is traced for example by a moving bicycle [1]. As in the foregoing examples, the volume of each bracelet is the volume of the limiting sphere obtained when the oval cylinder shrinks to a point. In Figure 9c, a double triangle moves tangentially around the oval cylinder to sweep out a bracelet whose outer surface is a ruled surface resembling the hyperboloid of one sheet in Figure

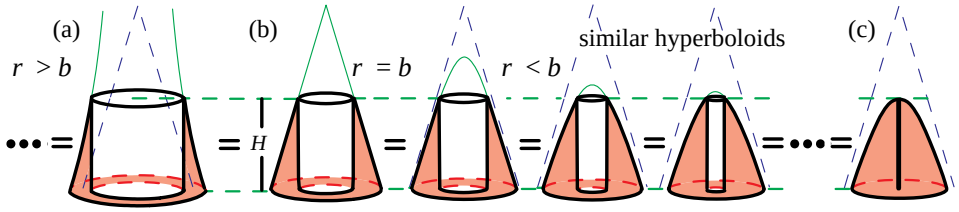

Figure 8. Hyperboloidal bracelets of one sheet in (a) and of two sheets in (b), all having equal height and equal volume, that of the limiting case in (c).

6b. A typical cross section is an oval ring, as in Figure 9b. The volume of the bracelet is that of the limiting cone as in Figure 6b.

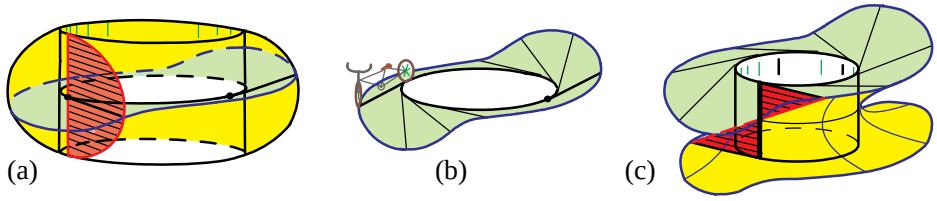

Figure 9. (a) Bracelet formed by semicircular disk swept tangentially around an oval cylinder. The volume of the solid tangent sweep is the same as that of its solid tangent cluster, a sphere. (b) Typical horizontal cross section of the bracelet in (a). (c) Bracelet formed by right triangle swept tangentially around an oval cylinder. A typical horizontal cross section is like that in (b).

2. TANGENTIAL SWEEPING AROUND A GENERAL CYLINDER

The tangentially swept solids treated above can be generalized as shown in Figure 10a. Start with a plane region S between two graphs in the same half-plane. To be specific, let S consist of all points (x, y) satisfying the inequalities

$$f(x) \le y \le g(x), \quad a \le x \le b$$

where f and g are nonnegative piecewise monotonic functions related by the inequality $0 \le f(x) \le g(x)$ for all x in an interval $[a, b]$. In Figure 10a, the x axis is oriented vertically, and S is in the upper half-plane having the x axis as one edge. If we rotate S around the x axis we obtain a solid of revolution swept by region S as indicated in the right portion of Figure 10a.

More generally, place the x axis along the generator of a general cylinder (not necessarily circular or closed) and, keeping the upper half-plane tangent to the cylinder, move it along the cylinder as suggested in Figure 10a. Then S generates a tangentially swept solid we call a *solid tangent sweep*. The corresponding *solid tangent cluster* is that obtained by rotating S around the x axis. When the smaller function f defining S is identically zero, the swept solid is called a *bracelet*. Clearly, by Figure 10b, any swept solid can be produced by removing one bracelet from another. We now have:

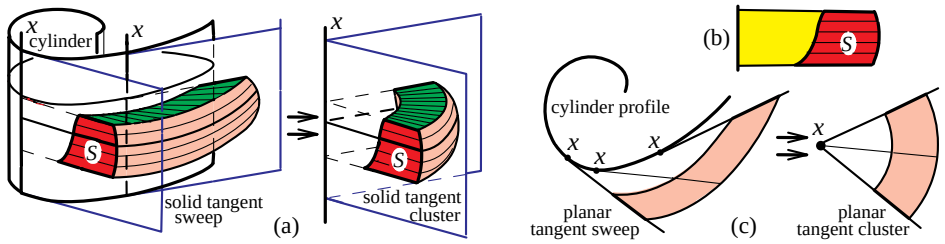

Figure 10. (a) The volume of the solid tangent sweep is the same as that of its solid tangent cluster. (b) Region S lies between two ordinate sets. (c) Top view of a typical cross section.

Theorem 1. *The volume of the solid tangent sweep does not depend on the profile of the cylinder, so it is equal to the volume of the solid tangent cluster, a portion of a solid of revolution.*

Figure 10 provides a geometric proof. A typical cross section cut by a plane perpendicular to the x axis is shown in Figure 10c. The area of the shaded band outside the cylinder is the difference of areas of two tangent sweeps of the profile of the cylinder. The area of the portion of the adjacent circular annulus swept about the x axis is the difference in areas of the corresponding tangent clusters. Therefore, by Mamikon's theorem, the shaded band and annulus in Figure 10c have equal areas. Apply the slicing principle to the solids in Figure 10a to obtain Theorem 1. □

In Section 1 we treated families of bracelets with a common property: all members of the family have the same height and the same volume, because when a given family is cut by a horizontal plane, all planar sections have equal areas.

Consequently, by simply slicing any such family by two horizontal planes at a

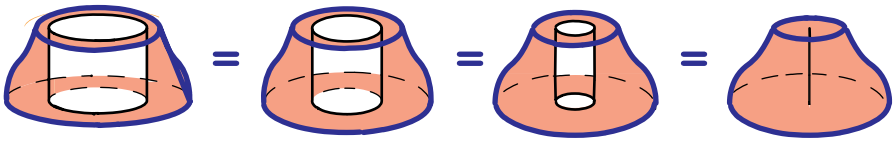

Figure 11. A family of bracelets obtained by parallel slicing of another family of bracelets. The slices also have equal height and equal volume.

given distance apart we obtain infinitely many new families with the same property because corresponding horizontal slices have equal volume. In particular, parallel slicing of families that have a horizontal plane of symmetry leads to many new families of solids with equal height and equal volume that have no horizontal plane of symmetry, as depicted in Figure 11. This greatly increases the range of applicability of our results.

3. APPLICATIONS TO TOROIDAL SOLIDS

Persoids of revolution. A torus is the surface of revolution generated by rotating a circle about an axis in its plane. The curve of intersection of a torus and a plane

parallel to the axis of rotation is called a *curve of Perseus*, examples of which are shown in Figure 12. Classical examples include ovals of Cassini and leminscates of Booth and Bernoulli. Each such curve of Perseus has an axis of symmetry parallel to the axis of rotation. When the *persoidal region*, bounded by a curve of Perseus, is rotated about this axis of symmetry it generates a solid that we call a *persoid of revolution*.

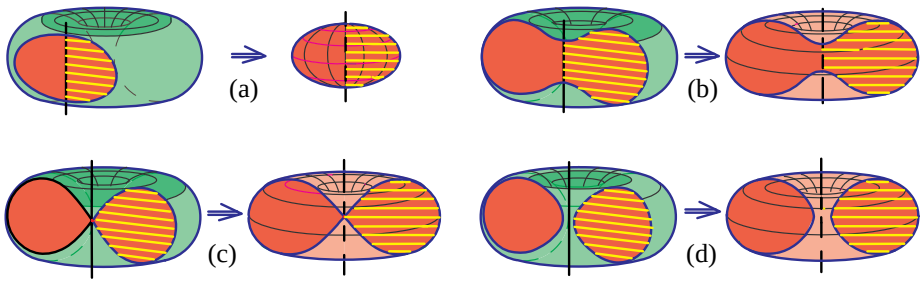

Figure 12. Each persoidal region (left) generates a solid persoid of revolution (right).

How can we calculate the volume of a persoid of revolution? We use the example in Figure 12a to illustrate a method that applies to all persoids of revolution.

When half the persoidal region in Figure 12a is swept tangentially around a circular cylinder it generates a solid tangent sweep which, by Theorem 1, has the same volume as its solid tangent cluster, in this case the persoid of revolution. To calculate this volume, we observe that the same solid can be swept by a circular segment *normal* to the cylinder as indicated in Figure 13a and in Figure 14a.

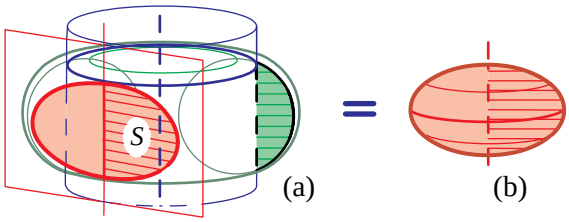

Figure 13. A tangentially swept solid with the same volume as the persoid of revolution. The same solid is swept by a circular segment normal to the cylinder.

Figure 14b shows a typical horizontal cross section of the solid, a circular annulus swept by tangential segments and by normal segments. By Pappus' theorem on solids of revolution, the volume of the solid is equal to Ad, where A is the area of the circular segment and d is the distance through which the centroid of the segment moves in sweeping out the solid. Both A and d can be determined by elementary geometry, thus giving an elementary calculation of the volume of the solid, hence also of the volume of the persoid of revolution. Moreover, according to Theorem 1, *all solids tangentially swept by a given persoidal region around a*

cylinder of any shape have the same volume as the persoid of revolution. Only one of these solids is a solid torus.

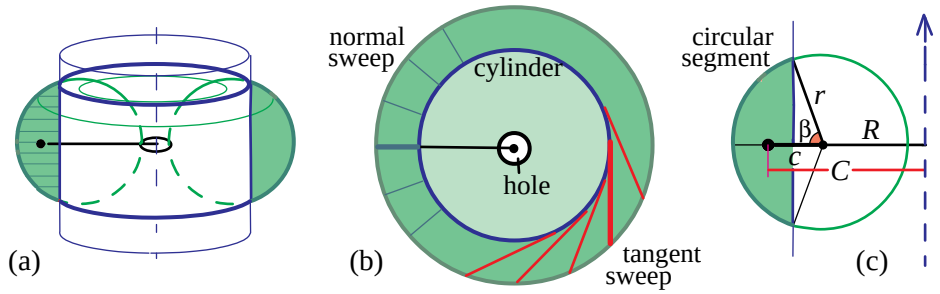

Figure 14. Calculating the volume of a swept solid using Pappus' theorem.

Volumes of classical persoids generated by ovals of Cassini and the Bernoulli lemniscate can be calculated by finding equations of the Perseus curves and using integral calculus. The foregoing discussion provides an elementary derivation that does not require equations or integration. In particular, the curve of Perseus in Figure 12c, known as a Booth lemniscate (with a cusp), generates a persoid of revolution whose volume is equal to that of the entire solid torus, $2\pi^2 r^2 R$. Here r is the radius of the circle that generates the torus as its center moves around a circle of radius R. Cassinian ovals can be defined as sections cut by a plane at a distance r from the axis of the torus. Their shapes are represented by the examples in Figure 12. When $R > 2r$, the oval consists of two symmetric disconnected pieces as in Figure 12d, and again the persoid of revolution has volume equal to that of the torus. When $R = 2r$, the Cassinian oval and the Booth lemniscate in Figure 12c become a Bernoulli lemniscate, and the persoid of revolution has volume $4\pi^2 r^3$. We summarize as follows:

Proposition. *When $R \geq 2r$ the persoid of revolution has volume $2\pi^2 r^2 R$, which is that of the solid torus.*

When $R < 2r$, as in Figures 12a and b, the persoidal region consists of one piece, and the volume V of the persoid of revolution is given by Pappus' theorem as

$$V = 2\pi CA, \tag{1}$$

where A is the area of the circular segment shaded in Figure 14c, and C is the centroidal distance of the segment from the axis of rotation. We show now that this volume is given by the explicit formula

$$V = \frac{4}{3}\pi(r\sin\beta)^3 + \pi R r^2(2\beta - \sin 2\beta). \tag{2}$$

Here r is the radius of the circle that generates the torus as its center moves around a circle of radius R, and β is half the angle that subtends the circular segment of radius r. In our geometric proof we assume that $0 \leq \beta \leq \pi/2$, but formula (2) is valid for all β. The area A of the segment is

$$A = r^2(\beta - \sin\beta\cos\beta). \tag{3}$$

Figure 14c shows that $C = c + R$, where c is the centroidal distance of the segment from the center of the circle of radius r. Hence $CA = cA + RA$. But $2\pi cA = \frac{4}{3}\pi(r\sin\beta)^3$, the volume of a spherical bracelet of height $r\sin\beta$, so (1) and (3) give (2).

For a Cassinian oval as depicted in Figures 12b and c, we have $R + r\cos\beta = r$, which gives $\cos\beta = 1 - R/r$. This determines the value of β to used in (2).

Hierarchy of toroidal solids. We can construct a hierarchy of toroidal solids as follows. Start with a plane oval region and rotate it around an axis at a positive distance from the oval to generate a toroidal solid, which we call the *initial toroid*. Cut this toroid through its hole by planes parallel to the axis at varying distances from it. Each cut produces two new oval sections with an axis of symmetry between them. Rotation of one them about the axis of symmetry generates a new toroidal solid, and the family of such toroidal solids obtained by all possible cuts we call toroids of the 1st generation. By analogy to the persoid of revolution treated in Figure 12d, each solid in this generation has the same volume as the initial toroidal solid. This extends the result for initial circular toroids described in the foregoing Proposition.

Now we repeat the process, taking as initial toroid any member of the 1st generation. For each such member we can produce a new family of toroids of the 2nd generation. Each member of the 2nd generation can also be taken as initial toroid to produce a 3rd generation, and so on. Remarkably, *all toroids so produced have the same volume as the initial toroid* we started with. It seems unbelievable that so many families exist sharing the same volume property as the classical family of drilled bracelets in Figure 1.

The next section describes another principle that aids in calculating volumes of solid clusters (hence of solid sweeps) without using calculus.

4. VOLUME OF SOLID CLUSTERS VIA CONICAL SHELLS

Conical shell principle. Figure 15a shows a triangle with its base on a horizontal axis. The area centroid of the triangle is at a distance one-third its altitude from the base, which we denote by c. When the same triangle is translated so that the upper vertex is on the axis, its centroid is at distance $2c$ from the axis.

By rotating each triangular configuration about the horizontal axis we form two solids of revolution, called *conical shells*, shown in Figure 15b. By a theorem of

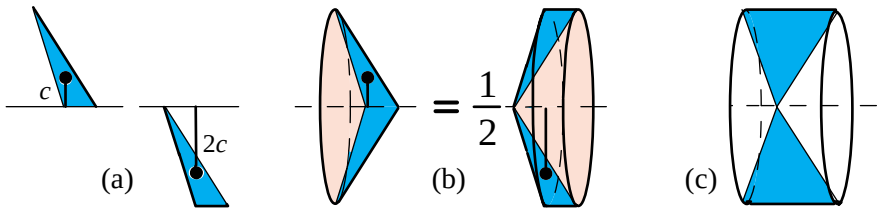

Figure 15. A conical shell principle for volumes of solids of revolution.

Pappus, the volume of each shell is the area of the triangle times the length of the path of the centroid of the triangle. Apply this to the solids in Figure 15b to obtain:

Conical shell principle. *The solid on the right of Figure 15b has twice the volume of that on the left.*

This principle implies that the punctured cylinder in Figure 15c has volume 2/3 that of the cylinder. It also leads to a basic theorem (Theorem 2 below) concerning tangent sweeps and tangent clusters that we turn to next.

Figure 16a shows the graph of a monotonic function we use as a tangency curve. Tangent segments (not necessarily of the same length) from this curve to the hor-

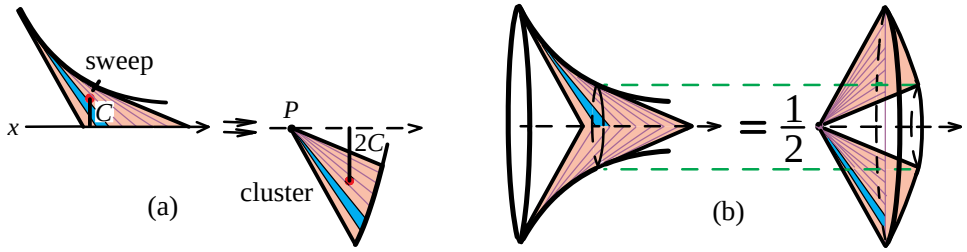

Figure 16. Geometric meaning of Theorem 2.

izontal axis generate the tangent sweep of this curve. Figure 16a also shows the tangent cluster obtained by translating all the tangent segments so the points of tangency are brought to a common point P on the horizontal axis. Consider the region between any two tangent segments in the tangent sweep, and the corresponding portion of the tangent cluster, both shown shaded in Figure 16a. We know from Mamikon's sweeping-tangent theorem that these two shaded regions have equal areas.

Now we obtain a simple relation connecting their area centroids and also the volumes of the two solids they generate by rotation about the axis. Decompose each region into tiny triangles akin to those shown in Figure 15a. We deduce that if C is the centroidal distance of the tangent sweep from the horizontal axis, then the centroidal distance of the tangent cluster from the same axis is $2C$, as indicated in Figure 16a. This proves part (a) of Theorem 2. Part (a), together with Pappus' theorem, gives part (b) of Theorem 2.

Theorem 2. (a) *If C is the centroidal distance of the tangent sweep from a horizontal axis, then the centroidal distance of the tangent cluster from the same axis is $2C$.*

(b) *The volume of the solid obtained by rotating the tangent sweep about the horizontal axis is one-half the volume of the solid obtained by rotating the corresponding tangent cluster about the same axis.*

Now we apply Theorem 2 to several examples of solids of revolution.

Tractrix and pseudosphere. When the tangent sweep of the entire tractrix shown in Figure 17a is rotated about the x axis it generates a solid of revolution which is half

a pseudosphere. If the cusp of the tractrix is at height H above its asymptote, the

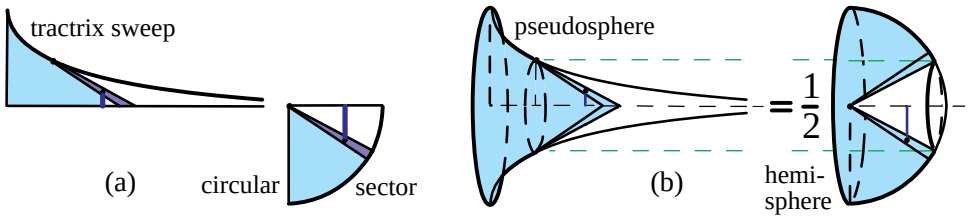

Figure 17. Determining the volume of a portion of a pseudosphere without calculus.

volume of half the pseudosphere is $\frac{2}{3}\pi H^3$, half the volume of a sphere of radius H, a result known from integral calculus. We shall obtain the same result and more (without calculus) as a direct application of Theorem 2b. Because all tangent segments to the tractrix cut off by the x axis have constant length, the tangent cluster shown in Figure 17a is a circular sector, and each small triangle contributing to the tangent sweep has a corresponding translated triangle in the tangent cluster. Therefore, Theorem 2b tells us that *the volume of any portion of the half pseudosphere is half that of the corresponding portion of the hemisphere*, as indicated in Figure 17b.

Exponential. Next we rotate the tangent sweep of an exponential function, shaded in Figure 18a, around the x axis to form a solid of revolution shown in Figure 18b. To determine its volume, refer to Figure 18a which shows the corresponding tangent cluster, a right triangle whose base is the constant length of the subtangent

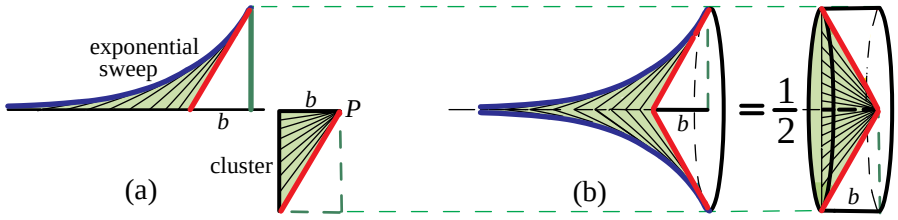

Figure 18. The volume of the solid generated by rotating an exponential ordinate set is half that of a cylinder whose altitude is the length of the constant subtangent.

to the tangency curve indicated as b in Figure 18a. (See [2; p. 16] or [3]). When this tangent sweep is rotated about the x axis it generates a solid of revolution whose volume, according to Theorem 2, is half that of the solid cluster of revolution. Consequently, *the volume of the solid obtained by rotating the ordinate set of the exponential (which includes the unshaded right triangle) is equal to half the volume of the circular cylinder whose altitude is the length b of the constant subtangent.*

Generalized pursuit curve. Figure 19a shows a tangency curve with tangent segments cut off by a horizontal axis. At each point, a tangent segment of length t cuts off a subtangent of length b. For a tractrix, t is constant, and for an exponential, b

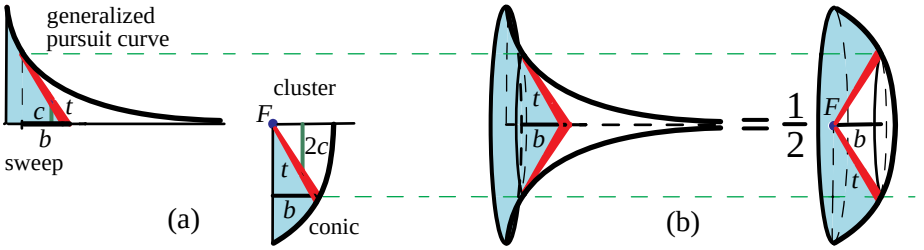

Figure 19. (a) Tangent cluster of a generalized pursuit curve is bounded by a portion of a conic section. (b) Solid obtained by rotating the generalized pursuit curve has half the volume of the solid of revolution of the conic.

is constant. If a convex combination of t and b is constant, say $\mu t + \nu b = C$ for some choice of nonegative μ and ν, with $\mu + \nu = 1$, the tangency curve is called a generalized pursuit curve. We know (see [2; p. 348], or [3]) that the tangent cluster of a generalized pursuit curve is bounded by a conic section with eccentricity ν/μ and a focus at the common point F to which each tangent segment is translated, as shown in Figure 19a. For example, when $\mu = \nu$ the pursuit curve is the classical dog-fox pursuit curve. A fox runs along the horizontal line with constant speed and is chased by a dog running at the same speed. In this case, the tangent cluster is bounded by part of a parabola.

When the general pursuit curve is rotated about the horizontal axis, its tangent sweep generates a solid of revolution as depicted in Figure 19b. By Theorem 2, *the volume of this solid is half that of the solid generated by rotating the tangent cluster.*

Paraboloidal segment. Figure 20a shows the parabola $y = x^2$ with the tangent sweep consisting of tangent segments cut off by the y axis. A corresponding tangent cluster is shaded in Figure 20b, whose curved boundary is easily shown to be the vertically dilated parabola $y = 2x^2$. Now we form two solids by rotating the tangent sweep and tangent cluster about the y axis. According to Theorem 2,

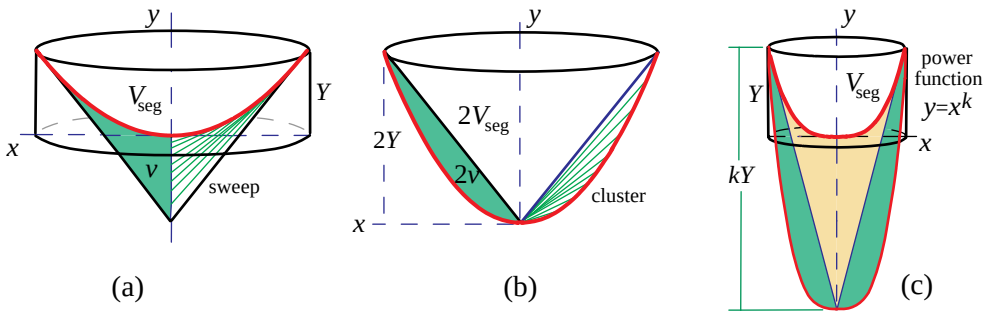

Figure 20. Volume of a paraboloidal segment.

the volume v of the solid obtained by rotating the sweep is one-half the volume

V obtained by rotating the cluster. This enables us to determine the volume V_{seg} of the paraboloidal segment obtained by rotating the parabola $y = x^2$ about the y axis. The volume of the paraboloidal segment in Figure 20b is $2V_{\text{seg}}$. Both Figures 20a and 20b show the same cone of volume V_{cone}. From Figure 20a we see that $V_{\text{seg}} = V_{\text{cone}} - v$, and from Figure 20b we find $2V_{\text{seg}} - V_{\text{cone}} = 2v$. Eliminating v we find $4V_{\text{seg}} = 3V_{\text{cone}}$. But $3V_{\text{cone}}$ is twice the volume of the circumscribing cylinder shown in Figure 20a. Consequently, we find Archimedes' result: *The volume V_{seg} of a paraboloidal segment is one-half that of its circumscribing cylinder.* In other words, the surface of revolution obtained by rotating the parabola around the y axis divides its circumscribing cylinder into two pieces of equal volume. Theorem 2 also yields a corresponding result for the power function $y = x^k$ in Figure 20c. The surface of revolution about the y axis divides the circumscribing cylinder into two solids whose volumes are in the ratio $k : 2$.

5. MODIFIED TREATMENT FOR VOLUMES OF SOLID CLUSTERS

The next theorem modifies the conical shell principle for treating volumes of solids obtained by rotating the ordinate set of a monotonic function about the x axis.

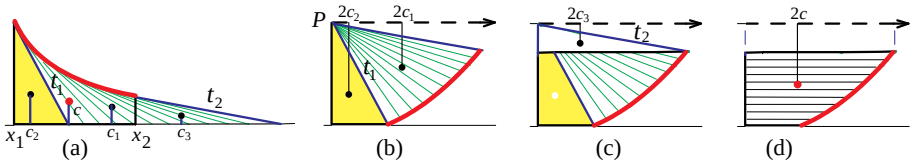

Figure 21. An abscissa set in (d) formed from the ordinate set in (a). They have equal areas and centroidal distances in the ratio 2:1.

Figure 21a shows the graph of a monotonic function and part of its tangent sweep between the graph and the x axis determined by two tangential segments t_1 and t_2 as shown. We are interested in the ordinate set above the interval $[x_1, x_2]$. This ordinate set can be formed from the tangent sweep by adding the right triangle with hypotenuse t_1 and subtracting the right triangle with hypotenuse t_2. The tangency points of t_1 and t_2 are brought to the same point P on the tangent cluster. From the corresponding tangent cluster we form its *abscissa set* shown in Figure 21d in two steps: add right triangle with hypotenuse t_1 as in Figure 21b, and subtract right triangle with hypotenuse t_2 as in Figure 21c. The resulting abscissa set in Figure 21d has the same area as the ordinate set in Figure 21a above $[x_1, x_2]$. The 2:1 relation of centroidal distances in Figure 15a yields the same relation for the components in Figures 21 a, b, and c. Now rotate the ordinate set about the x axis, and rotate the abscissa set about the polar axis p (the axis through P parallel to the x axis) to produce the two solids in Figure 22a. Argue as in Theorem 2 to get:

Theorem 3. (a) *The area of the ordinate set of any monotonic graph is equal to the area of the abscissa set of the corresponding tangent cluster.*

(b) *If C is the centroidal distance of the ordinate set from the horizontal axis, then the centroidal distance of the abscissa set of the corresponding tangent cluster from the polar axis is $2C$.*

(c) *The volume of the solid obtained by rotating the ordinate set about the horizontal axis is one-half the volume of the solid obtained by rotating the abscissa set of the corresponding tangent cluster about the polar axis.*

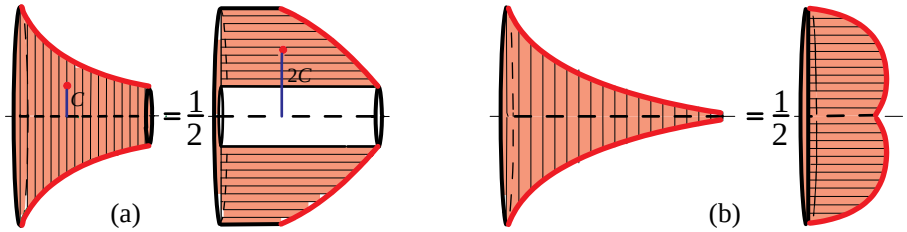

Figure 22. (a) Theorem 3a, b and c. (b) Special case where graph touches the x axis.

The geometric meaning of Theorem 3 is shown in Figure 22a. Figure 22b illustrates the special case where the graph touches the x axis.

Cut pseudosphere. When Theorem 3 is applied to a cut portion of a pseudosphere and its mirror image obtained from Figure 17b, it reveals that *the volume of that portion of a pseudosphere is half the volume of a spherical bracelet*, as indicated in Figure 23.

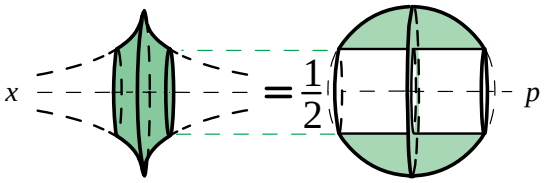

Figure 23. Cut pseudosphere has half the volume of a spherical bracelet.

Paraboloidal solid funnel. The shaded region in Figure 24a is a parabolic segment between the curve $y = x^2$ and the interval $[0, X]$. Figure 24b shows a tangent sweep of the parabola and a corresponding tangent cluster, whose curved boundary is part of the parabola $y = (2x)^2$. This figure was used in [2; p. 476] and in [3] to calculate the area of the parabolic segment in Figure 24a by Mamikon's sweeping tangent method. Now we use it to determine the volume v of the paraboloidal funnel in Figure 24c which is obtained by rotating the ordinate set in Figure 24a about the x axis. The upper shaded region in Figure 24b is the abscissa set of the cluster. By Theorem 3, v is one-half the volume V of the solid obtained by rotating the upper shaded region about the x axis. This implies that v is one-fourth the volume of the solid obtained by rotating the unshaded region in Figure 24a around the x axis. Hence the curved surface of the funnel divides its circumscribing cylinder into two pieces whose volumes are in the ratio $4 : 1$. Therefore *the volume*

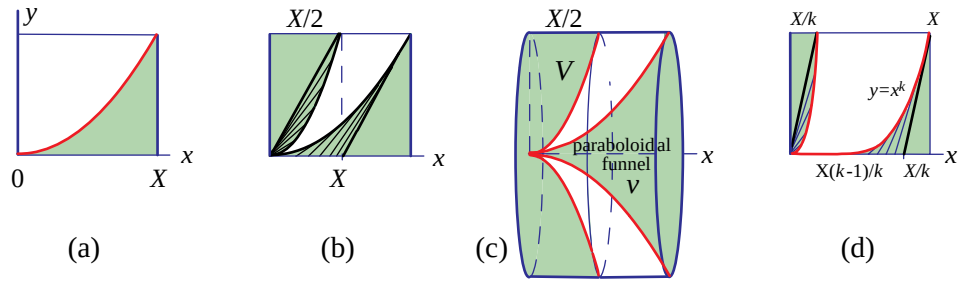

Figure 24. Volume of a paraboloidal solid funnel.

of the paraboloidal funnel is 1/5 *that of its circumscribing cylinder*. In the same manner, Theorem 3 shows that if we rotate the curve $y = x^k$ in Figure 24d about the x axis, the surface of revolution divides the circumscribing cylinder into two pieces whose volumes are in the ratio $2k : 1$

Rotated cycloidal cap. Figure 25 shows one arch of a cycloid generated by a point on the boundary of a rolling circular disk, together with a circumscribing rectangle. The disk rolls along the base of this rectangle, and a tangent sweep is the "cap" formed by drawing tangent segments from the cycloid to the upper edge of the

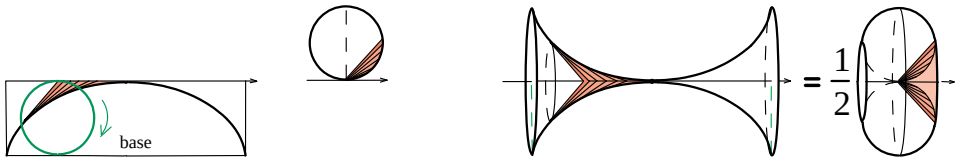

Figure 25. Solid of revolution swept by cycloidal cap.

rectangle as indicated. It is known that the area of the cap is equal to that of the disk because the disk is the tangent cluster of this tangent sweep (see [2; p. 35], or [4]). By Theorem 3, *the horn-shaped solid obtained by rotating the cycloidal cap about the upper edge has volume equal to half that of the toroidal-type solid obtained by rotating the disk about the same edge.* If the disk has radius a this volume is $\pi^2 a^3$.

A family generalizing the cycloid and tractrix. Figure 26 shows a cycloid (flipped over) and a tractrix, with tangent clusters to each obtained in similar fashion. For the cycloid the tangent cluster segments emanate from a common point P at one

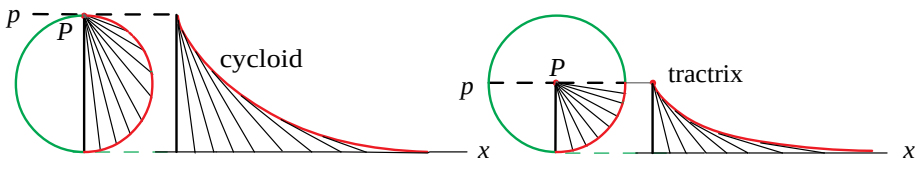

Figure 26. Common method for generating cycloid and tractrix.

end of the vertical diameter of a circle; for the tractrix they emanate from the center P of a circle.

Figure 27 shows how to produce a family of curves generalizing the cycloid and tractrix by allowing the tangent segments of the cluster to emanate from a common point P anywhere on the diameter. We consider the symmetric solids of revolution

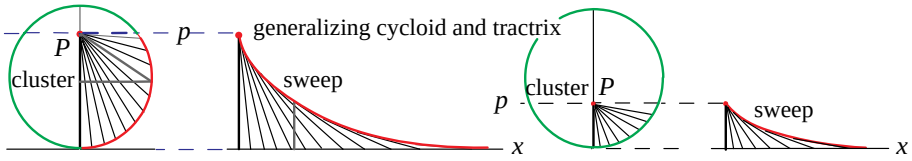

Figure 27. Family that includes cycloid and tractrix.

swept by rotating about the x axis the ordinate sets of these curves together with their mirror images through the y axis. Figure 28 shows how Theorem 3 determines the volume of a symmetrically cut portion of such solids. *Each volume is half that of a toroidal bracelet*, the corresponding rotated abscissa set of the cluster, whose volume can be easily found by Pappus' rule as was done earlier for persoids of revolution.

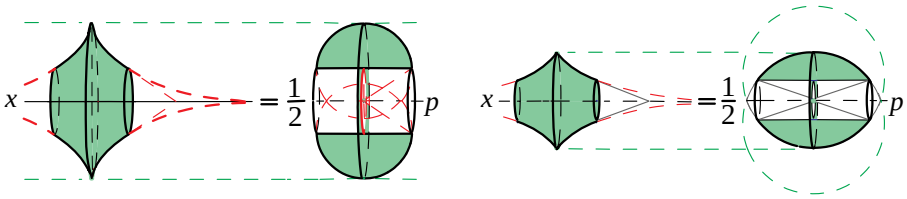

Figure 28. Volume relations for solids obtained by rotating the ordinate sets in Figure 27.

6. VOLUMES SWEPT BY COMPLEMENTARY REGIONS

According to Pappus, the solid of revolution obtained by rotating a plane region of area A around an axis has volume $V = 2\pi cA$, where c is the centroidal distance of the region from the axis of rotation. Therefore, for a region of given area A, determining V is equivalent to determining centroidal distance c. We exploit this fact to derive a surprising and useful comparison lemma for volumes swept by two complementary regions whose union is a rectangle.

Figure 29a shows a rectangle divided into two complementary regions of areas A_1 and A_2. In Figure 29b, the region of area A_1 has been rotated about the lower edge l_1 of the rectangle to generate a solid of revolution of volume V_1. In Figure 29c, the complementary region of area A_2 has been rotated about the upper edge l_2 of the rectangle to generate another solid of revolution of volume V_2. Both solids are circumscribed by a cylinder of volume $V = \pi RH$ obtained by rotating the rectangle of area R and height H around either horizontal edge. Let $a_1 = A_1/R$

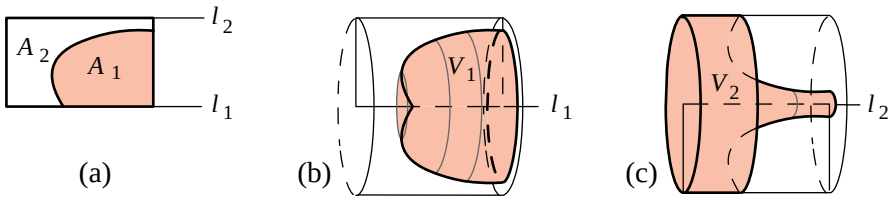

Figure 29. Solids obtained by rotating complementary parts of a rectangle around its lower and upper edges.

and $a_2 = A_2/R$ denote the fractional areas relative to the rectangle, so that $a_1 + a_2 = 1$. Similarly, let $v_1 = V_1/V$ and $v_2 = V_2/V$ denote the fractional volumes relative to the cylinder. (Relative areas and relative volumes are dimensionless.) Then we have the following surprising relation, which we state as a lemma:

Comparison Lemma for Complementary Regions. *The difference of relative volumes is equal to the corresponding difference of relative areas:*

$$v_2 - v_1 = a_2 - a_1. \tag{4}$$

To prove (4), let c_1 denote the distance of the area centroid of A_1 from the lower axis l_1, and let c_2 denote the centroidal distance of area A_2 from the upper axis l_2. Then $c = H/2$ is the centroidal distance of the area R of the rectangle from either axis. By equating area moments about the lower axis l_1 we find $c_1a_1 + (2c - c_2)a_2 = c$, which can be rewritten as follows:

$$c_1a_1 - c_2a_2 = c(1 - 2a_2) = c(a_1 - a_2). \tag{5}$$

From Pappus' theorem we have

$$v_2 - v_1 = \frac{2\pi}{V}(c_2A_2 - c_1A_1) = \frac{2}{H}(c_2a_2 - c_1a_1) = \frac{1}{c}(c_2a_2 - c_1a_1),$$

which, together with (5), gives (4).

Examples: Cycloidal and paraboloidal solids. To illustrate how this can be used in practice, refer to Figure 30. Figure 30a shows the solid swept by rotating one arch of a cycloid around its base. If the rolling disk generating the cycloid has radius a, then the volume V_{cap} of the solid of revolution swept by the cycloidal cap in Figure 25 is $V_{\text{cap}} = \pi^2a^3$. The arch and cap are complementary regions with relative areas 3/4 and 1/4, whose difference is 1/2. The cylinder has volume $8\pi^2a^3$ so the volume of the cap relative to that of the cylinder is $v_{\text{cap}} = 1/8$. By (4) in the comparison lemma, the volume of the arch relative to that of the cylinder is $v_{\text{arch}} = v_{\text{cap}} + 1/2 = 5/8$. Therefore $V_{\text{arch}} = 5\pi^2a^3$.

Now we use the lemma again to determine the relative volume v_2 of the solid in Figure 30b obtained by rotating the complement of the parabolic segment in Figure 24a about the upper edge of the circumscribing rectangle. In Figure 24c we found that the volume v_1 of a paraboloidal funnel is 1/5 that of the circumscribing cylinder, so by (4) we have $v_2 = v_1 + a_2 - a_1 = 1/5 + 2/3 - 1/3 = 8/15$. In Figure 30b, *the volume of the shaded solid is* 8/15 *that of its circumscribing cylinder*.

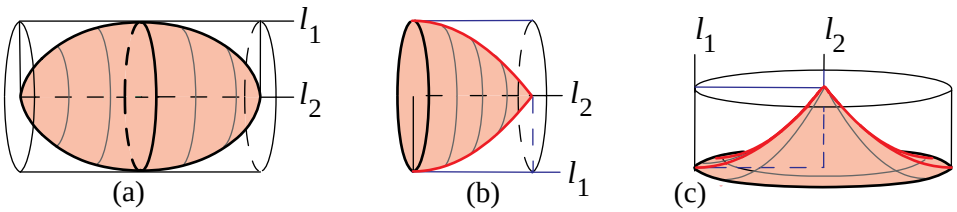

Figure 30. (a) Cycloidal arch rotated about its base has volume 5/8 that of its circumscribing cylinder. (b) Solid obtained by rotating a parabolic region around the upper edge has volume 8/15 that of the circumscribing cylinder. (c) Paraboloidal funnel has volume 1/6 that of its circumscribing cylinder.

Finally, we use the lemma once more to determine the relative volume v_2 of the paraboloidal funnel in Figure 30c obtained by rotating the parabolic segment in Figure 24a around axis l_2. In Figure 20 we found that the relative volume v_1 of the complementary paraboloidal segment rotated around l_1 is $1/2$, so by (4) we have $v_2 = 1/2 + a_2 - a_1 = 1/2 + 1/3 - 2/3 = 1/6$. In other words, in Figure 30c *the volume of the paraboloidal funnel is* 1/6 *that of the circumscribing cylinder*.

The lemma has a surprising consequence. For the special case in which $a_1 = a_2$ we find $v_1 = v_2$. In other words:

If the rectangle is divided into two regions of equal area, then the two solids obtained by rotating one region about the upper edge and the other about the lower edge have equal volumes!

Figure 31 shows three interesting examples. In Figure 31a, a cycloid generated by a rolling disk of radius 1 divides the shaded rectangle of altitude 3/2 into two regions of equal area. Hence the solid obtained by rotating the portion of the rectangle above the arch around the upper edge of this rectangle has the same volume as the solid obtained by rotating the cycloidal arch around the lower edge, which was treated in Figure 30a.

In Figure 31b a parabolic segment of height 1 is inside a rectangle of altitude 4/3. The parabola divides the shaded rectangle into two regions of equal area, so the solid obtained by rotating one region around the upper edge has the same volume as the solid obtained by rotating the complementary region around the lower edge. Figure 31c is similar, with the regions rotated about the right and left edge of the rectangle.

Examples. Generalized strophoidal solids.

(a) Solid of revolution generated by tangent sweep to unit circle. The shaded region in Figure 32a is the tangent sweep to a unit circle, where each tangent segment is cut off by a horizontal line p through the center of the circle. The corresponding tangent cluster is shown in Figure 32b. Now we rotate each of these regions about the horizontal axis to produce two solids of revolution. The volume V_a of the solid in Figure 32a (inside the cone and outside the sphere) is easy to find. It is equal to that of the cone minus the volume of the inscribed spherical segment. The volume

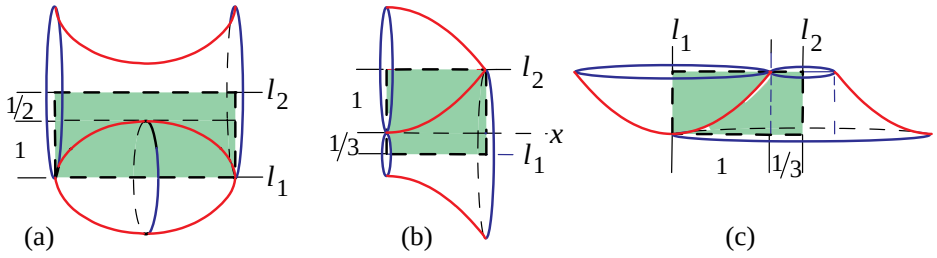

Figure 31. Three examples of solids of equal volume obtained by rotating complementary regions of equal area around opposite edges of a rectangle.

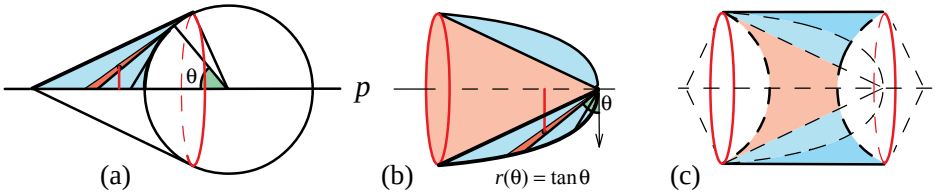

Figure 32. Solids swept by (a) tangent sweep to unit circle, and by (b) its tangent cluster. (c) Calculating the volume of the full solid in (b).

V_b of the solid in Figure 32b (outside the cone) is twice V_a, according to Theorem 2, so V_b is twice the volume of the cone minus twice that of the spherical segment in Figure 32a. The cones in Figures 32a and 32b are congruent. Therefore, if we adjoin the inside cone to the solid of volume V_b in Figure 32b, we obtain a solid whose volume is three times that of the cone minus twice that of the spherical segment in Figure 32a. But three times the volume of cone is the volume of its circumscribed cylinder, shown in Figure 32c. Consequently, *the volume of the full solid is that of the circumscribing cylinder minus twice that of the spherical segment.*

The full solid in Figure 32b can be generated another way. It is part of the solid of revolution obtained by rotating the plane curve with polar equation $r = \tan\theta$ around its horizontal axis of symmetry. The volume of that solid can also be calculated by using integral calculus, but the foregoing calculation is simpler and more revealing.

(b) Solid of revolution generated by strophoid. Figure 33a shows a tangent sweep like that in Figure 32a, except that the tangent segments to the unit circle are cut off by a horizontal line p tangent to the circle at point P. The corresponding tangent cluster, with the points of tangency brought to the common point P, is shown in the lower part of Figure 33a. This cluster is bounded by a curve which, as we will show later, is a classical right strophoid. The strophoid consists of two parts, a loop and a leftover portion with a horizontal asymptote. The region bounded by the loop is the tangent cluster of the portion of the tangent sweep circumscribed by the rectangle in Figure 33b. Therefore the loop area is $2 - \pi/2$. Tangent sweeping

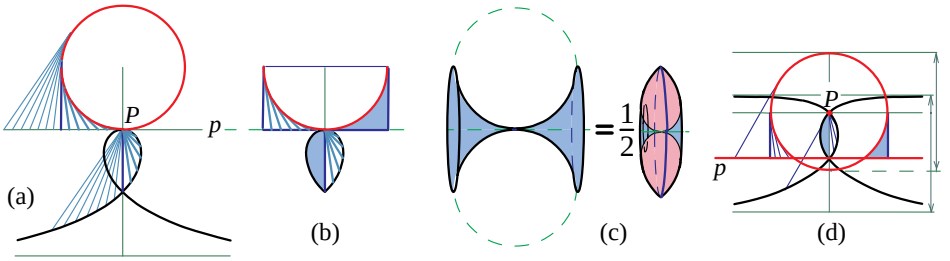

Figure 33. (a) Tangent sweep to a circle and its tangent cluster. (b) Portion of sweep in (a) corresponding to the loop. (c) Volume relation for solids obtained by rotating regions in (b). (d) Generalized strophoid.

can also be used to show that the area of the region between the strophoid and its asymptote is $2 + \pi/2$.

Now we determine the volume of the solid obtained by rotating the loop about the horizontal axis p. According to Theorem 2, *its volume is twice that of a toroidal cavity* (the solid obtained by rotating the corresponding tangent sweep around p). To find that volume, in turn, we apply the Comparison Lemma. Rotation of the complementary region about the upper edge of the rectangle in Figure 33b gives a sphere of volume $4\pi/3$, which means that the relative volume v_1 is $2/3$ that of its circumscribing cylinder. The relative areas of the complementary regions are $a_1 = \pi/4$ and $a_2 = 1 - \pi/4$, so $a_2 - a_1 = 1 - \pi/2$ and (4) gives $v_2 = 5/3 - \pi/2$ as the relative volume of the rotated tangent sweep. Therefore the absolute volume of the solid on the left of Figure 33c is $2\pi(5/3 - \pi/2) = \pi(10/3 - \pi)$. The volume of the solid obtained by rotating the loop is twice that.

The volume of the solid generated by rotating, about the asymptote, the region in Figure 33a between the strophoid and its asymptote can also be determined, but we omit the details.

An infinite family of generalized strophoids can be constructed by parallel motion of the line p which cuts off the tangent segments to the circle, as indicated in Figure 33d. Tangent sweeping can be used to determine corresponding areas and volumes of revolution, but we shall not present the details.

Different descriptions of the classical strophoid. The classical strophoid has been described in three different ways by Roberval, Barrow, and Newton. Figure 34a shows Newton's description as the locus of corner A of a carpenter's square, as the end point B of edge BA slides along a horizonal line while the perpendicular edge touches a fixed peg P at distance AB above B. Figure 34b shows that our description of the strophoid in Figure 33a is equivalent to that of Newton. And Figure 34c leads to a known polar description of the right strophoid.

7. APPLICATIONS TO HYPERBOLOIDS

Hyperboloid of two sheets. Figure 35a shows the lower half of right circular cone with a cylindrical hole drilled through its axis. A tangent plane to the cylinder intersects the cone along one branch of a hyperbola, forming a hyperbolic cross

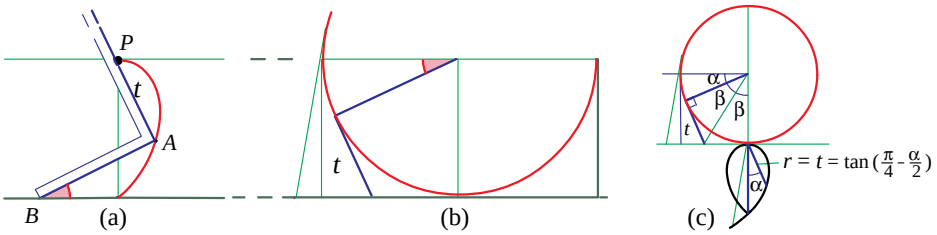

Figure 34. (a) Newton's description of strophoid. (b) Tangent sweep to a unit circle used to describe strophoid. (c) Polar equation describing strophoid.

section that generates a bracelet by tangential sweeping. *The volume of the hyperboloidal bracelet shown is equal to the volume of the solid of revolution generated by the hyperbolic cross section.*

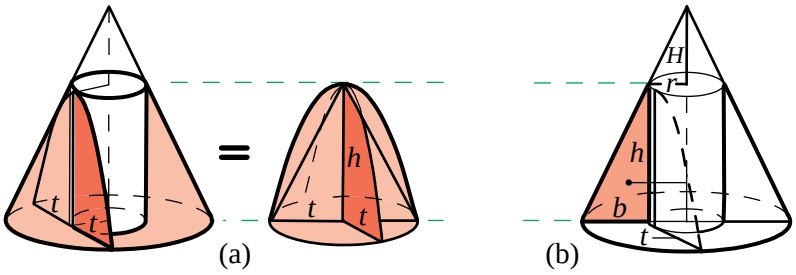

Figure 35. (a) Bracelet cut from a cone by an axial hole has the same volume as that of a hyperboloid of revolution. (b) Diagram for proving Archimedes' volume relation in (6).

Archimedes showed in [6; *On Conoids and Spheroids*, Prop. 25] that this volume (call it V) bears a simple relation to the volume V_{cone} of the inscribed right circular cone in Figure 35a with the same base and axis. This cone has altitude h and base t, the base radius of the hyperboloid of revolution. Archimedes showed that

$$\frac{V}{V_{\text{cone}}} = \frac{3H+h}{2H+h}, \tag{6}$$

where H, indicated in Figure 35b, is the length of the semimajor axis of the hyperbola. A simple proof of (6) can be given from our observation that the bracelet can be swept by rotating tangentially around the cylindrical hole the shaded triangle of base b and altitude h in Figure 35b. The area of the triangle is $bh/2$, and the area centroid of the triangle is at distance $r + b/3$ from the axis of rotation, where r is the radius of the cylindrical hole.

By Pappus, volume V is the product of the area of the triangle and the distance its centroid moves in one revolution, giving us

$$V = 2\pi(r + \frac{b}{3})\frac{bh}{2} = \frac{\pi}{3}(b+3r)bh. \tag{7}$$

The cone with the same base and axis has altitude h and base t, where t is the length of the tangent to the hole in Figure 35b. By similar triangles, $b/t = t/(2r + b)$, so $t^2 = (b + 2r)b$. Hence

$$V_{\text{cone}} = \frac{\pi}{3}t^2h = \frac{\pi}{3}(b + 2r)bh. \tag{8}$$

Now divide (7) by (8) and use the similarity relation $r/b = H/h$ to obtain (6).

Equilateral hyperbola rotated about an asymptote. Figure 36a shows an equilateral hyperbola and its orthogonal asymptotes. The portion of any tangent to the hyperbola between the asymptotes is bisected at the point of tangency. As the point of tangency moves to the right, the lower half of the tangent segment forms a tangent sweep with the hyperbola as tangency curve. A corresponding tangent cluster is formed by translating each tangent segment so the point of tangency is at the origin. The free end of the translated segment traces the mirror image of the original hyperbola, as suggested in Figure 36b. By Theorem 2, the volume of the solid obtained by rotating the tangent sweep about the horizontal axis is one-half the volume of the solid obtained by rotating the corresponding tangent cluster about the same axis. As the point of tangency moves from some initial position to ∞, the swept solid is a hyperboloid of revolution of volume V_{hyp}, say, punctured by a right circular cone of volume V_{cone} generated by rotating the initial tangent segment. On the other hand, the cluster solid is the same hyperboloid together with a cone congruent to the puncturing cone. Consequently, $V_{\text{hyp}} + V_{\text{cone}} = 2(V_{\text{hyp}} - V_{\text{cone}})$, hence $V_{\text{hyp}} = 3V_{\text{cone}}$, which, in turn, is the volume of the cylinder attached to the hyperboloid, as shown in Figure 36c.

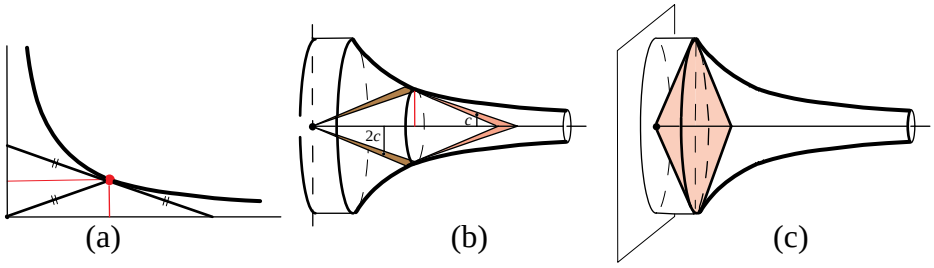

Figure 36. Hyperboloid of revolution and attached cylinder of equal volume.

Figure 37 shows an interesting interpretation of the foregoing result. The hyperboloid of revolution can be regarded as a "monument" of infinite extent supported by a cylindrical pedestal whose base rests on a plane through the other asymptote. We have just shown that *the volume of such a monument is equal to the volume of its pedestal*. It seems appropriate to refer to this as a "monumental result." It can, of course, also be easily verified by integration.

General hyperbola rotated about one asymptote. An even deeper monumental result will be obtained for a general hyperbola rotated about one of its asymptotes. The volume of the solid hyperboloid is again equal to the volume of its pedestal, but now the more general pedestal consists of two parts, a cylindrical part together with

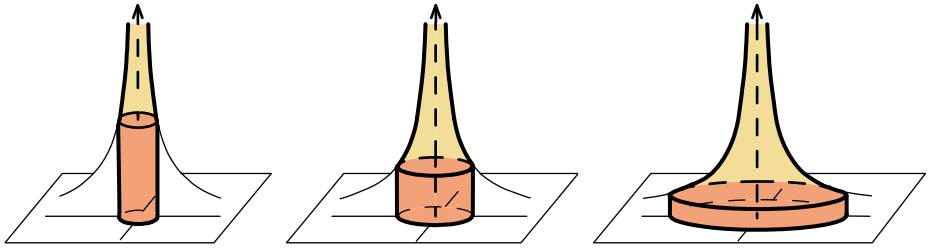

Figure 37. Each hyperbolic monument has the same volume as its cylindrical pedestal.

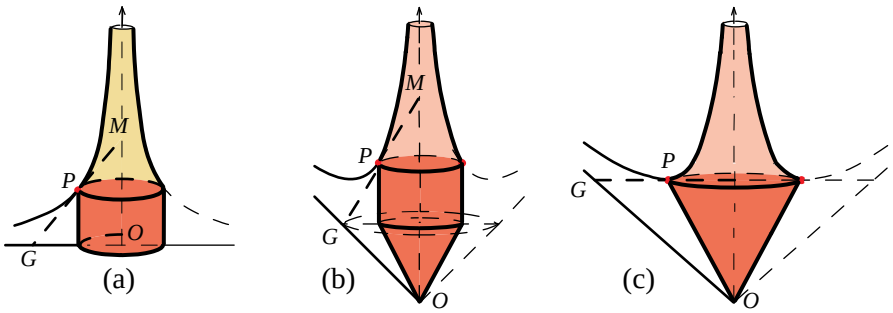

Figure 38. Hyperboloid of revolution and attached pedestal of equal volume.

an attached conical part whose shape depends on the angle between the asymptotes, as illustrated in Figure 38b. The conical part disappears when the asymptotes are orthogonal as in Figure 38a, and the cylindrical part disappears when the monument touches the ground, as in Figure 38c.

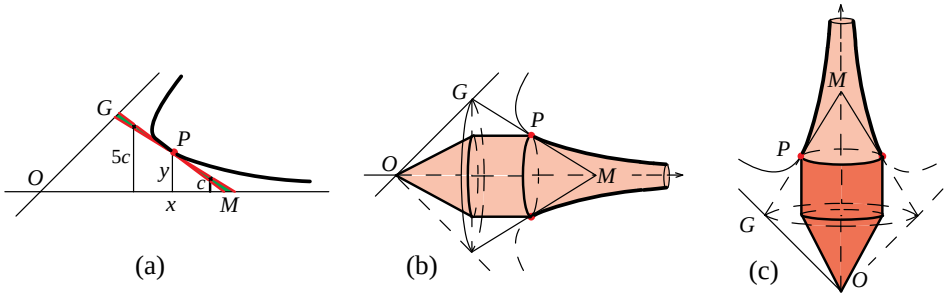

Figure 39. (a) Centroidal distance to upper tangent sweep is 5 times that to the lower tangent sweep. (b) and (c) Hyperboloid of revolution and attached pedestal of equal volume.

Figure 39a shows one branch of the hyperbola oriented so that the asymptote of rotation is along the x axis, together with a tangent segment at a point $P = (x, y)$ cut off by the two asymptotes at points G and M in Figure 39b. The asymptotes intersect at O. For any hyperbola, the point of tangency P bisects segment GM.

We wish to determine the volume of the solid of revolution obtained by rotating about the x axis the ordinate set of this hyperbola above the interval $[x, \infty)$.

The ordinate set consists of two parts, a lower tangent sweep generated by moving PM from x to ∞, plus the triangle between the initial tangent PM and its subtangent. Figure 39a shows a small triangle contributing to the lower tangent sweep; its centroid is at height $c = y/3$ above the x axis. The corresponding triangle cut off by the other asymptote, which is part of the another (upper) tangent sweep, has its centroid at height $y + 2y/3 = 5c$ above the x axis. The ratio 5 to 1 of these centroidal distances for the hyperbola has the following profound consequence which we state as a lemma:

Lemma. *The solid obtained by rotating the upper tangent sweep of the hyperbola about the x axis has volume 5 times that of the solid obtained by rotating the lower tangent sweep about the same axis.*

The lemma follows from Pappus' theorem. The volume of the conical shell generated by rotating each small triangle in the lower tangent sweep is $2\pi c$ times the area of the triangle. The corresponding triangle in the upper tangent sweep has the same area, so the corresponding conical shell has volume 5 times as great.

The lemma now follows from the fact that each solid of rotation is the union of such conical shells.

Now we show that *the volume of the hyperboloid of revolution is equal to the volume of the composite pedestal, cone plus cylinder.* First, we express each of these volumes in terms of the volume V_{hyp} of the hyperboloid of revolution and various related cones. The volume generated by the lower tangent sweep is $V_{\text{hyp}} - V_{\text{cone}}$, where V_{cone} is the volume of the cone of slant height PM swept by the right triangle below the initial tangent segment. The volume generated by the upper tangent sweep is equal to that generated by the lower tangent sweep plus the volume V_{double} of the double cone generated by rotating triangle OGM in Figure 39b. By the lemma we have

$$(V_{\text{hyp}} - V_{\text{cone}}) + V_{\text{double}} = 5(V_{\text{hyp}} - V_{\text{cone}}),$$

which gives us

$$4V_{\text{hyp}} = V_{\text{double}} + 4V_{\text{cone}}. \tag{9}$$

From Figure 39b it is easy to see that $V_{\text{double}} = 8V_{\text{cone}} + V_O$, where V_O is the volume of the cone with slant height OG. But $V_O = 4V_{\text{base}}$, where V_{base} is the volume of the base cone with vertex O and radius y. Hence (9) implies

$$V_{\text{hyp}} = V_O + 3V_{\text{cone}} = V_O + V_{\text{cyl}}, \tag{10}$$

where V_{cyl} is the volume of the cylinder joining the bases of the base cone and the cone with slant height PM. This completes the proof that the volume of the hyperboloid of revolution is equal to the volume of the composite pedestal, cone plus cylinder.

8. FURTHER EXAMPLES OF TANGENTIALLY SWEPT SOLIDS

Cardioid. In the next example we rotate one lune of a cardioid about the axis of the cardioid to generate a solid of revolution. Here the cardioid is a pedal curve as described in [2; p. 24]. (Point P is the pedal point and F denotes the foot of the perpendicular from P to an arbitrary tangent line to the large circle. The cardioid is the locus of all such points F constructed for all tangent lines.) One lune of the cardioid is swept by tangents to the large circle as indicated in Figures 40a and b. The left half of the small disk is the tangent cluster of that part of the lune swept

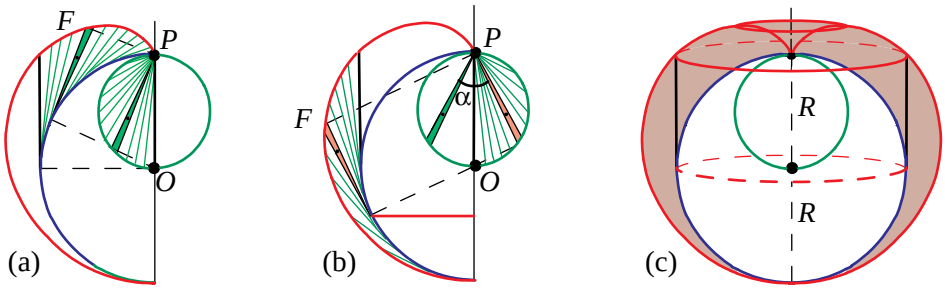

Figure 40. (a) and (b): Tangential sweeping of one lune of a cardioid. (c) Solid of revolution.

by tangents from the horizontal position at P to the vertical position in Figure 40a. The right half of the small disk is the tangent cluster of the remaining part of the lune as in Figure 40b. Hence, the area of the lune is equal to the area of the small disk.

When we rotate the cardioid about its axis of symmetry it generates an apple-like solid depicted in Figure 40c. Classical integration in polar form shows that its volume is twice the volume of the large central sphere. In other words, *the punctured apple (the shaded portion between the sphere and the apple) has the same volume as the sphere.* We shall give a geometric proof of this result.

In Figure 41 a thin shaded triangle of altitude t of the tangent sweep of the upper part of the lune makes an angle α with the axis of rotation. The corresponding triangle of the same altitude for the lower part of the lune that makes the same angle α is also shown. The two triangles have equal area (which we denote by ΔA) and the sum of their centroidal distances from the axis of rotation is $(R\cos\alpha - c) + (R\cos\alpha + c) = 2R\cos\alpha$, where R is the radius of the large central circle. When rotated together around the axis they sweep a solid of volume $4\pi(R\cos\alpha)\Delta A$, according to a theorem of Pappus.

The two thin triangles can be combined to form a rectangle shown in Figure 41a as a thin horizontal slice of the large semicircular disk. The area of the rectangle is $2\Delta A$ and its centroidal distance from the axis is $\frac{1}{2}R\cos\alpha$. Two symmetric copies of this rectangle are shown. When the rectangles are rotated around the axis they generate two symmetric slices of the sphere which together, by Pappus, have the same volume as the solid swept by the two thin triangles. As α varies from 0 to $\pi/2$, the rotated triangles sweep the punctured apple, and the corresponding rectangles

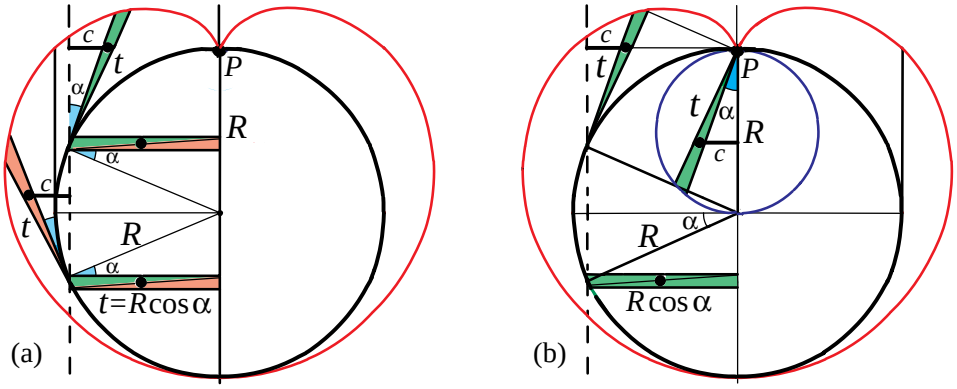

Figure 41. Diagram showing that punctured apple has same volume as the sphere.

sweep the large interior sphere. This shows that *the punctured apple has the same volume as the sphere.*

We can gain further insight by regarding the punctured apple as a piece of pottery with two parts, an upper one (the cap) shown in Figure 42a, and a lower one shown in Figure 42b. We will show that *the volume* V_{upper} *of the cap is equal to that of the large hemisphere minus that of the small sphere* obtained by rotating the tangent cluster disk in Figure 42 whose area is that of the lune. Consequently, the *volume* V_{lower} *of the lower part is that of the large hemisphere plus the volume of the small sphere.*

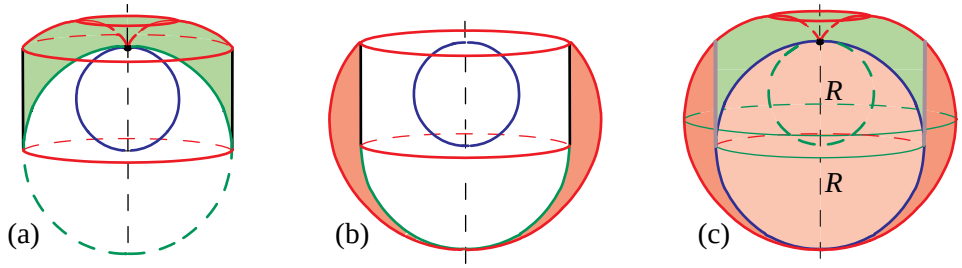

Figure 42. Upper part (a) and lower part (b) of punctured apple. Volume of upper part is that of the large hemisphere in (c) minus that of small sphere. Volume of lower part is that of large hemisphere plus that of small sphere.

Volume of the upper part: Figure 41b shows a thin triangle in the tangent sweep of the upper part of the lune and its counterpart in the tangent cluster, which makes an angle α with the axis of rotation. The triangles have equal area (which we call ΔA), and the sum of their centroidal distances from the axis of rotation is $R\cos\alpha$. The triangles of this part of the tangent sweep generate the cap and those of the tangent cluster generate the small interior sphere. The two thin triangles can be combined to form the familiar rectangle shown in Figure 41b as a thin

horizontal slice of the large semicircular disk. The area of the rectangle is $2\Delta A$ and its centroidal distance from the axis is $\frac{1}{2}R\cos\alpha$. When all these rectangles are rotated around the axis they sweep a hemispherical solid whose volume is equal that of the volume swept by all the above triangles. This shows that V_{upper} is the volume of the large hemisphere minus the volume of the small sphere.

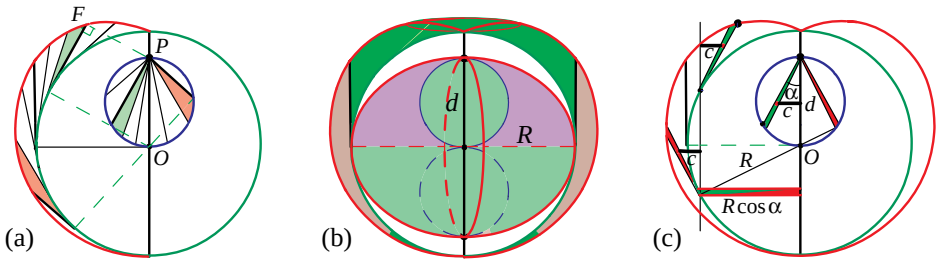

Figure 43. Analysis for cardioid modified for the Limaçon of Pascal.

Limaçon. Not surprisingly, a similar argument works when the cardioid is replaced by any Limaçon of Pascal, an example of which is shown in Figure 43. In this case, *the volume of the punctured apple is equal to that of an ellipsoid of revolution* obtained by rotating an ellipse of semiaxes R and d around the major axis, as indicated in Figure 43b. We also note that volume V_{upper} of the upper part is equal to that of the large semiellipsoid minus that of the small sphere of diameter d in Figure 43b. The volume V_{lower} of the lower part is that of the same semiellipsoid plus that of the small sphere of diameter d. For the proof observe that the thin triangles now have area smaller than the area ΔA for the cardioid by a factor $(d/R)^2$, where d is the diameter of the small circle in Figure 43c. The rest of the argument is like that for the cardioid.

Catenoid. Figure 44a shows a portion of a catenary, the graph of a hyperbolic cosine, $y = \cosh x$, for $0 \le x \le X$. When the ordinate set of this graph is rotated about the x axis the solid of revolution is a catenoid whose volume, expressed as an integral, is $V_{\text{ch}} = \pi \int_0^X \cosh^2 x\, dx$. The corresponding volume of the solid obtained by rotating the ordinate set (Figure 44b) of a hyperbolic sine, $y = \sinh x$, over the same interval is $V_{\text{sh}} = \pi \int_0^X \sinh^2 x\, dx$. But $\cosh^2 x - \sinh^2 x = 1$, so the difference of the volumes is

$$V_{\text{ch}} - V_{\text{sh}} = \pi X. \tag{11}$$

The result in (11) can be obtained without integration by using sweeping tangents to show geometrically that the difference of volumes $V_{\text{ch}} - V_{\text{sh}}$ is the volume of the cylinder of altitude X and radius 1 shown in Figure 44c.

The method of sweeping tangents also reveals the nonobvious result that the sum of the volumes is the same as the volume of another solid of revolution, shown in Figure 45a. This solid is generated by rotating the rectangle in Figure 45b with vertex X about the x axis. That rectangle appears in [2; p. 346] and in [5; p. 413] where its area is shown by tangent sweeping to be equal to that of the ordinate set

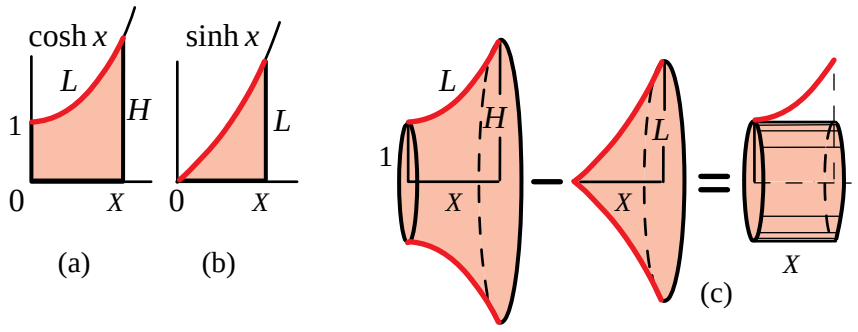

Figure 44. The difference of volumes $V_{\text{ch}} - V_{\text{sh}}$ is the volume of a cylinder.

of the catenary. The rectangle has base 1, altitude L and diagonal of length H.

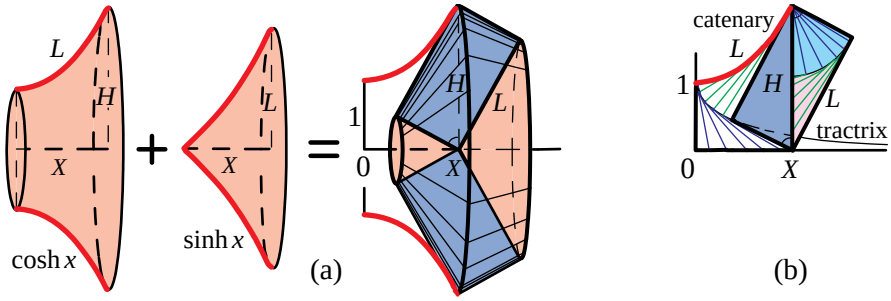

Figure 45. The sum of volumes $V_{\text{ch}} + V_{\text{sh}}$ is the volume of a solid obtained by rotating the rectangular region in (b).

Here $L = \sinh X$ is the arclength of the catenary, and $H = \cosh X$. The rectangle reveals that $H^2 = L^2 + 1$. An easy calculation shows that the solid has volume

$$V_{\text{ch}} + V_{\text{sh}} = \pi LH. \tag{12}$$

From (11) and (12) we obtain V_{ch} and V_{sh} separately without integration:

$$V_{\text{ch}} = \frac{\pi}{2}(LH + X), \quad V_{\text{sh}} = \frac{\pi}{2}(LH - X). \tag{13}$$

9. VERTICAL SECTIONS OF SOLID SWEEP AND CLUSTER

We know that a solid tangent sweep and its solid tangent cluster have equal volumes because corresponding horizontal cross sections of these solids have equal areas. We turn next to surprising properties relating their *vertical* cross sections.

Area balance of axial sections. Figure 46 shows vertical cross sections of bracelets in Figures 1, 4, 5a, 6 and 8 taken through the axis of revolution, indicated by the arrow. The section of the solid tangent cluster is shown on the right of the axis, and a section of a typical solid tangent sweep is shown on the left.

From Pappus' rule for volumes, we obtain the following balance-revolution principle (introduced in [2; p. 410].) *The areas of two plane regions are in equilibrium*

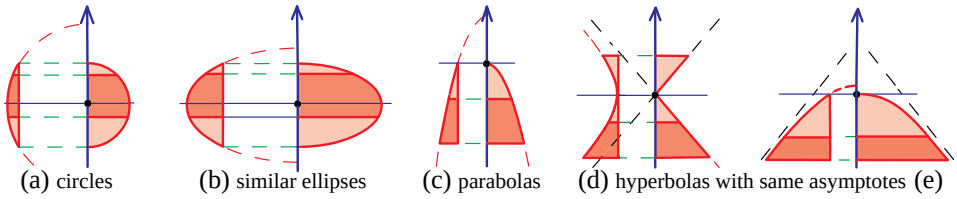

Figure 46. Area equilibrium of axial sections of bracelets with respect to the axis of rotation.

with respect to a balancing axis if, and only if, the solids of revolution generated by rotating them about the balancing axis have equal volumes. Applying this to the solids in Figure 1, we find that the semicircular disk in Figure 46a is in area balance with the circular segment on the left of the axis. The same holds true for the semielliptical disk in Figure 46b, the semiparabolic segment in Figure 46c, and the hyperbolic segments in Figures 46d and e. Because any slice of a family of bracelets has the equal height-equal volume property, each area equilibrium in Figure 46 holds slice-by-slice and, in the limiting case, chord-by-chord.

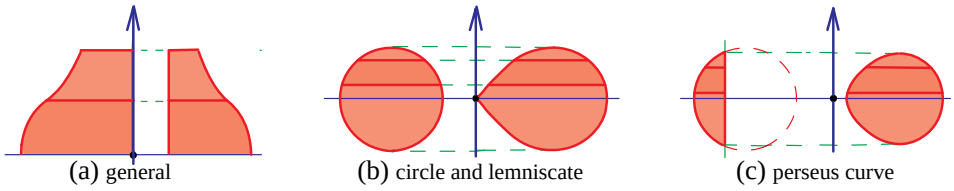

Figure 47. Area equilibrium of axial sections of more general sweeps and clusters.

Figure 47a shows the same principle applied to vertical cross sections of a more general tangentially swept solid and its solid cluster. Figures 47b and c are special cases obtained by vertical cross sections in Figure 13. We were pleasantly surprised to learn that the circular disk and lemniscate in Figure 47b are in chord-by-chord equilibrium. Tangential sweeping reveals unexpected area balancing relations without knowing the areas themselves, their centroids, or cartesian equations representing the boundary curves.

Congruent sections. Figure 48 reveals a new fact concerning vertical sections of a solid sweep around a circular cylinder of radius a and its solid cluster, for a general sweeping region S.

Each vertical section of the solid cluster at distance d from its rotation axis is geometrically congruent to the vertical section of the solid sweep at distance D from its rotation axis, where $D = (d^2 + a^2)^{1/2}$.

To prove this it suffices to show that their corresponding chords PQ and $P'Q'$ in a typical two-dimensional horizontal section of the two vertical sections are congruent.

Figure 48 shows a typical horizontal section of (a) a solid sweep, and (b) it solid cluster. In (a) the inner circle is the profile of the tangency cylinder, and AT is the

horizontal section of the tangent plane to the cylinder. Point A is the outer edge of the tangent segment of the sweeping region S. Its inner edge B, where the vertical

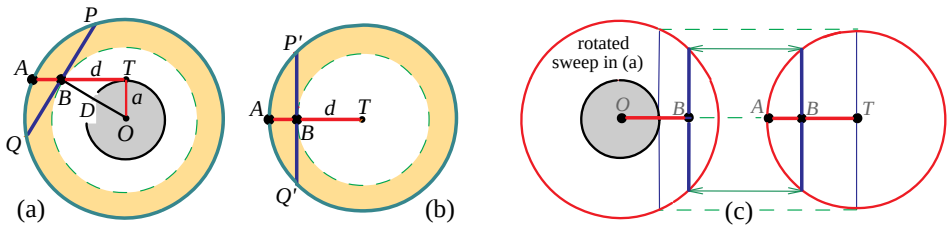

Figure 48. Chord PQ in (a) and $P'Q'$ in (b) are congruent because they sweep out annuli of equal area. (c) Matching congruent vertical sections of the sweep and cluster.

section intersects AT, and can be anywhere on AT. In (b), the circle through A has as radius the translated segment AT, with the position of B at distance d from T. In (a) and (b), the points B of all horizontal sections lie on a vertical line, which is an axis of symmetry of the corresponding vertical section. The outer edge A and corresponding inner edge can vary from layer to layer.

To prove congruency of chords PQ and $P'Q'$, we note that the annulus swept by AT in (a) has the area of the circle of radius AT in (b). Also, the annulus swept by BT in (a) has the area of the circle of radius BT in (b). Hence their area differences (those of the lighter shaded annuli) are also equal. Therefore the tangent segments BP in (a) and BP' in (b) are congruent (otherwise the areas they sweep would not be equal). Because B is the midpoint of PQ in Figure 48a, and of $P'Q'$ in Figure 48b, chords PQ and $P'Q'$ are congruent. Figure 48c shows how to match directly any two congruent vertical sections of the sweep and cluster.

Example: Bernoulli lemniscate. A Bernoulli lemniscate (see Section 3) is the boundary of a vertical cross section internally tangent to a solid torus generated by a circular disk S of radius r rotated around an axis at distance $2r$ from the center of S. Using the axis as the edge of a half-plane as in Figure 10a, rotate the same disk S tangentially around any circular cylinder to produce a solid tangent sweep whose solid cluster is the solid torus. When the solid sweep is cut by a vertical plane internally tangent to the sweep, its cross section is a region congruent to that bounded by the Bernoulli lemniscate. Because the radius of the tangency cylinder is arbitrary, this process produces infinitely many congruent Bernoulli lemniscates, all generated by the same disk S.

10. CONCLUDING REMARKS

We began this paper with the classical calculus result that all bracelets obtained by drilling cylindrical holes of given height through solid spheres of different radii have equal volume. We derived this result without calculus, and then showed that the same bracelets can be produced differently by a method of tangential sweeping of plane regions around general cylinders. Tangential sweeping, in turn, leads to infinitely many new families of solids that share the equal height-equal volume

property and also gives a new way of calculating volumes of many solids of revolution, some familiar and some unfamiliar, without the use of calculus. A knowledge of the volume of a solid of revolution, in turn, also gives the centroidal distance from the axis of the planar sweeping region if its area is known, which is the case in most of our examples. Some results of this paper also appear in [7].

Another view of swept solids and their clusters. Figure 49 shows another way to see visually why a solid tangent sweep has the same volume as its solid cluster. In Figure 49a we take a solid of revolution and slice it into wedges by vertical planes passing through its axis. The vertical faces are shown there as rectangles, but they could have a more general shape like that in Figure 10a, as suggested by the shading. Now slide the wedges radially away from the axis in such a way that common faces continually touch each other. The new configuration is a prismatic

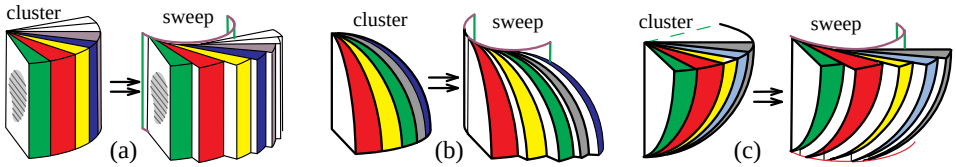

Figure 49. (a) Solid of revolution sliced into wedges that are spread tangentially around a cylinder. Sliced upper hemisphere in (b), lower hemisphere in (c).

solid of the same volume, surrounding a prismatic cavity. As the number of wedges increases indefinitely, the cavity becomes more like a cylinder along which the prismatic solid is swept tangentially. The original solid of revolution is its tangent cluster. Figure 49 also reveals that *the volume centroids of any solid tangent sweep and its cluster lie in the same horizontal plane.*

Extensions to n-space. Many results in this paper can be readily extended to higher dimensions. For example, to extend the results for the family of spherical bracelets in Figure 1, we puncture an n-sphere by a coaxial n-cylinder to produce an n-dimensional bracelet. As in Figure 1, those bracelets of equal height also have equal volume, that of the n-sphere with diameter equal to the height of the cylindrical hole. We can also regard the general n-dimensional tangent sweep as being swept tangentially by an $(n-1)$-dimensional hemisphere as in Figure 3.

References

[1] T. M. Apostol, A visual approach to calculus problems. *Engineering and Science*, vol. LXIII, no. 3, (2000) 22–31; `www.its.caltech.edu/~mamikon/VisualCalc.html`.

[2] T. M. Apostol and M. A. Mnatsakanian, *New Horizons in Geometry*. Dolciani Mathematical Expositions No. 47, Mathematical Association of America, 2012.

[3] T. M. Apostol and M. A. Mnatsakanian, Subtangents–an aid to visual calculus, *Amer. Math. Monthly*, 109 (2002) 525–533.

[4] T. M. Apostol and M. A. Mnatsakanian, Tangents and subtangents used to calculate areas, *Amer. Math. Monthly*, 109 (2002) 900–908.
[5] T. M. Apostol and M. A. Mnatsakanian, The method of sweeping tangents, *Mathematical Gazette*, 92 (2008) 396–417.
[6] T. L. Heath, *The Works of Archimedes*, Dover, New York, 1953.
[7] M. A. Mnatsakanian, On the area of a region on a developable surface, *Dokladi Armenian Acad. Sci.*, 73 (2) (1981) 97–101. (Russian);
www.its.caltech.edu/~mamikon/Article.html;
English translation: http://mamikon.com/Article81.pdf.

Tom M. Apostol: California Institute of Technology, 253-37 Caltech, Pasadena, California 91125 USA
E-mail address: apostol@caltech.edu

Mamikon A. Mnatsakanian: California Institute of Technology, 253-37 Caltech, Pasadena, California 91125 USA
E-mail address: mamikon@caltech.edu

Forum Geometricorum
Volume 15 (2015) 45–72.

FORUM GEOM
ISSN 1534-1178

Volumes of Solids Swept Tangentially Around General Surfaces

Tom M. Apostol and Mamikon A. Mnatsakanian

Abstract. In Part I ([2]) the authors introduced solid tangent sweeps and solid tangent clusters produced by sweeping a planar region S tangentially around cylinders. This paper extends [2] by sweeping S not only along cylinders but also around more general surfaces, cones for example. Interesting families of tangentially swept solids of equal height and equal volume are constructed by varying the cylinder or the planar shape S. For most families in this paper the solid tangent cluster is a classical solid whose volume is equal to that of each member of the family. We treat many examples including familiar quadric solids such as ellipsoids, paraboloids, and hyperboloids, as well as examples obtained by puncturing one type of quadric solid by another, all of whose volumes are obtained with the extended method of sweeping tangents. Surprising properties of their centroids are also derived.

1. Tangential sweeping around a general cylinder

Figure 1 recalls the concepts of solid tangent sweep and solid tangent cluster introduced in [2]. Start with a plane region S between two graphs in the same

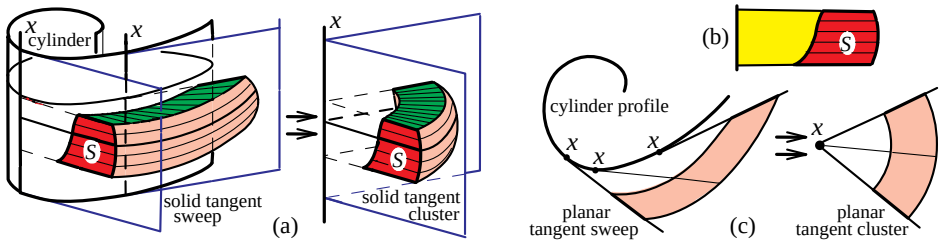

Figure 1. (a) Volume of a solid tangent sweep is equal to that of its solid tangent cluster. (b) Region S lies between two ordinate sets. (c) Top view of a horizontal cross section.

half-plane. To be specific, assume S consists of all points (x, y) satisfying the inequalities

$$f(x) \le y \le g(x), \quad a \le x \le b$$

where f and g are nonnegative functions related by the inequality $0 \le f(x) \le g(x)$ for all x in an interval $[a, b]$. In Figure 1a, the x axis is oriented vertically, and S is in the upper half-plane having the x axis as one edge. If we rotate S around the x axis we obtain a solid of revolution swept by region S, as indicated in the right portion of Figure 1a. More generally, place the x axis along the generator of a general cylinder (not necessarily circular or closed) and, keeping the upper

Publication Date: January 27, 2015. Communicating Editor: Paul Yiu.

half-plane tangent to the cylinder, move it along the cylinder. Then S generates a tangentially swept solid we call a *solid tangent sweep*. The corresponding *solid tangent cluster* is that obtained by rotating S around the x axis.

When the smaller function f defining S is identically zero, the swept solid is called a *bracelet*. Examples are shown in Figures 2 and 3. Clearly, by Figure 1b, any swept solid can be produced by removing one bracelet from another. In [2] we proved:

Theorem 1. *The volume of the solid tangent sweep does not depend on the profile of the cylinder, so it is equal to the volume of the solid tangent cluster, a portion of a solid of revolution.*

The proof used the fact that the shaded band and annulus in Figure 1c have equal areas, together with the slicing principle: *Two solids have equal volumes if their horizontal cross sections taken at any height have equal areas*.

Families of solid tangent sweeps with the same solid tangent cluster. For a given region S we can allow the cylinder to vary and thus obtain a *family* of solid tangent sweeps, all with the same solid tangent cluster. Thus, from Theorem 1 we obtain the following corollary:

Corollary 1. *Each member of the family has the same volume as their common solid tangent cluster.*

Moreover, from such a family one can obtain infinitely many new families with the same property by slicing the solids of the given family by two horizontal planes at given distance apart. Not only are the volumes of the slices equal because of the slicing principle, but we also have the following corollary:

Corollary 2. *For any such family of slices, the altitudes of the volume centroids above a fixed horizontal base plane are also equal.*

This property of centroids is another consequence of the slicing principle (see [3; p.150]). In Section 6 we use Corollary 2 to locate centroids of many solids.

2. CONIC SECTIONS SWEEPING AROUND CIRCULAR CYLINDERS

In Figure 2a, S is a semielliptical disk, and the swept solid is an ellipsoidal bracelet whose volume is that of its solid cluster, an ellipsoid of revolution. In

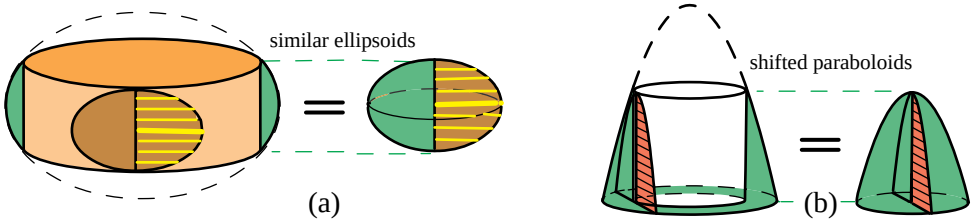

Figure 2. (a) All ellipsoidal bracelets have the same volume as the ellipsoid. (b) All paraboloidal bracelets have the same volume as the paraboloid of revolution.

Figure 2b, S is half a parabolic segment, and the solid sweep is a paraboloidal bracelet whose volume is that of its solid cluster, part of a paraboloid of revolution.

If Figure 3a, S is a double right triangle sweeping around a circular cylinder. The swept solid is a hyperboloidal bracelet of one sheet whose volume is that of its solid cluster, a portion of a solid cone. In Figure 3b, S is a portion of a hyperbolic segment sweeping around a circular cylinder. The solid sweep is a hyperboloidal bracelet of two sheets (only one of which is shown), whose volume is that of its solid cluster, a portion of a hyperboloid of revolution.

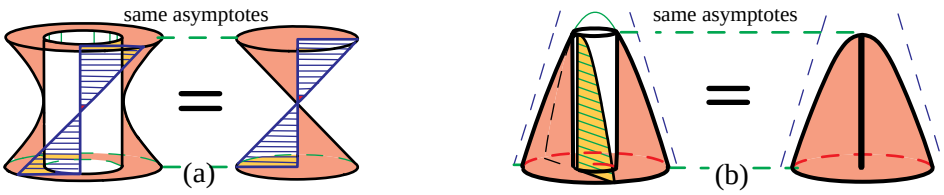

Figure 3. (a) Double triangle sweeps a hyperboloidal bracelet with the same volume as its solid cluster, a portion of a solid cone with the same volume. (b) Hyperbolic segment sweeps a hyperboloidal bracelet. The solid cluster is part of a hyperboloid of revolution of the same volume.

These results are summarized in Figure 4, where E and P denote the ellipsoid and paraboloid in Figure 2, H_1 is a hyperboloid of one sheet in Figure 3a (a degenerate case shown), and H_2 is a hyperboloid of two sheets in Figure 3b. Vertical sections of a circular cylinder, C, are also included, regarded as swept by a degenerate conic.

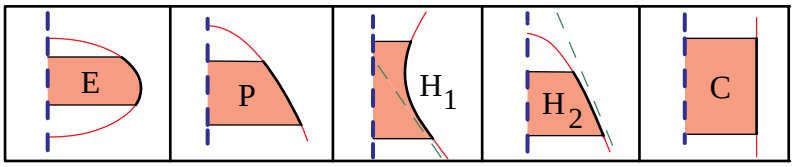

Figure 4. Special sweeping regions S bounded by conics.

Because the tangent sweeps in the foregoing examples are taken around a circular cylinder, the same solids can be obtained by using this cylinder to drill a hole through the axis of a solid bounded by a quadric surface. The volume of each drilled solid depends only on the height of the cylindrical hole and not on its radius. When the radius is zero, the drilled solid is the solid cluster, a quadric surface of revolution. A classical case is when the solid being drilled is a sphere, a result usually treated by integral calculus. All spherical bracelets of a given height have equal volume.

Solids sweeps and clusters whose outer lateral boundary is a quadric surface. When a conic is rotated around one of its axes of symmetry, the solid of revolution has a lateral surface that is a portion of a quadric surface. Rotation around a different

axis will not produce a quadric surface. For example, rotating a circle around a line not through its center produces a torus, which is a *quartic* surface. When a conic is swept tangentially around a circular cylinder, with the symmetry axis of the conic lying on a generator of the cylinder, the solid tangent sweep and its solid cluster have outer lateral surfaces that are similar quadric surfaces.

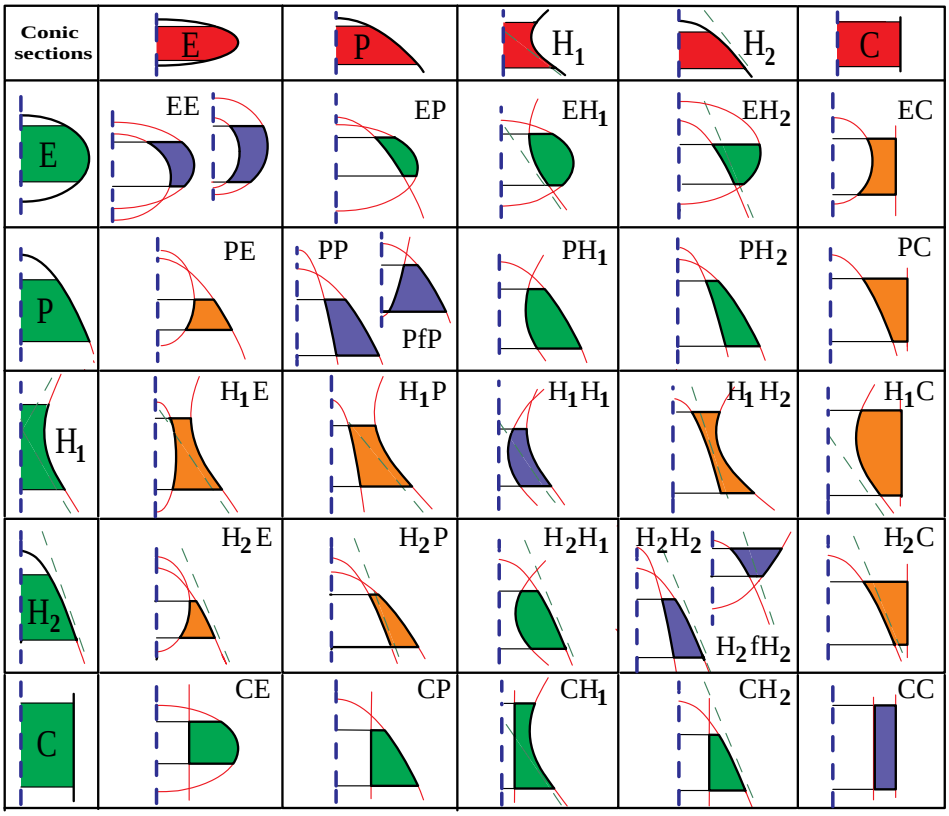

Figure 5. Table summarizing sweeping regions S bounded by two conics.

Solids swept by combinations of conics. Now we consider solids swept by regions S in Figure 1 where both functions f and g that define S have portions of conic sections as their graphs. The table in Figure 5 shows various possible combinations. The examples in Figure 4 are used as the top row and leftmost column of the table, with E meaning ellipse, P meaning parabola, H_1 a hyperbola whose rotation about its axis produces a hyperboloid of one sheet, H_2 a hyperbola whose rotation about its axis produces a hyperboloid of two sheets, and C meaning circular cylinder. Conics in the top row form the outer boundary of S and those in the left column form the inner boundary. The dashed vertical line in each entry of the table is a common axis of symmetry of the two conics.

The first diagonal entry in the table shows two possible cases when both boundaries are ellipses, one when the ellipses intersect, and another when they do not

intersect. The second diagonal entry shows two possible cases when both boundaries are parabolas, one when they open in the same direction, the other when they open in opposite direction, with fP indicating 'flipped' parabola. Similarly, the next-to-last diagonal entry shows two possible cases of two hyperbolas of type H_2 opening in the same or opposite direction, with fH_2 indicating 'flipped' hyperbola.

When a region S from the table is rotated about the common fixed vertical axis of symmetry it generates a solid of revolution, a solid cluster, whose inner and outer surfaces are quadric surfaces. When the axis of symmetry is allowed to move tangentially around a *circular* cylinder, S generates a solid tangent sweep having the solid of revolution as its solid tangent cluster. Because the cylinder is circular, the inner and outer surfaces of each tangent sweep are quadric surfaces, similar to the corresponding surfaces of the cluster. The sweep and cluster have equal volumes, and cross sections produced by any horizontal plane have equal areas. *As the radius of the cylinder changes, a family of solid tangent sweeps is produced, each with the same volume as the solid tangent cluster.*

Dual solids. Figure 6a shows a family of spherical bracelets of a given height. They are of type CE in Figure 5, where ellipse E is a circle. Figure 6b shows a family of circular cylinders of given height from which inscribed spherical portions have been removed. They are of type EC in Figure 5, where again E is a circle. When swept solids of type CE and EC have the same height, we call them *dual* solids. The solid cluster in Figure 6a is a sphere, and its dual in Figure 6b is a cylinder with a spherical hole. Archimedes showed that the volume of a sphere is 2/3 that

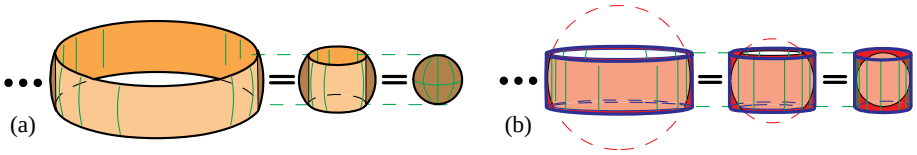

Figure 6. (a) Family of spherical bracelets of given height. (b) Family of solids dual to those in (a).

of its smallest circumscribing cylinder (a result inscribed on his tombstone), so the volume of the solid cluster in Figure 6b is exactly half that of the solid cluster in Figure 6a. The same ratio holds for any two dual members of these families. The term *dual* is used more generally to refer to two solids of the same height swept by regions S in Figure 5 that are symmetrically located with respect to the main

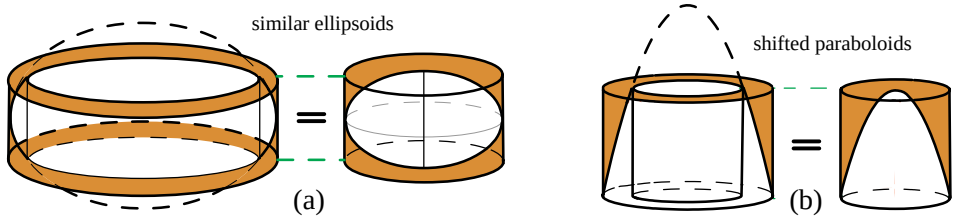

Figure 7. Family dual (a) to ellipsoidal bracelets and (b) to paraboloidal bracelets.

diagonal. In dual solids the types of outer and inner surfaces are interchanged. Figure 7a shows two members of a family of ellipsoidal bracelets dual to those in Figure 2a, and Figure 7b displays two members of a family dual to the paraboloidal bracelets in Figure 2b.

Figures 8a and 8b show two members of families of hyperboloidal bracelets dual to those in Figure 3a and 3b, respectively. In a given family of dual bracelets the volume of each punctured cylinder depends only on the height of the cylinder and not on its radius.

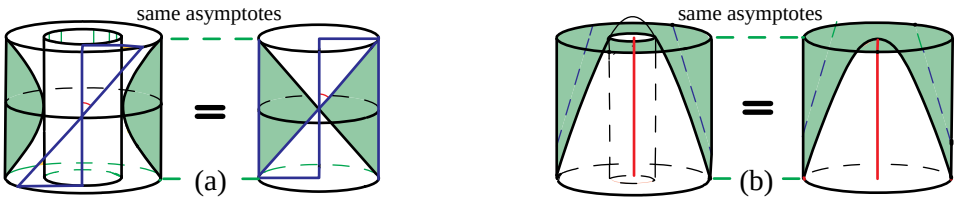

Figure 8. Family dual to hyperboloidal bracelets in Figure 3. (a) Bracelets of one sheet. (b) Bracelets of two sheets.

In all the foregoing examples, the volume of a swept solid plus that of its dual solid is equal to the volume of the circumscribing cylinder.

Solids swept by combinations of regions bounded by conics. Theorem 1 can be extended to include any solid swept by a suitable combination of regions S of the type shown in Figure 1. Figure 9 indicates several examples obtained by combining re-

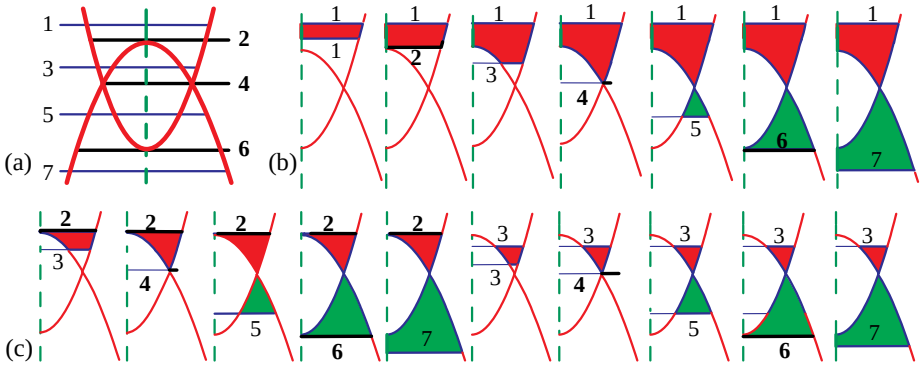

Figure 9. (a) Sweeping regions S bounded by two parabolas. (b) Strips with line 1 as upper boundary. (c) Strips with lines 2 and 3 as upper boundaries.

gions of type PfP in Figure 5, a parabola and an intersecting flipped parabola. There are seven numbered horizontal lines in Figure 9a. The even numbered lines, shown darker, are fixed. Line 2 passes through the vertex of one parabola, line 4 passes through the intersection points of the two parabolas, and line 6 passes through the vertex of the flipped parabola. They divide the plane into four horizontal strips, and the odd numbered lines lie somewhere inside these strips as indicated. As the

odd numbered lines vary in position they generate different types of plane regions between the two parabolas that can be swept around the common axis of symmetry. Samples are shown in Figures 9b and 9c. Images symmetric with respect to line 4 are not shown.

3. TANGENTIAL SWEEPING BY VARIABLE PLANE REGIONS ALONG SPECIAL CYLINDERS

In Figure 1, solid sweeps and their clusters were generated by sweeping a fixed plane region S tangentially along a general cylinder. This section treats special cylinders and includes cases in which S is allowed to vary. Further examples of variable sweeping regions are given in Section 8.

Tractrix as profile of the cylinder. Figure 10 shows a *tractrix cylinder*, whose profile is a tractrix, with various regions swept tangentially along the same tractrix cylinder. In Figure 10a a rectangle of fixed size is swept tangentially along a tractrix cylinder; the corresponding solid tangent cluster is part of a circular cylinder. In Figure 10b a semielliptical disk inscribed in the rectangle of Figure 10a is swept along the same tractrix cylinder; the corresponding solid tangent cluster is part of an ellipsoid of revolution. (The ellipsoid in Figure 10b is almost spherical.) Both solid tangent clusters are familiar solids whose volumes are well known or are easily calculated. The corresponding tangentially swept solids are not well known, and integral calculus does not easily yield their volumes. But Theorem 1 does the job with little effort! The volume of each solid sweep is simply equal to that of its solid tangent cluster, which is easily calculated.

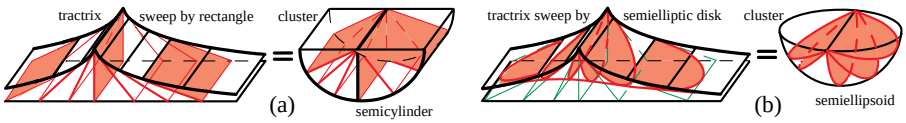

Figure 10. Tangentially swept solids generated by (a) a rectangle, and (b) a semielliptical disk moving tangentially along a tractrix cylinder.

Exponential as profile of the cylinder. Figure 11 shows two solids swept tangentially along an *exponential cylinder*, whose profile is an exponential curve. The solid in Figure 11a is swept by a rectangle whose base is of fixed length and whose altitude

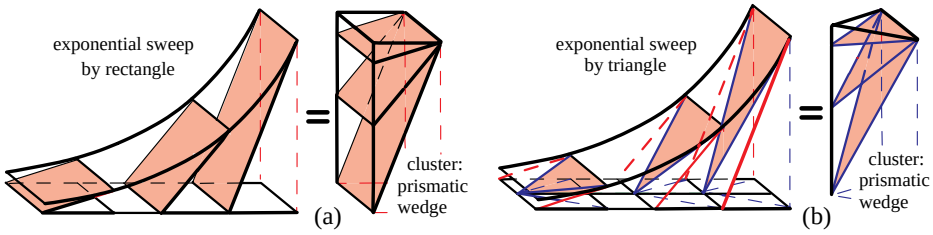

Figure 11. Solids swept tangentially along an exponential cylinder by (a) variable rectangle, and (b) variable isosceles triangle.

is the length of the tangent segment from the exponential curve to its asymptote. Because the subtangents of an exponential have constant length, the solid tangent cluster is a portion of half a rectangular prism. The solid in Figure 11b is swept by an isosceles triangle inscribed in the tangential rectangle of Figure 11a. Its solid tangent cluster is a portion of a triangular prism.

The solid in Figure 12a is swept by a semielliptical disk inscribed in the rectangle of Figure 11a. Its solid cluster is part of a cylindrical wedge with a semielliptical base. In Figure 12b the semielliptical disk of Figure 12a is flipped over. The corresponding solid cluster is the complementary part of the cylindrical wedge in Figure 12a.

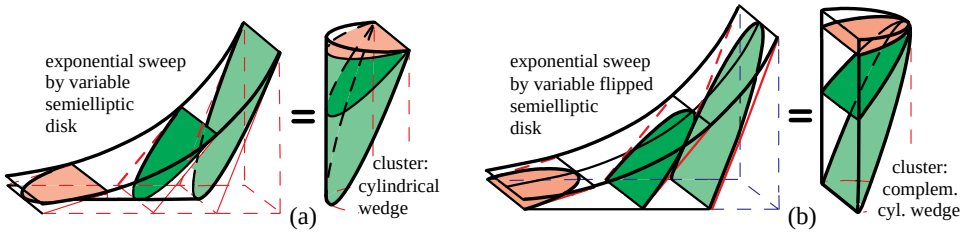

Figure 12. Solids swept tangentially along an exponential cylinder by (a) variable semielliptical disk, and (b) flipped variable semielliptical disk.

Cycloid as profile of the cylinder. In Figure 13a, a solid is swept by a variable rectangle moving tangentially along a *cycloidal cylinder*, whose profile is a cycloid. Figure 13b shows the solid swept by an isosceles triangle inscribed in the rectangle of Figure 13a.

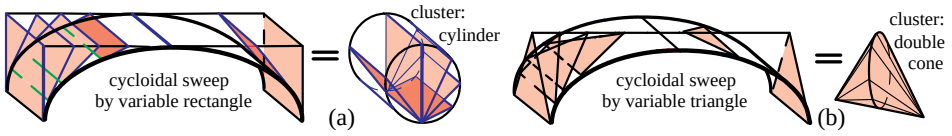

Figure 13. Solids swept tangentially along a cycloidal cylinder by (a) variable rectangle, and (b) variable isosceles triangle.

The solid in Figure 14a is swept by a variable elliptical disk inscribed in the rectangle of Figure 13a, and that in Figure 14b is swept by a semielliptical disk inscribed in the same rectangle.

The foregoing examples show that many infinite families of tangentially swept solids can be generated by plane regions moving along various cylinders. We have discussed a few special cases for which the volume of the solid tangent cluster is known or, as we shall see presently, can be easily determined without using integral calculus.

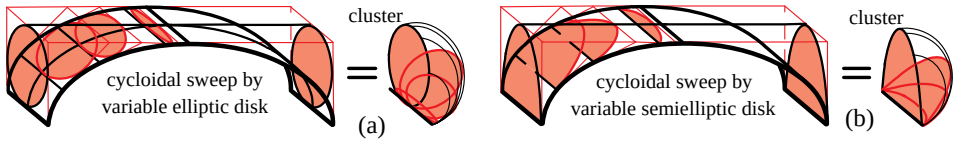

Figure 14. Solids swept tangentially along a cycloidal cylinder by a full elliptical disk in (a) and a semielliptical disk in (b).

Calculating the volumes of solid clusters. Each solid cluster is a portion of a solid of revolution. In the examples treated above we can calculate the volume of the solid cluster directly or by invoking a new comparison lemma that extends Pappus' rule on volumes of solids of revolution.

Take a plane region that may change its shape as it rotates about an axis. Let $A(\theta)$ denote the area of the region and let $c(\theta)$ denote the distance of its area centroid from the axis when the region has rotated through an angle θ from some initial position. By Pappus' rule, the volume ΔV of the solid of revolution generated by rotating through a small angle $\Delta\theta$ is given by

$$\Delta V = A(\theta)c(\theta)\Delta\theta.$$

This implies the following comparison lemma for volumes generated by two plane regions of areas $A_1(\theta)$ and $A_2(\theta)$ that change their shapes in a special way as they rotate about the same axis:

Comparison Lemma. *If at any stage of the rotation the ratio of their areas $A_1(\theta)/A_2(\theta)$ is a constant α, and the ratio of their centroidal distances $c_1(\theta)/c_2(\theta)$ is a constant γ, then the corresponding ratio of their volumes $V_1(\theta)/V_2(\theta)$, when swept through the same angle, is the constant $\alpha\gamma$, just as if the regions did not change their shapes. This ratio does not depend on the shape of the tangential cylinder.*

The comparison lemma allows us to calculate the volumes of the solid clusters treated in Figures 10 through 14.

In Figure 10b the solid cluster is a portion of an ellipsoid of revolution inscribed in the circular cylinder in Figure 10a, both rotated through the same angle. In this case we easily find that $\alpha = \pi/4$ and $\gamma = 8/(3\pi)$ giving $\alpha\gamma = 2/3$ for the ratio of their volumes, ellipsoid to cylinder. This is the famous 2/3 ratio for the volumes of a sphere and cylinder found on Archimedes' tombstone.

In Figure 11b the solid cluster is a portion of half a triangular prism inscribed in half the rectangular prism in Figure 11a. The two solid clusters are also solids of revolution for which the comparison lemma can be applied. In this case we find that $\alpha = 1/2$ and $\gamma = 2/3$, so the ratio of their volumes is $\alpha\gamma = 1/3$.

Similarly, we determine the volume of the solid cluster in Figure 12b by comparing it with that in Figure 11a. In this case we have $\alpha = \pi/4$ and $\gamma = 2(1 - \frac{4}{3\pi})$, giving $\alpha\gamma = \frac{\pi}{2} - \frac{2}{3}$. Figures 13 and 14 show four different solids swept along a cycloidal cylinder. The solid cluster in Figure 13a is a portion of a circular cylinder, so its volume is easily calculated. The other three solid clusters are not well

known solids, but we can determine their volumes in terms of that of the cylindrical cluster in Figure 13a by applying the comparison lemma. Comparing the solid cluster in Figure 14a with that in Figure 13a we find $\alpha = \pi/4$ and $\gamma = 1$ giving us $\alpha\gamma = \pi/4$.

4. TANGENTIAL SWEEPING AROUND A CONE

Instead of generating solids tangentially swept around a cylinder, we replace the

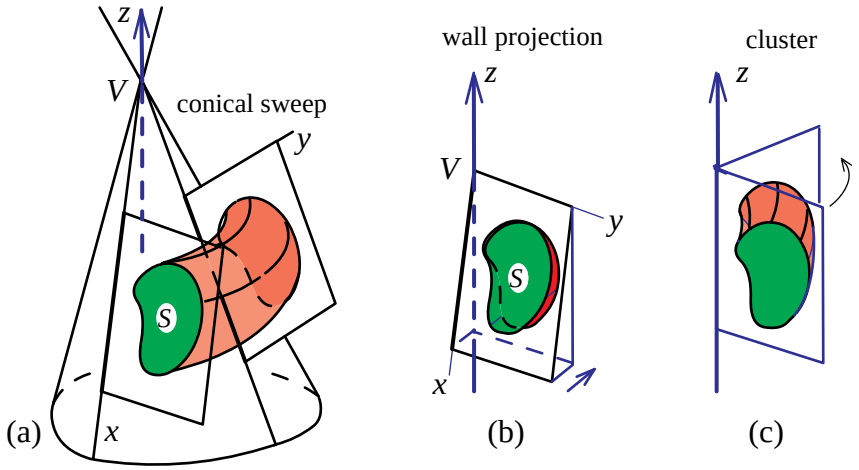

Figure 15. (a) Tangential sweeping by S around a cone. (b) Region S and its wall projection on the yz plane. (c) Rotation of wall projection in (b) around the z axis produces the cluster.

cylinder with a cone, as illustrated in Figure 15a. The cone can be quite general, not necessarily circular, but for the sake of simplicity we consider a right circular cone with vertex angle 2α, where $\alpha < \pi/2$.

Take a region S in the upper half of the xy plane tangent to the cone, with the x axis matching a generator of the cone. As this plane moves tangentially around the cone, region S sweeps out a toroid-like solid that we call a *conical sweep*. We are interested in determining the volume of the conical sweep.

Each cross section of the sweep cut by a plane perpendicular to the axis of the cone, which we call the z axis, is part of a planar ring whose area does not depend on the position of S, which can be near to or far away from the cone's vertex V. Consequently the volume of the conical sweep does not depend on the position of S. For convenience we take the origin of the xy plane to be the vertex V. Figure 15b shows a projection of S on the yz plane, called the *wall projection*, which makes an angle α with the x axis (half the vertex angle of the cone). The area of the wall projection of S is $\cos\alpha$ times the area of S. Figure 15c shows the solid of revolution obtained by rotating the wall projection around the z axis. We call this solid *the cluster of the conical sweep*. A plane perpendicular to the z axis cuts both the conical sweep and its cluster in regions of equal area so, by the slicing principle, their volumes are equal. This gives the following theorem, with the notation just introduced.

Theorem 3. (a) *The volume of a conical sweep of S does not depend on the distance of S from the vertex of the cone.*

(b) *The volume of a conical sweep is equal to the volume of its cluster.*

(c) *This common volume is equal to* cos α *times the volume of the solid of revolution obtained by rotating region S around a fixed axis.*

Ellipsoid of revolution. Our first application of Theorem 2 is to an ellipsoid of revolution shown in Figure 16b. When a semielliptical disk is swept tangentially

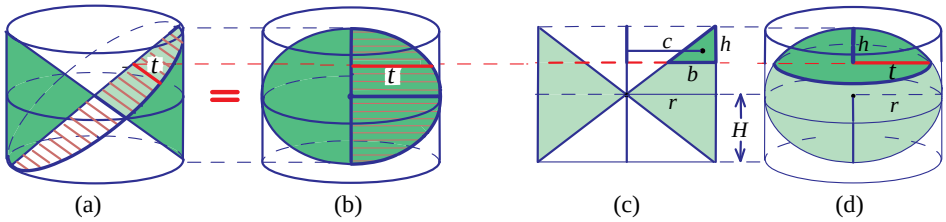

Figure 16. Finding the volume of an ellipsoid in (a) and (b), and of an ellipsoidal segment of altitude $h < H$ in (c) and (d).

around a circular cone as in Figure 16a it generates a punctured cylinder, a solid sweep lying between the cone and its circumscribing cylinder. The volume of this solid sweep is known to be 2/3 that of the cylinder. By Theorem 2 the volume of its cluster, the ellipsoid of revolution in Figure 16b, is also 2/3 that of its circumscribing cylinder. When the ellipsoid is a sphere this is Archimedes' tombstone result.

We shall determine, more generally, the volume $V(h)$ of the ellipsoidal segment of altitude h in Figure 16d in an alternative way by rotating the shaded triangle in Figure 16c about the vertical axis and applying Pappus's theorem. The shaded triangle of altitude h in Figure 16c sweeps out the upper portion of the punctured cylinder, which is the same as a portion of the solid sweep swept tangentially by the corresponding portion of the semielliptical disk in Figure 16a. The tangent cluster of this portion is the ellipsoidal segment of volume $V(h)$ in Figure 16d.

By Pappus, volume $V(h)$ is the product of the area of the triangle and the distance its centroid moves in one revolution. The area of the triangle is $bh/2$ and the area centroid of the triangle is at distance $c = r - b/3$ from the axis of rotation, hence

$$V(h) = 2\pi(r - \frac{b}{3})\frac{bh}{2} = \frac{\pi}{3}(3r - b)bh. \tag{1}$$

Archimedes [4; *On Conoids and Spheroids*, Proposition 27] showed that $V(h)$ bears a simple relation to the volume V_{cone} of the cone in Figure 17a with the same base and altitude (altitude h and base radius t, where t is the length of the chord in Figures 17a and 17b), namely

$$\frac{V(h)}{V_{\text{cone}}} = \frac{3H - h}{2H - h}, \tag{2}$$

where H is the length of the vertical semiaxis of the ellipsoid (half the height of the circumscribing cylinder) in Figure 16d, and $h < H$.

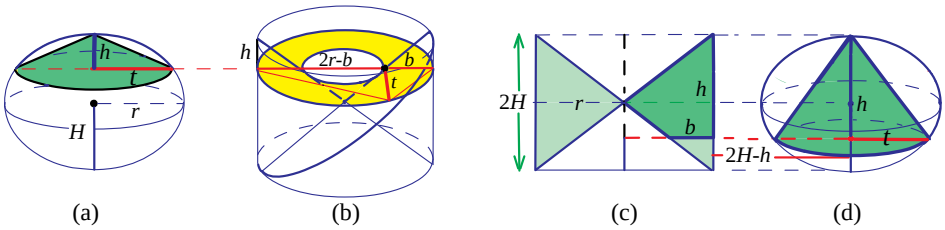

Figure 17. Proof of Archimedes's formula (2). In (d), $h \geq H$.

A simple proof of (2) can be given by observing that volume $V_{\text{cone}} = \pi t^2 h/3$. By similar triangles in Figure 17b, we find $b/t = t/(2r - b)$, so $t^2 = (2r - b)b$, hence

$$V_{\text{cone}} = \frac{\pi}{3} t^2 h = \frac{\pi}{3}(2r - b)bh. \tag{3}$$

Now divide (1) by (3) and use the similarity relation $r/b = H/h$ to obtain (2).

The same type of argument, using Figure 17d, proves (2) when $h \geq H$. (When h is replaced by $-h$, (2) becomes ratio (6) in [2] for a hyperboloidal segment.)

Paraboloid of revolution. Another result of Archimedes [4; *On Conoids and Spheroids*, Props. 21, 22], depicted in Figure 18b, states that *the volume of a paraboloidal solid of revolution is equal to half that of its circumscribing cylinder*. We shall deduce this by applying Theorem 2.

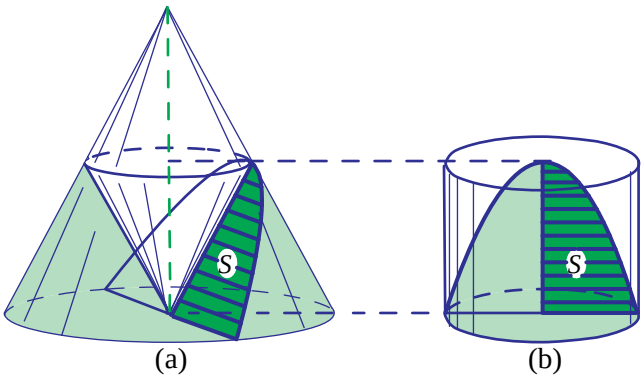

Figure 18. Tangential sweeping by half a parabolic sector around a cone produces a solid sweep in (a) whose cluster is a paraboloid of revolution in (b). The volume of the paraboloid is half that of its circumscribing cylinder.

Cut the large cone C in Figure 18a by a plane parallel to a generator through a point midway between the base and vertex of C. We take half the parabolic cross section as region S and and form a conical sweep by rotating S tangentially around the smaller cone c whose vertex is at the center of the base of the larger cone C. The corresponding conical cluster is the paraboloid of revolution in Figure 18b. By Theorem 2, its volume V is equal to that of the conical sweep in Figure 18a.

This solid sweep is inside the large cone C and outside the small cone c. Thus, $V = 6v(c)$, where $v(c)$ is the volume of the small cone c. But $v(c)$ is one-third the volume of the circumscribing cylinder through the base of c, so V is twice the volume of this cylinder which, in turn, is half that of the larger circumscribing cylinder in Figure 18b. This proves the result of Archimedes. The same result follows from (2) by keeping h fixed and allowing H to tend to ∞ so the ellipsoidal segment becomes paraboloidal.

General persoid of revolution. A torus is the surface of revolution generated by rotating a circle about an axis in its plane. The curve of intersection of a torus and a plane parallel to the axis of rotation is called a *curve of Perseus*, examples of which include the ovals of Cassini and leminscates of Booth and Bernoulli. Each such curve of Perseus has an axis of symmetry parallel to the axis of rotation. When the *persoidal region*, bounded by a curve of Perseus, is rotated about this axis of symmetry it generates a solid that we call a *persoid of revolution*.

In [2] we treated persoids of revolution obtained by rotating persoidal regions cut from a torus by planes parallel to the axis of the torus. Now we consider more general persoidal regions obtained by cutting planes that make an angle $\alpha < \pi/2$ with the toroidal axis. Examples are shown in Figures 19, 20, and 21.

In Figure 19a the axis of symmetry of the plane cross section S is designated as the x axis. In Figure 19b the x axis is oriented vertically and S is rotated about this fixed axis to generate a *general persoid of revolution*. By Theorem 2c, its

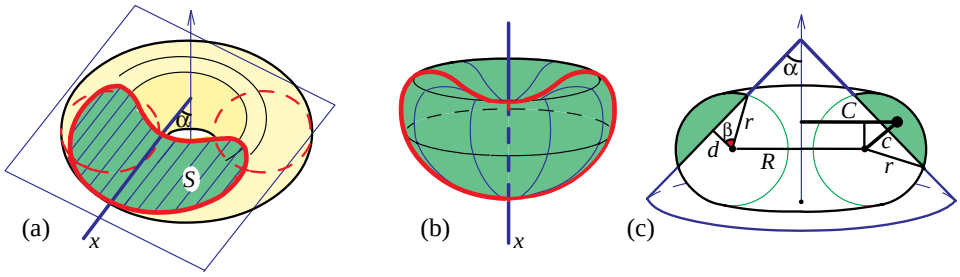

Figure 19. (a) Slanted toric section. (b) Its solid of revolution. (c) Diagram for calculating the volume by Pappus' theorem.

volume V is 1/cos α times the volume of the conical sweep obtained by tangential sweeping of S around a cone with vertex angle 2α. This cone is shown in Figure 19c together with a cross section of the torus through its axis. The tangential sweep is the portion of the solid torus outside the cone. This same solid is generated by rotating the circular segment in Figure 19c about the axis of the cone. By Pappus, the volume of this solid of revolution is $2\pi CA$, where A is the area of the circular segment, and C is the centroidal distance of the segment from the axis of rotation. Hence volume V of the solid of revolution in Figure 19b is given by

$$V = \frac{2\pi CA}{\cos\alpha}. \tag{4}$$

Now we show that

$$V = \frac{4}{3}\pi r^3 \sin^3\beta + \frac{\pi R r^2(2\beta - \sin 2\beta)}{\cos\alpha}, \tag{5}$$

where r is the radius of the circle that generates the torus as its center moves around a circle of radius R, α is half the vertex angle of the cone, and β is half the angle that subtends the circular segment of radius r. The first term in (5) is $\frac{4}{3}\pi(r\sin\beta)^3$, the volume of a spherical bracelet of altitude $r\sin\beta$.

Area A of the circular segment, expressed in terms of r and β, is

$$A = r^2(\beta - \sin\beta\cos\beta). \tag{6}$$

From Figure 19c we find $C = c\cos\alpha + R$, where c is the centroidal distance of the segment from the center of the circle of radius r. Hence $CA/\cos\alpha = cA + RA/\cos\alpha$. But $cA = \frac{4}{3}\pi(r\sin\beta)^3$ so (4) and (6) yield (5).

Figure 20a shows a vertical axial section of the torus and the end view of three parallel cutting planes that pass through the hole in the torus making an angle α with the vertical axis of the torus. They cut three curves of Perseus as indicated. We wish to find the volumes of each persoid of revolution about its own axis.

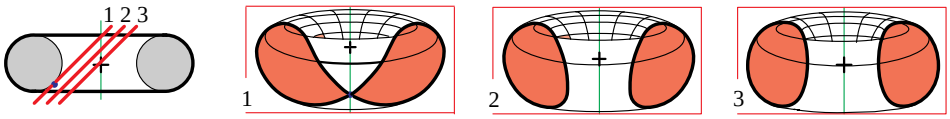

Figure 20. Slanted toric sections cut by parallel planes through the hole of the torus.

According to Theorem 2, this volume is equal to that of the conical sweep divided by $\cos\alpha$. In each of these example, the conical sweep is the entire solid torus, whose volume is $2\pi^2 r^2 R$, so the volume V of each persoid of revolution is

$$V = \frac{2\pi^2 r^2 R}{\cos\alpha}. \tag{7}$$

An interesting case occurs when the cutting plane is tangent internally to the inner part of the torus, as in Figure 21a. Here the curve of Perseus consists of two intersecting circles of radius R as seen from a direction perpendicular to the cutting plane. In Figure 21a, $r = R\cos\alpha$ so (7) gives $V = 2\pi^2 R^2 r$, which is the volume of a different torus generated by a circle of radius R rotated around a circle of radius r.

5. FAMILIES OF CONE-DRILLED SOLIDS OF EQUAL VOLUME

We turn next to examples of families of cone-drilled solids of equal volume obtained by sweeping simple shapes bounded by portions of conic sections (including degenerate conics) along a right circular cone. When the conic is attached to a generator of the cone along one of its axes of symmetry as in Figure 22, both the tangent sweep and the tangent cluster are solids bounded by quadric surfaces. Figure 22a shows a rectangular strip of given width attached tangentially to a right circular cone. Tangential sweeping produces a portion of a twisted cylinder outside

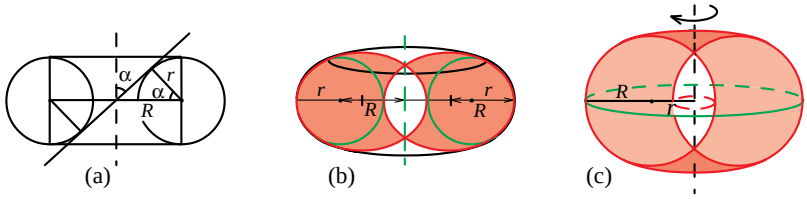

Figure 21. (a) Cross section showing cutting plane as a line doubly tangent internally to the inner part of the torus (side view). (b) Inclined view of the section in (a). (c) Normal view seen from a direction perpendicular to the cutting plane.

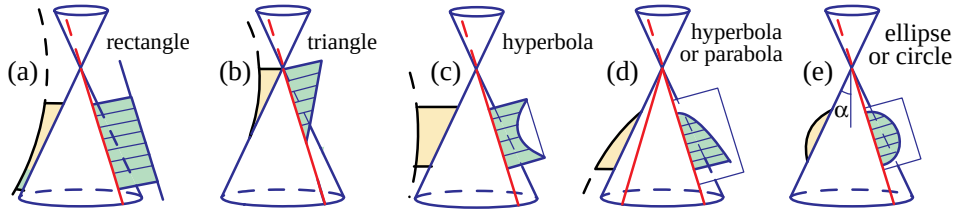

Figure 22. Regions bounded by conics sweeping tangentially around a cone.

the cone. A family (not shown) of equal height and equal volume is produced by shifting the rectangle up or down along the generator of the cone.

An interesting family is obtained by varying the vertex angle of the cone. By slicing all swept solids by parallel horizontal planes at distance H apart we get a family of slices of equal volume independent of the cone's vertex angle, as depicted in Figure 23. If the width of the strip is w, the volume of each slice in this family is equal to that of a circular cylinder of height H and radius w, or $\pi w^2 H$. In Figure

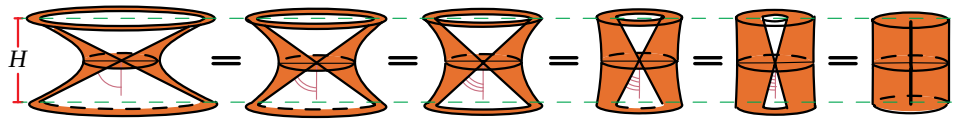

Figure 23. A family of cone-drilled hyperboloids of the same height and equal volume.

23 the swept solids are symmetric about the vertex of the central cone, but the same result holds if the tangential sweeping is done at any location relative to the vertex. The volume of each swept solid is equal to that of the circular cylinder.

One leg of a given right triangle can be attached tangent to a cone anywhere along a generator as in Figure 22b and rotated to sweep a portion of a twisted cylinder outside the cone. Varying the position of the right triangle produces a family of cone-drilled solids (not shown) having the same height and the same volume, that of the cone obtained by revolution of the vertical wall projection of the sweeping triangle.

We can attach a plane region bounded by a portion of a conic section as in Figures 22c, d and e, to produce more examples of interesting families of cone-drilled solids. A semielliptical disk will sweep a portion of an ellipsoid, or a paraboloid or hyperboloid of two sheets, depending on the proportions of the semiaxes of the ellipse.

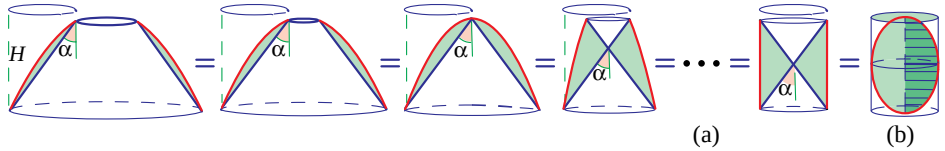

Figure 24. (a) Cone-drilled paraboloids of equal height and equal volume.
(b) Limiting case is a cylinder punctured by a cone.

If the ellipse is represented by a circle in its ceiling projection, then the solid is paraboloidal, drilled by a cone as in Figure 24. In this case all solids in this family have volumes equal to that of the ellipsoid obtained by revolution of the wall projection of the sweeping ellipse. If the lengths a and b of the semiaxes

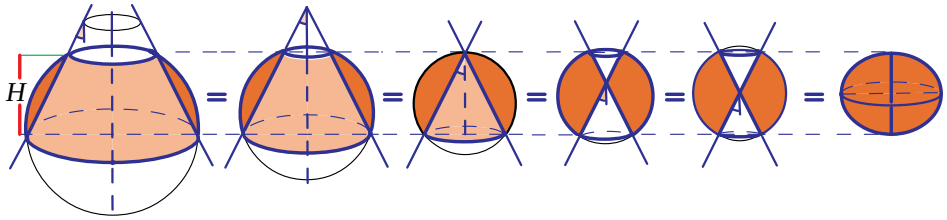

Figure 25. Cone-drilled spheres of equal height and equal volume.

of the ellipse satisfy $a/b < \sin\alpha$, where α is half the vertex angle of the cone, we obtain a family of cone-drilled similar ellipsoids of revolution. When $a = b$ the ellipse is a circle attached to a cone along its diameter as in Figure 22e and we obtain cone-drilled spheres of different sizes (Figure 25), all having the same height and the same volume. When a/b has a larger value we obtain a family of cone-drilled hyperboloids of two sheets, all having the same volume if their heights are equal.

The table in Figure 26 supplements that in Figure 5 by including a cone as a quadric surface. The first entry, labeled C, shows an axial vertical section of a cone punctured by a cylinder, and of a cylinder punctured by a cone. The second entry, labeled E, shows an axial vertical section of an ellipsoid punctured by a cone, and of a cone punctured by an ellipsoid. The remaining entries have analogous meanings, with P representing a paraboloid of revolution, H_1 a hyperboloid of one sheet, and H_2 one part of a hyperboloid of two sheets.

Combining families of drilled solids of equal height. Figure 27 shows a family of solids obtained by combining the families in Figure 24 and 25, where each member

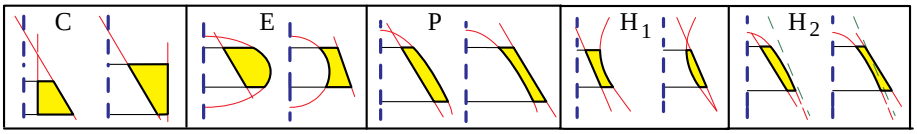

Figure 26. Axial vertical sections of quadric surfaces drilled by cones, and of cones punctured by quadric surfaces.

of the respective family is drilled by a congruent truncated cone of height H. The solids in this new family, shown with darker shading, also have the same volume, the difference of the volumes of those in Figure 24 and 25. That common volume, in turn, is that of a sphere.

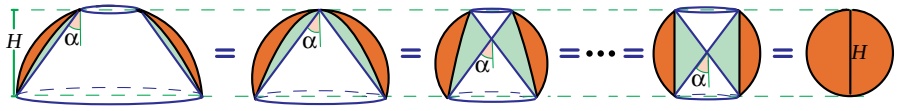

Figure 27. Paraboloidal-drilled spheres of height H and equal volume, that of a sphere of diameter H.

Similarly, Figure 28 shows a family of solids obtained by combining the families of the type in Figures 2 and 3 with the same height H. The limiting case in (c) is a portion of a sphere punctured by a cone, whose volume is that of the ellipsoid in (d).

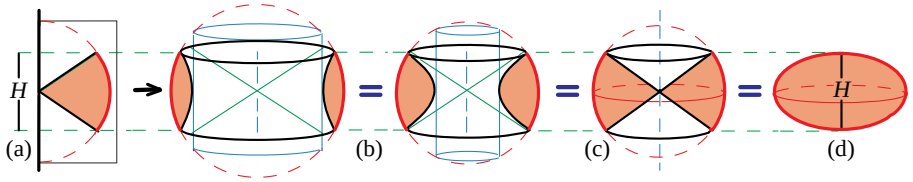

Figure 28. Spheres punctured by twisted cylinders of equal height produce solids of equal volume, that of an ellipsoid.

Special cases previously considered. Two special cases are treated by Polya [6; p. 202], where the volume of a conically and parabolically perforated sphere are obtained using integration. Polya's examples were extended by Alexanderson and Klosinski [1], who also used integration to calculate volumes of several solids obtained by rotating the region between two conic sections. They did not consider arbitrary horizontal slices as we did in Figure 5, but considered only special slices between common intersection points of the conics, so the entire boundary of each solid is made up of portions of quadric surfaces. Their examples are summarized in Figure 29, where now C represents a cone, a cylinder being a special case. Their list can be extended (without integration) as shown in Figure 30, where hyperboloids of two sheets H_2 are also considered. The notation H_2^2 indicates that both sheets are used. Similar examples were also treated in [5].

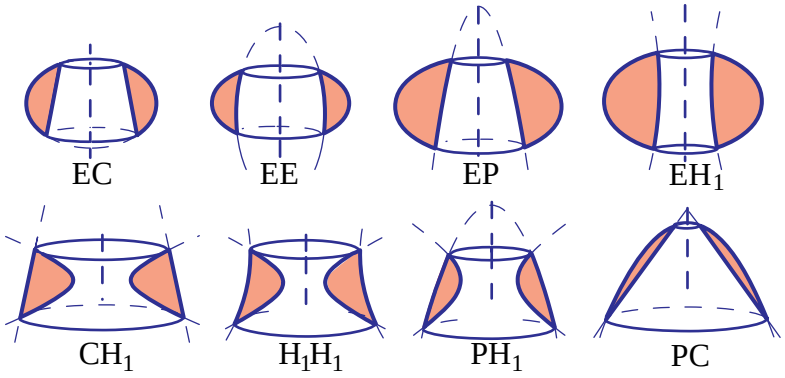

Figure 29. Solids generated by rotating regions between intersections of two conics.

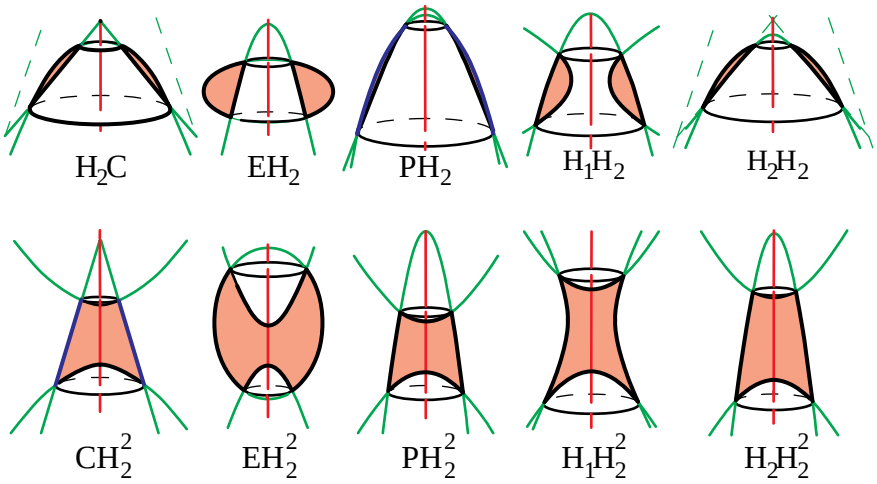

Figure 30. More solids like those in Figure 29 with hyperboloids of two sheets included.

In each entry of Figures 29 and 30 each conic can be scaled separately and shifted vertically so that the height of the hole in the punctured solid has a fixed value. Each entry yields a *family* of punctured solids having equal height and equal volume.

Alternative treatment. The equality of volumes for the families in Figures 27 or 28 can be obtained in an alternative manner, as illustrated in Figure 31 in a general setting. Take any plane region S between two graphs in the same half-plane as described in Section 2. Rotate this region tangentially along a cone (Figure 31a), or rotate its wall projection around a cylinder (Figure 31c). We generate a family of tangentially swept solids of equal volume by translating region S along the generator of the cone or by varying the radius of the cylinder. The common volume is that of the cluster in Figure 31b.

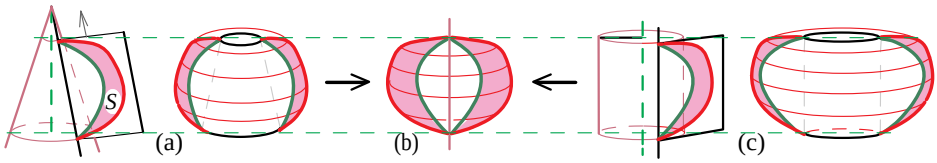

Figure 31. (a) Solid tangential sweep around a cone. (c) Solid tangential sweep of wall projection of (a) around a cylinder. (b) Solid tangent cluster of (a) and of (c).

Area balance of axial sections of swept solids. In [2] we showed that any vertical cross section of a general tangentially swept solid around a circular cylinder is in area balance with the corresponding vertical cross section of its solid cluster. This is a consequence of a balance-revolution principle introduced in [3; p. 410]. *The areas of two plane regions are in equilibrium with respect to a balancing axis if, and only if, the solids of revolution generated by rotating them about the balancing axis have equal volumes.* The same is true when the circular cylinder is replaced by a right circular cone. In fact, a stronger result holds. *Any vertical section of a tangentially swept solid around a circular cylinder or a right circular cone is in chord-by-chord balance with the corresponding vertical cross section of its solid cluster (with respect to the common axis of the cylinder or cone).*

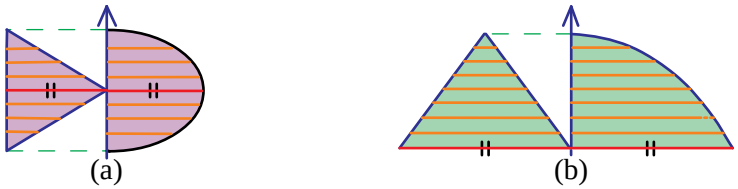

Figure 32. (a) Triangle and semielliptical disk in chord-by-chord balance. (b) Isosceles triangle and semiparabolic segment in chord-by-chord balance.

This follows from the fact that each horizontal cross section of the sweep is a circular ring whose area is equal to the corresponding circular cross section of the cluster, so by using Pappus we see that the horizontal chords are in balance. Examples of area balance of axial sections are exhibited by any two members of a family of solids of revolution generated by any entry in Figure 5. Figure 32a shows an example of area balance of axial sections of Figures 16a and 16b, a triangle and a semielliptical disk. Another example is shown in Figure 32b, area balance of axial sections of Figures 18a and 18b, an isosceles triangle and a semiparabolic segment. More examples appear in Figures 34 and 36.

6. CENTROIDS OF SOLID SWEEPS AND CLUSTERS

The property of volume centroids described in Corollary 2 of Section 1 also applies to solid sweeps obtained by sweeping around a cone instead of a cylinder. *The altitudes of the volume centroids of a solid sweep and its solid cluster are*

equal. Now we use this property to locate the volume centroids of several solids of revolution. The first two are the ellipsoidal and paraboloidal segments of revolution in Figures 33a and b. Archimedes treated the centroid of a spherical segment (a special case of an ellipsoidal segment), and of a paraboloid of revolution. The next two, shown in Figure 34, were not treated by Archimedes. Figure 34a shows the upper half of a hyperboloid of one sheet, and Figure 34b shows the lower half of a hyperboloid of two sheets.

Centroids of ellipsoidal segment and paraboloidal segment. For the ellipsoidal segment of height h shown Figure 33a, z denotes the distance of its volume centroid from the top. We shall show that

$$z = h\frac{8H - 3h}{4(3H - h)}, \tag{8}$$

where H is the altitude of a full semiellipsoidal solid. For a spherical segment, Equation (8) is equivalent to Proposition 9 in [4; *Method*, p.35]. When $h = H$ the ellipsoidal segment is half an ellipsoid and (8) gives $z = \frac{5}{8}H$.

To prove (8), recall that in Figure 16 we observed that the ellipsoidal segment is the solid tangent cluster of a solid tangent sweep obtained by rotating a triangle tangentially around a circular cylinder. By Corollary 2, distance z is equal to that for the cylinder of altitude h and radius r punctured by an inverted truncated cone as in Figure 33a, whose volume we denote by V_{TC}, and whose centroidal distance from the top we denote by z_{TC}. Let $V(h)$ denote the volume of the ellipsoidal segment. The solid cylinder of radius r and altitude h has centroidal distance $h/2$ from the top, so by equating moments about the top we find

$$zV(h) + z_{\text{TC}}V_{\text{TC}} = \frac{h}{2}\pi r^2 h. \tag{9}$$

The term $z_{\text{TC}}V_{\text{TC}}$ is also the difference of moments of a large cone of altitude H and radius r, and a smaller cone of altitude $H - h$ and radius $r(H - h)/H$, which gives

$$z_{\text{TC}}V_{\text{TC}} = \frac{H^2}{4}\pi\frac{r^2}{3} - (\frac{H}{4} + \frac{3h}{4})\frac{\pi}{3}(H - h)(\frac{H - h}{H}r)^2. \tag{10}$$

From (1) we have $V(h) = \frac{\pi}{3}(3r - b)bh$, where $b = hr/H$. This becomes $V(h) = \frac{\pi}{3}(3H - h)(rh/H)^2$, which when used in (9) together with (10) leads, after much algebraic simplification, to (8).

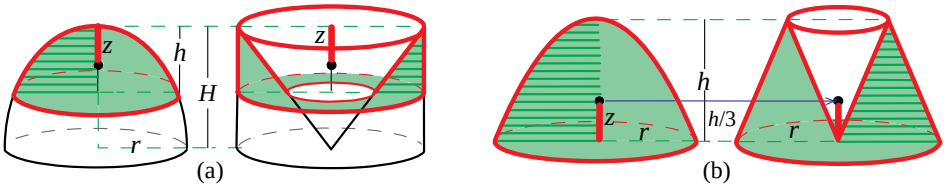

Figure 33. (a) Centroid of an ellipsoidal segment. (b) Centroid of a paraboloidal segment.

We treat next the paraboloidal segment of altitude h in Figure 33b. In this case the formula for centroidal distance z from its base is very simple:

$$z = \frac{h}{3}, \tag{11}$$

a result found by Archimedes in [4; *Method*, Proposition 5]. Figure 18 shows that the paraboloidal segment is the solid cluster of the tangential sweep, and we showed earlier that its volume V is six times the volume v of the small inverted cone of the same altitude in Figure 33b. To prove (11) we note that the solid tangent sweep in Figure 33b can be obtained by removing two smaller cones, each of volume v, from the large cone of altitude $2h$ in Figure 18a. Equating moments about the base of the configuration in Figure 18a we find

$$6zv + 2vh = 4vh,$$

which immediately gives (11).

Note that the centroidal distance $h/3$ of the paraboloidal segment is exactly the same as the planar centroidal distance of the isosceles triangle of base r and altitude h that sweeps out the punctured truncated cone in Figure 33b when rotated about the axis of the cone. As we will show later in this section, this is not a mere coincidence, but is a phenomenon shared by solids obtained by rotating planar regions with an axis of symmetry.

Centroids of hyperboloidal segments. First we treat a hyperboloidal segment of one sheet cut from the upper half of the unpunctured solid in Figure 3a. The segment has altitude h, lower circular base of radius r, and upper circular base of radius R, as shown in Figure 34a. We will show that its centroidal distance Z from the lower base is given by

$$Z = \frac{3}{4}h\frac{R^2 + r^2}{R^2 + 2r^2}. \tag{12}$$

We know that the punctured solid has the same volume and same centroidal distance from the base as its solid cluster, the cone of altitude h and radius t in Figure 34a.

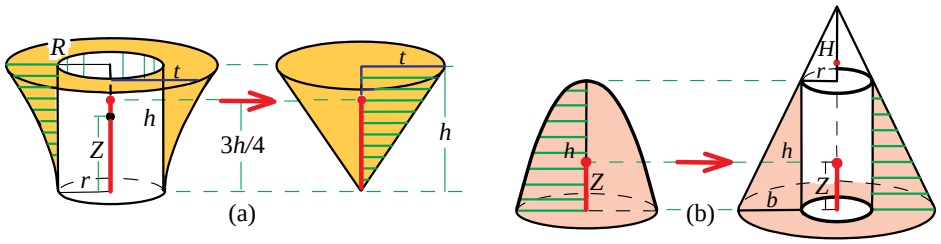

Figure 34. Centroid of hyperboloidal segments of (a) one sheet, and (b) one of two sheets.

Here $t^2 + r^2 = R^2$. Equating moments of the volume [cone] of the cone plus the volume [cyl] of the cylindrical hole with that of the volume [cone]+[cyl] of the

unpunctured hyperboloidal segment, we find

$$\frac{3}{4}h[\text{cone}] + \frac{1}{2}h[\text{cyl}] = Z([\text{cone}] + [\text{cyl}]). \tag{13}$$

But [cone]$= \pi t^2 h/3$ and [cyl]$= \pi r^2 h$. Use these in (13) and solve for Z to obtain (12).

For the hyperboloidal segment of two sheets, one of which, of altitude h, is shown in Figure 34b, the centroidal distance Z from the base is given by

$$Z = \frac{h}{4}\frac{4H+h}{3H+h}, \tag{14}$$

where H is the altitude of the small cone in Figure 34b.

To prove (14), we use the fact that the punctured truncated cone in Figure 34b has the same volume $V(h)$ and same centroidal distance Z from the base as its solid cluster, the hyperboloidal segment. Volume $V(h)$ is equal to that of the solid swept by the triangle of base b and altitude h in Figure 34b. By Pappus, we have

$$V(h) = 2\pi(r + \frac{b}{3})\frac{bh}{2} = \pi r^2(3 + \frac{h}{H})\frac{h^2}{3H}, \tag{15}$$

where we have used the similarity relation $b/r = h/H$. Equating moments of the configuration in Figure 34b about the base, we have

$$\frac{1}{4}(H+h)[\text{Cone}] = \frac{1}{2}h[\text{cyl}] + (h + \frac{1}{4}H)[\text{cone}] + ZV(h), \tag{16}$$

where [Cone] denotes the volume of the large cone of radius $r + b$ and altitude $H + h$, [cyl] denotes the volume of the cylinder of radius r and altitude H, and [cone] denotes the volume of the small cone of radius r and altitude H. Now use the volume formulas

$$[\text{Cone}] = \frac{1}{3}\pi(r+b)^2(H+h) = \frac{1}{3}\pi r^2(1+\frac{h}{H})^2(H+h), \;\; [\text{cone}] = \frac{1}{3}\pi r^2 H, \;\; [\text{cyl}] = \pi r^2 h$$

together with (15) in (16), and solve for Z to get (14) after algebraic simplification.

Special centroidal altitude lemma. Figure 35a shows a right triangular region of altitude h rotated to generate a solid cone of the same altitude. The areal centroidal distance of the triangle above its base is $h/3$, but the volume centroidal distance of the cone is $h/4$ (Figure 35a). Earlier we observed that the volume centroidal distance $h/3$ of the paraboloidal segment in Figure 33b is equal to the areal centroidal distance of an isosceles triangle of altitude h that sweeps out the punctured truncated cone. This surprising result is explained by the following lemma on centroidal altitudes, illustrated in Figure 35b.

Centroidal altitude lemma. *The area centroid of any axially symmetric plane region has the same altitude above any fixed base as the volume centroid of the solid of revolution swept by the plane region around any axis in that plane disjoint from the region that is parallel to the axis of symmetry.*

The idea of the proof is very simple. Because each horizontal chord of the plane region has its centroid on the axis of symmetry, during the revolution it sweeps an area proportional to the chord length. Therefore, the volume centroid of the solid

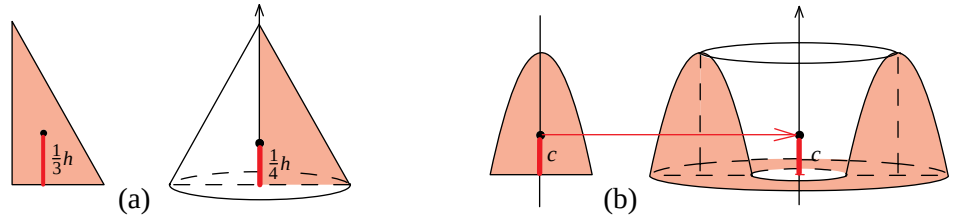

Figure 35. (a) Centroid of triangle and cone are different. (b) Centroidal altitude lemma.

having these areas as horizontal cross sections is at the same altitude as the areal centroid determined by the chords.

This idea can be converted into a rigorous proof by using integrals to represent the two centroids. If $l(h)$ denotes the length of the chord at altitude h, the altitudes of the area centroid and volume centroid are given, respectively, by

$$\text{area centroid} = \frac{\int l(h)h\,dh}{\int l(h)\,dh}, \quad \text{volume centroid} = \frac{\int A(h)h\,dh}{\int A(h)\,dh},$$

where $A(h)$ denotes the cross sectional area of the solid at altitude h. By Pappus, $A(h) = 2\pi R l(h)$, where R is the distance between the two parallel axes. The constant factor $2\pi R$ cancels in the second ratio of integrals, and we see that the area centroid and volume centroid are at the same altitude.

Now we apply the lemma to the upper half of a torus (Figure 36b) generated by revolving a semicircular disk of radius r (Figure 36a) around any axis at distance $R \geq r$ from its center. According to the lemma, the volume centroid of the semitorus is at the same altitude as the area centroid of the semicircular disk, regardless of R. Figure 36c shows a vertical section of the semitorus by a plane internally tangent to the torus, the upper half of a persoidal region consisting of two congruent pieces with an axis of symmetry. When one piece is swept tangentially around a cylinder through the hole of the torus its tangent sweep is the torus itself. When rotated around its own axis of symmetry it produces the semipersoid of revolution (d). According to Corollary 2, the semitorus in Figure 36b and solid in (d) have the same centroidal altitude. Consequently, the volume centroid of the semipersoid of revolution in (d) has the same altitude as that of the semicircular disk in (a).

The same property holds for any horizontal slice of the configuration in Figure 36 because any horizontal slice of a semicircular disk has an axis of symmetry.

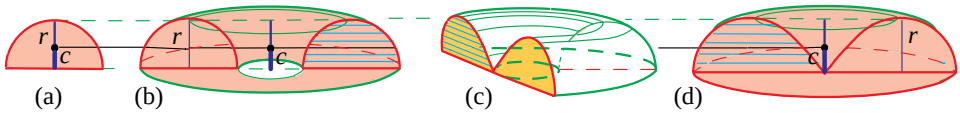

Figure 36. Semicircular disk (a), semitorus (b), and solid (d), obtained by revolution of the lemniscate in (c), all have their centroid at the same altitude.

More generally, the foregoing analysis applies to any persoidal region cut by a vertical plane passing through the hole of the torus. Moreover, it also applies when the circular disk in Figure 36a is replaced by any symmetric plane region generating a toroidal-like solid. For example, we can use an isosceles triangle as in Figure 37a and rotate it around any vertical axis disjoint from the triangle. The resulting toroidal-like solid will a punctured truncated cone, and the corresponding persoid-like solids will be bounded by two hyperboloids of revolution as shown in Figure 37b. Their centroids will be at the same altitude above the base, which in this case is one-third the altitude of the triangle.

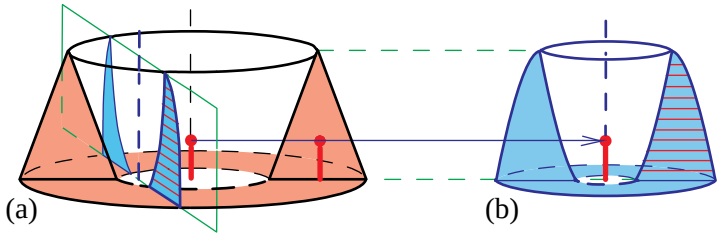

Figure 37. (a) Punctured truncated cone with a section bounded by two hyperbolas. (b) Hyperboloid of revolution punctured by another hyperboloid. The centroids of both solids have the same altitude as that of the triangle.

Finally, we note that the special centroidal altitude lemma is also valid when the symmetric plane region is swept tangentially along any cylinder whose generator is parallel to the symmetry axis of the region. In view of Corollary 2, the tangentially swept solid has its volume centroid at the same altitude as that of the plane region.

7. TANGENTIAL SWEEPING AROUND A GENERAL SURFACE

Earlier we generated solids by tangential sweeping along a cylinder or cone. Now we use a more general surface as depicted by the lightly shaded region in Figure 38, which we call a *tangency surface*. Take such a surface and slice it by a family of horizontal parallel planes, as indicated in Figure 38a. Take a typical curve of intersection as tangency curve, and construct a tangent sweep using vectors from the tangency curve to some free-end curve. The free-end curves lie on another surface, as illustrated in Figure 38a, which we call the *free-end surface*. For each horizontal tangent sweep, construct its planar tangent cluster by translating each tangent to a common point in that plane. The darker shaded regions in Figure 38 depict the tangent sweep and its cluster in the bottom plane. They have equal areas. As we move from the bottom horizontal plane to the top one in Figure 38a, the solid swept tangentially between the tangency surface and the free-end surface is called a *solid tangent sweep*. Now construct the *solid tangent cluster* as the union of the planar clusters with their common points lying on one vertical line P, as in Figure 38b.

Each horizontal plane intersects the solid tangent sweep and the solid tangent cluster along plane regions having equal area. By the slicing principle, we have:

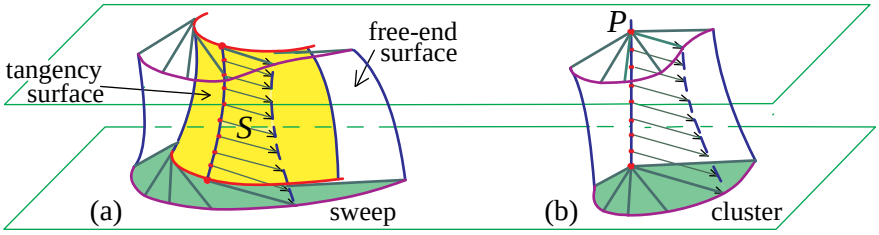

Figure 38. (a) Solid tangent sweep. (b) Solid tangent cluster.

Theorem 4. *The portion of a solid tangent sweep between any two horizontal planes has the same volume as its corresponding solid tangent cluster.*

Corollary 2 of Theorem 1 also is valid for solid sweeps and clusters in Theorem 3: *The altitudes of the volume centroids above a fixed horizontal base are equal.*

As in earlier examples, there is an alternative method for producing the solid tangent sweep. Choose an initial tangent vector in the bottom horizontal plane from the tangency surface to the free-end surface. As we move continuously from the bottom plane to the top, select those tangent vectors of the tangency curves parallel to the initial tangent vector. Their tangency points trace a curve which is a directrix for a cylindrical region containing all these parallel tangency vectors. This cylindrical region, which we call S, plays the same role as the plane region S used earlier for sweeping along a cylinder or cone. It can change its shape as it moves tangentially around the surface.

Tangency surfaces of revolution. In Figure 39a the tangency surface is a sphere of diameter H, and S is a rectangular strip of width w wrapped tangentially with one edge along a meridian joining the poles. As S rotates around the sphere, the opposite edge sweeps part of the surface of a larger sphere, so the solid tangent sweep is a solid spherical shell between two concentric spheres with the polar caps of the larger sphere removed, as depicted in Figure 39b. Figure 39c shows the

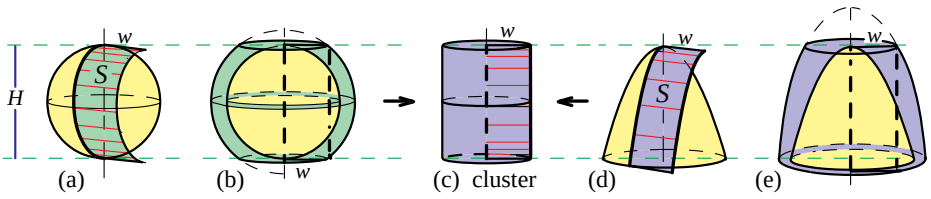

Figure 39. (a) Rectangle sweeping around a sphere. (b) Solid tangential sweep. (d) Rectangle sweeping around paraboloid. (e) Swept solid. (c) Common solid tangent cluster.

corresponding solid tangent cluster, a circular cylinder of radius w and altitude H. According to Theorem 3, the spherical shell and the cylinder have equal volumes. This was also noted in [3; Theorem 5.2]. When a rectangle of width w is wrapped around a paraboloid of altitude H as in Figure 39d, the corresponding solid tangent

sweep is the solid paraboloidal shell in Figure 39e. The cylinder in Figure 39c is its solid tangent cluster. Surprise: The volume of the paraboloidal shell in (e) is equal to that of the spherical shell in (b)! Two more examples, with the paraboloid

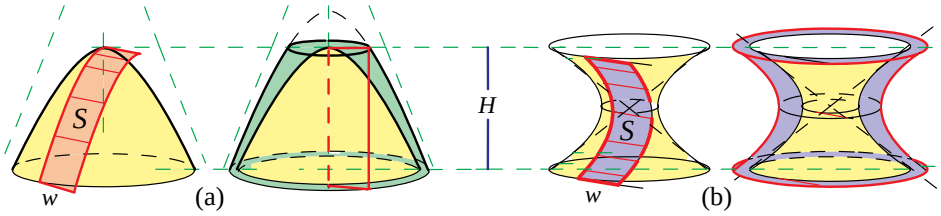

Figure 40. Rectangle sweeping around two types of hyperboloid in (a) and (c). Their solid tangent sweeps have the same volume as their common tangent cluster cylinder in (b).

replaced by two types of hyperboloid, are shown in Figure 40a and 40b. Another surprise: Each solid tangent sweep has volume equal to that of the cylinder in Figure 39c.

Figure 41a shows an example of Figure 39a in which the inner surface is produced by rotating a curve $y = y(x)$ around the x axis, and the outer surface is a coaxial cylinder of radius a. A horizontal tangent vector from the surface to the

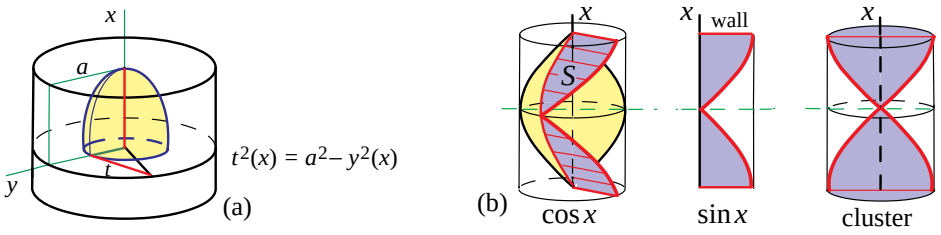

Figure 41. (a) Tangent of length $t(x)$ from inner surface of revolution to outer cylinder. (b) Tangential region S sweeps solid between rotated cosine curve and cylinder of radius 1. Its wall projection is the ordinate set of a sine curve; rotating it produces solid cluster.

cylinder has length $t = t(x)$ given by $t^2(x) = a^2 - y^2(x)$. The vectors of length t form a region S that generates a solid tangential sweep lying outside the surface and inside the cylinder, and the wall projection is a plane region formed by the ordinate set of $t(x)$. For example, if $a = 1$ and $y(x) = \cos x$ as shown in Figure 41b, then $t(x) = \sin x$, and the corresponding solid tangent cluster is a surface bounded by rotating a sine curve. Its volume is equal to that of the solid tangent sweep. Consequently, the solid between the cylinder and the rotated cosine has the same volume as the rotated cosine, each being half that of the circumscribing cylinder. The same is true, of course, for the solid between the cylinder and the rotated sine.

In Figure 42a, the inner surface is a paraboloid obtained by rotating the parabola $y^2(x) = x$ around the x axis, and the wall projection is bounded by a portion of the

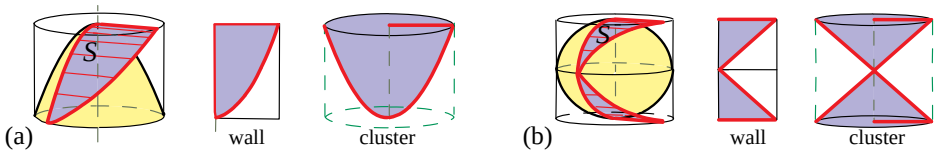

Figure 42. (a) Paraboloid inscribed in cylinder. (b) Ellipsoid inscribed in cylinder.

parabola $t^2(x) = a^2 - x$, which is a flipped version of the original parabola. (The flipped parabola also appears in another context in [3; p. 181].) The solid cluster, a flipped version of the original paraboloid, has the same volume of the solid tangent sweep. This example gives another proof of Archimedes' result that the volume of a paraboloid of revolution is half that of its circumscribing cylinder.

In Figure 42b an ellipsoid is inscribed in a cylinder, and the wall projection of the plane region that generates the solid tangent cluster is a right triangle, shown shaded. Rotating this triangle produces the tangent cluster, a right circular cone whose volume, one-third that of the cylinder, is also that of the solid tangent sweep. Finally, we remark that in the case of surfaces of revolution, the axial sections of the tangential sweep and cluster are in chord-by-chord balance and hence in area balance with respect to the axis of revolution.

8. CONCLUDING REMARKS

Start with any family of swept solids with circular horizontal cross sections. Figure 43a shows the cross section of a typical member of the family and of its

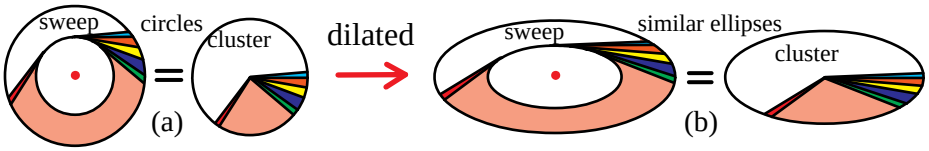

Figure 43. (a) Circular tangent sweep and cluster. (b) Horizontal dilation of (a).

tangent cluster, both cross sections having the same area. If all members of the family are dilated by a factor a in one horizontal direction, as indicated in Figure 44, all the cross sectional areas are multiplied by the factor a so all dilated cross sectional areas will be equal. Consequently, all the solids in the dilated family of equal height will have equal volumes and equal centroidal altitude above a fixed horizontal base. But now the cross sections are elliptic, as indicated in Figure 44b, and the dilated solids are elliptic quadrics punctured by elliptic quadrics.

We can also scale and dilate the elliptic cross sections so that they become parabolic, by moving one focus of the ellipse to infinity. This can be achieved on the cone that is cut by a plane to produce the ellipse. The plane that cuts an ellipse can be rotated so it becomes parallel to a generator of the cone to transform the ellipse to a parabola. Rotating the cutting plane further produces a hyperbola.

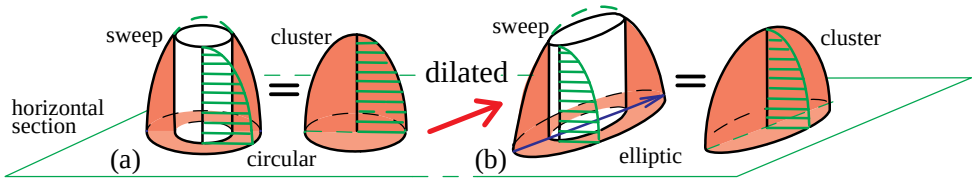

Figure 44. (a) Solid sweep and cluster. (b) Horizontal dilation of (a).

Consequently, proper scaling and dilation transforms punctured parabolic surfaces to punctured hyperbolic surfaces.

Thus we see that families of swept solids of equal height and equal volume can be extended to all types of quadric surfaces. These represent familiar examples of swept solids swept by *variable* plane regions S bounded by conic sections.

References

[1] G. L. Alexanderson and L. F. Klosinski, Some surprising volumes of revolution, *Two-Year College Mathematics Journal*, 6 (1975), 13–15.

[2] T. M. Apostol and M. A. Mnatsakanian, Volumes of solids swept tangentially around cylinders, *Forum Geom.*, 15 (2015) 13–44.

[3] T. M. Apostol and M. A. Mnatsakanian, *New Horizons in Geometry*, Dolciani Mathematical Expositions No. 47, Mathematical Association of America, 2012.

[4] T. L. Heath, *The Works of Archimedes*, Dover, New York, 1953.

[5] M. A. Mnatsakanian, On the area of a region on a developable surface, *Dokladi Armenian Acad. Sci.*, 73 (2) (1981) 97–101. (Russian);
`www.its.caltech.edu/~mamikon/Article.html`;
English translation: `http://mamikon.com/Article81.pdf`.

[6] G. Polya, *Mathematics and Plausible Reasoning, Vol. I, Induction and Analogy in Mathematics*, Princeton University Press, Princeton, 1954.

Tom M. Apostol: California Institute of Technology, 253-37 Caltech, Pasadena, California 91125 USA

E-mail address: `apostol@caltech.edu`

Mamikon A. Mnatsakanian: California Institute of Technology, 253-37 Caltech, Pasadena, California 91125 USA

E-mail address: `mamikon@caltech.edu`

Forum Geometricorum
Volume 15 (2015) 73–89.

FORUM GEOM
ISSN 1534-1178

From Electrostatic Potentials to Yet Another Triangle Center

Hrvoje Abraham and Vjekoslav Kovač

Abstract. We study the problem of finding a point of maximal electrostatic potential inside an arbitrary triangle with homogeneous surface charge distribution. In this article we derive several synthetic and analytic relations for its location in the plane. Moreover, this point satisfies the definition of a triangle center, different from any of previously discovered centers in Clark Kimberling's encyclopedia.

1. Introduction

The topic we are about to discuss was initiated by a concrete and practical question in physics that has eventually revealed its unexpectedly interesting geometrical flavor. Let us begin with a statement of this theoretical problem and postpone applied motivation to the end of this section.

Problem. Suppose that a planar triangle T is a continuous source of charge, which is homogeneously distributed over its surface, i.e. the charge density is constant over the triangle. At which point in the same plane the electrostatic potential of T attains its maximum value?

All physical notions will be accompanied with their precise definitions and the discussion will soon turn into elementary geometrical considerations. Let us recall that the potential of a point source with charge q evaluated at a point that is r units apart is given by $V(r) = kq/r$. This is merely a restatement of *Coulomb's law* and the constant k is not important for us. By "superposition principle" for multiple charges it is therefore reasonable to define the potential generated by the whole triangle T as

$$V(P) = \iint_T \frac{d\lambda(Q)}{|PQ|} \tag{1}$$

for any point P in the plane. Here λ denotes the two-dimensional Lebesgue measure (i.e. the area measure), Q is an integration variable, and $|PQ|$ denotes the distance between points P and Q. We are careless about the multiplicative constant or

Publication Date: February 3, 2015. Communicating Editor: Paul Yiu.

We are grateful to Clark Kimberling for including the point of maximal electrostatic potential as entry $X(5626)$ in his encyclopedia [7] shortly after the preprint of this paper became available. We would also like to thank Dragutin Svrtan for a useful discussion.

the charge density and we even omit them from writing. In Cartesian coordinates the above formula becomes simply

$$V(x,y) = \iint_T \frac{dx'dy'}{\sqrt{(x'-x)^2+(y'-y)^2}}.$$

It is easy to see that V is indeed a well-defined function on the whole plane. One can draw contour graphs of (1) for various choices of triangles using the Mathematica command ContourPlot [14] and the level sets will look as those in figure 1. Such drawings can make us suspect that V has the shape of a single "mountain

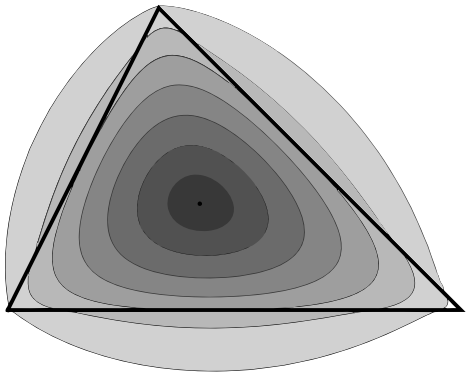

Figure 1. Contour graph of V.

peak," but this certainly could not pass as a rigorous argument. It is not immediately clear from the formula that there even exist a point $P_{\max}$ inside T where V attains its maximum and it is certainly not obvious that such point should be unique for every triangle. Moreover, we would like to locate this point, in a certain sense, for an arbitrary given triangle T.

What would be the physical meaning of the maximum potential point? It is the point where the electrostatic field $\vec{E}$ generated by T stabilizes. Let us perform a simple thought experiment. Assume that T is charged positively and place a negative point charge somewhere in the plane. It will necessarily be driven by electrostatic forces unless it is placed at a point where it "feels perfectly stable." Figure 2 illustrates several integral curves of the vector field $\vec{E}$, which are also known in physics as *lines of force* or *field lines*. Observe that they all meet at the same point inside T. This experiment is once again very far from a rigorous proof. Existence and uniqueness of the maximum potential point will follow from more general results in convex analysis and will be discussed in the next section. However, in the case of a triangle, they will also come as a byproduct of our attempts to specify its location throughout the rest of the paper.

We have just mentioned the notion of electrostatic field, so what would that field be in the case of our charged triangle T? It can be defined simply as $\vec{E} = -\nabla V$ at any point where the potential V is differentiable. In physics, the electric field is sometimes (but not always) given before the potential. We have intentionally

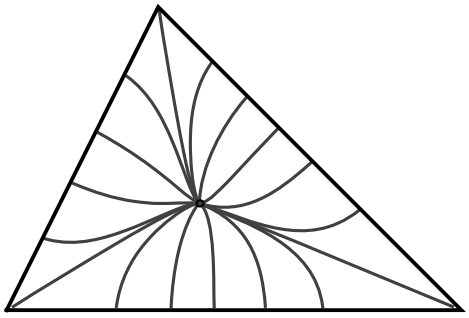

Figure 2. Integral curves of $\vec{E}$ that lie inside T.

ordered things this way, simply because the potential of T was easier to define mathematically. Going back to a point source, an easily derived and well-known formula is $\vec{E} = kq\vec{r}/r^3$. Here $\vec{r}$ denotes a directed line segment from the source to a point where the field is computed. Using the superposition principle once again we suspect that the correct corresponding expression is

$$\vec{E}(P) = \iint_T \frac{\overrightarrow{QP}}{|PQ|^3} d\lambda(Q) = -\iint_T \frac{\overrightarrow{PQ}}{|PQ|^3} d\lambda(Q), \tag{2}$$

or coordinate-wise with $\vec{i}$ and $\vec{j}$ being the standard unit vectors,

$$\vec{E}(x,y) = -\iint_T \frac{(x'-x)\vec{i} + (y'-y)\vec{j}}{((x'-x)^2 + (y'-y)^2)^{3/2}} dx'dy'.$$

However, the double integral in the above formula will not be absolutely convergent unless $P = (x,y)$ lies outside T. To explain the difficulty, assume that P is contained in the triangle interior, together with a "small" disk $\mathrm{D}_\varepsilon(P)$ of radius ε around it. We insert absolute values inside the double integral and only integrate over this disk. Changing to a polar coordinate system centered at P we obtain

$$\iint_{\mathrm{D}_\varepsilon(P)} \frac{|\overrightarrow{PQ}|}{|PQ|^3} d\lambda(Q) = \int_0^\varepsilon \int_0^{2\pi} \frac{r}{r^3} r dr d\varphi = +\infty,$$

because $\int_0^\varepsilon dr/r$ diverges.

In order to get a valid formula for $\vec{E}$ that would hold for points P in the interior of T, one simply has to observe that the contributions $\frac{\overrightarrow{PQ}}{|PQ|^3}$ of points $Q \in \mathrm{D}_\varepsilon(P)$ cancel out each other completely, see figure 3. Therefore,

$$\vec{E}(P) = -\iint_{T\setminus \mathrm{D}_\varepsilon(P)} \frac{\overrightarrow{PQ}}{|PQ|^3} d\lambda(Q) \tag{3}$$

should hold for P inside the triangle. Indeed, one can even let $\varepsilon \to 0$, obtaining the expression called the *principal value* of the integral:

$$\vec{E}(P) = -\text{p.v.}\iint_T \frac{\overrightarrow{PQ}}{|PQ|^3} d\lambda(Q). \tag{4}$$

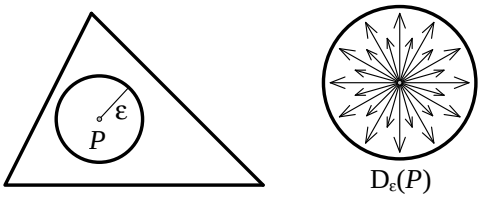

Figure 3. Cancellations in the singular part of the integral.

Things remain problematic for points P at the boundary, because the same argument shows that the expression for $\vec{E}(P)$ does not converge in any usual sense. Indeed, the potential is continuous but not differentiable at those points.

The main source of motivation for the problem comes from implementation of a certain type of *boundary element method (BEM)* for electrostatic problems [1], [5], [8], [12]. Boundary element methods are usually formulated by surface elements of a three-dimensional object and these elements are in turn most often represented by triangles. In the case of an electrostatic problem, a single triangle potential could be evaluated either at vertices, or at a certain interior point, depending on the formulation of the method. In the later case, it is common to take the center of mass (i.e. the centroid), but there is no reason or evidence why this would be the best choice. Indeed, one can argue that using the maximum potential point provides better results, but such discourse is out of the scope of this paper. Calculating its coordinates and discovering its properties proved to be challenges on their own.

2. Existence and uniqueness

In this section we start the rigorous mathematical treatment of the problem. Our potential is a particular instance of the so-called *fractional integral*,

$$(I_p f)(x,y) = \iint \Big((x'-x)^2 + (y'-y)^2\Big)^{p/2} f(x',y')\,dx'dy', \qquad (5)$$

which is also known as the *Riesz potential* [11] when $-2 < p < 0$ and when it is properly normalized. In order to obtain (1), one only has to take $p = -1$ and choose f to be the indicator function of T.

Extreme points of "regularized" versions of $I_p f$ when p is a real number and f is the characteristic function of a general convex set (even in higher dimensions) have already been studied in the literature. They were named *radial centers* by M. Moszyńska [9], who seems to be the first to establish their existence and uniqueness for $-2 < p \leq 1$, while the remaining cases were studied by I. Herburt [3] and J. O'Hara [10], who called these points r^p *centers*. Herburt, Moszyńska, and Peradzyński [4] gave physical interpretations of radial centers, mentioning gravitational and electrostatic potentials for $p = -1$, but do not specialize the discussion to triangles. On the other hand, we need to mention an unpublished text by K. Shibata [13] on a similarly defined but different point in a triangle, corresponding to $p = -2$, which we discuss briefly in the last section.

As we have already said, existence and uniqueness of the maximum point for V follows from general results of Moszyńska [9, Section 3] for general compacts convex sets T with nonempty interior. Moreover, Herburt [2] showed that the maximum point lies in the interior of T if the set T has piecewise smooth boundary. However, since we are only interested in a very special case when T is a triangle in $\mathbb{R}^2$, we are able to reprove these facts easily between the lines of the more precise results on the maximum point location. This keeps the material elementary and self-contained.

The following proposition is an easy exercise in vector calculus, so we only provide proofs of its nontrivial parts.

Proposition 1. (a) *Potential V is finite and continuous on the whole plane.*
(b) $V(P) \to 0$ *uniformly as the distance from P to T tends to ∞.*
(c) *Potential V is differentiable both in the interior and in the exterior of T.*
(d) *Field $\vec{E} = -\nabla V$ is given by* (2) *for exterior points P and by* (3) *or* (4) *for points P in the interior of T.*
(e) *Potential V cannot attain local maxima in the exterior or on the boundary of T.*

Proof. Parts (a) and (b) are very easy and follow simply from absolute integrability of the function in (1) and boundedness of the domain T.

(c) and (d) Fix a point P_0 inside T and choose $\varepsilon > 0$ twice smaller than the distance from P_0 to the boundary of T. We need to show that V is differentiable at P_0 and that $\nabla V(P_0) = -\vec{E}(P_0)$, where $\vec{E}(P_0)$ is given by formula (3). Take any point P such that $|PP_0| < \varepsilon$. Parts of the integrals in the expression $V(P)-V(P_0)$ corresponding to $\mathrm{D}_\varepsilon(P_0)\cap\mathrm{D}_\varepsilon(P)$ cancel out by symmetry, so this difference is equal to

$$\iint_{T\setminus(\mathrm{D}_\varepsilon(P_0)\cup\mathrm{D}_\varepsilon(P))} \Big(\frac{1}{|PQ|} - \frac{1}{|P_0Q|}\Big)\,d\lambda(Q).$$

Using

$$|P_0Q|^2 - |PQ|^2 = 2\overrightarrow{P_0Q}\cdot\overrightarrow{P_0P} - |P_0P|^2,$$

it can be rewritten as

$$V(P) - V(P_0) = \iint_{T\setminus(\mathrm{D}_\varepsilon(P_0)\cup\mathrm{D}_\varepsilon(P))} \frac{2\overrightarrow{P_0Q}\cdot\overrightarrow{P_0P} - |P_0P|^2}{|P_0Q||PQ|(|P_0Q| + |PQ|)}\,d\lambda(Q).$$

On the other hand, from (3),

$$\vec{E}(P_0)\cdot\overrightarrow{P_0P} = -\iint_{T\setminus\mathrm{D}_\varepsilon(P_0)} \frac{\overrightarrow{P_0Q}\cdot\overrightarrow{P_0P}}{|P_0Q|^3}\,d\lambda(Q).$$

After simple algebraic manipulations and by splitting

$$\mathrm{D}_\varepsilon(P_0) = \big(\mathrm{D}_\varepsilon(P_0)\cup\mathrm{D}_\varepsilon(P)\big)\setminus\big(\mathrm{D}_\varepsilon(P)\setminus\mathrm{D}_\varepsilon(P_0)\big),$$

we arrive at

$$\frac{1}{|P_0P|}\Big(V(P) - V(P_0) + \vec{E}(P_0)\cdot\overrightarrow{P_0P}\Big) = J_1 - J_2 - J_3,$$

where

$$J_1 = \iint_{T\setminus(\mathrm{D}_\varepsilon(P_0)\cup\mathrm{D}_\varepsilon(P))} \frac{\overrightarrow{P_0Q}\cdot\overrightarrow{P_0P}}{|P_0Q||P_0P|}\,\frac{2|P_0Q|+|PQ|}{|P_0Q|+|PQ|}\,\frac{|P_0Q|-|PQ|}{|P_0Q|^2|PQ|}\,d\lambda(Q),$$

$$J_2 = \iint_{T\setminus(\mathrm{D}_\varepsilon(P_0)\cup\mathrm{D}_\varepsilon(P))} \frac{|P_0P|}{|P_0Q||PQ|(|P_0Q|+|PQ|)}\,d\lambda(Q),$$

$$J_3 = \iint_{\mathrm{D}_\varepsilon(P)\setminus\mathrm{D}_\varepsilon(P_0)} \frac{\overrightarrow{P_0Q}\cdot\overrightarrow{P_0P}}{|P_0Q||P_0P|}\,\frac{1}{|P_0Q|^2}\,d\lambda(Q).$$

Using $|P_0Q|\geq\varepsilon$, $|PQ|\geq\varepsilon$, and $\big||P_0Q|-|PQ|\big|\leq|P_0P|$ the first integral is easily bounded as

$$|J_1|\leq\frac{2}{\varepsilon^3}\lambda(T)|P_0P|$$

and similarly we get

$$|J_2|\leq\frac{1}{2\varepsilon^3}\lambda(T)|P_0P|,\quad |J_3|\leq\frac{1}{\varepsilon^2}\lambda\big(\mathrm{D}_\varepsilon(P)\setminus\mathrm{D}_\varepsilon(P_0)\big).$$

Letting $P\to P_0$ we conclude

$$\lim_{P\to P_0}\frac{V(P)-V(P_0)+\vec{E}(P_0)\cdot\overrightarrow{P_0P}}{|P_0P|}=0,$$

which is precisely what we needed.

For points P_0 in the exterior of T the proof can follow the same lines. Moreover, an even shorter proof can be given for such P_0 by entirely standard arguments of interchanging limits and integrals, as the integral in (2) is an absolutely convergent one.

(e) Begin by taking a point P_0 outside T. Informally saying, the field does not vanish at P_0 since it has to "point" away from T. More rigorously, let l be any line passing though P_0 and containing T entirely in one of the two corresponding half-planes, see figure 4. If $\vec{n}$ is a vector normal to l and oriented in the opposite

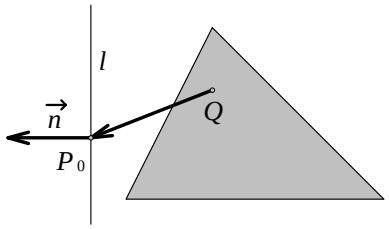

Figure 4. Treatment of exterior points.

direction, then formula (2) yields

$$\vec{E}(P_0)\cdot\vec{n}=\iint_T\frac{\overrightarrow{QP_0}\cdot\vec{n}}{|P_0Q|^3}d\lambda(Q)>0.$$

Consequently, $(\nabla V)(P_0) \neq \vec{0}$, so P_0 cannot be a stationary point for V.

The same argument "almost works" for points at the triangle boundary. Even though $\vec{E}(P_0)$ does not exist, we can imagine that it is a vector of infinite length pointing outwards. The reader can modify the proof of parts (c) and (d) to show that

$$\lim_{h\to 0} \frac{V(P_0 - h\vec{n}) - V(P_0)}{h} = +\infty$$

holds for the same choice of $\vec{n}$. Once again, we conclude that P_0 is not a local maximum point for V. □

It is now easy to conclude that potential V attains its maximum at some point inside triangle T and at each such point P one has $\vec{E}(P) = \vec{0}$. Indeed, by positivity and parts (a) and (b) of Proposition 1 it follows that V is bounded and has a maximum that is attained at some (finite) point in the plane. By part (e) we know that any such point must lie in the interior of T. Finally, the second assertion is a consequence of parts (c) and (d).

We need to remark that an explicit formula for V can be computed, although it is rather complicated and not practically useful. Instead, it will be more useful to transform formula (3) for $\vec{E}(P)$ in the next section.

3. Geometric relations

Throughout this section suppose that P is a stationary point inside a positively oriented triangle $T = \triangle ABC$, i.e. the corresponding vector field $\vec{E}$ vanishes at P. We already know that P has to coincide with the unique maximum point of V, but prefer to use condition $\vec{E}(P) = \vec{0}$ only, in order to reprove the uniqueness result. Denote its distances from vertices A, B, C respectively by

$$r_A = |PA|, \;\; r_B = |PB|, \;\; r_C = |PC|.$$

Let us also introduce convenient notation for the several angles it determines,

$$\begin{array}{lll} \alpha_1 = \angle BAP, & \beta_1 = \angle CBP, & \gamma_1 = \angle ACP, \\ \alpha_2 = \angle PAC, & \beta_2 = \angle PBA, & \gamma_2 = \angle PCB, \end{array}$$

as in figure 5. Finally, we use standard notation for triangle sidelengths and angles:

$$a = |BC|, \;\; b = |CA|, \;\; c = |AB|, \;\; \alpha = \angle BAC, \;\; \beta = \angle CBA, \;\; \gamma = \angle ACB.$$

The following theorem gives two simple relations that enable us to locate such point P in the plane. The first relation is in terms of distances from triangle vertices, while the second one is in terms of the angles defined above.

Theorem 2. *If P is a point inside triangle ABC such that $\vec{E}(P) = \vec{0}$, then*

$$\left(\frac{r_B + r_C - a}{r_B + r_C + a}\right)^{1/a} = \left(\frac{r_C + r_A - b}{r_C + r_A + b}\right)^{1/b} = \left(\frac{r_A + r_B - c}{r_A + r_B + c}\right)^{1/c} \qquad (6)$$

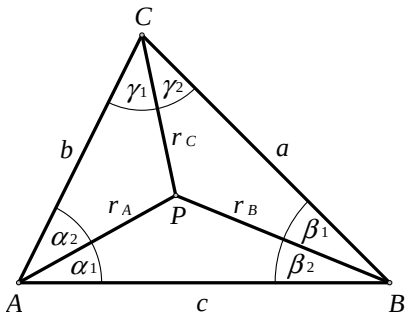

Figure 5. Convenient notation.

and

$$\left(\tan\frac{\beta_1}{2}\tan\frac{\gamma_2}{2}\right)^{\frac{1}{\sin\alpha}} = \left(\tan\frac{\gamma_1}{2}\tan\frac{\alpha_2}{2}\right)^{\frac{1}{\sin\beta}} = \left(\tan\frac{\alpha_1}{2}\tan\frac{\beta_2}{2}\right)^{\frac{1}{\sin\gamma}}. \quad (7)$$

In particular, equations (6) and (7) hold for the maximum point of potential V.

Proof. Take P to be the origin of the coordinate system and change to polar coordinates. Let us denote by M_φ the point at the intersection of the polar ray determined by an angle $\varphi \in [0, 2\pi)$ with the boundary of $\triangle ABC$. Furthermore, let us write $R(\varphi) = |PM_\varphi|$. For $\varepsilon > 0$ small enough formula (3) becomes

$$\begin{aligned}\vec{E}(P) &= -\int_\varepsilon^{R(\varphi)}\int_0^{2\pi} \frac{r(\cos\varphi)\vec{i} + r(\sin\varphi)\vec{j}}{r^3}\, r dr d\varphi \\ &= -\int_0^{2\pi} \big(\log R(\varphi) - \log\varepsilon\big)\Big((\cos\varphi)\vec{i} + (\sin\varphi)\vec{j}\Big) d\varphi\end{aligned}$$

and then using $\int_0^{2\pi}\cos\varphi\, d\varphi = 0 = \int_0^{2\pi}\sin\varphi\, d\varphi$ we get

$$\vec{E}(P) = -\int_0^{2\pi} \log R(\varphi)\,\Big((\cos\varphi)\vec{i} + (\sin\varphi)\vec{j}\Big) d\varphi.$$

For the rest of the proof it will be convenient to represent vectors by complex numbers, i.e. to work in the complex plane. Using $e^{i\varphi} = \cos\varphi + i\sin\varphi$ the condition $\vec{E}(P) = \vec{0}$ becomes simply

$$\int_0^{2\pi} \log R(\varphi)\, e^{i\varphi} d\varphi = 0. \quad (8)$$

The next step is to find an expression for $\log R(\varphi)$. Let vertices A, B, C have complex coordinates

$$r_A e^{i\varphi_A}, r_B e^{i\varphi_B}, r_C e^{i\varphi_C}$$

and let vectors $\overrightarrow{CB}, \overrightarrow{AC}, \overrightarrow{BA}$ be represented by complex numbers

$$a e^{i\theta_a}, b e^{i\theta_b}, c e^{i\theta_c}.$$

Without loss of generality suppose that M_φ lies on side AB of $\triangle ABC$, which is the same as saying $\varphi_A < \varphi < \varphi_B$, where we possibly need to adjust the angles by adding appropriate multiples of 2π. Let d_c denote the distance from P to the line AB and let ψ denote the angle $\angle BM_\varphi P$. From figure 6 we see that $\psi = \varphi - \varphi_A + \alpha_1$ and $R(\varphi) = d_c/\sin\psi$, i.e.

$$\log R(\varphi) = \log d_c - \log\sin\psi.$$

Observing that ψ ranges from α_1 to $\pi - \beta_2$ we get

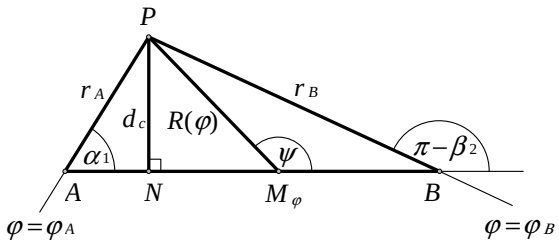

Figure 6. Discussion of the range $\varphi_A < \varphi < \varphi_B$.

$$\int_{\varphi_A}^{\varphi_B} \log R(\varphi)\, e^{i\varphi} d\varphi = \log d_c \int_{\varphi_A}^{\varphi_B} e^{i\varphi} d\varphi - \int_{\alpha_1}^{\pi-\beta_2} (\log\sin\psi)\, e^{i(\psi+\varphi_A-\alpha_1)} d\psi.$$

First, we use an immediate formula

$$\int_\eta^\vartheta e^{i\varphi} d\varphi = \big(-ie^{i\varphi}\big)\Big|_{\varphi=\eta}^{\varphi=\vartheta}. \tag{9}$$

Next, it is an easy exercise in integration by parts to obtain

$$\int_\eta^\vartheta (\log\sin\psi)\cos\psi\, d\psi = \Big(\big(\log\sin\psi - 1\big)\sin\psi\Big)\Big|_{\psi=\eta}^{\psi=\vartheta}$$

and

$$\int_\eta^\vartheta (\log\sin\psi)\sin\psi\, d\psi = \Big(-\big(\log\sin\psi - 1\big)\cos\psi + \log\tan\tfrac{\psi}{2}\Big)\Big|_{\psi=\eta}^{\psi=\vartheta}$$

for angles $0 < \eta < \vartheta < \pi$. Combining we get

$$\int_\eta^\vartheta (\log\sin\psi) e^{i\psi} d\psi = \Big(-i\big(\log\sin\psi - 1\big)e^{i\psi} + i\log\tan\tfrac{\psi}{2}\Big)\Big|_{\psi=\eta}^{\psi=\vartheta}. \tag{10}$$

From formulas (9), (10) we obtain

$$\begin{aligned}\int_{\varphi_A}^{\varphi_B} \log R(\varphi)\, e^{i\varphi} d\varphi = {} & -i\log d_c\, e^{i\varphi_B} + i\log d_c\, e^{i\varphi_A} \\ & + ie^{i(\varphi_A-\alpha_1+\pi-\beta_2)}(\log\sin\beta_2 - 1) - ie^{i\varphi_A}(\log\sin\alpha_1 - 1) \\ & - ie^{i(\varphi_A-\alpha_1)}\log\tan\tfrac{\pi-\beta_2}{2} + ie^{i(\varphi_A-\alpha_1)}\log\tan\tfrac{\alpha_1}{2},\end{aligned}$$

and then using

$$d_c/\sin\alpha_1 = r_A,\ \ d_c/\sin\beta_2 = r_B,\ \ \varphi_A-\alpha_1+\pi-\beta_2 = \varphi_B,\ \ \varphi_A-\alpha_1 = \theta_c$$

we get

$$\int_{\varphi_A}^{\varphi_B} \log R(\varphi)\, e^{i\varphi} d\varphi = -ie^{i\varphi_B}(\log r_B - 1) + ie^{i\varphi_A}(\log r_A - 1) + ie^{i\theta_c}\big(\log\tan\tfrac{\alpha_1}{2} - \log\cot\tfrac{\beta_2}{2}\big).$$

Adding this one and the two analogous relations, applying (8), and observing cancellations of $ie^{i\varphi_A}(\log r_A - 1)$ and the two alike terms gives

$$e^{i\theta_c}\log(\tan\tfrac{\alpha_1}{2}\tan\tfrac{\beta_2}{2}) + e^{i\theta_a}\log(\tan\tfrac{\beta_1}{2}\tan\tfrac{\gamma_2}{2}) + e^{i\theta_b}\log(\tan\tfrac{\gamma_1}{2}\tan\tfrac{\alpha_2}{2}) = 0.$$

We can interpret this using vectors once again as

$$\frac{\log(\tan\frac{\alpha_1}{2}\tan\frac{\beta_2}{2})}{c}\overrightarrow{BA} + \frac{\log(\tan\frac{\beta_1}{2}\tan\frac{\gamma_2}{2})}{a}\overrightarrow{CB} + \frac{\log(\tan\frac{\gamma_1}{2}\tan\frac{\alpha_2}{2})}{b}\overrightarrow{AC} = \vec{0}.$$

Next, we claim that

$$\tfrac{1}{c}\log(\tan\tfrac{\alpha_1}{2}\tan\tfrac{\beta_2}{2}) = \tfrac{1}{a}\log(\tan\tfrac{\beta_1}{2}\tan\tfrac{\gamma_2}{2}) = \tfrac{1}{b}\log(\tan\tfrac{\gamma_1}{2}\tan\tfrac{\alpha_2}{2}). \qquad (11)$$

To see (11) one only has to observe $\overrightarrow{AC} = -\overrightarrow{BA} - \overrightarrow{CB}$ and make use of linear independence of $\overrightarrow{BA}$ and $\overrightarrow{CB}$. If we apply the law of sines and exponentiate (11), we will complete the proof of (7).

In order to derive (6), we use trigonometric half-angle formulas, the law of cosines, and some factoring:

$$\tan^2\frac{\alpha_1}{2} = \frac{1-\cos\alpha_1}{1+\cos\alpha_1} = \frac{1-(r_A^2+c^2-r_B^2)/2r_Ac}{1+(r_A^2+c^2-r_B^2)/2r_Ac} = \frac{(r_A+r_B-c)(r_B-r_A+c)}{(r_A+r_B+c)(r_A-r_B+c)}.$$

Multiplying this one with an analogous expression for $\tan\frac{\beta_2}{2}$ and taking square roots gives

$$\tan\frac{\alpha_1}{2}\tan\frac{\beta_2}{2} = \frac{r_A+r_B-c}{r_A+r_B+c},$$

so that (11) becomes

$$\frac{1}{c}\log\Big(\frac{r_A+r_B-c}{r_A+r_B+c}\Big) = \frac{1}{a}\log\Big(\frac{r_B+r_C-a}{r_B+r_C+a}\Big) = \frac{1}{b}\log\Big(\frac{r_C+r_A-b}{r_C+r_A+b}\Big). \qquad (12)$$

Exponentiation proves relation (6). □

4. Cartesian coordinates

Here we address the problem of determining the coordinates of P, given the coordinates of triangle vertices. The starting point are equalities (6), i.e. their logarithmic version (12). It is easy to see that these expressions are less than 0, so it is natural to consider their negatives. Multiply them further by the semiperimeter $s = \frac{1}{2}(a+b+c)$ of triangle ABC in order to make them "dimensionless" and denote the obtained common value by λ:

$$-\frac{s}{a}\log\Big(\frac{r_B+r_C-a}{r_B+r_C+a}\Big) = -\frac{s}{b}\log\Big(\frac{r_C+r_A-b}{r_C+r_A+b}\Big) = -\frac{s}{c}\log\Big(\frac{r_A+r_B-c}{r_A+r_B+c}\Big) = \lambda.$$

Concentrating on only one expression at a time, we can now write

$$\frac{r_B + r_C - a}{r_B + r_C + a} = e^{-a\lambda/s},$$

so that

$$r_B + r_C = a\,\frac{1 + e^{-a\lambda/s}}{1 - e^{-a\lambda/s}} = a\,\frac{e^{a\lambda/2s} + e^{-a\lambda/2s}}{e^{a\lambda/2s} - e^{-a\lambda/2s}} = a\coth\tfrac{a\lambda}{2s}$$

and similarly

$$r_C + r_A = b\coth\tfrac{b\lambda}{2s}, \quad r_A + r_B = c\coth\tfrac{c\lambda}{2s}.$$

Let us agree to write

$$u = a\coth\tfrac{a\lambda}{2s}, \;\; v = b\coth\tfrac{b\lambda}{2s}, \;\; w = c\coth\tfrac{c\lambda}{2s} \tag{13}$$

in all that follows. Hence,

$$r_A = \frac{1}{2}(v + w - u), \;\; r_B = \frac{1}{2}(w + u - v), \;\; r_C = \frac{1}{2}(u + v - w). \tag{14}$$

Now is the time to observe that the distances r_A, r_B, r_C are not independent. The simplest equation relating them can be derived from

$$\text{area}(\triangle PBC) + \text{area}(\triangle PCA) + \text{area}(\triangle PAB) = \text{area}(\triangle ABC)$$

using Heron's formula:

$$\begin{aligned}&\sqrt{s_a(s_a - a)(s_a - r_B)(s_a - r_C)} + \sqrt{s_b(s_b - b)(s_b - r_C)(s_b - r_A)}\\ &+ \sqrt{s_c(s_c - c)(s_c - r_A)(s_c - r_B)} = \sqrt{s(s - a)(s - b)(s - c)},\end{aligned}$$

with s_a, s_b, s_c, s being semiperimeters of the the four triangles respectively. Substituting (14), multiplying by 4, and simplifying we obtain

$$\begin{aligned}&\sqrt{(u^2 - a^2)\big(a^2 - (v - w)^2\big)} + \sqrt{(v^2 - b^2)\big(b^2 - (w - u)^2\big)}\\ &+ \sqrt{(w^2 - c^2)\big(c^2 - (u - v)^2\big)} = \sqrt{2(a^2b^2 + b^2c^2 + c^2a^2) - (a^4 + b^4 + c^4)}.\end{aligned} \tag{15}$$

This is a nonlinear equation for λ and then r_A, r_B, r_C are determined by (13) and (14).

It remains to explain how to express coordinates of $P(x_P, y_P)$ from its distances to triangle vertices $A(x_A, y_A)$, $B(x_B, y_B)$, $C(x_C, y_C)$. Using the formula for Euclidean distance in Cartesian coordinates we get an overdetermined quadratic system for x_P and y_P,

$$\begin{aligned}(x_P - x_A)^2 + (y_P - y_A)^2 &= r_A^2,\\ (x_P - x_B)^2 + (y_P - y_B)^2 &= r_B^2,\\ (x_P - x_C)^2 + (y_P - y_C)^2 &= r_C^2.\end{aligned}$$

Subtracting the third equation from the first two leads to a linear system

$$\begin{aligned}2(x_C - x_A)x_P + 2(y_C - y_A)y_P &= x_C^2 - x_A^2 + y_C^2 - y_A^2 + v(w - u),\\ 2(x_C - x_B)x_P + 2(y_C - y_B)y_P &= x_C^2 - x_B^2 + y_C^2 - y_B^2 + u(w - v),\end{aligned}$$

which can be quickly solved as

$$x_P = \frac{(x_A^2+y_A^2-vw)(y_B-y_C)+(x_B^2+y_B^2-wu)(y_C-y_A)+(x_C^2+y_C^2-uv)(y_A-y_B)}{2x_A(y_B-y_C)+2x_B(y_C-y_A)+2x_C(y_A-y_B)}, \tag{16}$$

$$y_P = \frac{(x_A^2+y_A^2-vw)(x_B-x_C)+(x_B^2+y_B^2-wu)(x_C-x_A)+(x_C^2+y_C^2-uv)(x_A-x_B)}{2y_A(x_B-x_C)+2y_B(x_C-x_A)+2y_C(x_A-x_B)}. \tag{17}$$

That way we have established the following theorem.

Theorem 3. *Suppose that P is a point inside $\triangle ABC$ satisfying $\vec{E}(P) = \vec{0}$. Its Cartesian coordinates satisfy* (16) *and* (17)*, where u, v, w are defined by* (13) *and $\lambda > 0$ is a solution of equation* (15)*.*

Turning back to equation (15), we might want to know the number of its positive solutions. We claim that the left-hand side is a strictly decreasing function of $\lambda \in (0, \infty)$. Since

$$\lambda \mapsto u^2 - a^2 = a^2\big(\coth^2 \tfrac{a\lambda}{2s} - 1\big)$$

is obviously strictly decreasing, it remains to show that

$$\lambda \mapsto |v - w| = \big|b \coth \tfrac{b\lambda}{2s} - c \coth \tfrac{c\lambda}{2s}\big|$$

increases and that its values stay below a. Without loss of generality suppose $b \geq c$. It is an easy calculus exercise to see that $t \mapsto t \coth t$ is increasing, so the expression inside the last modulus is always positive. Define

$$g(t) = b \coth bt - c \coth ct,$$

so that

$$g'(t) = -\frac{b^2}{\sinh^2 bt} + \frac{c^2}{\sinh^2 ct}.$$

Inequality $g'(t) \geq 0$ is equivalent with

$$\frac{\sinh bt}{b} \geq \frac{\sinh ct}{c},$$

which can also be verified easily, using the fact that $t \mapsto (\sinh t)/t$ increases. Finally, we observe that

$$\lim_{t\to\infty} g(t) = b - c < a,$$

by the triangle inequality.

Therefore, (15) can have at most one positive solution λ, which combines nicely with theorem 3 to prove the fact that there can be only one point P inside T such that $\vec{E}(P) = \vec{0}$. This leads us to the promised result on uniqueness of the maximum point for V.

From now on we denote this unique maximum potential point by $P_{\max}(x_{\max}, y_{\max})$. One could name it the *electrostatic center* of T, although the term *gravitational center* has already been used in the literature [3], [4] in the study of general convex bodies in $\mathbb{R}^n$. When we actually want to solve equation (15) for λ, we do not know how to do it analytically, so we need to use numerical techniques. For instance, by taking $A(-1, 0)$, $B(2, 0)$, and $C(0, 2)$ we get

$$\lambda_{\max} = 4.010297202743007522718690055346\ldots,$$

and then from (16) and (17),

$$\begin{aligned} x_{\max} &= 0.272557906914867702024319226991\ldots, \\ y_{\max} &= 0.704148189723077020171531030875\ldots. \end{aligned}$$

Even though equation (15) does not seem to be solvable in terms of elementary functions, we do not really have a rigorous proof of this fact.

Open problem 1. *Is it possible to express the Cartesian coordinates of $P_{\max}$ (or equivalently its parameter $\lambda_{\max}$) as elementary functions of triangle sides a, b, c?*

If one desires to write the coordinates of $P_{\max}$ as explicitly as possible, it will perhaps be easier to do so using a series expansion. We still require that each term of the series is given by an elementary formula.

Open problem 2. *Is it possible to express the Cartesian coordinates of $P_{\max}$ as two convergent series, $x_{\max} = \sum_{n=1}^{\infty} x_n$ and $y_{\max} = \sum_{n=1}^{\infty} y_n$, where both x_n and y_n are elementary functions of a, b, c, and n?*

Our desire to obtain a series expansion is motivated by a common practice in theoretical physics. We have to remark once again that numerical schemes for solving (15) actually do lead to approximations of $x_{\max}$ and $y_{\max}$ by sequences or series. However, in that case $(x_n)_{n=1}^{\infty}$ and $(y_n)_{n=1}^{\infty}$ are defined recursively, still without giving us a single explicit formula that would hold for each n.

Equation (15) seems to be a transcendental one, but at least the four square roots can be eliminated by squaring the equality three times. We do not write down the result of this procedure as it involves more complicated expressions.

5. Trilinear coordinates

The point $P_{\max}$ deserves to be called a triangle center, as purely physical reasons suggest that it always occupies the same relative position in any member of a family of mutually similar triangles. However, the notion of triangle center was rigorously defined in [6]. Let us begin by introducing a convenient choice of relative homogeneous coordinates with respect to a given triangle ABC. *Trilinear coordinates* of a point P inside $\triangle ABC$ are any real numbers $\tau_a : \tau_b : \tau_c$ such that

$$\frac{\tau_a}{d_a} = \frac{\tau_b}{d_b} = \frac{\tau_c}{d_c},$$

where d_a, d_b, d_c are (directed) distances from P to triangle sides BC, CA, AB respectively. Equivalently, $a\tau_a : b\tau_b : c\tau_c$ are the barycentric coordinates of P.

A real valued function f defined on the set of all possible triples of triangle side lengths (a, b, c) is called a *triangle center function* if it has the following properties.

- There exists a real constant ν such that $f(ta, tb, tc) = t^{\nu} f(a, b, c)$ for $t > 0$, i.e. f is homogeneous of order ν.
- Equality $f(a, c, b) = f(a, b, c)$ holds for any triple in the domain of f.
- f is not identically 0.

A *triangle center* associated to f is then the point given by trilinear coordinates

$$f(a, b, c) : f(b, c, a) : f(c, a, b). \tag{18}$$

We need to remark that the same center can be associated to many different center functions f.

What can we say about our point $P_{\max}$? Calculations from the previous section immediately give

$$\frac{\tau_a}{\tau_b} = \frac{\text{area}(\triangle PBC)/a}{\text{area}(\triangle PCA)/b} = \frac{\sqrt{((u/a)^2-1)(a^2-(v-w)^2)}}{\sqrt{((v/b)^2-1)(b^2-(w-u)^2)}},$$

so we see that a good choice of triangle center function for $P_{\max}$ is

$$f(a,b,c) = \sqrt{\Big(\coth^2\tfrac{a\lambda_{\max}}{a+b+c}-1\Big)\Big(a^2-\big(b\coth\tfrac{b\lambda_{\max}}{a+b+c}-c\coth\tfrac{c\lambda_{\max}}{a+b+c}\big)^2\Big)},$$

where $\lambda_{\max}$ is the unique positive solution to (15). Also, f obviously fulfills all three requirements above (with $\nu=1$). One only has to observe that $\lambda_{\max}$ remains the same if the triangle is scaled by a factor t. This proves the announced assertion that $P_{\max}$ is a non-trivial triangle center.

All interesting triangle centers are being collected systematically in C. Kimberling's encyclopedia [7], which contains 5622 entries $X(1)$–$X(5622)$ at the moment of writing of this paper. Trilinear coordinates are given for these characteristic points, justifying their worth to be mentioned. In order to detect new centers, the encyclopedia also offers the search among the existing ones using the numerical value of

$$d_a = \text{dist}(P, BC) = \frac{2\tau_a \text{area}(ABC)}{a\tau_a + b\tau_b + c\tau_c}$$

in the particular case of triangle with sides $a=6$, $b=9$, $c=13$. For point $P_{\max}$ it is now easy to compute this value to 30 decimal digits:

$$d_a = 2.11073179669028917745983688818 2\ldots$$

and realize that it does not appear in the list.

Trilinear coordinates for $P_{\max}$ are implicit due to the fact that $\lambda_{\max}$ is not explicitly given. Just in the case that the first open problem we stated turns out to have a positive answer, it will be interesting to see if the trilinear coordinates can be algebraic functions of triangle sides. Once again we are quite sceptical about that possibility.

Open problem 3. *Prove that $P_{\max}$ is a transcendental triangle center, i.e. it does not have a trilinear representation* (18)*, with f being an algebraic function of a, b, c.*

6. Approximation for the parameter

It remains to say a few words on estimation of $\lambda_{\max}$. Equation (15) degenerates for an equilateral triangle simply to

$$3a^2\sqrt{\coth^2\tfrac{\lambda}{3}-1} = a^2\sqrt{3},$$

which is easily solved as $\lambda_0 = 3\log(2+\sqrt{3})$. An interesting fact we obtained "experimentally" is that the exact value of $\lambda_{\max}$ for a general triangle ABC is "quite correlated" with the quantity

$$\log\frac{s^2}{27\rho^2} = \log\frac{s^3}{27(s-a)(s-b)(s-c)} \geq 0,$$

where ρ is radius of the inscribed circle. Figure 7 sketches graph of the ratio of $\lambda_{\max} - \lambda_0$ and this quantity as a function of two angles α and β. It is obtained

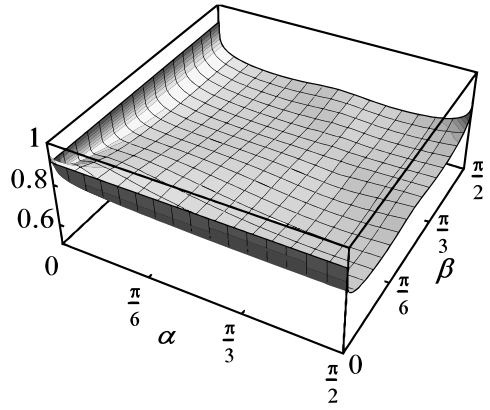

Figure 7. Ratio of $\lambda_{\max} - \lambda_0$ and $\log(s^2/27\rho^2)$.

using Plot3D command in Mathematica [14]. Note that it is enough to restrict the domain to $0 < \alpha, \beta < \pi/2$, because every triangle has at least two acute angles. The figure illustrates that the ratio is always between (say) $1/2$ and 1, although we have not established such inequalities rigorously. The moral of this remark could be that there are some wise choices of the initial approximation to λ when solving (15) numerically.

Another interesting observation is related to formulas (13), (16), and (17) for Cartesian coordinates of point P. If we now "free" the variable λ and treat it simply as a parameter that runs over interval $(0,\infty)$, then the point P traces some planar curve. Each specific choice of λ theoretically corresponds to a triangle center. It is easy to find limiting positions of P as $\lambda \to 0$ and $\lambda \to \infty$. These are respectively the centroid $X(2)$ and the incenter $X(1)$.

7. Related results

An interesting problem is to investigate extreme points of more general convolution potentials, such as (5) for parameter p taking values other than -1, and some of that work has been done by O'Hara [10] following "experimental speculations" by Shibata [13]. It is well-known that for $p = 2$ we obtain the centroid $X(2)$ and the case $p = -2$ will be discussed below. It seems that all other choices of p lead to unnamed triangle centers and it is not clear which of them satisfy any reasonably nice relations.

Observe that the integral in (5) diverges for $p \leq -2$. One can still define potential difference between two interior points, simply by cutting out small congruent disks around those points. More precisely, the expression

$$V_p(P) - V_p(P') = \iint_{T \setminus \mathrm{D}_\varepsilon(P)} |PQ|^p d\lambda(Q) - \iint_{T \setminus \mathrm{D}_\varepsilon(P')} |P'Q|^p d\lambda(Q)$$

is well-defined for interior points P, P' and $\varepsilon > 0$ small enough, and determines function V_p up to an additive constant. Our definition is a simpler alternative to the more common approach of subtracting the singular part from the limit as $\varepsilon \to 0$, as is done in [10].

Let us only comment on the case $p = -2$, as it is also quite interesting and has already appeared in the literature. Shibata [13] considered the problem of choosing the position of a street lamp in a triangular park, in a way that it maximizes the total brightness of the park. He further reformulates the problem as finding the maximum point of the potential V_{-2} and names it the *illuminating center* of T. Geometrical characterization of such point P inside $\triangle ABC$ that was given in [13] can be restated as

$$\frac{\angle BPC}{\text{area}(\triangle BPC)} = \frac{\angle CPA}{\text{area}(\triangle CPA)} = \frac{\angle APB}{\text{area}(\triangle APB)}.$$

Shibata's text does not contain a complete proof of this relation, so let us comment on how one can deduce it rather easily along the lines of previously presented results.

One can still derive a formula analogous to (8). Similarly as in §§2 and 3 we conclude that any stationary point P for V_{-2} in the interior of T now has to satisfy

$$\int_0^{2\pi} R(\varphi)^{-1} e^{i\varphi} d\varphi = 0. \tag{19}$$

Here we use the same notation as in the proof of Theorem 2. One then calculates

$$\begin{aligned}\int_{\varphi_A}^{\varphi_B} R(\varphi)^{-1} e^{i\varphi} d\varphi &= \int_{\alpha_1}^{\pi-\beta_2} \frac{\sin\psi}{d_c} e^{i(\psi+\varphi_A-\alpha_1)} d\psi \\ &= -\frac{ie^{i\varphi_B}}{4r_B} + \frac{ie^{i\varphi_A}}{4r_A} + \frac{e^{i\varphi_B}\cot\beta_2}{4r_B} + \frac{e^{i\varphi_A}\cot\alpha_1}{4r_A} - \frac{\angle APB}{2id_c} e^{i\theta_c},\end{aligned}$$

so that (19) gives

$$\begin{aligned}&\frac{e^{i\varphi_A}(\cot\alpha_1+\cot\alpha_2)}{4r_A} + \frac{e^{i\varphi_B}(\cot\beta_1+\cot\beta_2)}{4r_B} + \frac{e^{i\varphi_C}(\cot\gamma_1+\cot\gamma_2)}{4r_C} \\ &- \frac{\angle BPC}{2id_a} e^{i\theta_a} - \frac{\angle CPA}{2id_b} e^{i\theta_b} - \frac{\angle APB}{2id_c} e^{i\theta_c} = 0.\end{aligned}$$

Straightforward computation shows that the sum of the first three terms is 0 for just any point P, so the above equality becomes

$$\frac{\angle BPC}{d_a} e^{i\theta_a} + \frac{\angle CPA}{d_b} e^{i\theta_b} + \frac{\angle APB}{d_c} e^{i\theta_c} = 0,$$

i.e.

$$\frac{\angle BPC}{\text{area}(BPC)}\overrightarrow{CB}+\frac{\angle CPA}{\text{area}(CPA)}\overrightarrow{AC}+\frac{\angle APB}{\text{area}(APB)}\overrightarrow{BA}=\vec{0}.$$

It is easy to fill in the details.

References

[1] C. A. Brebbia and J. Dominguez, Boundary element methods for potential problems, *Appl. Math. Modelling*, 1 (1977) 372–378.

[2] I. Herburt, Location of radial centres of convex bodies, *Adv. Geom.*, 8 (2008) 309–313.

[3] I. Herburt, On the uniqueness of gravitational centre, *Math. Phys. Anal. Geom.*, 10 (2007) 251–259.

[4] I. Herburt, M. Moszyńska, and Z. Peradzyński, Remarks on radial centres of convex bodies, *Math. Phys. Anal. Geom.*, 8 (2005) 157–172.

[5] M. A. Jaswon, Integral equation methods in potential theory I, *Proc. Royal Soc. London*, series A 275 (1963) 23–32.

[6] C. Kimberling, Central Points and Central Lines in the Plane of a Triangle, *Math. Mag.*, 67 (1994) 163–187.

[7] C. Kimberling, *Encyclopedia of Triangle Centers*, `http://faculty.evansville.edu/ck6/encyclopedia/ETC.html`.

[8] P. Lazić, H. Štefančić, and H. Abraham, The Robin Hood method — A novel numerical method for electrostatic problems based on a non-local charge transfer, *J. Comput. Phys.*, 213 (2006) 117–140.

[9] M. Moszyńska, Looking for selectors of star bodies, *Geom. Dedicata*, 83 (2000) 131–147.

[10] J. O'Hara, Renormalization of potentials and generalized centers, *Adv. in Appl. Math.*, 48 (2012) 365–392.

[11] M. Riesz, L'intégrale de Riemann-Liouville et le problème de Cauchy, *Acta Math.*, 81 (1949) 1–223.

[12] F. J. Rizzo, An integral equation approach to boundary value problems of classical elastostatics, *Q. Appl. Math.*, 25 (1967) 83–95.

[13] K. Shibata, Where should a streetlight be installed in a triangular-shaped park?, `http://www1.rsp.fukuoka-u.ac.jp/kototoi/igi-ari-4_E.pdf`

[14] Wolfram Research, Inc., *Mathematica*, Version 9.0.1, Champaign, IL (2013).

Hrvoje Abraham: Artes Calculi, Derenčinova 1, 10000 Zagreb, Croatia
E-mail address: `ahrvoje@gmail.com`

Vjekoslav Kovač: University of Zagreb, Faculty of Science, Department of Mathematics, Bijenička cesta 30, 10000 Zagreb, Croatia
E-mail address: `vjekovac@math.hr`

Forum Geometricorum
Volume 15 (2015) 91–92.

FORUM GEOM
ISSN 1534-1178

The Golden Section in the Inscribed Square of an Isosceles Right Triangle

Tran Quang Hung

Abstract. We prove the occurrence of the golden section with the inscribed square of an isosceles right triangle on its hypotenuse and its circumcircle.

Given a right isosceles triangle ABC and its circumcircle, inscribed a square $DEFG$ with a side FG along the hypotenuse AB. If the side DE is extended to intersect the circumcircle at P, then E divides DP in the golden ratio (see Figure 1). This is reminiscent of the golden section by Odom's construction [2]; see also [1].

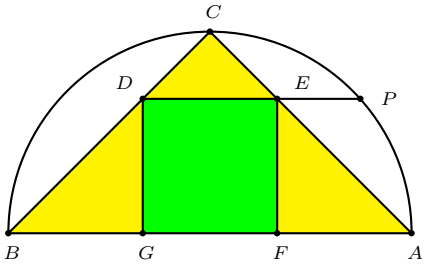

Figure 1

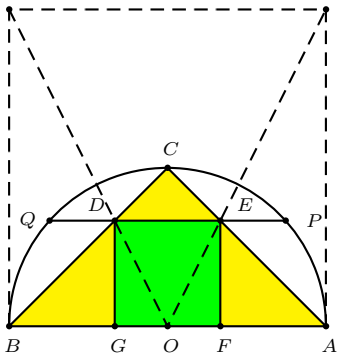

Figure 2

A simple construction of the inscribed square (see Figure 2) leads to a simple calculation giving the ratio $\frac{DP}{DE} = \frac{\sqrt{5}+1}{2}$, the golden ratio. We give a synthetic proof here.

From the similarity of the isosceles right triangles DEC and AEF, we have

$$\frac{DE}{EC} = \frac{AE}{EF} \implies DE^2 = DE \cdot EF = AE \cdot EC.$$

If the line DE intersects the circumcircle again at Q, then $EQ = DP$. By the intersecting chords theorem, $AE \cdot EC = PE \cdot EQ = PE \cdot DP$. Therefore, $DE^2 = EP \cdot DP$, and E divides DP in the golden ratio.

Publication Date: February 5, 2015. Communicating Editor: Paul Yiu.

References

[1] K. Hofstetter, A simple construction of the golden section, *Forum Geom.*, 2 (2002) 65–66.
[2] G. Odom and J. van de Craats, Elementary Problem 3007, *Amer. Math. Monthly*, 90 (1983) 482; solution, 93 (1986) 572.

Tran Quang Hung: High school for Gifted students, Hanoi University of Science, Vietnam National University, Hanoi, Vietnam
E-mail address: analgeomatica@gmail.com

Forum Geometricorum
Volume 15 (2015) 93–98.

FORUM GEOM
ISSN 1534-1178

Reflections on Poncelet's Pencil

Roger C. Alperin

Abstract. We illustrate properties of the conics in Poncelet's pencil using some new insights motivated by some elementary triangle constructions of García.

1. Introduction

The conics passing through the vertices A, B, C of a triangle and its orthocenter H is the Poncelet pencil; any conic of this pencil is an equilateral hyperbola. The isogonal transform of a line through the circumcenter O gives a conic of this pencil and conversely. We described this pencil in [1] and used it to solve some triangle constructions in [2].

Here is a brief review of some properties of the conics in this pencil. For a triangle Δ and an equilateral hyperbola $\mathcal{K}$ passing through the vertices of Δ, let $\mathcal{C}$ be the circumcircle of Δ and S the fourth point of intersection of these two conics. Let S' be the antipodal of S on $\mathcal{C}$. Let L be the line through O parallel to the Wallace-Simson line of S'. Then the isogonal transform of L is $\mathcal{K}$. The center of $\mathcal{K}$ is denoted Z. The nine point circle of any triangle on the equilateral hyperbola passes through Z since the same equilateral hyperbola serves for any triangle on it.

García [4] has recently introduced some elementary triangle constructions which we will use to give some alternate constructions of some of the data of the conics in the Poncelet pencil. This provides some new insights into the properties of the conics in Poncelet's pencil.

2. Review of García's results and some extensions

Consider triangle $\Delta = \Delta ABC$; symmetries of a point P in the midpoints of Δ gives $\Delta_1 = \Delta_1(P)$ with vertices A_1, B_1, C_1. A second triangle $\Delta_2 = \Delta_2(P)$ is constructed with vertices A_2, B_2, C_2 which are the reflections of the vertices of Δ_1 in corresponding sides of triangle Δ (see Figure 1).

We review García's Theorems and develop some useful corollaries.

The triangles Δ and Δ_1 have centroids G and G_1.

Let Z be obtained by application of the similarity $\sigma = \sigma_{G,-\frac{1}{2}}$ (centered at G with scale factor $-\frac{1}{2}$) to P.

Theorem 1 (García)**.** *Triangle Δ_1 is a symmetry of Δ about Z.*

Corollary 2. *The points P, G, Z, G_1 lie on a line.*

Proof. σ transforms P to Z, so P, Z, G lie on a line. Then also G_1 lies on this line since it is a symmetry about Z of G. □

Publication Date: April 8, 2015. Communicating Editor: Paul Yiu.

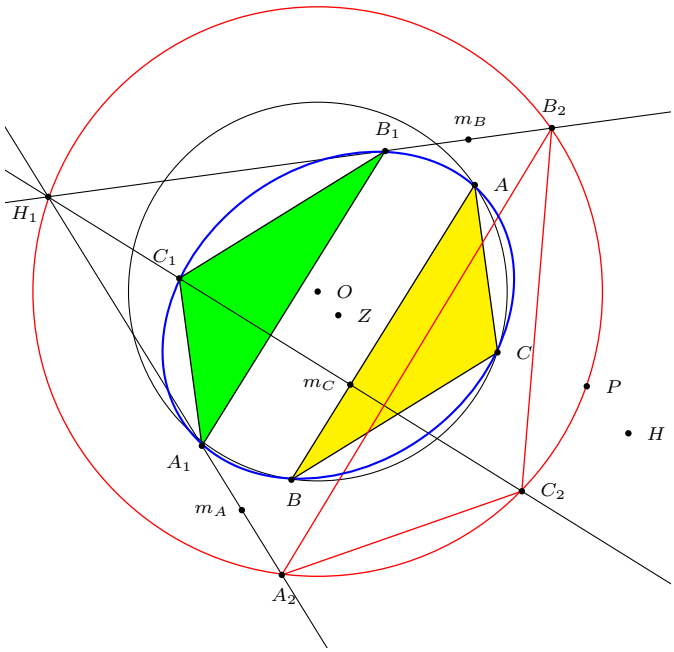

Figure 1. García's triangles and a conic

Theorem 3 (García)**.** *The point P lies on the circumcircle of Δ_2. The circumcenter of Δ_2 is O, the circumcenter of Δ.*

Corollary 4. *The orthocenter H_1 of Δ_1 is antipodal to P on the circumcircle of Δ_2.*

Proof. The two similarities $\sigma_{H,\frac{1}{2}}$, $\sigma_{G,-\frac{1}{2}}$ take the circumcircle of Δ to the circumcircle to the midpoint triangle Δ_m, hence $\sigma_{H,2}\sigma_{G,-\frac{1}{2}}$ preserves the circumcircle of Δ and hence its center O. Thus $\sigma_{H,2}\sigma_{G,-\frac{1}{2}} = \sigma_{O,-1}$.

Now evaluating both sides at P we get that $\sigma_{H,2}\sigma_{G,-\frac{1}{2}}(P) = \sigma_{H,2}(Z) = H_1$ is antipodal to P. □

Corollary 5. *Δ_2 and Δ_1 are in perspective from H_1.*

Proof. Since Δ_2 is obtained by reflection of the vertices of Δ_1 across the sides of Δ, which are parallel to the sides of Δ_1, then the altitudes of Δ_1 (concurrent at H_1) pass through the vertices of Δ_2. □

Corollary 6. *The midpoints of corresponding vertices of Δ_1 and Δ_2 lie on the corresponding sides of Δ.*

Proof. This follows immediately from the construction. □

2.1. *Similarity.*

Proposition 7. *Let H denote the orthocenter of Δ. Let $\mathcal{C}$ be a circle passing though H. The intersections of the altitudes of Δ with $\mathcal{C}$ give a triangle $\Delta' = \Delta_{\mathcal{C}}$ oppositely similar to Δ.*

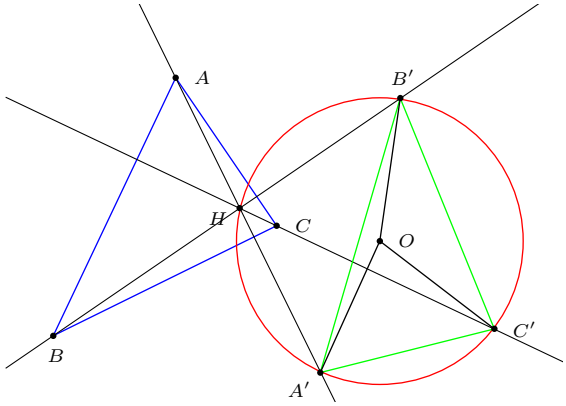

Figure 2. Similarity via H

Proof. The angles of Δ are related to the angles of Δ' via H and angles on $\mathcal{C}$ subtended at H. There are two angles at A formed by the altitude there and the adjacent sides. Consider the angle with side AC. This altitude passes through the vertex A' of Δ'. The altitude perpendicular to AC passes through B'. The angle formed by these altitudes at H is half the central angle of $A'B'$, which is the angle $OA'B'$. Similarly we can determine $OA'C'$. The sum of these two angles is $\angle A'$; using this we get the same sum as $\angle A$ since the altitudes through H are perpendicular to the adjacent sides at A. The argument is similar at the other vertices. □

Corollary 8. *Δ_2 and Δ_1 are similar with scale factor R_2/R_1.*

Proof. By Corollary 5 Δ_2 is in perspective with Δ_1 though H_1, with H_1 on the circumcircle of Δ_2; and by Proposition 7 Δ_2 is oppositely similar to Δ_1.

Using the formula for area $\frac{abc}{4R}$ in terms of the side lengths and circumradius then we easily deduce that the scale factor of the similarity is R_2/R_1. □

2.2. *A conic.*

Theorem 9. *The six points of Δ and Δ_1 lie on a conic $\mathcal{K} = \mathcal{K}_{\Delta,P}$ having center Z.*

Proof. Corresponding sides of the triangles meet on the line at infinity so an application of the converse of Pascal's Theorem shows that there is a conic passing through all six vertices. The point Z is the center of symmetry taking one triangle to the other; hence it must be the center of the conic. □

3. P lies on circumcircle of Δ

Corollary 10. *If P is on the circumcircle of Δ then Δ_2 is also on this circumcircle and is anti-congruent to Δ. The point H_1 is antipodal to P on the circumcircle of Δ.*

Proof. The circumcircle of Δ_2 has center O and passes through P so Δ_2 is also the circumcircle of Δ. The similarity factor is 1 by Corollary 8 so the two triangles are anti-congruent. This circumcircle also passes through H_1 using Theorem 3. □

Theorem 11. *Suppose P lies on the circumcircle of Δ then $\mathcal{K} = \mathcal{K}_{\Delta,P}$ is in Poncelet's pencil with circumcircle point H_1.*

Proof. Consider the conic passing through Δ, H and H_1. Then it is an equilateral hyperbola in Poncelet's pencil since H is on the conic. Since the conic also passes through H_1, then H_1 is the circumcircle point of this conic. Since both points H, H_1 are on the equilateral hyperbola then the midpoint Z is the center of the conic . Hence also Δ_1 is on the conic by Theorem 3. Thus the conic is $\mathcal{K}_{\Delta,P}$ by Bezout's Theorem [3]. □

Corollary 12. *As P varies on the circumcircle of Δ then the family of conics $\mathcal{K}_{\Delta,P}$ is Poncelet's pencil for Δ.*

Proof. Given a conic in Poncelet's pencil let P be the antipodal to its circumcircle point then by the Theorem above this conic is $\mathcal{K}_{\Delta,P}$. □

Corollary 13. *The conic $\mathcal{K}_{\Delta,P}$ is tangent to the circumcircle iff P is antipodal to a vertex of Δ.*

Proof. The circumcircle is tangent to $\mathcal{K}$ iff the circumcircle point H_1 is a vertex of the triangle iff (Corollary 4) P is antipodal to a vertex of Δ. □

Theorem 14. *Suppose P lies on the circumcircle of Δ. The reflections of P in the sides of Δ lie on a line M parallel to the line L, the isogonal transform of $\mathcal{K}_{\Delta,P}$. This line M is also parallel to the Wallace-Simson line of P and passes through H. Thus $L = \sigma_{G,-\frac{1}{2}}(M)$.*

Proof. This follows immediately from Corollary 7 of [2] since P is antipodal the circumcircle point H_1. The second and third statements follow from Theorems 5, 6 of [2]. Also since M passes through H, then $\sigma_{G,-\frac{1}{2}}(M)$ passes through O since $\sigma_{G,-\frac{1}{2}}(H) = O$ and thus $L = \sigma_{G,-\frac{1}{2}}(M)$. □

Theorem 15. *If P is on the circumcircle of Δ, then the midpoints of Δ_1 and Δ_2 lie on L_1, the Wallace-Simson line of H_1. The line L_1 passes through the center Z of $\mathcal{K}_{\Delta,P}$. The lines L_1 and L are perpendicular.*

Proof. As shown already in Corollary 6 and Corollary 5 these midpoints are on the sides of Δ and since the two triangles are congruent and in perspective from H_1 the midpoints are on the lines of perspectivity. But the vertices of Δ_2 are by definition the reflections of the vertices across the sides of Δ_1. Hence the midpoints are the

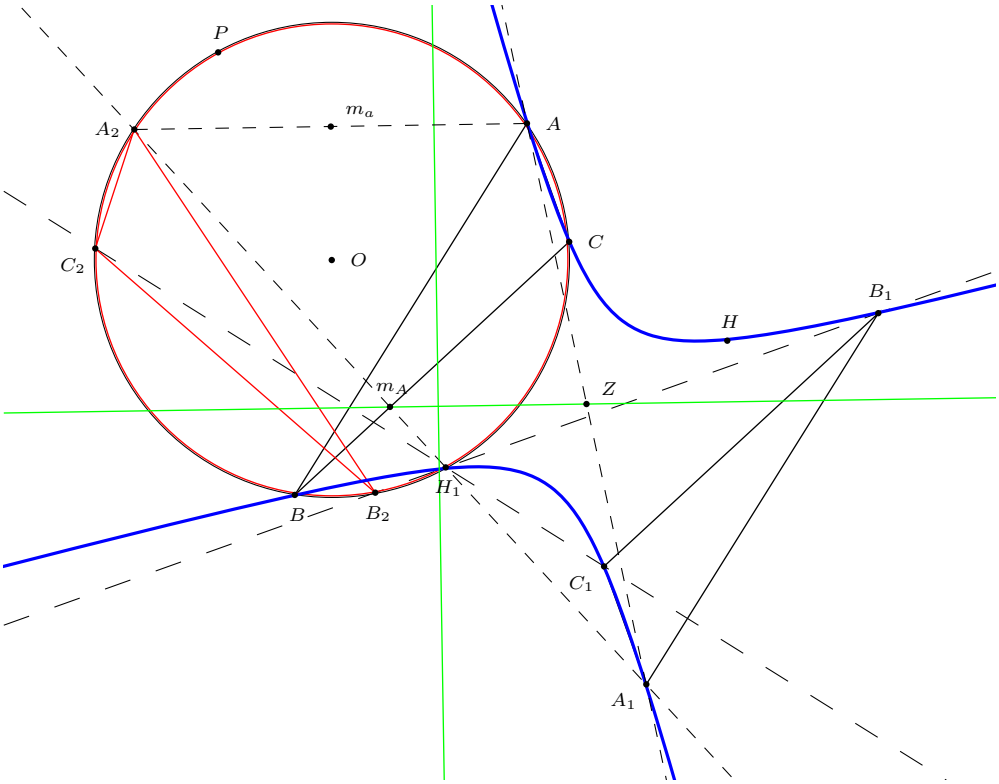

Figure 3. P on circumcircle equilateral hyperbola

feet of the altitudes from H_1 and lie on the Wallace-Simson line of H_1. Since H_1 is the circumcircle point of $\mathcal{K}_{\Delta,P}$ this line passes through Z, [2] Theorem 6. The Wallace-Simson lines of H_1 and P are perpendicular since these these points are antipodal. □

Theorem 16. *If P is on the circumcircle of Δ, then the midpoints of Δ and Δ_2 lie on line L.*

Proof. From point A_1 the midpoints to A and A_2 are on the line L_1. Thus the midpoint m_A of A and A_2 lies on a line parallel to L_1. Since Δ and Δ_2 lie on the circumcircle centered at O the perpendicular bisector of A and A_2 passes through O and is perpendicular to L_1. Thus m_A lies on L. The argument is similar for the other pairs of points and hence the desired result follows.. □

4. Equilateral triangles on equilateral hyperbolas

Proposition 17. *Suppose ΔABC is an equilateral triangle on the right hyperbola $\mathcal{K}$. The circumcircle meets $\mathcal{K}$ at the fourth intersection point S. The center of $\mathcal{K}$, Z, is the midpoint of OS where O is the circumcenter of Δ.*

Proof. Since Δ is equilateral $H = O$ and the result follows since Z is the midpoint of HS [2]. □

Proposition 18. *Let M be a line through Z the center of the equilateral hyperbola $\mathcal{K}$ meeting at points O and S. Construct a circle $\mathcal{C}$ with center at O and passing through S. The three intersections of $\mathcal{K}$ and $\mathcal{C}$ other than S give the vertices of an equilateral triangle Δ.*

Proof. By construction O is the circumcenter of Δ and S is the circumcircle point. In general the point Z is the midpoint of HS [2]. By our construction Z is the midpoint of OS so $H = O$. Thus the triangle is equilateral. □

References

[1] R. C. Alperin, The Poncelet pencil of rectangular hyperbolas, *Forum Geom.*, 10 (2010) 15–20.
[2] R. C. Alperin, Solving Euler's triangle problems with Poncelet's pencil, *Forum Geom.*, 11 (2011) 121–129.
[3] W. Fulton, *Algebraic Curves: An Introduction to Algebraic Geometry*, Benjamin, 1969.
[4] E. A. J. García, A note on reflections, *Forum Geom.*, 14 (2014) 155–161.

Roger C. Alperin: Department of Mathematics, San Jose State University, San Jose, CA 95192 USA

E-mail address: rcalperin@gmail.com

Forum Geometricorum
Volume 15 (2015) 99–103.

FORUM GEOM
ISSN 1534-1178

Bounds for Elements of a Triangle Expressed by R, r, and s

Temistocle Bîrsan

Abstract. Assume that a triangle is defined by the triple (R, r, s) fulfilling the conditions (1) and (2) (R - the circumradius, r - the inradius, s - the semiperimeter). We find some bounds for the trigonometric functions of the angles and for the sides of the triangle expressed by R and r (see the formulas (3) and (7) - (13)).

It is well-known that the positive numbers R, r, s may be the circumradius, the inradius, and, respectively, the semi-perimeter of a triangle if and only if these numbers satisfy Euler's inequality

$$R \geq 2r, \tag{1}$$

and the fundamental double inequality

$$\begin{aligned} &2R^2 + 10Rr - r^2 - 2\left(R - 2r\right)\sqrt{R^2 - 2Rr} \\ \leq\ & s^2 \leq 2R^2 + 10Rr - r^2 + 2\left(R - 2r\right)\sqrt{R^2 - 2Rr}. \end{aligned} \tag{2}$$

This double inequality was found in 1851 and it was subsequently rediscovered in many different forms. It often appears in the literature under the name of *Blundon's inequality*. A history of this inequality can be found in [2, pp.1–5].

In the following, we consider that the triangles are given by triples (R, r, s) that verify (1) and (2). The objective of this note is to find some bounds (expressed by R, r) for the sides and trigonometric functions of angles of the triangle. We recall a well-known result on the conditions in which the inequalities in (2) become equalities. There is a rich literature on this subject. In a recent short paper [1], we have presented a simple geometrical proof of Theorem 1 below.

We say that a triangle is wide-isosceles if it is isosceles with the base greater than or equal to the congruent sides, and is tall-isosceles if it is isosceles with the congruent sides greater than or equal to the base. The equilateral triangle is both wide-isosceles and tall-isosceles (see Figure 1).

Theorem 1. *In the fundamental double inequality,*
(a) *the first inequality is an equality if and only if the triangle is wide-isosceles;*
(b) *the second inequality is an equality if and only if the triangle is tall-isosceles;*
(c) *both inequalities are equalities if and only if the triangle is equilateral.*

We now state and prove our first result.

Publication Date: April 9, 2015. Communicating Editor: Paul Yiu.

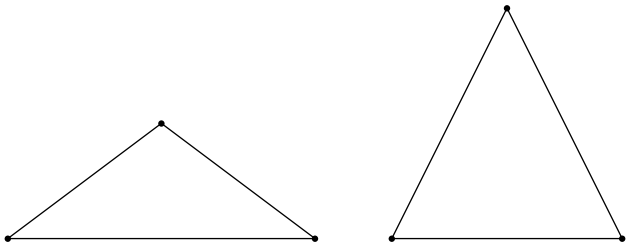

Figure 1

Proposition 2. *In any triangle ABC,*

$$\frac{1}{2}\left(1-\sqrt{1-\frac{2r}{R}}\right)\leq \sin\frac{A}{2}\leq \frac{1}{2}\left(1+\sqrt{1-\frac{2r}{R}}\right). \tag{3}$$

Moreover,
(a) *the first inequality is an equality if and only if the triangle is tall-isosceles;*
(b) *the second inequality is an equality if and only if the triangle is wide-isosceles;*
(c) *both inequalities are equalities if and only if the triangle is equilateral.*

Proof. Let O and I be the circumcenter and the incenter of the triangle ABC. Applying the triangle inequality for the triangle AOI, we have

$$AO-OI\leq AI\leq AO+OI. \tag{4}$$

The left-side of (4) is positive because I is contained in the circumcicle of triangle ABC. Taking into account the formulas $OA=R$, $OI^2=R^2-2Rr$, and $AI=\frac{r}{\sin\frac{A}{2}}$, we can write (4) in the form

$$R-\sqrt{R^2-2Rr}\leq \frac{r}{\sin\frac{A}{2}}\leq R+\sqrt{R^2-2Rr}$$

or

$$\frac{R-\sqrt{R^2-2Rr}}{2R}\leq \sin\frac{A}{2}\leq \frac{R+\sqrt{R^2-2Rr}}{2R}.$$

Therefore, the inequalities (3) are valid.

To prove the assertion (a) (resp. (b)) is equivalent to the fact that the right (respectively left) inequality of (4) becomes an equality if and only if the triangle ABC is tall-isosceles (respectively wide-isosceles).

(a) The equality $AI=AO+OI$ is equivalent with the fact that the triangle ABC is isosceles, with $AB=AC$, and O lying in the segment AI. Obviously, O and I coincide if and only if ABC is an equilateral triangle.

In the remaining case, we have $AO<AI$, i.e., $R<\frac{r}{\sin\frac{A}{2}}$. Let a and l denote the lengths of the base and congruent sides of the isosceles triangle. Then, using the formulas $4R\Delta=abc$ and $\Delta=rs$, we easily derive $R=\frac{l^2}{\sqrt{4l^2-a^2}}$, $r=\frac{a\sqrt{4l^2-a^2}}{2(2l+a)}$, and $\sin\frac{A}{2}=\frac{a}{2l}$. Consequently, we find that $R<\frac{r}{\sin\frac{A}{2}}$ is equivalent to $a<l$. Thus, in the second case the triangle ABC is tall-isosceles.

(b) If $AI = AO - OI$, then A, O, I are collinear and $I \in (AO]$. We proceed similarly. Again, we have to consider two cases. If O and I coincide, the triangle ABC is equilateral. If $I \in (AO)$,then $AO > AI$, and $R > \frac{r}{\sin\frac{A}{2}}$, i.e., $a > l$. In this case, ABC is wide-isosceles.

(c) follows from (a) and (b). □

We restate Proposition 2 in a symmetrical form.

Corollary 3. *In triangle ABC,*

$$\max\left(\sin\frac{A}{2}, \sin\frac{B}{2}, \sin\frac{C}{2}\right) \leq \frac{1}{2}\left(1 + \sqrt{1 - \frac{2r}{R}}\right), \tag{5}$$

$$\min\left(\sin\frac{A}{2}, \sin\frac{B}{2}, \sin\frac{C}{2}\right) \geq \frac{1}{2}\left(1 - \sqrt{1 - \frac{2r}{R}}\right). \tag{6}$$

Moreover,
(a) *equality holds in* (5) *if and only if the triangle is wide-isosceles;*
(b) *equality holds in* (6) *if and only if the triangle is tall-isosceles.*

Starting from (3), we shall obtain new inequalities by using appropriate formulas in trigonometry. Thus, we obtain from (3), after squaring and simplifying, the following inequalities:

$$\frac{1}{2}\left(1 - \frac{r}{R} - \sqrt{1 - \frac{2r}{R}}\right) \leq \sin^2\frac{A}{2} \leq \frac{1}{2}\left(1 - \frac{r}{R} + \sqrt{1 - \frac{2r}{R}}\right). \tag{7}$$

Also, taking into account the identity $\cos^2 t + \sin^2 t = 1$, we deduce that

$$\frac{1}{2}\left(1 + \frac{r}{R} - \sqrt{1 - \frac{2r}{R}}\right) \leq \cos^2\frac{A}{2} \leq \frac{1}{2}\left(1 + \frac{r}{R} + \sqrt{1 - \frac{2r}{R}}\right). \tag{8}$$

Because the left-side term in (8) is positive, it follows that

$$\frac{\sqrt{2}}{2}\sqrt{1 + \frac{r}{R} - \sqrt{1 - \frac{2r}{R}}} \leq \cos\frac{A}{2} \leq \frac{\sqrt{2}}{2}\sqrt{1 + \frac{r}{R} + \sqrt{1 - \frac{2r}{R}}}. \tag{9}$$

From (7) or (8), using the identities $2\sin^2\frac{A}{2} = 1 - \cos A$ or $2\cos^2\frac{A}{2} = 1 + \cos A$, we obtain the following inequalities:

$$\frac{r}{R} - \sqrt{1 - \frac{2r}{R}} \leq \cos A \leq \frac{r}{R} + \sqrt{1 - \frac{2r}{R}}. \tag{10}$$

Remark. As it is natural, the left-side term of (10) is not always positive. We have $\frac{r}{R} - \sqrt{1 - \frac{2r}{R}} \geq 0$ if and only if $r - \sqrt{R^2 - 2Rr} \geq 0$, that is $r \geq OI$. (Geometricaly, O is in the interior or on the incircle of the triangle ABC).

By using the double angle formula, we obtain from (3) and (9),

$$\frac{\sqrt{2}}{2}\left(1-\sqrt{1-\frac{2r}{R}}\right)\sqrt{1+\frac{r}{R}-\sqrt{1-\frac{2r}{R}}}$$
$$\leq \sin A \leq \frac{\sqrt{2}}{2}\left(1+\sqrt{1-\frac{2r}{R}}\right)\sqrt{1+\frac{r}{R}+\sqrt{1-\frac{2r}{R}}} \tag{11}$$

or, by squaring,

$$2-\frac{2r}{R}-\frac{r^2}{R^2}-2\sqrt{1-\frac{2r}{R}} \leq \sin^2 A \leq 2-\frac{2r}{R}-\frac{r^2}{R^2}+2\sqrt{1-\frac{2r}{R}}. \tag{12}$$

From (11) and (12), and taking into account the law of sines, we easily obtain upper bounds and lower bounds for the lengths of the sides. Thus, we have

$$8R^2-8Rr-4r^2-8R\sqrt{R^2-2Rr} \leq a^2 \leq 8R^2-8Rr-4r^2+8R\sqrt{R^2-2Rr}. \tag{13}$$

Because the inequality in previous section has been found by simple transformations of the inequalities (3), we can obtain the necessary and sufficient conditions for equality to occur in the inequalities (7) - (13) as immediate consequences of those specified in Proposition 2. Next we state some results along this order of ideas, leaving the details to the reader.

Proposition 4. (a) *Equality occurs in the first inequality of* (7) *if and only if triangle ABC is tall-isosceles.*
(b) *Equality occurs in the second inequality of* (7) *if and only if triangle ABC is wide-isosceles.*
(c) *Equality occurs in both cases if and only if triangle ABC is equilateral.*

Proposition 5. (a) *Equality occurs in the first inequality of* (8), (9), (10) *if and only if triangle ABC is wide-isosceles.*
(b) *Equality occurs in the second inequality of* (8), (9), (10) *if and only if triangle ABC is tall-isosceles.*
(c) *Equality occurs in both cases if and only if triangle ABC is equilateral.*

Proposition 6. *In each of the double inequalities* (11), (12) *and* (13), *equality occurs in one or both side if and only if the triangle is equilateral.*

Remarks. (1) We can formulate the inequalities (7) - (13) in a symmetrical form as we have made in Corollary 3 with the inequalities (3).

(2) Of course, one can obtain further inequalities by proceeding in the same way as above. But, it appears the risk of complicated expressions in R and r for the leftmost and rightmost sides of the derived inequalities. For example, using the formula $1+\tan^2 t = \cos^{-2} t$, it is possible to obtain some inequality for $\tan\frac{A}{2}$, $\tan A$ starting from (9), (10).

Finally, we turn our attention to the left-side of the inequalities (13), i.e., to the inequality

$$a^2 \geq 8R^2-8Rr-4r^2-8R\sqrt{R^2-2Rr}, \tag{14}$$

with equality if and only if ABC is equilateral.

If ABC is an acute triangle, this inequality can be improved. Indeed, by (10) we have

$$\cos A \leq \frac{r}{R} + \sqrt{1 - \frac{2r}{R}}.$$

In our hypothesis, $\cos A \gneqq 0$. Thus, after squaring we obtain

$$\sin^2 A \geq \frac{2r}{R} - \frac{r^2}{R^2} - 2\frac{r}{R}\sqrt{1 - \frac{2r}{R}}$$

or, equivalently,

$$a^2 \geq 8Rr - 4r^2 - 8r\sqrt{R^2 - 2Rr}. \tag{15}$$

As in (10), the equality in (15) holds if and only if the acute triangle ABC is tall-isosceles.

It is easy to see that (15) improves (14). Indeed, it is straightforward to verify that

$$8Rr - 4r^2 - 8r\sqrt{R^2 - 2Rr} \geq 8R^2 - 8Rr - 4r^2 - 8R\sqrt{R^2 - 2Rr},$$

as well as the fact that the equality sign holds only if ABC is equilateral. Consequently, apart from (14), the equality sign holds for (15) not only for equilateral triangles but also for tall-isosceles ones.

References

[1] T. Bîrsan, Blundon's double inequality revisited, *Recreaţii Matematice*, 14 (2012) 22–24 (in Romanian).

[2] D. S. Mitrinović, J. E. Pečarić, and V. Volenec, *Recent Advances in Geometric Inequalities*, Kluwer Academic Publishers, 1889.

Temistocle Bîrsan: Department of Mathematics and Informatics, "Gheorghe Asachi" Tehnical University, Iaşi, Romania

E-mail address: t_birsan@yahoo.com

Forum Geometricorum
Volume 15 (2015) 105–114.

FORUM GEOM
ISSN 1534-1178

Equilateral Triangles and Kiepert Perspectors in Complex Numbers

Dao Thanh Oai

Abstract. We construct two equilateral triangles associated with an arbitrary hexagon, and show that they are perspective.

1. Two equilateral triangles associated with a hexagon

Consider a hexagon $A_1A_2A_3A_4A_5A_6$ with equilateral triangles $B_jA_jA_{j+1}$ constructed on the six sides externally. Here we take the subscripts modulo 6. Let G_j be the centroid of triangle $B_jA_jA_{j+1}$. We first establish the following interesting result.

Theorem 1. *The midpoints of the segments G_1G_4, G_2G_5, G_3G_6 form an equilateral triangle.*

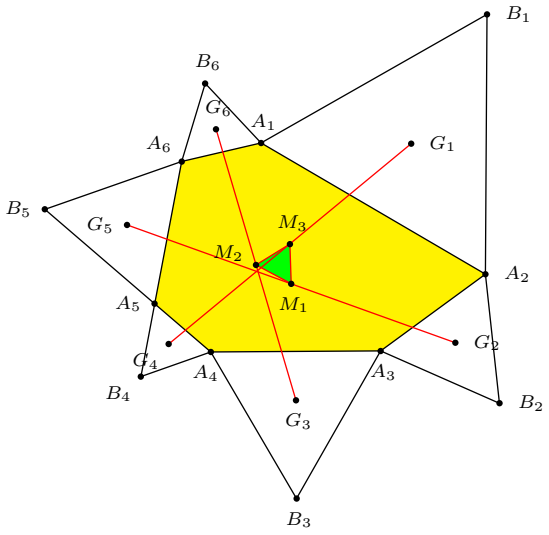

Figure 1.

We prove this theorem by using complex number coordinates of the points. Suppose the hexagon is in the complex plane. Each of the vertices A_j, $j = 1, 2, \ldots, 6$, has a complex affix α_j. We shall often simply identify a point with its complex

Publication Date: April 10, 2015. Communicating Editor: Paul Yiu.
The author thanks Dr. Paul Yiu for his help in the preparation of this paper.

affix. Throughout this note, ω denotes a complex cube root of unity. It satisfies $1+\omega+\omega^2=0$. The other complex cube root of unity is ω^2.

Lemma 2. (a) *A triangle with vertices z_1, z_2, z_3 is equilateral if and only if $z_1+\omega z_2+\omega^2 z_3=0$ for a complex cube root of unity ω.*

(b) *The center of an equilateral triangle with $\alpha_j\alpha_{j+1}$ as a side is γ_j, where*

$$(1-\omega)\gamma_j = -\omega\alpha_j+\alpha_{j+1}$$

for a complex cube root of unity ω.

Proof of Theorem 1. Let M_1, M_2, M_3 be the midpoints of G_2G_5, G_3G_6, G_1G_4 respectively. These have complex affixes $z_j=\frac{1}{2}(\gamma_{j+1}+\gamma_{j+4})$ for $j=1,2,3$. By Lemma 2(b),

$$\begin{aligned}
&2(1-\omega)(z_1+\omega^2 z_2+\omega z_3)\\
&=(1-\omega)((\gamma_2+\gamma_5)+\omega^2(\gamma_3+\gamma_6)+\omega(\gamma_4+\gamma_1))\\
&=(-\omega\alpha_2+\alpha_3)+(-\omega\alpha_5+\alpha_6)+\omega^2(-\omega\alpha_3+\alpha_4)\\
&\quad+\omega^2(-\omega\alpha_6+\alpha_1)+\omega(-\omega\alpha_4+\alpha_5)+\omega(-\omega\alpha_1+\alpha_2)\\
&=0.
\end{aligned}$$

Therefore, $z_1+\omega^2 z_2+\omega z_3=0$, and by Lemma 2(a), z_1, z_2, z_3 are the vertices of an equilateral triangle.

This completes the proof of Theorem 1.

By replacing ω by ω^2 in Lemma 2(b), we have an analogous result of Theorem 1 with the equilateral triangle constructed on the sides of the given hexagon internally. In other words, if for $j=1,2,\ldots,6$, G_j' is the reflection of G_j in the side A_jA_{j+1}, then the midpoints M_1' of $G_2'G_5'$, M_2' of $G_3'G_6'$, and M_3' of $G_1'G_4'$ also form an equilateral triangle (see Figure 2).

What is more interesting is that the two equilateral triangles $M_1M_2M_3$ and $M_1'M_2'M_3'$ are perspective. We shall prove this by explicitly computing the complex affix of the point of concurrency (Theorem 6 below).

Lemma 3. *The line joining α, β and the line joining γ, δ intersect at*

$$\theta=\frac{(\overline{\gamma}\delta-\overline{\delta}\gamma)(\alpha-\beta)-(\overline{\alpha}\beta-\overline{\beta}\alpha)(\gamma-\delta)}{(\overline{\gamma-\delta})(\alpha-\beta)-(\overline{\alpha-\beta})(\gamma-\delta)}.$$

Proof. Note that the denominator of θ is purely imaginary. Rewrite the numerator as

$$\begin{aligned}
&(\overline{\gamma}\delta-\overline{\delta}\gamma)(\alpha-\beta)+\overline{\beta}(\gamma-\delta)\alpha-\overline{\alpha}(\gamma-\delta)\beta\\
&=(\overline{\gamma}\delta-\overline{\delta}\gamma+\overline{\beta}(\gamma-\delta))\alpha-(\overline{\gamma}\delta-\overline{\delta}\gamma+\overline{\alpha}(\gamma-\delta))\beta\\
&=(\overline{\gamma}\delta-\overline{\delta}\gamma+\overline{\beta}(\gamma-\delta)-(\overline{\gamma-\delta})\beta)\alpha-(\overline{\gamma}\delta-\overline{\delta}\gamma+\overline{\alpha}(\gamma-\delta)-(\overline{\gamma-\delta})\alpha)\beta.
\end{aligned}$$

This is a linear combination of α and β with purely imaginary coefficients. It follows that θ is a real linear combination of α and β with coefficient sum equal to 1. It represents a point on the line joining α and β. Since θ is invariant under the

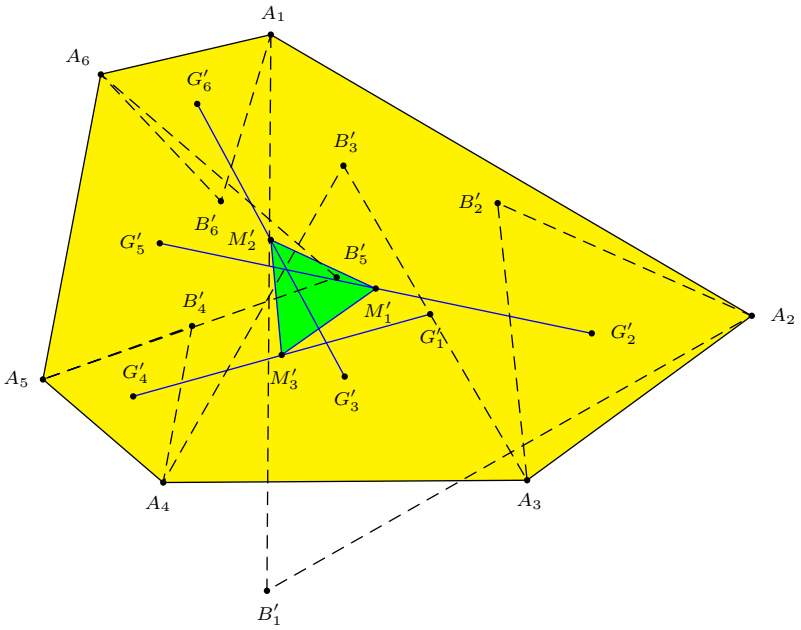

Figure 2.

permutation $(\alpha, \beta) \leftrightarrow (\gamma, \delta)$, it also represents a point on the line joining γ and δ. Therefore, it is the intersection of the two lines. □

We omit the proof of the next lemma.

Lemma 4. *Given two segments $\alpha\beta$ and $\alpha'\beta'$, let $\gamma(t)$ and $\gamma'(t)$ be the points dividing the segments $\alpha\beta$ and $\alpha'\beta'$ in the same ratio*

$$\alpha\gamma(t) : \gamma(t)\beta = \alpha'\gamma'(t) : \gamma'(t)\beta' = t : 1 - t,$$

the locus of the midpoint of $\gamma(t)\gamma'(t)$ is a straight line.

Consider the segments A_2A_3 and A_5A_6 with midpoints $\alpha = \frac{\alpha_2+\alpha_3}{2}$ and $\alpha' = \frac{\alpha_5+\alpha_6}{2}$. Let $\beta = \alpha + \frac{1}{2}(\alpha_2 - \alpha_3)i$ and $\beta' = \alpha' + \frac{1}{2}(\alpha_5 - \alpha_6)i$. These are vertices of isosceles right triangles constructed on the segments A_2A_3 and A_5A_6. Clearly, G_2 and G_5 divide the segment $\alpha\beta$ and $\alpha'\beta'$ in the same ratio; so do G'_2 and G'_5. An application of Lemma 4 identifies the line joining the midpoints of G_2G_5 and $G'_2G'_5$.

Corollary 5. *The line $M_1M'_1$ is the same as the line joining $\frac{\alpha_2+\alpha_5+\alpha_3+\alpha_6}{4}$ and $\frac{\alpha_2+\alpha_5+\alpha_3+\alpha_6}{4} + i \cdot \frac{\alpha_2+\alpha_5-\alpha_3-\alpha_6}{4}$.*

Theorem 6. *The lines $M_1M'_1$, $M_2M'_2$, and $M_3M'_3$ are concurrent at the point*

$$\frac{|\alpha_1+\alpha_4|^2(\alpha_2+\alpha_5-\alpha_3-\alpha_6)+|\alpha_2+\alpha_5|^2(\alpha_3+\alpha_6-\alpha_1-\alpha_4)+|(\alpha_3+\alpha_6|^2(\alpha_1+\alpha_4-\alpha_2-\alpha_5)}{2((\overline{\alpha_1+\alpha_4})(\alpha_2+\alpha_5-\alpha_3-\alpha_6)+(\overline{\alpha_2+\alpha_5})(\alpha_3+\alpha_6-\alpha_1-\alpha_4)+(\overline{\alpha_3+\alpha_6})(\alpha_1+\alpha_4-\alpha_2-\alpha_5))}.$$

Proof. Let $w_j = \frac{\alpha_j+\alpha_{j+3}}{2}$ for $j = 1, 2, 3$. By Corollary 5, $M_1M'_1$ is the line joining $\frac{w_2+w_3}{2}$ and $\frac{w_2+w_3}{2} + i \cdot \frac{w_2-w_3}{2}$. Similarly, $M_2M'_2$ is the line joining $\frac{w_3+w_1}{2}$

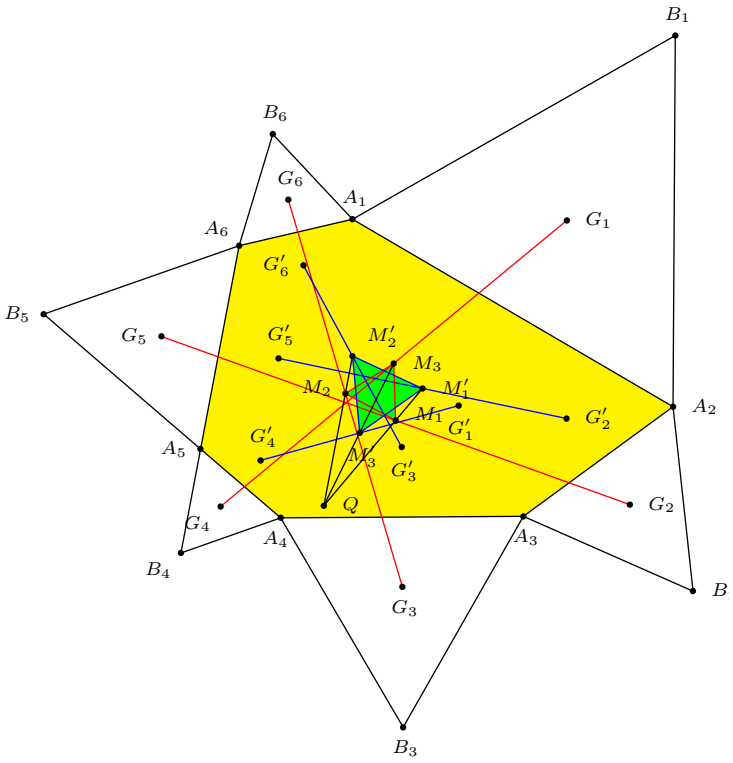

Figure 3.

and $\frac{w_3+w_1}{2}+i\cdot\frac{w_3-w_1}{2}$, and $M_3M'_3$ is the one joining $\frac{w_1+w_2}{2}$ and $\frac{w_1+w_2}{2}+i\cdot\frac{w_1-w_2}{2}$. By Lemma 3, the intersection of these last two lines is

$$Q=\frac{|w_1|^2(w_2+w_3)+|w_2|^2(w_3+w_1)+|w_3|^2(w_1+w_2)}{\overline{w_1}(w_2+w_3)+\overline{w_2}(w_3+w_1)+\overline{w_3}(w_1+w_2)}.$$

The cyclic symmetry of Q in w_1, w_2, w_3 shows that it lies also on the line $M_1M'_1$, and is therefore the point of concurrency of the three lines. Explicitly in terms of α_j for $j=1,2,\ldots,6$, this is given in the statement of the theorem above. □

2. Kierpert perspectors

2.1. Theorem 1 is a generalization of Napoleon's theorem. If we put $A_1=A_4=A$, $A_2=A_5=B$, and $A_3=A_6=C$, then $B_1=B_4$, $G_1=G_4=M_1$. Similarly, $G_2=G_5=M_2$ and $G_3=G_6=M_3$. In this case, $M_1M_2M_3$ is the Napoleon triangle of triangle $A_1A_2A_3$. The vertices of the other Napoleon equilateral triangle $M'_1M'_2M'_3$ are the reflections of M_1, M_2, M_3 in BC, CA, AB respectively. The two equilateral triangles are perspective at the circumcenter O.

On the other hand, if we put $A_1=A_2=A$, $A_3=A_4=B$, and $A_5=A_6=C$, then $M_1M_2M_3$ and $M'_1M'_2M'_3$ are the inferior of the Napoleon triangles of ABC. They are perspective at the nine-point center.

2.2. Let ABC be a given triangle. Assume the circumcircle the unit circle in the complex plane, so that the vertices are unit complex numbers α, β, γ.

$$\alpha_1 = \alpha, \quad \alpha_2 = \frac{\alpha+\gamma}{2}, \quad \alpha_3 = \gamma, \quad \alpha_4 = \frac{\beta+\gamma}{2}, \quad \alpha_5 = \beta, \quad \alpha_6 = \frac{\beta+\alpha}{2}.$$

For $j = 1, 2 \ldots, 6$, let G_j be the apex of an isosceles triangle with base A_jA_{j+1} and base angle θ. Thus,

$$G_j = \frac{\alpha_j + \alpha_{j+1}}{2} + \tan\theta \cdot \frac{\alpha_j - \alpha_{j+1}}{2} i.$$

In this case,

$$\begin{aligned} M_1 &= \frac{1}{2}(G_2 + G_5) \\ &= \frac{1}{2}\left(\frac{\alpha+3\gamma}{4} + \tan\theta \cdot \frac{\gamma-\alpha}{4} i + \frac{\alpha+3\beta}{4} + \tan\theta \cdot \frac{\alpha-\beta}{4} i\right) \\ &= \frac{1}{8}\left(2\alpha + 3\beta + 3\gamma - \tan\theta(\beta-\gamma)i\right) \\ &= \frac{1}{4}\alpha + \frac{3}{4}\left(\frac{\beta+\gamma}{2} - \frac{\tan\theta}{3} \cdot \frac{\beta-\gamma}{2} i\right) \end{aligned}$$

Note that $\frac{\beta+\gamma}{2} - \frac{\tan\theta}{3} \cdot \frac{\beta-\gamma}{2} i$ is the affix of the vertex of the isosceles triangle on BC with base angle $\arctan\left(\frac{1}{3}\tan\theta\right)$, on the same side as A. Similarly, M_2 and M_3 lie respectively on the lines joining B, C to the vertices of similar isosceles triangles on CA, and AB, constructed on the same sides of the vertices (see Figure 4).

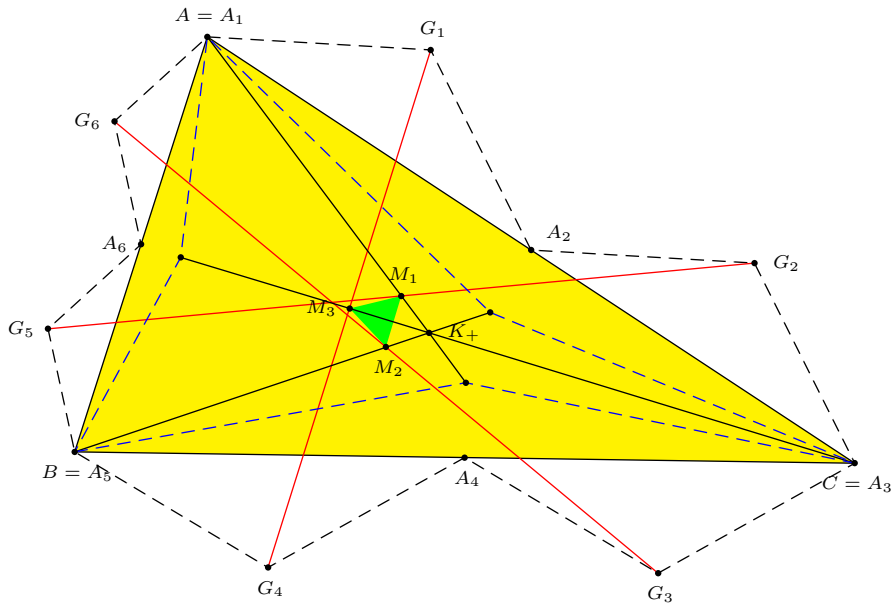

Figure 4.

Proposition 7. (a) *The triangle $M_1M_2M_3$ is perspective with ABC at the Kiepert perspector $K\left(-\arctan\left(\frac{1}{3}\tan\theta\right)\right)$.*

(b) *The triangle $M_1'M_2'M_3'$ is perspective with ABC at the Kiepert perspector $K\left(\arctan\left(\frac{1}{3}\tan\theta\right)\right)$* (see Figure 5).

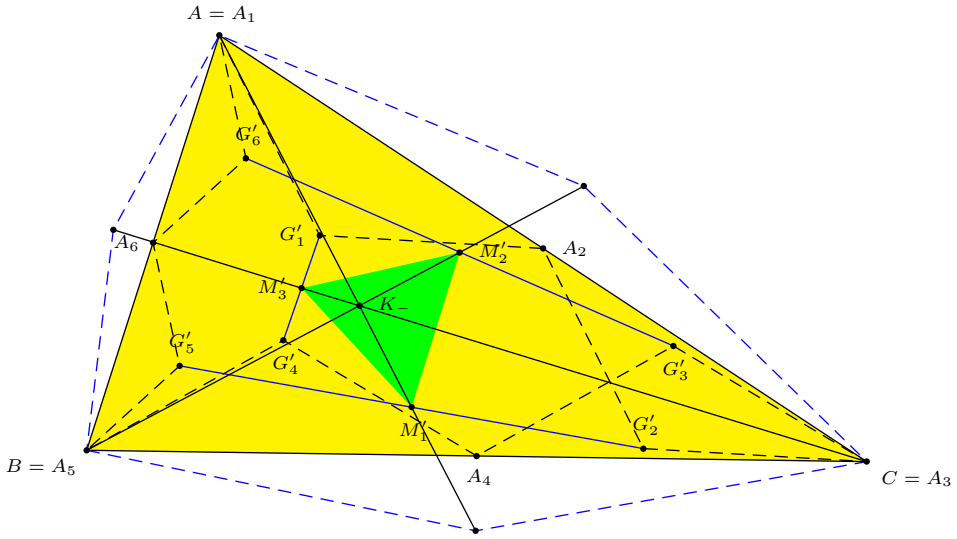

Figure 5.

Finally, we identify the perspector Q of the equilateral triangles $M_1M_2M_3$ and $M_1'M_2'M_3'$ (see Figure 6). The lines in question are

$$\begin{array}{lcccc} M_1M_1' & \text{joining} & \frac{2\alpha+3\beta+3\gamma}{8} & \text{and} & \frac{2\alpha+3\beta+3\gamma}{8} - i\cdot\frac{\beta-\gamma}{8} \\ M_2M_2' & \text{joining} & \frac{3\alpha+2\beta+3\gamma}{8} & \text{and} & \frac{3\alpha+2\beta+3\gamma}{8} - i\cdot\frac{\gamma-\alpha}{8} \\ M_3M_3' & \text{joining} & \frac{3\alpha+3\beta+2\gamma}{8} & \text{and} & \frac{3\alpha+3\beta+2\gamma}{8} - i\cdot\frac{\alpha-\beta}{8} \end{array}$$

By Theorem 6, the perspector Q has complex affix $\frac{1}{4}(\alpha+\beta+\gamma)$. Since the orthocenter H of triangle ABC has complex affix $\alpha+\beta+\gamma$ (see, for example, [3, p.74]), Q is the point dividing OH in the ratio $OQ : OH = 1 : 4$. In terms of the nine-point center N and the centroid G, this satisfies $NG : GQ = 2 : 1$. Therefore, Q is the nine-point center of the inferior (medial) triangle. This is the triangle center $X(140)$ in [2] (see Figure 6).

2.3. Given triangle ABC, consider points X, X' on BC, Y, Y' on CA, and Z, Z' on AB such that

$$BX : XX' : X'C = CY : YY' : Y'A = AZ : ZZ' : Z'B = t : 1-2t : t$$

for some real number t. Construct similar isosceles triangles of base angles θ on the sides XX', $X'Y$, YY', $Y'Z$, ZZ', $Z'X$, all outside or inside the hexagon according as θ is positive or negative. Denote the new apices of the isosceles

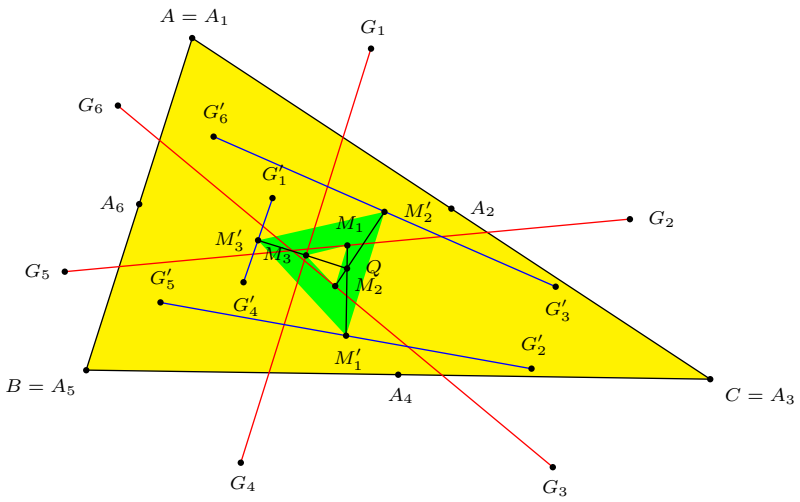

Figure 6.

triangles by A', C'', B', A'', C', B'' respectively. If the complex affixes of A, B, C are α, β, γ respectively, then

$$A' = \frac{\beta+\gamma}{2} + (1-2t)\tan\theta \cdot \frac{\beta-\gamma}{2}i,$$
$$A'' = (1-t)\alpha + t \cdot \frac{\beta+\gamma}{2} - t\tan\theta \cdot \frac{\beta-\gamma}{2}.$$

The midpoint of the segment $A'A''$ is

$$\begin{aligned} M_a &= \frac{1-t}{2}\alpha + \frac{1+t}{2} \cdot \frac{\beta+\gamma}{2} + \frac{1-3t}{2}\tan\theta \cdot \frac{\beta-\gamma}{2}i \\ &= \frac{1-t}{2}\alpha + \frac{1+t}{2}\left(\frac{\beta+\gamma}{2} + \frac{1-3t}{1+t}\tan\theta \cdot \frac{\beta-\gamma}{2}i\right) \end{aligned}$$

Note that $\frac{\beta+\gamma}{2} + \frac{1-3t}{1+t}\tan\theta \cdot \frac{\beta-\gamma}{2}i$ is the apex of the isosceles triangle on BC with base angle $\arctan\left(\frac{1-3t}{1+t}\tan\theta\right)$. Similar expressions hold for the coordinates of the midpoints M_b of $B'B''$ and M_c of $C'C''$. From these we conclude that the triangles $M_aM_bM_c$ and ABC are perspective at the Kiepert perspector $K\left(\arctan\left(\frac{1-3t}{1+t}\tan\theta\right)\right)$. (see Figure 7).

By reversing the sign of θ, we obtain $M'_aM'_bM'_c$ perspective with ABC at the Kiepert perspector $K\left(-\arctan\left(\frac{1-3t}{1+t}\tan\theta\right)\right)$. The line joining these two perspectors passes through the symmedian point of ABC.

These two triangles are equilateral if $\theta = \pm\frac{\pi}{6}$.

2.4. Given triangle ABC and an angle θ, consider the Kiepert triangle $A'B'C' := \mathcal{K}(\theta)$. On the sides of the hexagon $BA'CB'AC'$, construct, similar isosceles triangles of base angles ϕ. Let X_b be the apex of the triangle on CB' and X_c the one

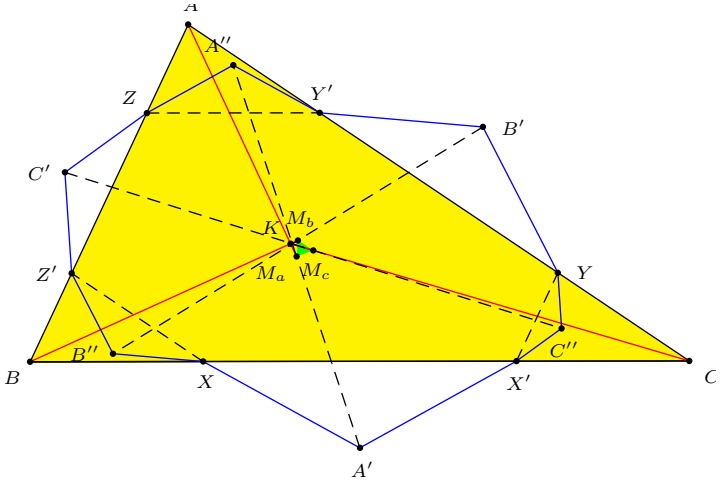

Figure 7

on $C'B$. The midpoint of X_bX_c has affix

$$\frac{\beta+\gamma}{2}+\frac{1}{8}(1-\tan\theta\tan\phi)(2\alpha-\beta-\gamma)-\frac{1}{8}(\tan\theta+\tan\phi)(\beta-\gamma)i$$
$$=\frac{1-\tan\theta\tan\phi}{4}\alpha+\frac{3+\tan\theta\tan\phi}{4}\left(\frac{\beta+\gamma}{2}-\frac{\tan\theta+\tan\phi}{3+\tan\theta\tan\phi}\cdot\frac{\beta-\gamma}{2}i\right)$$

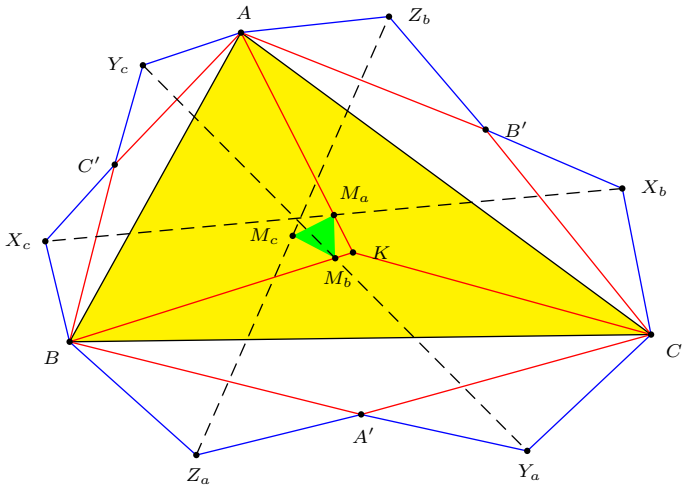

Figure 8

With similar expressions of the midpoints of the two other segments, we conclude that the midpoints of the three segments are perspective with ABC at the

Kiepert perspector

$$K\left(-\arctan\left(\frac{\tan\theta+\tan\phi}{3+\tan\theta\tan\phi}\right)\right).$$

3. Generalizations

Proposition 8 (Fritsch and Pickert [1]). *Given a quadrilateral $ABCD$, let A', B', C', D' be the centers of squares on the sides AB, BC, CD, DA, all constructed externally or internally of the quadrilateral. The midpoints of the diagonals of $ABCD$ and $A'B'C'D'$ form a square.*

Proposition 9 (van Aubel's theorem). *Given an octagon $A_1A_2\cdots A_8$, let C_j, $j=1,2,\ldots,8$* (indices taken modulo 8)*, be the centers of the squares on A_jA_{j+1}, all externally or internally of the octagon. The midpoints of C_1C_5, C_2C_6, C_3C_7, C_4C_8 form a quadrilateral with equal and perpendicular diagonals* (see Figure 9).

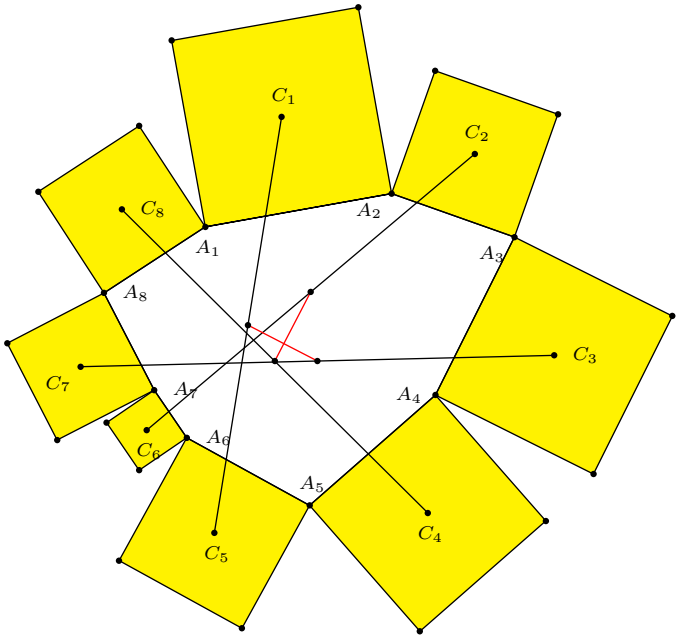

Figure 9

Proposition 10 (Thébault's theorem). *Given an octagon $A_1A_2\cdots A_8$, let B_j be the midpoint of A_jA_{j+1} for indices $j=1,2,\ldots,8$* (modulo 8)*. If C_j, $j=1,2,\ldots,8$, are the centers of the squares on B_jB_{j+1}, all externally or internally of the octagon, then the midpoints of C_1C_5, C_2C_6, C_3C_7, C_4C_8 are the vertices of a square* (see Figure 10).

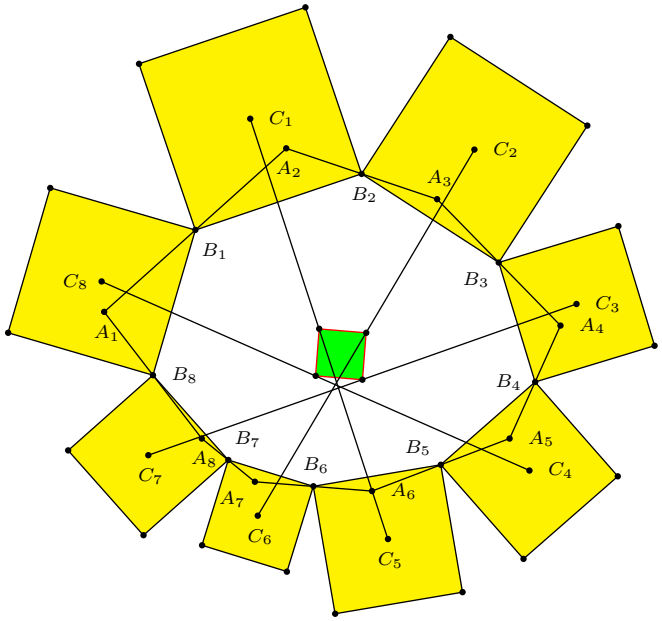

Figure 10

Proposition 8 is a special case of Proposition 10 with $A_1 = A_2$, $A_3 = A_4$, $A_5 = A_6$, $A_7 = A_8$.

References

[1] R. Fritsch and G. Pickert, A quadrangle's centroid of vertices and van Aubel's square theorem, *Crux Math.*, 39 (2013) 362–367.

[2] C. Kimberling, *Encyclopedia of Triangle Centers*, available at `http://faculty.evansville.edu/ck6/encyclopedia/ETC.html`.

[3] P. Yiu, *Euclidean Geometry*, Florida Atlantic University Lecture Notes, 1998; available at `http://math.fau.edu/Yiu/Geometry.html`

Dao Thanh Oai: Cao Mai Doai, Quang Trung, Kien Xuong, Thai Binh, Viet Nam
E-mail address: `daothanhoai@hotmail.com`

Forum Geometricorum
Volume 15 (2015) 115–122.

FORUM GEOM
ISSN 1534-1178

Two Conjectures of Victor Thébault Linking Tetrahedra with Quadrics

Blas Herrera

Abstract. We prove two of Thébault's conjectures. The first (1949) links four lines, that they are rulings of hyperbolic paraboloids or that they are coplanar, with orthocentric or isodynamic tetrahedra, respectively. The second (1953) links the radical center of four spheres with elements of tetrahedra.

1. Introduction

It is very well known that an Euclidean tetrahedron $T \equiv ABCD \subset \mathbb{A}^3$, where $\mathbb{A}^3$ is the Euclidean affine space, is called *orthocentric*, by definition, if the lines through the vertices which are orthogonal to the opposite faces are concurrent; and T is called *isodynamic*, by definition, if the segments that join the vertices with the incenter of the opposite faces are concurrent. It is also very well known that the radical center of four spheres is a point P such that the four powers of P with respect to the four spheres are are equal.

In [12] the famous French problemist Victor Thébault (1882-1960) conjectured the following: In a tetrahedron $T \equiv ABCD$, the planes tangent at A, B, C, D to the circumsphere of T cut the planes of the opposite faces in four lines. A necessary and sufficient condition for these four lines to be rulings of a hyperbolic paraboloid is that T be orthocentric, and a necessary and sufficient condition for these four lines to be coplanar is that T be isodynamic.

But the above conjecture, since 1949 has remained open.

Also, in [13] Victor Thébault conjectured the following: In a tetrahedron $ABCD$, let A', B', C', D' be the feet of the altitudes AA', BB', CC', DD'. The planes drawn through the midpoints of $B'C'$, $C'A'$, $A'B'$, $D'A'$, $D'B'$, $D'C'$ perpendicular to BC, CA, AB, DA, DB, DC respectively, are concurrent at a point P, which is the radical center of the spheres described with the vertices A, B, C, D as centers and with the altitudes AA', BB', CC', DD' as radii.

This conjecture, since 1953 has remained open.

In this paper we prove affirmatively these two results; we will call them theorems.

Publication Date: April 13, 2015. Communicating Editor: Paul Yiu.

Readers can see recent references of research papers about tetrahedra in [5], [6], [15], [16], [17], and about Thébault's problems in [2], [3], [4], [7], [8], [9], [10], [11] and [14].

2. Results

Theorem 1. *In a tetrahedron $T \equiv ABCD$, the planes tangent at A, B, C, D to the circumsphere of T cut the planes of the opposite faces in four lines. A necessary and sufficient condition for these four lines to be rulings of a hyperbolic paraboloid is that T be orthocentric, and a necessary and sufficient condition for these four lines to be coplanar is that T be isodynamic.*

Proof. To prove the result, we consider a Cartesian system of coordinates such that $A = (0,0,0)$, $B = (1,0,0)$, $C = (\alpha,\beta,0)$, $D = (\gamma,\delta,\varepsilon)$ with $\alpha > 0$, $\beta > 0$ and $\varepsilon > 0$. Let π_A, π_B, π_C and π_D be the planes tangent at A, B, C, D to the circumsphere of T, respectively. Let σ_A, σ_B, σ_C, σ_D be the planes containing the faces BCD, ACD, ABD, ABC respectively. Let $r_A = \pi_A \cap \sigma_A$, $r_B = \pi_B \cap \sigma_B$, $r_C = \pi_C \cap \sigma_C$ and $r_D = \pi_D \cap \sigma_D$ be the four lines of the problem. We can calculate two points for every line r_A, r_B, r_C and r_D:

$$\begin{aligned}
r_A &\equiv \left(\tfrac{\alpha-\Phi}{1-\Phi}, \tfrac{\beta}{1-\Phi}, 0\right) \wedge \left(\tfrac{\Phi(\varepsilon+\gamma-1)+\Psi(1-\alpha)+\alpha(1-\varepsilon)-\gamma}{\varepsilon(\Phi-1)}, \tfrac{\beta(\Psi+(\varepsilon-1))+\delta(1-\Phi)}{\varepsilon(1-\Phi)}, 1\right),\\
r_B &\equiv \left(\tfrac{\alpha}{2\alpha-\Phi}, \tfrac{\beta}{2\alpha-\Phi}, 0\right) \wedge \left(\tfrac{\Phi\gamma-\alpha(\Psi+\varepsilon)}{\varepsilon(\Phi-2\alpha)}, \tfrac{\Phi\delta+\beta(2\gamma-\varepsilon-\Psi)-2\alpha\delta}{\varepsilon(\Phi-2\alpha)}, 1\right), \qquad (1)\\
r_C &\equiv \left(\tfrac{\Phi}{2\alpha-1}, 0, 0\right) \wedge \left(\tfrac{\delta(2\beta-\Phi)-\Psi+\gamma}{\delta(1-2\alpha)}, 1, \tfrac{\varepsilon}{\delta}\right),\\
r_D &\equiv \left(\tfrac{\Psi}{2\gamma-1}, 0, 0\right) \wedge \left(\tfrac{\beta(2\delta-\Psi)-\Phi+\alpha}{\beta(1-2\gamma)}, 1, 0\right).
\end{aligned}$$

Here, we denote a line l through two points M and N as $l \equiv M \wedge N$, and $\Phi = \alpha^2 + \beta^2 = AC^2$, $\Psi = \gamma^2 + \delta^2 + \varepsilon^2 = AD^2$.

First, we note that this problem concerns the case of the Euclidean affine space but not the projective space. That is to say, the thesis of the problem is only true in the case that the four lines exist into the affine space and not into the plane of the infinite. For example: if $\alpha = \frac{1}{2}$, $\beta = 1$, $\gamma = \frac{1}{2}$, $\delta = \frac{1}{4}$ and $\varepsilon = \frac{1}{4}\sqrt{11}$, then T is isodynamic with $r_C \subseteq \pi_\infty$ (i.e. π_C is parallel to σ_C) and $r_D \subseteq \pi_\infty$, but $r_A \nsubseteq \pi_\infty$ and $r_B \nsubseteq \pi_\infty$. Therefore T is not equilateral, and we may assume that $\Psi \neq \Phi$ because T is not equilateral.

After a calculation, we find that the center of the circumsphere of T is $O = \frac{1}{2\beta}\left(\beta, \Phi-\alpha, \frac{\delta\alpha-\gamma\beta+\beta\Psi-\delta\Phi}{\varepsilon}\right)$. Because the four lines are affine, we have $\alpha \neq \frac{1}{2}$, $\gamma \neq \frac{1}{2}$, $\Phi \neq 1$ and $\Phi \neq 2\alpha$; see Equations (1). Also we may assume $\Psi \neq 1$ because if $\Psi = 1$, since $\Psi \neq \Phi$ we can choose another orientation of T with $AD = \Psi \neq 1$ and $AC = \Phi = 1$, and with Equations (1) the lines r_A and r_B are not affine. We note that T is isodynamic, by definition, if the segments that join the vertices with the incenter of the opposite faces are concurrent. It is very well known (see for example [1]) that T is isodynamic if and only if the three products

of the pairs formed by the opposite edges are equal:

$$\begin{aligned} &AB\cdot CD = AC\cdot BD = AD\cdot BD \\ \Leftrightarrow &\sqrt{\Phi+\Psi-2\alpha\gamma-2\beta\delta} = \sqrt{\Phi}\sqrt{\Psi+1-2\gamma} = \sqrt{\Psi}\sqrt{\Phi+1-2\alpha}; \end{aligned}$$

and this condition is true if and only if

$$\Psi = \Phi\frac{2\gamma-1}{2\alpha-1} = \frac{2\gamma\Phi-2\alpha\gamma-2\beta\delta}{\Phi-1} = \frac{2\alpha\gamma+2\beta\delta-\Phi}{2\alpha-\Phi}. \tag{2}$$

And we have the equivalencies

$$\begin{aligned} &\Phi\frac{2\gamma-1}{2\alpha-1} = \frac{2\gamma\Phi-2\alpha\gamma-2\beta\delta}{\Phi-1} \Leftrightarrow \Phi\frac{2\gamma-1}{2\alpha-1} = \frac{2\alpha\gamma+2\beta\delta-\Phi}{2\alpha-\Phi} \\ &\Leftrightarrow \frac{2\gamma\Phi-2\alpha\gamma-2\beta\delta}{\Phi-1} = \frac{2\alpha\gamma+2\beta\delta-\Phi}{2\alpha-\Phi} \Leftrightarrow \\ &\Leftrightarrow 2\gamma\Phi\left(2\alpha-\Phi\right)+\Phi\left(\Phi-1\right)+2\left(1-2\alpha\right)\left(\alpha\gamma+\beta\delta\right)=0. \end{aligned} \tag{3}$$

We note that T is orthocentric, by definition, if the lines through the vertices which are orthogonal to the opposite faces are concurrent. It is very well known (see for example [1]) that T is orthocentric if and only if the sum of the squares of the pairs formed by the opposite edges are equal:

$$\begin{aligned} &AB^2+CD^2 = AC^2+BD^2 = AD^2+BC^2 \\ \Leftrightarrow\ &1-2\alpha\gamma-2\beta\delta+\Phi+\Psi = 1-2\gamma+\Phi+\Psi = 1-2\alpha+\Phi+\Psi, \end{aligned}$$

and this condition is true if and only if

$$\gamma=\alpha, \qquad \delta=\frac{\alpha-\alpha^2}{\beta}. \tag{4}$$

Now, if the four lines r_A, r_B, r_C, r_D are coplanar, then the three points $M_1 = \left(\frac{\alpha}{2\alpha-\Phi}, \frac{\beta}{2\alpha-\Phi}, 0\right)$, $M_2 = \left(\frac{\Phi}{2\alpha-1}, 0, 0\right)$, $M_3 = \left(\frac{\Psi}{2\gamma-1}, 0, 0\right)$ are collinear because the eight points in Equations (1) above are not in the plane $z=0$; therefore $\frac{\Phi}{2\alpha-1} = \frac{\Psi}{2\gamma-1}$ because $\beta\neq 0$. Then if the four lines are coplanar we have $\Psi = \Phi\frac{2\gamma-1}{2\alpha-1}$. Also, the plane σ_1, which contains the four lines, also contains the points M_1, $M_2 = M_3$, and $M_4 = \left(\frac{\delta(2\beta-\Phi)-\Psi+\gamma}{\delta(1-2\alpha)}, 1, \frac{\varepsilon}{\delta}\right)$. Then, if we impose that the point $M_5 = \left(\frac{\Phi\gamma-\alpha(\Psi+\varepsilon)}{\varepsilon(\Phi-2\alpha)}, \frac{\Phi\delta+\beta(2\gamma-\varepsilon-\Psi)-2\alpha\delta}{\varepsilon(\Phi-2\alpha)}, 1\right)$ lies in the plane σ_1 we find that $2\gamma\Phi\left(2\alpha-\Phi\right)+\Phi\left(\Phi-1\right)+2\left(1-2\alpha\right)\left(\alpha\gamma+\beta\delta\right)=0$ because this is the condition that we find when we impose that $\det(\overrightarrow{M_2M_5}, \overrightarrow{M_2M_1}, \overrightarrow{M_2M_4}) = 0$ with $\Psi = \Phi\frac{2\gamma-1}{2\alpha-1}$. Therefore, using Equations (2) and (3), if the four lines are coplanar (in fact if r_B, r_C, r_D are coplanar) then T is isodynamic. Reciprocally, if T is isodynamic, the points $X=(x,y,z)$ in the plane σ_1 through the points M_1, $M_2 = M_3$ and M_4 verify $\sigma_1 \equiv \det(\overrightarrow{M_2X}, \overrightarrow{M_2M_1}, \overrightarrow{M_2M_4}) = 0$. An easy calculation, using Equations (2) and (3), proves that the eight points of Equations (1) are in σ_1. Therefore, the four lines are coplanar. Now, if we consider that T is orthocentric, then we calculate determinants and we find that r_A, r_B, r_C and r_D are parallel to the same plane. The plane by M_3 and r_C

is $\sigma_2 \equiv \det(\overrightarrow{M_3X}, \overrightarrow{M_3M_2}, \overrightarrow{M_3M_4}) = 0$, or equivalently using Equation (4), $\sigma_2 \equiv \varepsilon\beta y + \left(\alpha^2 - \alpha\right) z = 0$ and $\sigma_2 \cap r_A = P = \left(\frac{\Psi-\alpha}{\Psi-1}, \frac{\alpha(\alpha-1)}{\beta(\Psi-1)}, \frac{\varepsilon}{1-\Psi}\right)$. And with a calculation we have $P \in \sigma_3$, where σ_3 is the plane by M_3 and r_B because $\sigma_3 \equiv \det(\overrightarrow{M_3X}, \overrightarrow{M_3M_1}, \overrightarrow{M_3M_5}) = 0$, or using Equation (4),

$$\sigma_3 \equiv ax + by + cz + \Psi\beta^2\varepsilon = 0,$$

where

$$\begin{aligned}
a &= (1-2\alpha)\,\beta^2\varepsilon,\\
b &= \left((2\alpha-1)\,\alpha + \Psi\Phi - 2\Psi\alpha\right)\varepsilon\beta,\\
c &= d + e,\\
d &= \Psi\left((\Phi-2\alpha)\,\alpha\,(\alpha-1) + \beta^2\,(\Psi-2\alpha)\right),\\
e &= \alpha\,(1-2\alpha)\left(\alpha - \left(\alpha^2+\beta^2\right)\right).
\end{aligned}$$

Therefore, the line l_1 through M_3 which cuts r_B and r_C is a line that also cuts r_A in P. As before, we can calculate the plane by $M_6 = \left(\frac{\beta(2\delta-\Psi)-\Phi+\alpha}{\beta(1-2\gamma)}, 1, 0\right)$ and r_C which is $\sigma_4 \equiv \det(\overrightarrow{M_6X}, \overrightarrow{M_6M_2}, \overrightarrow{M_6M_4}) = 0$, and using Equation (4), $\sigma_4 \cap r_A = Q = (Q_1, Q_2, Q_3)$ with

$$\begin{aligned}
Q_1 &= \tfrac{\Phi-\Phi\alpha+\Psi\beta+\alpha(2\alpha-\beta-2)}{(\Psi-1)\beta},\\
Q_2 &= \tfrac{\Phi\left(\alpha\left((1-\alpha)(\Phi+\beta+1)+2\alpha^2-2\right)-\beta^2\Psi+\beta^2\right)+\beta\alpha(\Psi(2\beta+\alpha-1)-2\beta)+2\alpha^2(1-\alpha)}{(\Phi-\Psi-\Psi\Phi+\Psi^2)\beta^2},\\
Q_3 &= \varepsilon\tfrac{2\alpha-\Phi-2\Phi\alpha+\Phi\beta-\Psi\beta+\Phi^2}{\beta(\Phi-\Psi-\Psi\Phi+\Psi^2)}.
\end{aligned} \tag{5}$$

Note that $\Psi \neq \Phi \Rightarrow \Phi - \Psi - \Psi\Phi + \Psi^2 \neq 0$. As before, using Equation (4), with a calculation we have $Q \in \sigma_5$, where σ_5 is the plane by M_6 and r_B with equation $\sigma_3 \equiv \det(\overrightarrow{M_3X}, \overrightarrow{M_3M_1}, \overrightarrow{M_3M_5}) = 0$. The line l_2 through M_6 which cuts r_B and r_C is a line that also cuts r_A in Q. Therefore, the four lines r_A, r_B, r_C, r_D cut the two lines l_1, l_2. These two lines l_1, l_2 are not parallel, for otherwise we find that $\Phi = 2\alpha$. Also, they do not intersect each other, for otherwise we find that $\Phi = 2\alpha$ or $\Phi = 1$. In fact, with a longer calculation we can prove that the four lines r_A, r_B, r_C, r_D cut the two lines l_1, l_2, without any condition; that is, without the condition of Equation (4). For example, $\sigma_2 \cap r_A = P = \left(\frac{\gamma-\Psi}{1-\Psi}, \frac{\delta}{1-\Psi}, \frac{\varepsilon}{1-\Psi}\right)$ and always the four lines r_A, r_B, r_C, r_D of Equations (1) cut the two lines l_1, l_2. Also, $r_D \cap r_C = \varnothing$ because $\Psi \neq \Phi$, and $r_D \cap r_B = \varnothing$ because $\Psi \neq 1$. Then the four lines are not in the same plane, for otherwise they should be parallel and they are in the sides of the tetrahedron T, which is impossible. In conclusion: the four lines r_A, r_B, r_C, r_D are parallel to the same plane, they are not in the same plane and they cut two lines l_1, l_2 which are not parallel and do not intersect each other. Therefore, they are four rulings of a hyperbolic paraboloid. Reciprocally, we consider that the four lines r_A, r_B, r_C, r_D are rulings of a hyperbolic paraboloid

H. First we make calculations and we have that

$$\begin{aligned}
r_A \cap r_B \neq \varnothing \Rightarrow \Psi &= \Phi\frac{2\gamma-1}{2\alpha-1},\\
r_A \cap r_C \neq \varnothing \Rightarrow \Psi &= \frac{2\alpha\gamma+2\delta\beta-\Phi}{2\alpha-\Phi},\\
r_A \cap r_D \neq \varnothing \Rightarrow \Psi &= \frac{2\gamma\Phi-2\alpha\gamma-2\delta\beta}{\Phi-1},\\
r_B \cap r_C \neq \varnothing \Rightarrow \Psi &= \frac{2\gamma\Phi-2\alpha\gamma-2\delta\beta}{\Phi-1},\\
r_B \cap r_D \neq \varnothing \Rightarrow \Psi &= \frac{2\alpha\gamma+2\delta\beta-\Phi}{2\alpha-\Phi},\\
r_C \cap r_D \neq \varnothing \Rightarrow \Psi &= \Phi\frac{2\gamma-1}{2\alpha-1}.
\end{aligned} \tag{6}$$

Note that $r_A \cap r_B \neq \varnothing$ and $r_B \cap r_C \neq \varnothing$ imply, using Equations (2) and (3), that T is isodynamic, and the four lines are in the same plane, in contradiction with that they are four rulings of H. If $r_B \cap r_C \neq \varnothing$, then $r_A \cap r_B = \varnothing$. The lines are rulings of H; if $r_B \cap r_C \neq \varnothing$, we must also have $r_A \cap r_C \neq \varnothing$. Therefore, using Equations (2) and (3), T is again isodynamic in contradiction. In conclusion $r_B \cap r_C = \varnothing$. Then $r_A \cap r_B = \varnothing$, because if not then $r_A \cap r_B \neq \varnothing$ and $r_A \cap r_C \neq \varnothing$, and, using Equations (2) and (3), T is again isodynamic in contradiction. Also $r_B \cap r_D = \varnothing$, because if not then $r_B \cap r_D \neq \varnothing$ and $r_B \cap r_C \neq \varnothing$, and, using Equations (2) and (3), T is again isodynamic in contradiction. Therefore r_A, r_B, r_C, r_D are four rulings of H parallel to the same plane. Then we impose that the director vectors of r_A, r_B, r_C, r_D are linearly dependent; we calculate determinants and we find that

$$\begin{aligned}
0 = {} & \Psi\left(\Phi\gamma+\alpha\left(2\alpha\gamma+2\beta\delta-3\gamma+1-\Phi\right)-\delta\beta\right)\\
& +\Phi\left(\beta\delta+\gamma\left(-2\alpha\gamma-2\beta\delta+3\alpha-1\right)\right)+2\alpha\left(\gamma^2-\alpha\gamma-\delta\beta\right)+2\beta\gamma\delta.
\end{aligned} \tag{7}$$

But since $\Psi = \gamma^2 + \delta^2 + \varepsilon^2$ for infinitely many $\varepsilon \in \mathbb{R}$,

$$0 = \Phi\gamma+\alpha\left(2\alpha\gamma+2\beta\delta-3\gamma+1-\Phi\right)-\delta\beta. \tag{8}$$

This implies that

$$\begin{aligned}
\gamma &= \frac{\alpha^3+\alpha\beta^2-2\delta\beta\alpha+\delta\beta-\alpha}{-3\alpha+3\alpha^2+\beta^2},\\
\delta &= -\frac{-\alpha^3-\alpha\beta^2+3\alpha^2\gamma+\gamma\beta^2-3\alpha\gamma+\alpha}{\beta\left(2\alpha-1\right)},\\
0 &= \Phi\left(\beta\delta+\gamma\left(-2\alpha\gamma-2\beta\delta+3\alpha-1\right)\right)+2\alpha\left(\gamma^2-\alpha\gamma-\delta\beta\right)+2\beta\gamma\delta.
\end{aligned} \tag{9}$$

The last equation of (9) implies that

$$\delta = -\gamma\frac{-3\alpha^3-3\alpha\beta^2+3\alpha^2-2\alpha\gamma+2\alpha^3\gamma+2\alpha\gamma\beta^2+\beta^2}{\beta\left(2\alpha^2\gamma+2\gamma\beta^2-\beta^2-2\gamma+2\alpha-\alpha^2\right)} \tag{10}$$

With (10), the second equation of (9), and the condition $\gamma \neq \frac{1}{2}$, we have $\gamma = \alpha$. Finally with this result and the first equation of (9), we obtain $\delta = \frac{\alpha - \alpha^2}{\beta}$. Then T is orthocentric. □

Theorem 2. *In a tetrahedron $ABCD$, let A', B', C', D' be the feet of the altitudes AA', BB', CC', DD'.* [1] *The planes drawn through the midpoints of $B'C'$, $C'A'$, $A'B'$, $D'A'$, $D'B'$, $D'C'$ perpendicular to BC, CA, AB, DA, DB, DC respectively, are concurrent at a point P, which is the radical center of the spheres described with the vertices A, B, C, D as centers and with the altitudes AA', BB', CC', DD' as radii.*

Proof. To prove the result, we consider a Cartesian system of coordinates such that $A = (0,0,0)$, $B = (1,0,0)$, $C = (\alpha, \beta, 0)$, $D = (\gamma, \delta, \varepsilon)$ with $\alpha > 0$, $\beta > 0$ and $\varepsilon > 0$. In this system, the feet of the altitudes are

$$\begin{aligned}
A' &= \frac{\beta\varepsilon}{M_a}\left(\beta\varepsilon, (1-\alpha)\,\varepsilon, \delta\,(\alpha-1) - \beta\,(\gamma-1)\right),\\
B' &= \frac{\beta\varepsilon}{M_b + \beta^2\varepsilon^2}\left(\frac{M_b}{\beta\varepsilon}, \alpha\varepsilon, \beta\gamma - \alpha\delta\right),\\
C' &= \frac{\beta\delta}{\delta^2+\varepsilon^2}\left(\frac{\alpha}{\beta\delta}\left(\delta^2+\varepsilon^2\right), \delta, \varepsilon\right),\\
D' &= (\gamma, \delta, 0),
\end{aligned}$$

where

$$\begin{aligned}
M_a = {} & \left(\alpha^2 - 2\alpha + 1\right)\left(\delta^2+\varepsilon^2\right) + 2\beta\delta\,(\alpha-1) + \beta^2\left(1+\varepsilon^2\right)\\
& + \beta\gamma\,(\beta\gamma - 2\alpha\delta + 2\delta - 2\beta),\\
M_b = {} & \alpha^2\left(\delta^2+\varepsilon^2\right) + \beta\gamma\,(\beta\gamma - 2\alpha\delta).
\end{aligned}$$

Also we calculate the planes drawn through the midpoints of $B'C'$, $C'A'$, $A'B'$, $D'A'$, $D'B'$, $D'C'$ perpendicular to BC, CA, AB, DA, DB, DC respectively. They are

$$\begin{aligned}
\pi_{BC} &\equiv 2\,(1-\alpha)\,x - 2\beta y + \alpha^2 + \frac{\beta^2\delta^2}{\delta^2+\varepsilon^2} - \frac{M_b}{M_b + \beta^2\varepsilon^2} = 0,\\
\pi_{CA} &\equiv 2\alpha x + 2\beta y - \frac{\beta^2\delta^2}{\delta^2+\varepsilon^2} - \frac{\alpha^2 M_a + \beta^2\varepsilon^2}{M_a} = 0,\\
\pi_{AB} &\equiv 2x - \frac{\beta^2\varepsilon^2}{M_a} - \frac{M_b}{M_b + \beta^2\varepsilon^2} = 0,\\
\pi_{DA} &\equiv 2\gamma x + 2\delta y + 2\varepsilon z - \delta^2 - \gamma^2 - \frac{\beta^2\varepsilon^2}{M_a} = 0,\\
\pi_{DB} &\equiv 2\,(1-\gamma)\,x - 2\delta y - 2\varepsilon z + \delta^2 + \gamma^2 - \frac{M_b}{M_b + \beta^2\varepsilon^2} = 0,\\
\pi_{DC} &\equiv 2\,(\alpha-\gamma)\,x + 2\,(\beta-\delta)\,y - 2\varepsilon z - \alpha^2 + \gamma^2 + \delta^2 - \frac{\delta^2\beta^2}{\delta^2+\varepsilon^2} = 0.
\end{aligned}$$

[1] "Altitude AA'" means that AA' is the straight line segment which joins the vertex A with the point A' on the opposite side plane BCD such that the segment AA' is orthogonal to plane BCD; and this point A' is called "foot of the altitude".

Another calculation shows that all these planes are concurrent at the point

$$P = (P_1, P_2, P_3) = \left(\phi, -\frac{\xi + \alpha\phi}{\beta}, \frac{\beta\varphi + \delta\xi + (\alpha\delta - \beta\gamma)\,\phi}{\beta\varepsilon}\right),$$

with

$$\begin{aligned} 2\xi &= -\alpha^2 - \frac{\beta^2\delta^2}{\delta^2 + \varepsilon^2} + \frac{\beta^2\varepsilon^2}{M_a}, \\ 2\phi &= \frac{M_b}{M_b + \beta^2\varepsilon^2} + \frac{\beta^2\varepsilon^2}{M_a}, \\ 2\varphi &= \gamma^2 + \delta^2 + \frac{\beta^2\varepsilon^2}{M_a}. \end{aligned}$$

Finally, we calculate the power of P with respect to the spheres described with the vertices A, B, C, D as centers and with the altitudes AA', BB', CC', DD' as radii respectively. These are

$$\begin{aligned} P_a &= P_1^2 + P_2^2 + P_3^2 - \frac{\beta^2\varepsilon^2}{M_a}, \\ P_b &= (P_1 - 1)^2 + P_2^2 + P_3^2 - \frac{\beta^2\varepsilon^2}{M_b + \beta^2\varepsilon^2}, \\ P_c &= (P_1 - \alpha)^2 + (P_2 - \beta)^2 + P_3^2 - \frac{\beta^2\varepsilon^2}{\delta^2 + \varepsilon^2}, \\ P_d &= (P_1 - \gamma)^2 + (P_2 - \delta)^2 + (P_3 - \varepsilon)^2 - \varepsilon^2. \end{aligned}$$

It is easy to check that $P_a - P_b = P_a - P_c = P_a - P_d = 0$. Therefore, P is the radical center of the four spheres. □

References

[1] N. Altshiller-Court, *Modern Pure Solid Geometry*, Chelsea Publications, New York, 1964.
[2] J-L. Ayme, Sawayama and Thébault's theorem, *Forum Geom.*, 3 (2003) 225–229.
[3] Z. Čerin, On Thébault's problem 3887, *J. Geom. Graph.*, 15 (2011) 113–127.
[4] V. Darko and V. Volenec, Thébault's theorem, *Elem. Math.*, 63 (2008) 6–13.
[5] L. S. Evans, A tetrahedral arrangement of triangle centers, *Forum Geom.*, 3 (2003) 181–186.
[6] H. Havlicek and G. Weiß, Altitudes of a tetrahedron and traceless quadratic forms, *Amer. Math Monthly*, 110 (2003) 679–693.
[7] R. Kolar-Šuper, Z. Kolar-Begović, and V. Volenec, Thébault circles of the triangle in an isotropic plane, *Math. Commun.*, 15 (2010) 437–442.
[8] S-C. Liu, A generalization of Thébault's theorem on the concurrency of three Euler lines, *Forum Geom.*, 8 (2008) 205–208.
[9] A. Ostermann and G. Wanner, A dynamic proof of Thébault's theorem, *Elem. Math.* 65 (2010) 12–16.
[10] W. Reyes, An application of Thébault's theorem, *Forum Geom.*, 2 (2002) 183–185.
[11] R. Shail, A proof of Thébault's theorem, *Amer. Math. Monthly*, 108 (2001) 319–325.
[12] V. Thébault, Problem 4368, *Amer. Math. Monthly*, 56 (1949) 637.
[13] V. Thébault, Problem 4530, *Amer. Math. Monthly*, 60 (1953) 193.
[14] V. Volenec, Z. Kolar-Begović, and R. Kolar-Šuper, Thébault's pencil of circles in an isotropic plane, *Sarajevo J. Math.*, 6 (2010) 237–239.

[15] K. Wirth and A. S. Dreiding, Edge lengths determining tetrahedrons, *Elem. Math.*, 64 (2009) 160–170.
[16] K. Wirth and A. S. Dreiding, Tetrahedrons classes based on edge lengths, *Elem. Math.* 68 (2013) 56–64.
[17] Y-D. Wu and Z-H. Zhang, The Egde-tangent sphere of a circumscriptible tetrahedron, *Forum Geom.*, 7 (2007) 19–24.

Blas Herrera: Departament d'Enginyeria Informàtica i Matemàtiques, Universitat Rovira i Virgili, Avinguda Països Catalans, 26, 43007 Tarragona, Spain.
E-mail address: blas.herrera@urv.net

Forum Geometricorum
Volume 15 (2015) 123–125.

FORUM GEOM
ISSN 1534-1178

Lemniscates and a Locus Related to a Pair of Median and Symmedian

Francisco Javier García Capitán

Abstract. We show that the lemniscate of Bernoulli arises from a locus problem related to the orthogonality of a pair of median and symmedian of a triangle with a given side, and study a generalization of the locus problem.

1. A locus problem on the orthogonality of a pair of median and symmedian

Given a segment BC, consider the locus of A such that the median AM and the symmedian AL of triangle ABC are orthogonal to each other.

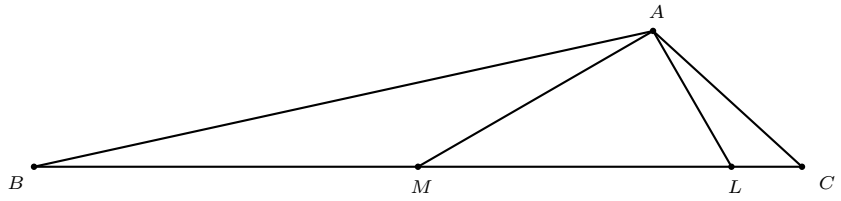

Figure 1.

In a Cartesian coordinate system, let the origin be the midpoint M of BC, and $B = (-a, 0)$ and $C = (a, 0)$ (see Figure 1). If $A = (u, v)$, the perpendicular to AM at A is the line $u(x - u) + v(y - v) = 0$. It intersects the x-axis at $L = \left(\frac{u^2+v^2}{u},\ 0\right)$. Now, AL is a symmedian if and only if $\frac{BL}{LC} = \frac{AB^2}{AC^2}$.

$$\frac{au + u^2 + v^2}{au - (u^2 + v^2)} = \frac{u^2 + v^2 + 2au + a^2}{u^2 + v^2 - 2au + a^2}.$$

Simplifying, we have

$$(u^2 + v^2)^2 = a^2(u^2 - v^2).$$

In polar coordinates, this is the curve $r^2 = a^2 \cos 2\theta$, the lemniscate with endpoints B and C (see Figure 2).

2. A generalization

Suppose instead of orthogonality, we require to A-median and A-symmedian to make a given angle $\alpha \neq 0$. If the *directed angle* $(AM,\ AL) = \alpha$, the slope of the line AL is

$$\tan\left(\alpha + \arctan\frac{v}{u}\right) = \frac{u\sin\alpha + v\cos\alpha}{u\cos\alpha - v\sin\alpha},$$

Publication Date: April 14, 2015. Communicating Editor: Paul Yiu.

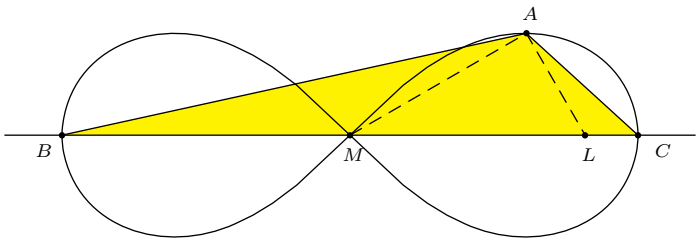

Figure 2.

and L is the point $\left(\frac{\sin\alpha(u^2+v^2)}{u\sin\alpha+v\cos\alpha},\ 0\right)$. The condition $\frac{BL}{LC}=\frac{AB^2}{AC^2}$ reduces in this case to

$$\sin\alpha(u^2+v^2)^2=a^2(\sin\alpha(u^2-v^2)+\cos\alpha\cdot 2uv).$$

In polar coordinates, $(u,v)=(r\cos\theta,\ r\sin\theta)$, this becomes

$$\mathscr{L}(\alpha):\qquad r^2=\frac{a^2}{\sin\alpha}\cdot\sin(2\theta+\alpha)=\frac{a^2}{\sin\alpha}\cdot\cos(2\theta-\frac{\pi}{2}+\alpha).$$

In particular, $\mathscr{L}\left(\frac{\pi}{2}\right)$ is the lemniscate $r^2=a^2\cos 2\theta$. $\mathscr{L}(\alpha)$ is the image of $\mathscr{L}\left(\frac{\pi}{2}\right)$ under a rotation by $\frac{\pi}{4}-\frac{\alpha}{2}$ about the center M, followed by a magnification of factor $\frac{1}{\sqrt{\sin\alpha}}$.

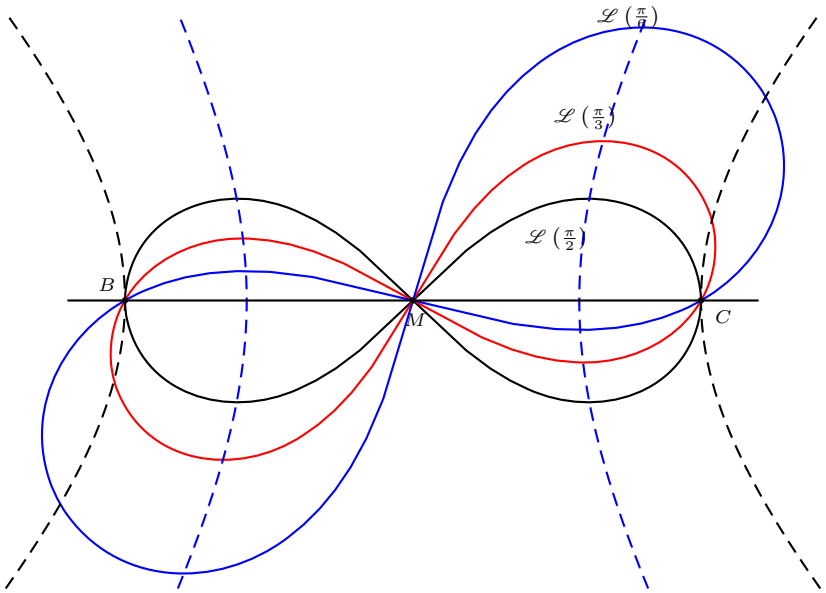

Figure 3.

3. On the family of lemniscates $\mathscr{L}(\alpha)$

For varying α, the extreme points of the lemniscate $\mathscr{L}(\alpha)$ are the points with polar coordinates $\left(\frac{a}{\sqrt{\sin\alpha}}, \frac{\pi}{4} - \frac{\alpha}{2}\right)$. This lies on the polar curve $r = \frac{a}{\sqrt{\cos 2\theta}}$ or $r^2 \cos 2\theta = a^2$. This is the rectangular hyperbola $x^2 - y^2 = a^2$, precisely the inverse of the lemniscate with respect to the circle with radius a and centered at the origin ([1, pp. 111–117], [2, pp. 143–147]; see Figure 3).

For each α, the "highest" point of the lemniscate $\mathscr{L}(\alpha)$ gives the largest triangle ABC with orthogonal A-median and A-symmedian. For points (x, y) on $\mathscr{L}(\alpha)$, $y_{\max}$ occurs at $\theta = \frac{\pi-\alpha}{3}$. Writing α in terms of θ, we have $\alpha = \pi - -3\theta$ and $2\theta + \alpha = \pi - \theta$. Therefore, this highest point lies on the polar curve

$$r^2 = \frac{a^2 \sin(\pi - \theta)}{\sin(\pi - 3\theta)} = \frac{a^2 \sin\theta}{\sin 3\theta}.$$

Further simplifying,

$$r^2 = \frac{a^2}{3 - 4\sin^2\theta} \implies 3r^2 - 4y^2 = a^2 \implies 3x^2 - y^2 = a^2.$$

Therefore, the locus of A for which triangle ABC is the *largest* among those with A-median and A-symmedian making a fixed angle is the hyperbola $3x^2 - y^2 = a^2$ (see Figure 3).

In particular, the largest triangle with orthogonal A-median and A-symmedian is constructible with ruler and compass. For $\alpha = \frac{\pi}{2}$, this is the point with polar coordinates $\left(\frac{a}{\sqrt{2}}, \frac{\pi}{6}\right)$. In Figure 4, O is the center of the square $MCDE$, A_0ME is an equilateral triangle. Construct the circular arc with center M and radius MO to intersect MA_0 at A, the highest point of the lemniscate $\mathscr{L}\left(\frac{\pi}{2}\right)$. In this case, $\cos BAC = -\frac{1}{\sqrt{3}}$.

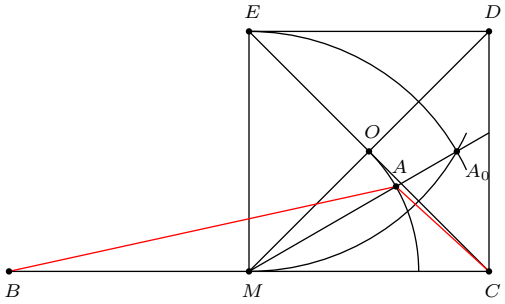

Figure 4.

References

[1] E. H. Lockwood, *A Book of Curves*, Cambridge University Press, 1967.
[2] R. C. Yates, *A Handbook on Curves and Their Properties*, J. W. Edwards, Ann Arbor, MI; 1952.

Francisco Javier García Capitán: Departamento de Matemáticas, I.E.S. Alvarez Cubero, Avda. Presidente Alcalá-Zamora, s/n, 14800 Priego de Córdoba, Córdoba, Spain
E-mail address: garciacapitan@gmail.com

Forum Geometricorum
Volume 15 (2015) 127–128.

FORUM GEOM
ISSN 1534-1178

Another Archimedean Circle in an Arbelos

Emmanuel Antonio José García

Abstract. The incircle of a triangle associated with an arbelos is Archimedean.

We make an addition to recent contributions to the Archimedean circles associated to an arbelos. See [1, 3, 4, 5] and the catalogue [2].

Consider an arbelos bounded by semicircles AB, AC, CB of radii $a+b$, a, b, and centers O, D, E respectively. Construct the semicircles with diameters AE, DB (and centers K, L respectively), and the common tangent of these semicircles touching AE at M, DB at N, and intersecting the semicircle AB at F and G (see Figure 1). If the tangents to the semicircle AB at F and G intersect at H, we prove that the incircle of triangle FGH is an archimedean circle of the arbelos, namely, its radius is $\frac{ab}{a+b}$.

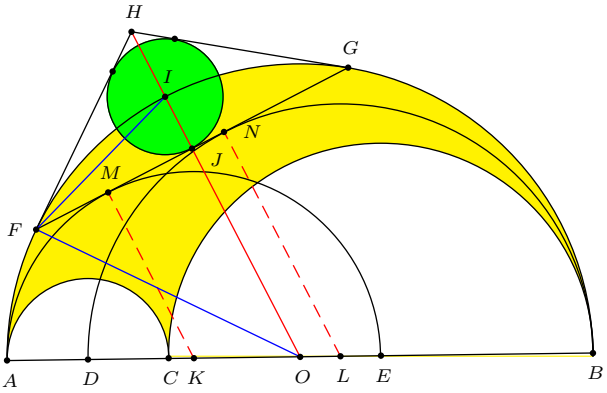

Figure 1

Let OH intersect the semicircle AB and the chord FG at I and J respectively. Since

$$\begin{aligned}\angle IFH &= 90^\circ - \angle OFI = 90^\circ - \frac{1}{2}(180^\circ - \angle IOF)\\ &= \frac{1}{2}\angle IOF = \frac{1}{2}\angle JOF = \frac{1}{2}\angle JFH.\end{aligned}$$

FI bisects angle GFH. Since I also lies on the bisector of angle FHG, it is the incenter of triangle FGH. The radius of the incircle of triangle FGH is $IJ = IO - OJ = (a+b) - OJ$.

Publication Date: April 16, 2015. Communicating Editor: Floor van Lamoen.

To find the length of OJ, note that it is parallel to both KM and LN of the trapezoid $KMNL$. Since $OL = \frac{a}{2}$ and $KO = \frac{b}{2}$, $OL : KO : KL = a : b : a + b$, and

$$\begin{aligned} OJ &= \frac{OL}{KL} \cdot KM + \frac{KO}{KL} \cdot LN \\ &= \frac{a}{a+b}\left(a + \frac{b}{2}\right) + \frac{b}{a+b}\left(\frac{a}{2} + b\right) \\ &= \frac{a^2 + ab + b^2}{a+b}. \end{aligned}$$

It follows that

$$IJ = (a+b) - \frac{a^2 + ab + b^2}{a+b} = \frac{ab}{a+b}.$$

This is the radius of an Archimedean circle in the arbelos.

References

[1] T. O. Dao, Two pairs of Archimedean circles in the arbelos, *Forum Geom.*, 14 (2014) 201–202.
[2] F. M. van Lamoen, Online catalogue of Archimedean circles, `http://home.kpn.nl/lamoen/wiskunde/Arbelos/Catalogue.htm`
[3] F. M. van Lamoen, A special point in the Arbelos leading to a pair of Archi-medean circles, *Forum Geom.*, 14 (2014) 253–254.
[4] Q. H. Tran, Two more pairs of Archimedean circles in the arbelos, *Forum Geom.*, 14 (2014) 249–251.
[5] P. Yiu, Three constructions of Archimedean circles in an arbelos, *Forum Geom.*, 14 (2014) 255–260.

Emmanuel Antonio José García: Universidad Dominicana O & M, Ave. Independencia # 200, Santo Domingo, Dominican Republic.
E-mail address: `emmanuelgeogarcia@gmail.com`

Forum Geometricorum
Volume 15 (2015) 129–157.

FORUM GEOM
ISSN 1534-1178

About Two Characteristic Points Concerning Two Nested Circles and Their Use in Research of Bicentric Polygons

Mirko Radić

Abstract. This paper is a companion to [8], which primarily deals with two characteristic points defined for two separated circles and their use in research of bicentric polygons with excircle. This paper primarily deals with two characteristic points defined for two nested circles and their use in research of bicentric polygons with incircle. Some useful properties and relations are established and some old and difficult problems are solved using these points.

1. The characteristic points of nested circles

We begin with the following definition.

Definition 1. Let C_1 and C_2 be two given circles such that C_2 is complete inside C_1. Let R, r, d be lengths (positive numbers) such that $R =$ radius of C_1, $r =$ radius of C_2, $d = |OI|$, where O is the center of C_1 and I is the center of C_2. Let xOy be a co-ordinate system with origin O, and positive x-axis containing I. The points $S_i(s_i, 0),\ i = 1, 2$ where

$$s_{1,2} = \frac{R^2 + d^2 - r^2 \mp \sqrt{(R^2 + d^2 - r^2)^2 - 4R^2d^2}}{2d}, \tag{1a}$$

will be called the *characteristic points* of the circles C_1 and C_2, or of the triple (R, r, d).

It is easy to see that lengths s_1 and s_2 given by (1a) can be written as

$$s_1 = \frac{R^2 + d^2 - r^2 - t_M t_m}{2d} \quad \text{or} \quad s_1 = \frac{(t_M - t_m)^2}{4d}, \tag{1b}$$

where

$$t_m^2 = (R - d)^2 - r^2, \quad t_M^2 = (R + d)^2 - r^2. \tag{2}$$

See Figure 1a. As can be seen, t_M is the length of the longest tangent that can be drawn from C_1 to C_2, and t_m is the length of the shortest. These lengths will be often used in the following.
In this connection see also Figure 1b. Later it will be shown that the characteristic point $S_1(s_1, 0)$ is the intersection of the chords $T_1\hat{T}_1$ and $T_2\hat{T}_2$ of C_1. From this it will be clear that $s_1 > d$ if $d \neq 0$, but $s_1 = 0$ if $I = O$. Also it will be shown that the point $S_2(s_2, 0)$ is the intersection of the line through the points T_1 and T_2 with the x-axis.

First we prove the following theorem.

Publication Date: May 27, 2015. Communicating Editor: Paul Yiu.

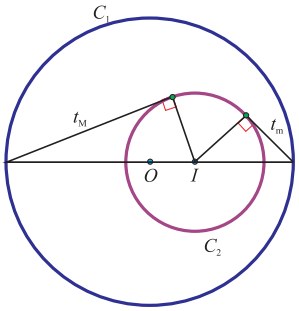

Figure 1a

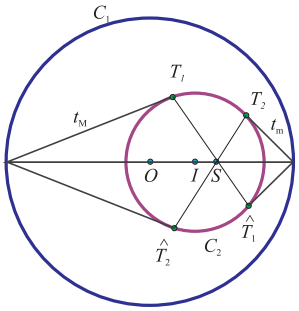

Figure 1b

Theorem 1. *Let C_1, C_2 and R, r, d be as in Definition 1. Let PQ be any given chord of the circle C_1 containing the point $S_1(s_1, 0)$, and PT_1 and QT_2 the tangents from P and Q to C_2 and let*

$$t_1 = |PT_1|, \qquad \hat{t}_1 = |QT_2|. \tag{3}$$

See Figure 2. Finally, let the coordinates of P, Q, T_1 and T_2 with reference to xOy be given by

$$P(u_1, v_1), Q(u_2, v_2), T_1(x_1, y_1), T_2(x_2, y_2). \tag{4}$$

Then

$$t_1\hat{t}_1 = t_m t_M, \tag{5}$$

that is,

$$\left((u_1 - x_1)^2 + (v_1 - y_1)^2\right)\left((u_2 - x_2)^2 + (v_2 - y_2)^2\right) - t_m^2 t_M^2 = 0. \tag{6}$$

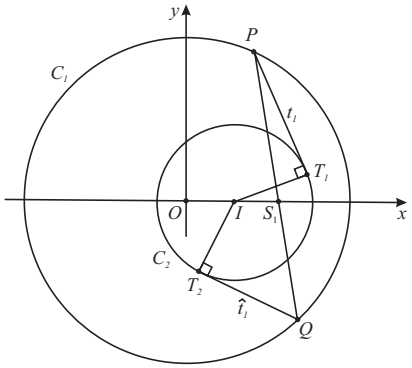

Figure 2

Proof. First it is clear that, if $v_1 > 0$, then $v_2 < 0$ and

$$v_1 = \sqrt{R^2 - u_1^2}, \qquad v_2 = -\sqrt{R^2 - u_2^2}. \tag{7}$$

The equation of the straight line through points $P(u_1, v_1)$ and $S_1(s_1, 0)$ is given by

$$y = \frac{v_1}{u_1 - s_1}(x - s_1). \tag{8}$$

It can be easily found that

$$\begin{aligned} u_2 &= \frac{sv_1^2 + \sqrt{s_1^2 v_1^4 - ((u_1 - s_1)^2 + v_1^2)(s_1^2 v_1^2 - R^2(u_1 - s_1)^2)}}{(u_1 - s_1)^2 + v_1^2}, \\ v_2 &= \frac{v_1}{u_1 - s_1}(u_2 - s_1). \end{aligned} \tag{9}$$

One solution of the system

$$(x - d)^2 + y^2 = r^2, \quad (u_1 - d)(x - d) + v_1 y = r^2 \tag{10}$$

is given by

$$\begin{aligned} x_1 &= d + \frac{r^2(u_1 - d) + \sqrt{r^4(u_1 - d)^2 - r^2(r^2 - v_1^2)(v_1^2 + (u_1 - d)^2)}}{(u_1 - d)^2 + v_1^2}, \\ y_1 &= \frac{r^2 - (u_1 - d)(x_1 - d)}{v_1}. \end{aligned} \tag{11}$$

In the same way, it can be found that a solution of the system

$$(x - d)^2 + y^2 = r^2, \quad (u_2 - d)(x - d) + v_2 y = r^2 \tag{12}$$

is given by

$$\begin{aligned} x_2 &= d + \frac{r^2(u_2 - d) + \sqrt{r^4(u_2 - d)^2 - r^2(r^2 - v_2^2)(v_2^2 + (u_2 - d)^2)}}{(u_2 - d)^2 + v_2^2}, \\ y_2 &= \frac{r^2 - (u_2 - d)(x_2 - d)}{v_2}. \end{aligned} \tag{13}$$

Starting from relation (6), using relations (7), (9), (11), (13) and with the help of a computer algebra system, we get, after rationalization and factorization, the following relation

$$\begin{aligned} &-4d(R - s_1)^2(R + s_1)^2\left(-dR^2 + d^2 s_1 - r^2 s_1 + R^2 s_1 - ds_1^2\right) \\ &\quad (R - u_1)^3(s_1 - u_1)^4(R + u_1)^3(d^2 + R^2 - 2du_1)^4(R^2 + s_1^2 - 2s_1 u_1)^7 \\ &\qquad \left(-dR^2 + d^2 u_1 - r^2 u_1 + R^2 u_1 - du_1^2\right) = 0. \end{aligned}$$

It can be easily seen that above relation is valid for every u_1 if the fourth factor $(-dR^2 + d^2 s_1 - r^2 s_1 + R^2 s_1 - ds_1^2)$ is equal to zero, that is, if s_1 is given by (1). This proves Theorem 1. □

This theorem will be proved later in an other way which may be interesting in itself. See Theorem 13 below.

Example 1. Let $R = 8$, $r = 3$, $d = 2$. Then

$$t_m = 5.196152423\ldots, \quad t_M = 9.539392014\ldots, \quad s_1 = 2.357966268\ldots.$$

If $u_1 = -2.5$, then $v_1 = 7.599342077\ldots$,
$u_2 = 5.847826086\ldots$, $v_2 = -5.459205922\ldots$,
$x_1 = 3.908649086\ldots$, $y_1 = 2.31453262\ldots$,
$x_2 = 0.585482934\ldots$, $y_2 = -2.64558906\ldots$,
$t_1 = 8.306623863\ldots$, $\hat{t}_1 = 5.967302209\ldots$.

$$t_1\hat{t}_1 = t_m t_M = 49.56813493\ldots\ .$$

Theorem 2 (Converse of Theorem 1)**.** *Let R, r, d be as in Theorem 1 and let PQ be any given chord of C_1 such that*

$$|PT_1| \cdot |QT_2| = t_m t_M, \tag{14}$$

where PT_1 is tangent of C_2 drawn from P and QT_2 is tangent of C_2 drawn from Q. Then the chord PQ contains the point $S_1(s_1, 0)$.

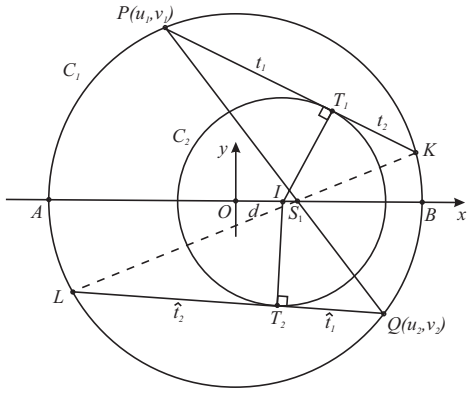

Figure 3

Proof. Since $|PT_1|^2 + |T_1I|^2 = |PI|^2$, we have

$$(u_1 - d)^2 + v_1^2 - r^2 = t_1^2$$

from which follows

$$u_1 = \frac{R^2 + d^2 - r^2 - t_1^2}{2d}. \tag{15}$$

In the same way it can be seen that

$$u_2 = \frac{R^2 + d^2 - r^2 - \hat{t}_1^2}{2d}. \tag{16}$$

Since

$$v_1 = \sqrt{R^2 - u_1^2}, \quad v_2 = -\sqrt{R^2 - u_2^2}, \tag{17}$$

the equation of the straight line through P and Q can be written as

$$y - v_1 = \frac{v_1 - v_2}{u_1 - u_2}(x - u_1),$$

where u_1 and u_2 are given by (15) and (16). Putting $y = 0$ we get the following equation in x

$$-v_1 = \frac{v_1 - v_2}{u_1 - u_2}(x - u_1). \tag{18}$$

In this equation we put $\hat{t}_1 = \frac{t_m t_M}{t_1}$ from (5). After rationalization and factorization we get

$$\begin{aligned}(d^2 - r^2 - 2dR + R^2 - t_1^2)(d^2 - r^2 + 2dR + R^2 - t_1^2)\\ (d^4 - 2d^2r^2 + r^4 - 2d^2R^2 - 2R^2r^2 + R^4 - t_1^4)\\ (-dR^2 + d^2x - r^2x + R^2x - dx^2) = 0.\end{aligned} \tag{19}$$

Only the fourth factor gives the point of intersection with x-axis and we have

$$x = \frac{R^2 + d^2 - r^2 - \sqrt{(R^2 + d^2 - r^2)^2 - 4R^2d^2}}{2d}. \tag{20}$$

First it can be seen that

$$(R^2 + d^2 - r^2)^2 - 4R^2d^2 = t_m^2 t_M^2. \tag{21}$$

Concerning the first three factors in (19) it is easily seen that these, respectively, can be written as

$$t_m^2 - t_1^2, \quad t_M^2 - t_1^2, \quad t_m^2 t_M^2 - t_1^4.$$

The first and the second expressions occur when $PQ = AB$ (see Figure 3); the third when $t_1 = \hat{t}_1$. Thus, the point of intersection with the x-axis in the general case is given by (20), with x replaced by $s_{1,2}$. This proves Theorem 2. □

Theorem 3. *Let T_1 and T_2 be as in Theorem 1* (see Figure 2). *The point S_1 lies on the segment T_1T_2.*

Proof. It is easy to show that the equation of the line through points $T_1(x_1, y_1)$ and $T_2(x_2, y_2)$ is satisfied by $S_1(s_1, 0)$, that is $-y_1 = \frac{y_1 - y_2}{x_1 - x_2}(s_1 - x_1)$. □

Theorem 4. *Let t_2 and $\hat{t}_2$ be as in Figure 3. Then $t_2\hat{t}_2 = t_1\hat{t}_1$, that is,*

$$t_2\hat{t}_2 = t_m t_M.$$

Proof. The proof is in the same way as the proof of Theorem 1. □

2. Characteristic points associated with bicentric polygons

One corollary of this theorem, which will be stated (see [2,3]), refers to bicentric polygons. Before stating it let us mention that a polygon which is both chordal and tangential is simply called a *bicentric* polygon. The following question can be raised: If C_1 and C_2 are circles such that C_2 is completely inside C_1, is there an n-sided polygon inscribed in C_1 and circumscribed around C_2? The first who considered this problem for $n = 4$ was the Swiss mathematician Nicolaus Fuss (1755 – 1826). See [2]. He found that for $n = 4$ the following condition must be fulfilled:

$$(R^2 - d^2)^2 - 2r^2(R^2 + d^2) = 0, \tag{22}$$

where $R =$ radius of C_1, $r =$ radius of C_2, and $d =$ distance between centers of C_1 and C_2.

Fuss also found conditions for $n = 5, 6, 7, 8$ (see [3]). Subsequently, such conditions are also found for many integers $n > 8$. In honor of Fuss all such conditions are called Fuss' relations.

It seems that many problems concerning bicentric polygons can be proved using properties of the characteristic points in Theorems 1, 2.

In establishing Fuss' relations, Poncelet's celebrated closure theorem [4] plays an important role.

Theorem (Poncelet's closure theorem)**.** Let C and D be two nested conics such that there is an n-sided polygon inscribed in D and circumscribed around C. Then for every point $x \in D$, there is an n-sided polygon with x as a vertex, inscribed in D and circumscribed around C.

Remark. (1) In the following we shall mostly deal with two circles C_1 and C_2, where C_2 is completely inside C_1. For brevity in the expression in this dealing we shall say that C_1 and C_2 are determined by triple (R, r, d) if and only if $(R, r, d) \in \mathbb{R}^3_+$ and

$$R > d + r, \tag{23}$$

where $R =$ radius of C_1, $r =$ radius of C_2, $d =$ distance between centers of C_1 and C_2.

In the following it will be shown that relations concerning the characteristic points of these circles are closely connected with bicentric polygons.

Definition A below is a slight modification of Definition 1 in [7].

Definition A. Let S be a set given by

$$S = \left\{(R, r, d) : (R, r, d) \in R^3_+ \text{ and } R > r + d\right\}.$$

For a given $(R_0, r_0, d_0) \in S$, we have

$$f_1(R_0, r_0, d_0) = (R_1, r_1, d_1),$$
$$f_2(R_0, r_0, d_0) = (R_2, r_2, d_2),$$

where R_1, r_1, d_1 and R_2, r_2, d_2 are given by

$$R_1^2 = R_0\left(R_0 + r_0 + \sqrt{(R_0 + r_0)^2 - d_0^2}\right), \tag{24a}$$

$$d_1^2 = R_0\left(R_0 + r_0 - \sqrt{(R_0 + r_0)^2 - d_0^2}\right), \tag{24b}$$

$$r_1^2 = (R_0 + r_0)^2 - d_0^2, \tag{24c}$$

$$R_2^2 = R_0\left(R_0 - r_0 + \sqrt{(R_0 - r_0)^2 - d_0^2}\right), \tag{25a}$$

$$d_2^2 = R_0\left(R_0 - r_0 - \sqrt{(R_0 - r_0)^2 - d_0^2}\right), \tag{25b}$$

$$r_2^2 = (R_0 - r_0)^2 - d_0^2, \tag{25c}$$

It can be proved that

$$R_1 > r_1 + d_1, \quad R_2 > r_2 + d_2, \tag{26a}$$

$$R_1 d_1 = R_2 d_2 = R_0 d_0, \tag{26b}$$

$$R_1^2 + d_1^2 - r_1^2 = R_2^2 + d_2^2 - r_2^2 = R_0^2 + d_0^2 - r_0^2. \tag{26c}$$

$$r_1 r_2 = t_M t_m, \tag{27a}$$

where

$$t_M^2 = (R_0 + d_0)^2 - r_0^2, \quad t_m^2 = (R_0 - d_0)^2 - r_0^2. \tag{27b}$$

Also,

$$(R_1 + d_1)^2 - r_1^2 = t_M^2, \quad (R_1 - d_1)^2 - r_1^2 = t_m^2. \tag{28a}$$

$$\frac{R_1^2 - d_1^2}{2r_1} = \frac{R_2^2 - d_2^2}{2r_2} = R_0, \quad \frac{2R_1 d_1 r_1}{R_1^2 - d_1^2} = \frac{2R_2 d_2 r_2}{R_2^2 - d_2^2} = d_0, \tag{28b}$$

$$\begin{aligned} &-\left(R_1^2 + d_1^2 - r_1^2\right) + \left(\frac{R_1^2 - d_1^2}{2r_1}\right)^2 + \left(\frac{2R_1 d_1 r_1}{R_1^2 - d_1^2}\right)^2 \\ &= -\left(R_2^2 + d_2^2 - r_2^2\right) + \left(\frac{R_2^2 - d_2^2}{2r_2}\right)^2 + \left(\frac{2R_2 d_2 r_2}{R_2^2 - d_2^2}\right)^2 = r_0^2. \end{aligned} \tag{28c}$$

More about this and the functions f_1 and f_2 can be seen in [7, Theorem 1].

Theorem 5. *Let R_0, r_0, d_0 and R_i, r_i, d_i, $i = 1, 2$, be as in Definition A. Then*

$$d_i s_i = d_0 s_0, \quad i = 1, 2, \tag{29}$$

where

$$s_0 = \frac{(t_M - t_m)^2}{4d_0}, \tag{30a}$$

$$s_i = \frac{(t_M - t_m)^2}{4d_i}. \tag{30b}$$

Proof. From (28a) and (30) it follows $4d_0 s_0 = 4d_i s_i,\ i = 1, 2.$ □

Theorem 6. *Let K_1 and K_2 be circles determined by triple (R_1, d_1, r_1), where R_1, r_1, d_1 are given by* (24)*. Then characteristic point of the triple (cR_1, cd_1, cr_1), where $c = \frac{R_0}{R_1}$, is the same as that of the triple (R_0, d_0, r_0), that is,*

$$cs_1 = s_0, \tag{31}$$

where s_0 and s_1 are given by (30)*.*

Proof. We can write

$$cs_1 = c \cdot \frac{(t_M - t_m)^2}{4d_1} = \frac{(t_M - t_m)^2}{4\frac{1}{c}d_1} = \frac{(t_M - t_m)^2}{4d_0} = s_0,$$

since, by (26b),

$$\frac{1}{c}d_1 = \frac{R_1}{R_0}d_1 = \frac{R_0 d_0}{R_0} = d_0.$$

□

Relations (25) hold analogously if the triple (R_1, d_1, r_1) is replaced by (R_2, d_2, r_2). In this case we have $c = \frac{R_0}{R_2}$, and $cs_2 = s_0$.

Some important properties concerning bicentric n-gons will be now established. Some of these are extension and completion of theorems proved earlier (see [7, 8]).

Theorem 7. *Let $n \geq 4$ be an even integer. Let $(R_1, r_1, d_1) \in R_+^3$ be any given solution of Fuss' relation $F_n(R, r, d) = 0$. Let C_1 and C_2 be circles (in the same plane) such that*
R_1 = radius of C_1,
r_1 = radius of C_2,
d_1 = distance between points O and I, where O is the center of C_1 and I is the center of C_2.

Further, let xOy denotes a coordinate system with origin O and positive x-axis containing I. Finally, let $P(u, v)$ be any given point of C_1. Then there is a unique point $Q(\hat{u}, \hat{v})$ of C_1 such that

$$\hat{u} = \frac{-2R_1^2 d_1 + \left(R_1^2 + d_1^2 - r_1^2\right) u}{2d_1 u - \left(R_1^2 + d_1^2 - r_1^2\right)}, \tag{32a}$$

$$\hat{v} = \sqrt{R_1^2 - \hat{u}^2} \text{ or } \quad -\sqrt{R_1^2 - \hat{u}^2}, \tag{32b}$$

and the line determined by points PQ contains the characteristic point $S_1(s_1, 0)$ of the triple (R_1, r_1, d_1).

Proof. From the equation of the line through $P(u, v)$ and $Q(\hat{u}, \hat{v})$, that is,

$$y - \hat{v} = \frac{v - \hat{v}}{u - \hat{u}}(x - \hat{u}), \tag{33}$$

putting $y = 0$, we obtain

$$\frac{\hat{u} - x}{u - x} = \frac{\hat{v}}{v}.$$

We have to prove that this has solution $x = s_1$ if and only if $\hat{u}$ and $\hat{v}$ are given by (32) and s_1 is given by

$$s_1 = \frac{(t_M - t_m)^2}{4d_1} = \frac{\left(\sqrt{(R_1 + d_1)^2 - r_1^2} - \sqrt{(R_1 - d_1)^2 - r_1^2}\right)^2}{4d_1}. \tag{34}$$

See also Figure 4.

Using computer algebra it can be easily shown that the relation

$$\frac{\hat{u}-s_1}{u-s_1}=\frac{\hat{v}}{v}$$

is satisfied if $\hat{u}$ and $\hat{v}$ are given by (32) and s_1 is given by (34). □

We remark that instead of the equation (33), the relation (34) can also be established by using the equation of the line through $P(u,v)$ and $S_1(s_1,0)$, that is

$$y=\frac{v}{u-s_1}(x-s_1), \tag{35}$$

and replacing x and y by $\hat{u}$ and $\hat{v}$ given by (32).

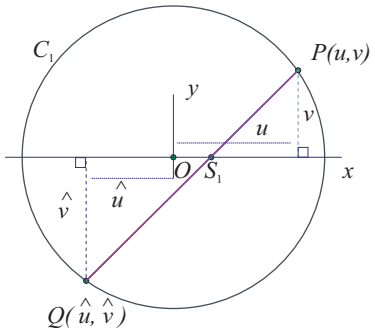

Figure 4: $(-\hat{u}+s_1):(u-s_1)=-\hat{v}:v$.

Corollary 8. *The relation* (32a) *is equivalent to*

$$u=\frac{-2R_1^2d_1+\left(R_1^2+d_1^2-r_1^2\right)\hat{u}}{2d_1\hat{u}-\left(R_1^2+d_1^2-r_1^2\right)}. \tag{36}$$

The proof is straightforward.

Theorem 9. *Let u and $\hat{u}$ be as in Theorem 7. Then*

$$t\hat{t}=t_Mt_m, \tag{37}$$

where

$$t^2=R_1^2+d_1^2-r_1^2-2d_1u, \qquad \hat{t}^2=R_1^2+d_1^2-r_1^2-2d_1\hat{u}, \tag{38}$$

$$t_M^2=(R_1+d_1)^2-r_1^2, \qquad t_m^2=(R_1-d_1)^2-r_1^2. \tag{39}$$

Proof. Replacing u in the relation (32a) by

$$\frac{R_1^2+d_1^2-r_1^2-t^2}{2d_1}$$

obtained from t^2 given by (38) we easily get the relation

$$\left(R_1^2+d_1^2-r_1^2-2d_1\hat{u}\right)t^2=t_M^2t_m^2$$

or

$$\hat{t}^2t^2=t_M^2t_m^2.$$

This theorem can be also proved in the following way.

If in the relation $(t\hat{t})^2 = \left(R_1^2 + d_1^2 - r_1^2 - 2d_1u\right)\left(R_1^2 + d_1^2 - r_1^2 - 2d_1\hat{u}\right)$ we replace $(t\hat{t})^2$ by $(t_M t_m)^2 = \left(R_1^2 + d_1^2 - r_1^2\right)^2 - 4d_1^2R_1^2$, then we get

$$-4d_1^2R_1^2 = -2d_1\hat{u}\left(R_1^2 + d_1^2 - r_1^2\right) - 2d_1u\left(R_1^2 + d_1^2 - r_1^2\right) + 4d_1^2u\hat{u},$$

which is equivalent to the relation (32a). □

Remark. (2) As can be seen, proving Theorem 9 we in fact prove Theorem 1 in an another way which may be interesting in itself.

Theorem 10. *Let $P(u,v)$, $Q(\hat{u},\hat{v})$ and $S_1(s_1,0)$ be as in Theorem 7. Then*

$$|PS|\,|QS| = R_1^2 - s_1^2. \tag{40}$$

Proof. First let us remark that $R_1 > s_1$ since

$$s_1 = \frac{(t_M - t_m)^2}{4d_1} = \frac{t_M^2 - 2t_Mt_m + t_m^2}{4d_1} = \frac{R_1^2 + d_1^2 - r_1^2 - t_Mt_m}{2d_1},$$

$$\begin{aligned} &2R_1d_1 > R_1^2 + d_1^2 - r_1^2 - 2t_Mt_m \\ \Longrightarrow\ &0 > (R_1 - d_1)^2 - r_1^2 - t_Mt_m \text{ or } 0 > t_m^2 - t_mt_M. \end{aligned} \tag{41}$$

Now,

$$\begin{aligned} |PS|^2 \cdot |QS|^2 &= \left((u - s_1)^2 + v^2\right)\left((\hat{u} - s_1)^2 + \hat{v}^2\right) \\ &= \left(R_1^2 - 2us_1 + s_1^2\right)\left(R_1^2 - 2\hat{u}s_1 + s_1^2\right). \end{aligned}$$

This is equal to $(R_1^2 - s_1^2)^2$ if and only if

$$-2R_1^2\hat{u}s_1 - 2R_1^2us_1 + 4u\hat{u}s_1^2 - 2us_1^3 - 2\hat{u}s_1^3 = 4R_1^2s_1^2. \tag{42}$$

This can be rewritten as

$$\hat{u}\left(R_1^2s + s_1^3 - 2s_1^2u\right) = 2R_1^2s_1^2 - \left(R_1^2s_1 + s_1^3\right)u.$$

From this,

$$\hat{u} = \frac{2R_1^2s_1 - (R_1^2 + s_1^2)u}{-2s_1u + R_1^2 + s_1^2}. \tag{43}$$

Replacing s_1 by $\dfrac{R_1^2 + d_1^2 - r_1^2 - t_Mt_m}{2d_1}$ (see (1b)) it is easy to find that the above relation can be written as

$$\hat{u} = \frac{2R_1^2d_1 - \left(R_1^2 + d_1^2 - r_1^2\right)u}{-2d_1u + \left(R_1^2 + d_1^2 - r_1^2\right)}.$$

Thus, the relation (40) is valid if $\hat{u}$ is given by (32a). □

Theorem 11. *Let $P(u,v)$, $Q(\hat{u},\hat{v})$ and $S_1(s_1,0)$ be as in Theorem 7. Then*

$$\frac{|PQ|}{t + \hat{t}} = \frac{2R_1}{\sqrt{(R_1 + d_1)^2 - r_1^2} + \sqrt{(R_1 - d_1)^2 - r_1^2}}, \tag{44}$$

where t and $\hat{t}$ are given by (38)*.*

Proof. We have to prove that

$$\frac{(u-\hat{u})^2+(v-\hat{v})^2}{(t+\hat{t})^2}=\left(\frac{2R_1}{t_M+t_m}\right)^2, \tag{45}$$

where t_M and t_m are given by (39). The proof goes in the same way as the proofs of the previous two theorems. Of course, in this theorem there is some more calculations since there are some terms which need to be rationalized. If obtained relation after rationalization is denoted by $f(u,\hat{u})$ then $f(u,\hat{u})=0$ for $\hat{u}$ given by (32a). This proves Theorem 11. □

Remark. (3) In [6, Theorem1] it is proved that for $n=4$ it holds

$$\frac{|PQ|}{t+\hat{t}}=\sqrt{\frac{2R_1^2}{R_1^2+d_1^2}}. \tag{46}$$

In the following theorem some results in [5, pp. 52–53] will be used. It was proved that for the lengths of tangents to a bicentric polygons,

$$(t_2)_{1,2}=\frac{(R^2-d^2)t_1\pm r\sqrt{(t_M^2-t_1^2)(t_1^2-t_m^2)}}{r^2+t_1^2}. \tag{47}$$

If t_1 is given tangent length, then one of $(t_2)_{1,2}$ is consecutive and other is proceeding.

Theorem 12. *Let $A_1\dots A_n$ be any given bicentric n-gon whose circumcircle is C_1 and incircle C_2 as it is described in Theorem 7. Let xOy be a coordinate system as in Figure 3 and let the vertices $A_1,\dots,A_n$ be given by $A_i(u_i,v_i),\ i=1,\dots,n$. Finally, let $t_1,\dots,t_n$ be tangent lengths from the vertices $A_i(u_i,v_i)$ of the n-gon $A_1\dots A_n$, that is,*

$$t_i^2=R_1^2+d_1^2-r_1^2-2d_1u_i,\quad i=1,\dots,n. \tag{48}$$

If $t_1^2=R_1^2+d_1^2-r_1^2-2d_1u_1$ is given, then the consequent of u_1 is $(u_2)_1$ or $(u_2)_2$ given by

$$\begin{aligned}(u_2)_1=\frac{1}{\left(d_1^2+R_1^2-2d_1u_1\right)^2}&\left(-d_1^4u_1+2r_1^2R_1^2u_1-R_1^4u_1+2d_1^2\left(r_1^2-3R_1^2\right)u_1\right.\\&-2\sqrt{r_1^2\left(R_1^2-d_1^2\right)^2\left(d_1^2-r_1^2+R_1^2-2d_1u_1\right)\left(R_1^2-u_1^2\right)}\\&\left.+2d_1^3\left(R_1^2+u_1^2\right)+2d_1R_1^2\left(R_1^2+u_1^2-2r_1^2\right)\right)\end{aligned} \tag{49a}$$

$$\begin{aligned}(u_2)_2=\frac{1}{\left(d_1^2+R_1^2-2d_1u_1\right)^2}&\left(-d_1^4u_1+2r_1^2R_1^2u_1-R_1^4u_1+2d_1^2\left(r_1^2-3R_1^2\right)u_1\right.\\&+2\sqrt{r_1^2\left(R_1^2-d_1^2\right)^2\left(d_1^2-r_1^2+R_1^2-2d_1u_1\right)\left(R_1^2-u_1^2\right)}\\&\left.+2d_1^3\left(R_1^2+u_1^2\right)+2d_1R_1^2\left(R_1^2+u_1^2-2r_1^2\right)\right).\end{aligned} \tag{49b}$$

Proof. From relation (47) (rewriting t_2 instead of $(t_2)_2$) it follows that

$$\left(t_2^2+\frac{(R_1^2-d_1^2)^2t_1^2}{(R_1^2+d_1^2-r_1^2-2d_1u_1)^2}-\frac{4d_1^2r_1^2(R_1^2-u_1^2)}{(R_1^2+d_1^2-r_1^2-2d_1u_1)^2}\right)^2$$
$$=\left(\frac{2(R_1^2-d_1^2)t_1t_2}{R_1^2+d_1^2-2d_1u_1}\right)^2, \tag{50}$$

where

$$t_1=\sqrt{R_1^2+d_1^2-r_1^2-2d_1u_1},\quad t_2=\sqrt{R_1^2+d_1^2-r_1^2-2d_1u_2}. \tag{51}$$

Replacing t_1 and t_2 in the relation (50) by the right sides of the above two relations, we get

$$au_2^2+bu_2+c=0, \tag{52a}$$

where

$$\begin{aligned}a&=-4d_1^2r_1^2R_1^2+4r_1^4R_1^2+4d_1^2R_1^4-4r_1^2R_1^4-4d_1^3R_1^2u_1\\&\quad+8d_1r_1^2R_1^2u_1-4d_1R_1^4u_1+d_1^4u_1^2+2d_1^2R_1^2u_1^2,\\b&=2\left(d_1^2-2r_1^2+R_1^2-2d_1u_1\right)\left(-2d_1R_1^2+d_1^2u_1+R_1^2u_1\right),\\c&=d_1^2+R_1^2-2d_1u_1.\end{aligned} \tag{52b}$$

Using computer algebra it can be easily found that the solution of the equation given by (52) are given by (49). □

Here is an example.

Example 2. Let $n=6$ and (R_1,r_1,d_1) be a solution of Fuss' relation $F_6(R,r,d)=0$ such that

$$R_1=8.340410321\ldots,\ r_1=6.812488532\ldots,\ d_1=1.198981793\ldots.$$

(For brevity in the following the points (sign) ... after calculated values will be omitted.)

The values t_M and t_m are given by

$$t_M=\sqrt{(R_1+d_1)^2-r_1^2}=6.7677574552,$$
$$t_m=\sqrt{(R_1-d_1)^2-r_1^2}=2.14242886.$$

Let t_1 be a length such that $t_M\geq t_1\geq t_m$, say $t_1=4$. Then, as can be easily concluded, there is a bicentric hexagon $A_1\ldots A_6$ such that its first tangent is $t_1=4$. The other tangent lengths of this hexagon can be calculated using formula (47) and find that

$$t_2=2.3947586766,\qquad t_3=2.2572852505,\qquad t_4=3.5765564793,$$
$$t_5=5.973973936,\qquad t_6=6.3378015311.$$

These tangent lengths can also be calculated using u_1 given by

$$u_1=\frac{R_1^2+d_1^2-r_1^2-t_1^2}{2d_1}=3.58220619 \tag{53}$$

and formulas given by (49). For example, taking u_1 given by (53) and using relation (49a) we get

$$(u_2)_1 = 7.862976314, \quad (u_2)_2 = 6.49623254.$$

It can be verified that

$$(u_2)_1 = \frac{R_1^2 + d_1^2 - r_1^2 - t_2^2}{2d_1}, \quad (u_2)_2 = \frac{R_1^2 + d_1^2 - r_1^2 - t_6^2}{2d_1}.$$

Thus,

$$(t_2)^2 = \frac{R_1^2 + d_1^2 - r_1^2 - 2d_1(u_2)_1}{2d_1}, \quad (t_6)^2 = \frac{R_1^2 + d_1^2 - r_1^2 - 2d_1(u_2)_2}{2d_1}.$$

In the same way we can proceed and get t_3, t_4, t_5.

Here, let us remark that the relations (49) may be very useful in some investigations concerning bicentric polygons.

Theorem 13. *Let $A_1 \dots A_n$ be n-gon as in Theorem 12 with vertices $A_i = A_i(u_i, v_i)$, $i = 1, \dots, n$. Let $t_1, \dots, t_n$ be the tangent lengths of the n-gon from the vertices $A_i = A_i(u_i, v_i)$, $i = 1, \dots, n$, that is*

$$t_i^2 = R_1^2 + d_1^2 - r_1^2 - 2d_1 u_i, \quad i = 1, \dots, n. \tag{54}$$

Let $n \geq 4$ be an even integer. Then

$$u_{i+\frac{n}{2}} = \frac{2R_1^2 d_1 - \left(R_1^2 + d_1^2 - r_1^2\right) u_i}{-2d_1 u_i + \left(R_1^2 + d_1^2 - r_1^2\right)}, \quad i = 1, \dots, \frac{n}{2}. \tag{55}$$

In other words, the chords $A_i A_{i+\frac{n}{2}}$, $i = 1, \dots, \frac{n}{2}$, of the circle C_1 contain the points $S_1(s_1, 0)$ such that the points $A_i(u_i, v_i)$ and $A_{i+\frac{n}{2}}(u_{i+\frac{n}{2}}, v_{i+\frac{n}{2}})$, $i = 1, \dots, \frac{n}{2}$, have the properties as the points $P(u, v)$ and $Q(\hat{u}, \hat{v})$ in the previous theorems, that is

$$t_i t_{i+\frac{n}{2}} = t_M t_m, \quad i = 1, \dots, \frac{n}{2}, \tag{56}$$

where t_M and t_m are given by (39).

Proof. First let us remark that the notation used in Theorems 7 and 9 will be used. So, if u and $\hat{u}$ are as in Theorem 7 and t is given by $t^2 = R_1^2 + d_1^2 - r_1^2 - 2d_1 u$, then $\hat{t}^2 = R_1^2 + d_1^2 - r_1^2 - 2d_1 \hat{u}$.

In the first way we prove that $\hat{t}_1, \hat{t}_2$ are consequent if t_1 and t_2 are consequent. In other words, we prove that

$$\hat{t}_1 + \hat{t}_2 = \sqrt{(\hat{u}_1 - \hat{u}_2)^2 + (\hat{v}_1 - \hat{v}_2)^2}, \tag{57}$$

where t_1 and t_2 are consecutive tangent lengths of the n-gon $A_1 \dots A_n$, that is, the relation (47) is valid and can be written as

$$t_2 = \frac{t_1(R^2 - d^2) - k}{r^2 + t_1^2}, \tag{58}$$

where

$$k=\sqrt{t_1^2\left(R^2-d^2\right)^2+\left(r^2+t_1^2\right)\left(4R^2d^2-r^2t_1^2-\left(R^2+d^2-r^2\right)^2\right)}.$$

Also let us remark that

$$\hat{v}_i^2=R_1^2-\hat{u}_i^2,\quad i=1,2.$$

It can be easily shown (even by hand, without using computer algebra) that the relation (57) implies the following relation

$$\left(8\hat{t}_1\hat{t}_2\hat{v}_1\hat{v}_2\right)^2=\left(\left(2R_1^2-2\hat{u}_1\hat{u}_2-\hat{t}_1^2-\hat{t}_2^2\right)^2-4(\hat{t}_1\hat{t}_2)^2-4(\hat{v}_1\hat{v}_2)^2\right)^2.$$

Replacing $\hat{u}_i,\ i=1,2$, with

$$\frac{-2R_1^2d_1+\left(R_1^2+d_1^2-r_1^2\right)u_i}{2d_iu_i-\left(R_1^2+d_1^2-r_1^2\right)},\quad i=1,2,$$

respectively, we get

$$\begin{aligned}
&(d_1-r_1-R_1)^2(d_1+r_1-R_1)^2(d_1-r_1+R_1)^2(d_1+r_1+R_1)^2\\
&\big(d_1^4u_1^2+2d_1^4u_1u_2+d_1^4u_2^2-4d_1^3R_1^2u_1-4d_1^3R_1^2u_2-4d_1^3u_1^2u_2\\
&\quad-4d_1^3u_1u_2^2-4d_1^2r_1^2R_1^2-4d_1^2r_1^2u_1u_2+4d_1^2R_1^4+2d_1^2R_1^2u_1^2\\
&\quad+12d_1^2R_1^2u_1u_2+2d_1^2R_1^2u_2^2+4d_1^2u_1^2u_2^2+8d_1r_1^2R_1^2u_1\\
&\quad+8d_1r_1^2R_1^2u_2-4d_1R_1^4u_1-4d_1R_1^4u_2-4d_1R_1^2u_1^2u_2-4d_1R_1^2u_1u_2^2\\
&\quad+4r_1^4R_1^2-4r_1^2R_1^4-4r_1^2R_1^2u_1u_2+R_1^4u_1^2+2R_1^4u_1u_2+R_1^4u_2^2\big)=0.
\end{aligned}\tag{59a}$$

Now, if in the fifth (last) factor of the above relation we put

$$\frac{\left(R_1^2+d_1^2-r_1^2\right)-t_i^2}{2d_1},\quad i=1,2,$$

instead of $u_i,\ i=1,2$, respectively, then we get

$$\begin{aligned}
&\left(d_1^4-2d_1^2r_1^2-2d_1^2R_1^2+2d_1^2t_1t_2+r_1^4-2r_1^2R_1^2+r_1^2t_1^2+r_1^2t_2^2+R_1^4-2R_1^2t_1t_2+t_1^2t_2^2\right)\\
&\left(d_1^4-2d_1^2r_1^2-2d_1^2R_1^2-2d_1^2t_1t_2+r_1^4-2r_1^2R_1^2+r_1^2t_1^2+r_1^2t_2^2+R_1^4+2R_1^2t_1t_2+t_1^2t_2^2\right)=0.
\end{aligned}\tag{59b}$$

Finally, if t_2 in the above relation be replaced by the right side of the relation (58), then the second factor of the above relation vanishes.

This proves the validity of (57).

Now, using this result, the proof of Theorem 13 follows from Poncelet's closure theorem. Namely, by this theorem there is a bicentric n-gon whose first tangent has length $\hat{t}_1$ and beginning point $\hat{A}_1(\hat{u}_1,\hat{v}_1)$. This n-gon is obtained such that we proceed in the same way with t_2, t_3, then with $t_3,t_4,\ldots$, finally with t_n,t_1. In this way we get closure:

$$\{\hat{A}_1,\ldots,\hat{A}_n\}=\{A_1\ldots,A_n\},$$

where

$$\hat{A}_i=A_{i+\frac{n}{2}}\text{ and }\hat{t}_i=t_{i+\frac{n}{2}},\quad i=1,\ldots,\frac{n}{2}.$$

Thus,

$$A_1A_2\cdots A_{\frac{n}{2}}\hat{A}_1\hat{A}_2\cdots\hat{A}_{\frac{n}{2}} = A_1A_2\cdots A_{n-1}A_n.$$

This proves Theorem 13. □

Remark. (4) As it is seen, the proof of Theorem 13 is rather involved and we have solved one of the old and difficult problems concerning bicentric polygons.

Here is an example. With the hexagon $A_1\dots A_6$ from Example 2, we have

$$t_1t_4 = t_2t_5 = t_3t_6 = t_Mt_m.$$

Theorem 14. *Let the triple (R_1, r_1, d_1) and the bicentric n-gon $A_1\dots A_n$ be as in Theorem 7. Let $t_i,\ i = 1,\dots,n$, be the tangent lengths of the n-gon $A_1\dots A_n$ and let $T_i,\ i = 1,\dots,n$ be the touching points of the segments $A_iA_{i+1},\ i = 1,\dots,n$, and the circle C_2, respectively. In other words*

$$t_i = |A_iT_i|, \quad i = 1,\dots,n. \tag{60}$$

Let

$$(k^iR_1, k^ir_1, k^id_1), \quad i = 1, 2,\dots \tag{61}$$

be a set of triples such that

$$k = \frac{r_1}{R_1}. \tag{62}$$

Then for each $i = 1, 2,\dots$ there is a bicentric n-gon from the class $C(k^iR_1, k^ir_1, k^id_1)$ such that its tangent lengths are $k^it_1,\dots,k^it_n$.

Proof. The triples given by (61) also satisfy Fuss' relation $F_n(R, r, d) = 0$ as the triple (R_1, r_1, d_1). □

Corollary 15. *Let $S_i(s_i, 0)$ denote the characteristic point of the triple $\left(k^iR_1, k^ir_1, k^id_1\right)$. Then*

$$s_i = k^{i-1}s_1, \tag{63}$$

where

$$s_1 = \frac{(t_M - t_m)^2}{4d_1}, \tag{64}$$

$$t_M^2 = (R_1 + d_1)^2 - r_1^2, \quad t_m^2 = (R_1 - d_1)^2 - r_1^2. \tag{65}$$

Proof. This follows from

$$s_i = \frac{\left(k^{i-1}t_M - k^{i-1}t_m\right)^2}{4k^{i-1}d_i} = \frac{k^{i-1}(t_M - t_m)^2}{4d_1}.$$

□

Example 3. Let $n = 6$ and let the triple (R_1, r_1, d_1), where

$$R_1 = 8.340410321,\ r_1 = 6.812488532,\ d_1 = 1.198981793$$

be a solution of Fuss' relation $F_6(R, r, d) = 0$.

Now, using these values we get

$$t_M = 6.67757441, \quad t_m = 2.142428529, \quad k = 0.816804971,$$

$$s_1 = 4.288544723, \quad s_2 = 3.502904648, \quad s_3 = 2.86118993, \text{ and so on.}$$

Let R_{i+1}, r_{i+1}, d_{i+1} be given by

$$R_{i+1} = k^i R_1, \quad r_{i+1} = k^i r_1, \quad d_{i+1} = k^i d_1, i = 1, 2, \ldots .$$

Thus

$$R_2 = 6.81248861, \quad r_2 = 5.564474498, \quad d_2 = 0.979334288,$$
$$R_3 = 5.564474498, \quad r_3 = 4.545090431, \quad d_3 = 0.799925115, \text{ and so on.}$$

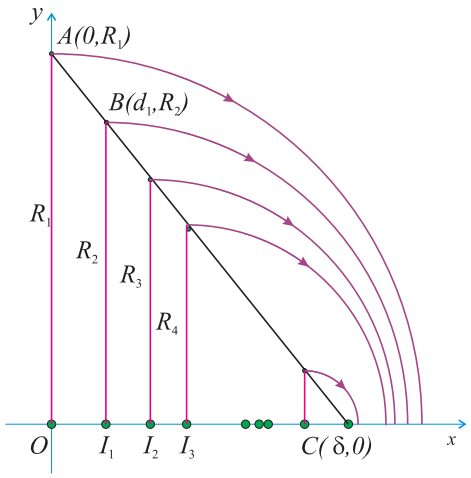

Figure 5

The following properties may be interesting. In Figure 5,

$$\delta = d_1 + d_2 + d_3 + \cdots = \frac{d_1}{1-k} = 6.544838032.$$

First, let us remark that the line determined by points $A(0, R_1)$ and $B(d_1, R_2)$, where $R_2 = r_1$, contains the point $C(\delta, 0)$ and the points whose coordinates are (d_2, R_3), (d_3, R_4) and so on. Also, let us remark that there are points $S_i(s_i, 0)$, $i = 1, 2, \ldots, n$, on the positive x-axis such that

$$s_1 = |OS_1| < r_1, \quad s_2 = |I_1S_2| < r_2, \quad s_3 = |I_2S_3| < r_3, \text{ and so on.}$$

Remark. (5) If instead of $k = \frac{r_1}{R_1}$, we take $K = \frac{R_1}{r_1}$ then we have analogous situation. Only in this case each of the values K^iR_1, K^ir_1, $K^id_1 \to \infty$ when $i \to \infty$.

Theorem 16. *Let $(R_0, r_0, d_0) \in \mathbb{R}^3_+$ be a solution of Fuss' relation $F_n(R, r, d) = 0$ and let $(R_1, r_1, d_1) \in \mathbb{R}^3_+$ be given by* (24)*, that is,*

$$(R_1, r_1, d_1) = \left(\sqrt{R_0(R_0 + r_0 + r_1)}, r_1, \sqrt{R_0(R_0 + r_0 - r_1)}\right)$$

where

$$r_1 = \sqrt{(R_0 + r_0)^2 - d_0^2}.$$

Let (R_1, r_1, d_1) be a solution of Fuss' relation $F_{2n}(R, r, d) = 0$ and let C_1, C_2, K_1, K_2 be circles in the same plane such that O is the center of C_1 and K_1 (see Figure 6)*. The center of C_2 is denoted by I_0 and center of K_2 is denoted by I_1 and*

$$\begin{aligned} R_0 &= \text{ radius of } C_1, \quad r_0 = \text{ radius of } C_2, \\ d_0 &= \text{ distance between centers of } C_1 \text{ and } C_2. \\ R_1 &= \text{ radius of } K_1, \quad r_1 = \text{ radius of } K_2, \\ d_1 &= \text{ distance between centers of } K_1 \text{ and } K_2. \end{aligned}$$

Let xOy be a coordinate system with origin O and positive x-axis containing the centers I_0 and I_1. Then there are bicentric n-gon $A_1 \cdots A_n$ inscribed in C_1 and circumscribed around C_2 and bicentric $2n$-gon inscribed in K_1 and circumscribed around K_2 such that the following is valid:

> *If $t_1 \ldots, t_n$ are tangent lengths of the n-gon $A_1 \cdots A_n$ and $u_1, \ldots, u_{2n}$ are tangent lengths of the $2n$-gon $B_1 \cdots B_{2n}$ then*
>
> $$u_{2i-1} = t_i, \quad i = 1, \ldots, n. \tag{66}$$

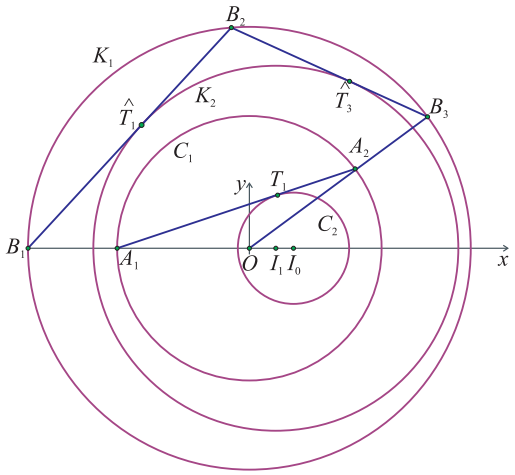

Figure 6: A_1 and A_2 are two consequent vertices of an n-gon $A_1 \ldots A_n$ inscribed in C_1 and circumscribed around C_2.

Proof. The point A_1 is given by $A_1(u_1, 0)$, where $u_1 = -R_0$, and the point A_2 (as a consequent of A_1) is given by $A_2(u_2, v_2)$, where u_2 (by Theorem 12) is given by

$$u_2 = \frac{R_0}{(R_0 + d_0)^4} \left(d_0^4 - 2R_0^2 r_0^2 + R_0^4 - 2r_0^2 d_0^2 + 6R_0^2 d_0^2 + 4R_0 d_0^3 + 4R_0^3 d_0 - 4R_0 d_0 r_0^2 \right). \tag{67}$$

Of course, $v_2^2 = R_0^2 - u_2^2$.

The point B_1 and B_3 are elements of K_1 given by $B_1(\hat{u}_1, 0)$ and $B_3(\hat{u}_3, \hat{v}_3)$, where

$$\hat{u}_1 = cu_1 = -R_1, \quad \hat{u}_3 = cu_2, \text{ where } c = \frac{R_1}{R_0}. \tag{68}$$

First we prove that

$$|A_1T_1| = \left|B_1\hat{T}_1\right|, \quad |A_2T_1| = \left|B_3\hat{T}_3\right|, \tag{69}$$

where relations

$$R_0^2 + d_0^2 - r_0^2 = R_1^2 + d_1^2 - r_1^2, \quad R_0d_0 = R_1d_1$$

given by (28b) and (28c) will be used. The proof is as follows:

$$|A_1T_1|^2 = R_0^2 + d_0^2 - r_0^2 - 2d_0u_1 = R_0^2 + d_0^2 - r_0^2 + 2d_0R_0, \tag{70a}$$

$$\left|B_1\hat{T}_1\right|^2 = R_1^2 + d_1^2 - r_1^2 - 2d_1\hat{u}_1 = R_1^2 + d_1^2 - r_1^2 + 2d_1R_1, \tag{70b}$$

since

$$R_1^2 + d_1^2 - r_1^2 = R_0^2 + d_0^2 - r_0^2, \quad 2d_1cu_1 = 2d_1R_1\frac{R_1}{R_0}u_1 = 2\frac{d_0R_0}{R_0}u_1 = 2d_0u_1.$$

In the same way it can be shown that the second relation given by (69) is also valid. That the tangent length is given by $t^2 = R^2 + d^2 - r^2 - 2du$ can be seen in the proof of Theorem 2.

Now we prove that there is a point $B_2 \in K_1$ between B_1 and B_3 such that B_2 is a consequent of B_1 and B_3 is a consequent of B_2. The proof is as follows.

By Theorem 12 the consequent of B_1 is given by $B_2(\hat{u}_2, \hat{v}_2)$, where

$$\hat{u}_2 = \frac{R_1}{(R_1+d_1)^4}\left(d_1^4 - 2R_1^2r_1^2 + R_1^4 - 2r_1^2d_1^2 + 6R_1^2d_1^2 + 4R_1d_1^3 + 4R_1^3d_1 - 4R_1d_1r_1^2\right). \tag{71}$$

From this, using computer algebra, it is easy to show that B_3 is consequent of B_2.

Now, if we take $A_3 \in C_1$ which is consequent of A_2, then for A_2 and A_3 analogously holds as for A_1 and A_2. So, in this way we can proceed and get closure, that is, a bicentric $2n$-gon inscribed in K_1 and circumscribed around K_2 whose tangent lengths are such that holds (66). □

For example, from (70) and Figure 6 it can be seen that

$$t_1 = |A_1T_1| = \left|B_1\hat{T}_1\right| = u_1,$$
$$t_2 = |A_2T_1| = \left|B_3\hat{T}_3\right| = u_3,$$

analogously for A_3 and B_5, and so on.

Remark. (6) If we take A_1 on the x-axis we get (with less calculation) a bicentric $2n$-gon inscribed in K_1 and circumscribed around K_2 symmetric about the x-axis. By Poncelet's closure theorem, it follows that for every point $X \in K_1$ we get a bicentric $2n$-gon inscribed in K_1 and circumscribed around K_2.

Now we state the following corollaries of Theorem 16.

Corollary 17. $u_iu_{i+n} = t_Mt_m$ *for* $i = 1, \ldots, n$.

See Theorem 13.

Corollary 18. *$A_1A_2 \parallel B_1B_3$ and $c\,|A_1A_2| = |B_1B_3|$ for c given by* (68) (see Figure 6).

Proof. Let f denote the homothety whose center is O and coefficient c is given by (68). This homothety maps A_1A_2 onto B_1B_3. □

Corollary 19. *Let $B_1 \dots B_{2n}$ be a bicentric $2n$-gon as described in Theorem 16. Then $B_1B_3 \dots B_{2n-1}$ and $B_2B_4 \dots B_{2n}$ are bicentric n-gons inscribed in K_1 and circumscribed around a circle $\hat{K}_2$ with center I_2 and radius cr_0 such that $|OI_2| = c\,|OI_0| = cd_0$.*

Proof. First it is clear that $F_n(R_0, r_0, d_0) = 0 \Longrightarrow F_n(cR_0, cr_0, cd_0) = 0$, that is, $F_n(R_0, r_0, d_0) = 0 \Longrightarrow F_n(R_1, cr_0, cd_0) = 0$ since $cR_0 = R_1$.

Also let us remark that from the Corollary 18 can be concluded that there are two bicentric n-gons $A_1 \dots A_n$ and $D_1 \dots D_n$ inscribed in C_1 and circumscribed around C_2 such that the first has sides parallel with the corresponding sides of the n-gon $B_1B_3 \dots B_{2n-1}$ and the second has sides parallel with the corresponding sides of the n-gon $B_2B_4 \dots B_{2n}$. □

Corollary 20. *Let $u_1, \dots, u_{2n}$ be tangent lengths of the $2n$-gon $B_1 \dots B_{2n}$. Then, $cu_i,\ i = 1, 3, 5, \dots, 2n-1$, are the tangent lengths of the n- gon $B_1B_3 \dots B_{2n-1}$, and*
$cu_i,\ i = 2, 4, 6, \dots, 2n$, are the tangent lengths of the n- gon $B_2B_4 \dots B_{2n}$.

Proof. It follows from the above corollaries. □

Here is an example where $n = 3$. See Figure 7.

Example 4. The incircle of the triangles $B_1B_3B_5$ and $B_2B_4B_6$ is denoted by $\hat{K}_2$. There are two triangles $A_1A_2A_3$ and $D_1D_2D_3$ inscribed in C_1 and circumscribed around C_2. The first is similar to the triangle $B_1B_3B_5$ and the second is similar to the triangle $B_2B_4B_6$. If $u_1 \dots, u_6$ are the tangent lengths of the hexagon $B_1 \dots B_6$, then

u_1, u_3, u_5 are the tangent lengths of the triangle $A_1A_2A_3$,

u_2, u_4, u_6 are the tangent lengths of the triangle $D_1D_2D_3$,

where, for example, $u_1 = |A_1T_1|$, $u_3 = |A_2T_1|$, $u_5 = |A_3T_3|$.

By Theorem 16, this holds analogously for each bicentric n-gon $A_1 \dots A_n$ and the corresponding bicentric $2n$-gon $B_1 \dots B_{2n}$.

Theorem 21. *Let the triple (R_0, r_0, d_0) be as in Theorem 16 and let the triple (R_2, r_2, d_2) be given by* (25)*, that is,*

$$(R_2, r_2, d_2) = \left(\sqrt{R_0(R_0 - r_0 + r_2)}, r_2, \sqrt{R_0(R_0 - r_0 - r_2)}\right), \tag{72a}$$

where

$$r_2 = \sqrt{(R_0 - r_0)^2 - d_0^2}. \tag{72b}$$

Then $F_{2n}(R_2, r_2, d_2) = 0$.

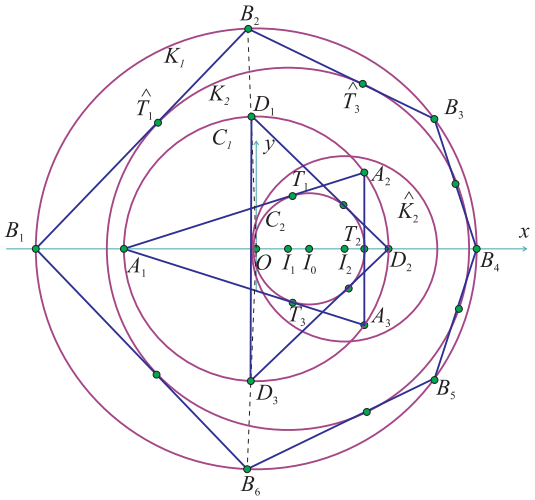

Figure 7: $R_0 = 5,\ r_0 = 2.1,\ d_0 = 2$ refers to circle C_1 and C_2. The chords B_1B_3, B_3B_5, B_5B_1 of the circle K_1 are tangential segments of the circle $\hat{K}_2$.

The proof is analogous to that of Theorem 16, and we have analogous corollaries.

3. The n-closure and related considerations

Let S denote the set of all ordered triples (R, r, d), where $(R, r, d) \in \mathbb{R}^3_+$ and $R > r + d$. Let f_1 and f_2 be functions defined on the set S as in Definition A. We have

$$f_1(R_0, r_0, d_0) = (R_1, r_1, d_1), \tag{73}$$

$$f_2(R_0, r_0, d_0) = (R_2, r_2, d_2), \tag{74}$$

where (R_1, r_1, d_1) and (R_2, r_2, d_2) are given by (24) and (25) respectively.

Let f be any given composition of the function f_1 and f_2. For example, $f = f_1^2 f_2 f_1 f_2^3 f_1$. Then it is appropriate to write this composition as

$$(R_{11212221}, r_{11212221}, d_{11212221}),$$

since

$$\begin{aligned} f_1^2 f_2 f_1 f_2^3 f_1(R_0, r_0, d_0) &= f_1^2 f_2 f_1 f_2^3 (R_1, r_1, d_1) \\ &= f_1^2 f_2 f_1 f_2^2 (R_{12}, r_{12}, d_{12}), \text{ and so on.} \end{aligned}$$

Concerning such indices let us remark that the situation is in some way connected with fact that there are 2^k integers with k digits from the set $\{1, 2\}$. So, if $k = 3$, we have indices

$$111, 112, 121, 122, 211, 212, 221, 222.$$

See also Figure 8, where instead of $(R_i, r_i, d_i),\ i = 0, 1, 2, \ldots,$ are (for brevity) written only corresponding indices.

Before stating some examples, we define some terms which will be used.

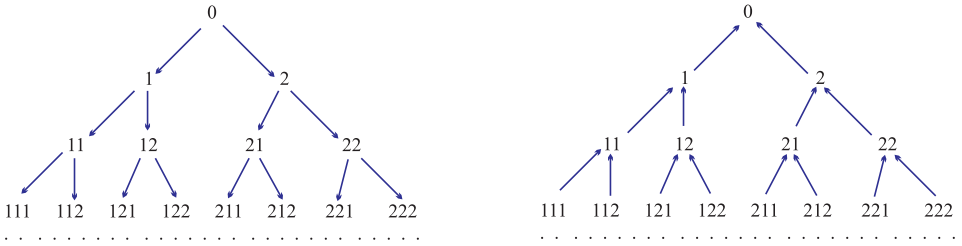

(a) (b)

Figure 8:
The Figure 8a geometrically represents functions f_1 and f_2 and their compositions, and the Figure 8b geometrically represents function g given by (80) and its compositions.

Definition 2. Let (R_0, r_0, d_0) be a triple such that $F_n(R_0, r_0, d_0) = 0$. We say that this triple has n-closure.

Now, let C_1 and C_2 be circles such that C_2 is completely inside C_1, and let R_0 = radius of C_1, r_0 = radius of C_2, d_0 = distance between centers of C_1 and C_2. Let $A_1 \dots A_n$ be an n-gon inscribed in C_1 and circumscribed around C_2. We say that this n-gon has k-circumscription if

$$\sum_{i=1}^{n} \arctan \frac{t_i}{r_0} = k\pi,$$

where $t_1, \dots, t_n$ are the tangent lengths of the n-gon $A_1 \dots A_n$. The number k in this case is called the *rotation number* for n.

Let (R_0, r_0, d_0) be as in Definition 2. Then $f_1(R_0, r_0, d_0)$ has $2n$-closure. Also, the triple $f_2(R_0, r_0, d_0)$ has $2n$-closure for every $n > 3$. But for $n = 3$, we get a bicentric hexagon which is a double triangle.

Here are some examples referred to Theorems 16 and 21 and composition of the functions f_1 and f_2.

Let $n = 3$ and let $(R_0, r_0, d_0) = (5, 2.1, 2)$. Then

$$f_1(5, 2.1, 2) = (R_1, r_1, d_1),$$
$$f_1^2(5, 2.1, 2) = (R_{11}, r_{11}, d_{11}),$$

where

$$R_1 = 8.340410221, \quad r_1 = 6.812488532, \quad d_1 = 1.198981793,$$
$$R_{11} = 15.886048415, \; r_{11} = 15.105389214, \; d_{11} = 0.629483163.$$

Since $t_M = \sqrt{(R_0 + d_0)^2 - r_0^2} = 6.67757441$, $t_m = \sqrt{(R_0 - d_0)^2 - r_0^2} = 2.142428529$, we should take t_1 such that $t_m < t_1 < t_M$. Let's say $t_1 = 4$. Now, let $A_1A_2A_3$ be a triangle from the class $C(R_0, r_0, d_0)$, and let $B_1, \dots, B_6$ and $C_1 \dots C_{12}$ be bicentric hexagon and bicentric 12-gon, the first from the class $C(R_1, r_1, d_1)$ and the second from the class $C(R_{11}, r_{11}, d_{11})$, such that their first tangent length is also $t_1 = 4$. Then the following are valid.

The tangent lengths of the triangle $A_1A_2A_3$ are

$$t_1 = 4,\ t_2 = 2.257285251,\ t_3 = 5.973973936. \tag{75a}$$

The tangent lengths of the bicentric hexagon $B_1 \dots B_6$ are

$$\begin{aligned} &u_1 = 4, && u_2 = 2.394578677, && u_3 = 2.257285251, \\ &u_4 = 3.576556479, && u_5 = 5.973973936, && u_6 = 6.337801531, \end{aligned} \tag{75b}$$

where $u_1 = t_1$, $u_3 = t_2$, $u_5 = t_3$.

The tangent lengths of the bicentric 12-gon $C_1 \dots C_{12}$ are

$$\begin{aligned} &v_1 = 4, && v_2 = 3.010399453, && v_3 = 2.394578677, \\ &v_4 = 2.148970243, && v_5 = 2.257285251, && v_6 = 2.727553891, \\ &v_7 = 3.576556479, && v_8 = 4.752268309, && v_9 = 5.973973936, \\ &v_{10} = 6.657247101, && v_{11} = 6.337801531, && v_{12} = 5.245075438, \end{aligned} \tag{75c}$$

where $v_1 = u_1$, $v_3 = u_2$, $v_5 = u_3$, $v_7 = u_4$, $v_9 = u_5$, $v_{11} = u_6$.

Here is a partition of the tangent lengths of the bicentric hexagon

$$\{\{u_1, u_3, u_5\}, \{u_2, u_4, u_6\}\}. \tag{76}$$

This partition has the property that there are two triangles from the class $C(R_0, r_0, d_0)$ such that the first has tangent lengths u_1, u_3, u_5 and the second has tangent lengths u_2, u_4, u_6.

Analogously for the tangent lengths $v_1, \dots, v_{12}$ of the bicentric 12-gon $C_1 \dots C_{12}$; in this case we have the following partition

$$\{\{v_1, v_5, v_9\}, \{v_3, v_7, v_{11}\}, \{v_2, v_6, v_{10}\}, \{v_4, v_8, v_{12}\}\}. \tag{77}$$

This partition has the property that there are four triangles from the class $C(R_0, r_0, d_0)$ such that their tangent lengths are

$$v_1, v_5, v_9, \tag{78a}$$

$$v_3, v_7, v_{11}, \tag{78b}$$

$$v_2, v_6, v_{10}, \tag{78c}$$

$$v_4, v_8, v_{12}, \tag{78d}$$

respectively.

In the same way we can proceed and find that this holds analogously for the tangent lengths of the corresponding bicentric 24-gon from the class $C(f_1^3(R_0, r_0, d_0))$, that is, from $C(R_{111}, r_{111}, d_{111})$. More generally, for any integer $m \geq 1$, there is a partition of the tangent lengths of the corresponding bicentric $3 \cdot 2^m$-gon from the class $C(f_1^m(R_0, r_0, d_0))$ such that this holds analogously as for $m = 1, 2, 3$.

Also from Theorem 16 and Theorem 21 analogous results can be concluded if instead of $n = 3$ we take $n > 3$ and any given composition of the function f_1 and f_2 given by Definition A.

In connection with Theorem 16 and Theorem 21 we state the following conjecture which is a modification of Conjecture 2 given in [5, page 56].

Conjecture 1. *Let (R_0, r_0, d_0) be as in Theorem 16 and let $P_1 \dots P_n$ and $Q_1 \dots Q_n$ be n-gons from the class $C(R_0, r_0, d_0)$ such that the sum of the tangent lengths of the n-gon $P_1 \dots P_n$ is minimal and the sum of the tangent lengths of the n-gon $Q_1 \dots Q_n$ is maximal. Then both of those two n-gons are axial symmetric in the x-axis. Let the sum of the tangent lengths of the n-gon $P_1 \dots P_n$ be denoted by a and the sum of the tangent lengths of the n-gon $Q_1 \dots Q_n$ be denoted by b. Then the following is valid:*

> *For every n-gon $A_1 \dots A_n$ from the class $C(R_0, r_0, d_0)$ there is an n-gon $B_1 \dots B_n$ from the same class such that*
>
> $$(t_1 + \dots + t_n)(u_1 + \dots + u_n) = ab, \tag{79}$$
>
> *where $t_1, \dots, t_n$ are the tangent lengths of the n-gon $A_1 \dots A_n$ and $u_1, \dots, u_n$ are the tangent lengths f the n-gon $B_1 \dots B_n$.*

Let such two n-gons be called conjugate n-gons. Thus for every n-gon from the class $C(R_0, r_0, d_0)$ there is an n-gon from the same class conjugate to it.

Here are some examples where $n = 3$ and $(R_0, r_0, d_0) = (5, 2.1, 2)$.

First, it can be easily found that for axial symmetric triangles from the class $C(5, 2.1, 2)$ we have $ab = 150.5559966$. Now using the tangent lengths $u_1, \dots, u_6$ given by (75b) and partition given by (76) it can be verified that triangle whose tangent lengths are u_1, u_3, u_5 is conjugate to triangle whose tangent lengths are u_2, u_4, u_6, that is, $(u_1 + u_3 + u_5)(u_2 + u_4 + u_6) = 150.5559966$. Also, using the tangent lengths given by (75c) (see also (77)) it can be verified that triangle whose tangent lengths are v_1, v_5, v_9 is conjugate to triangle whose tangent lengths are v_3, v_7, v_{11}, and triangle whose tangent lengths are v_2, v_6, v_{10} is conjugate to triangle whose tangent lengths are v_4, v_8, v_{12}. In other words,

$$(v_1 + v_5 + v_9)(v_3 + v_7 + v_{11}) = (v_2 + v_6 + v_{10})(v_4 + v_8 + v_{12}) = 150.5559966.$$

In order that the rule of obtaining conjugate bicentric polygons be more noticeable here will be also in short about bicentric 24-gon $D_1 \dots D_{24}$ from the class $C(R_{111}, r_{111}, d_{111})$ obtained starting from the triple $(5, 2.1, 2)$. Let $w_1, \dots, w_{24}$ denote tangent lengths of this 24-gon and let w_1 be 4 as in the previous examples. Then

$$\begin{aligned} & (w_1 + w_9 + w_{17})(w_5 + w_{13} + w_{21}) \\ = \; & (w_3 + w_{11} + w_{19})(w_7 + w_{15} + w_{23}) \\ = \; & (w_2 + w_{10} + w_{18})(w_6 + w_{14} + w_{22}) \\ = \; & (w_4 + w_{12} + w_{20})(w_8 + w_{16} + w_{24}) \\ = \; & 150.5559966. \end{aligned}$$

Thus in this case there are 4 pairs of conjugate triangles from the class $C(5, 2.1, 2)$ which refer to the 24-gon $D_1 \dots D_{24}$.

More generally, for a given $m > 1$, there are 2^{m-1} pairs of conjugate triangles from the class $C(5, 2.1, 2)$ which refer to bicentric polygons with $3 \cdot 2^m$ vertices. Analogously holds if instead $n = 3$ we take $n > 3$. Of course, this holds on the

supposition that Conjecture 1 is true. We hope that the Conjecture will be validated in the near future.

Figure 7 shows how conjugate bicentric polygons can be constructed. For example, $A_1A_2A_3$ and $D_1D_2D_3$ are conjugate triangles from the class $C(5, 2.1, 2)$.

Analogously can be concluded if instead of $n = 3$ we can take $n > 3$.

It is clear from Theorem 16 and Theorem 21 that the functions f_1 and f_2 play key roles in this work. These functions are given in [7], where some of their important properties are established. In the present article we have established some other of their important properties given by Theorem 16 and Theorem 21. In this connection let us mention that in [7] we have also defined a function g such that the following is valid: If

$$f_1(R_0, r_0, d_0) = (R_1, r_1, d_1), \quad f_2(R_0, r_0, d_0) = (R_2, r_2, d_2), \tag{80a}$$

then

$$g(R_1, r_1, d_1) = (R_0, r_0, d_0), \quad g(R_2, r_2, d_2) = (R_0, r_0, d_0). \tag{80b}$$

This function is given by

$$g(R, r, d) = \left(\frac{R^2 - d^2}{2r}, \sqrt{-(R^2 + d^2 - r^2) + \left(\frac{R^2 - d^2}{2r} \right)^2 + \left(\frac{2Rrd}{R^2 - d^2} \right)^2}, \frac{2Rrd}{R^2 - d^2} \right). \tag{81}$$

We have subsequently found that $\sqrt{-(R^2 + d^2 - r^2) + \left(\frac{R^2 - d^2}{2r} \right)^2 + \left(\frac{2Rrd}{R^2 - d^2} \right)^2}$ can be written rationally as $\frac{d^4 - 2d^2r^2 - 2d^2R^2 - 2r^2R^2 + R^4}{2r(d^2 - R^2)}$.

See Figure 8b, for example. Starting from the triple $(R_{112}, r_{112}, d_{112})$ we get

$$g^3(R_{112}, r_{112}, d_{112}) = (R_0, r_0, d_0).$$

Thus, using sequences like these in Theorem 16 we can get some other relations useful in research of bicentric polygons.

Also let us emphasize here that using the function g the following theorem can be easily proved.

Theorem 22. *The converses of Theorems 16 and 21 are also valid, that is, if the triples* $(R_i, r_i, d_i),\ i = 1, 2$, *are such that* $F_{2n}(R_i, r_i, d_i) = 0,\ i = 1, 2$, *then there is a triple* (R_0, r_0, d_0) *such that* $F_n(R_0, r_0, d_0) = 0$ *and* $f_i(R_0, r_0, d_0) = (R_i, r_i, d_i),\ i = 1, 2$.

Proof. If the triple (R, r, d) in the relation (81) is one of the triples $(R_i, r_i, d_i),\ i = 1, 2$, then we have a relation which can be written as $g(R_i, r_i, d_i) = (R_0, r_0, d_0),\ i = 1, 2$, that is, $F_{2n}(R_i, r_i, d_i) = 0 \to F_n(g(R_i, r_i, d_i)) = 0,\ i = 1, 2$.

Also let us remark that the system

$$Rd = R_0d_0, \quad R^2 + d^2 - r^2 = R_0^2 + d_0^2 - r_0^2, \quad R^2 - d^2 = 2R_0r$$

in R, r, d has two solutions given by (24) and (25), and that the solution of the above system in R_0, r_0, d_0 is given by (81), that is, $g(R, r, d) = (R_0, r_0, d_0)$.

□

Corollary 23. *Using relation* (27a) *and* (28b) *the triple* $c(R_0, r_0, d_0)$*, where* $c = \frac{R_1}{R_0}$*, can be written as*

$$\left(R_1,\ \frac{2R_1 t_M t_m}{R_1^2 - d_1^2},\ \frac{2R_1 r_1 d_1}{R_1^2 - d_1^2}\right),$$

where cr_0 *and* cd_0 *are also expressed only using* R_1*,* r_1*,* d_1*.*

Of course, the triple $c(R_0, r_0, d_0)$ can be also expressed as

$$\frac{2R_1 r_1}{R_1^2 - d_1^2}\left(\frac{R_1^2 - d_1^2}{2r_1}, \sqrt{-\left(R_1^2 + d_1^2 - r_1^2\right) + \left(\frac{R_1^2 - d_1^2}{2r_1}\right)^2 + \left(\frac{2R_1 r_1 d_1}{R_1^2 - d_1^2}\right)^2}, \frac{2R_1 r_1 d_1}{R_1^2 - d_1^2}\right).$$

4. Another type of characteristic points for two nested circles

About interesting geometrical properties of the triples (R_0, r_0, d_0) and $c(R_0, r_0, d_0)$ see Corollaries 17–20.

In the following we briefly consider one more characteristic point defined for two nested circles. Definition 1 will be extended as follows. Instead of R, r, d, we use R_0, r_0, d_0, and let the points $S_1(s_1, 0)$ and $S_2(s_2, 0)$ be given by

$$s_{1,2} = \frac{R_0^2 + d_0^2 - r_0^2 \mp \sqrt{(R_0^2 + d_0^2 - r_0^2)^2 - 4R_0^2 d_0^2}}{2d_0} \tag{82a}$$

or

$$s_{1,2} = \frac{R_0^2 + d_0^2 - r_0^2 \mp t_M t_m}{2d_0}, \tag{82b}$$

since

$$(R_0^2 + d_0^2 - r_0^2)^2 - 4R_0^2 d_0^2 = \left((R_0 + d_0)^2 - r_0^2\right)\left((R_0 - d_0)^2 - r_0^2\right) = t_M^2 t_m^2.$$

Then both of the points $S_1(s_1, 0)$ and $S_2(s_2, 0)$ can be called characteristic points determined by the triple (R_0, r_0, d_0).

It is easy to show that

$$s_{1,2} = \frac{(t_M \mp t_m)^2}{4d_0}. \tag{82c}$$

The point $S_1(s_1, 0)$ is the intersection of the x-axis and the line through the points T_1 and $\hat{T}_1$ drawn in Figure 1b given by

$$T_1\left(d_0 - \frac{r_0^2}{R_0 + d_0}, \frac{r_0 t_M}{R_0 + d_0}\right), \quad \hat{T}_1\left(d_0 + \frac{r_0^2}{R_0 - d_0}, -\frac{r_0 t_m}{R_0 - d_0}\right). \tag{83}$$

The point $S_2(s_2, 0)$ is the intersection of the x-axis and the line through the points T_1 given by (83) and

$$T_2\left(d_0 + \frac{r_0^2}{R_0 - d_0}, \frac{r_0 t_m}{R_0 - d_0}\right).$$

Now we consider the relation (43) as an equation in s given by

$$\hat{u} = \frac{2R_0^2 s - \left(R_0^2 + s^2\right) u}{-2su + R_0^2 + s^2}, \tag{84a}$$

where we here use notation R_0, r_0 d_0 instead of notation R_1, r_1, d_1. As will be shown, this relation plays a key role in using characteristic points. First it can be easily shown that this relation is equivalent to

$$\hat{u} = \frac{-2R_0^2 d_0 + \left(R_0^2 + d_0^2 - r_0^2\right) u}{2d_0 u - \left(R_0^2 + d_0^2 - r_0^2\right)}. \tag{84b}$$

Namely, if s in the relation (84a) is replaced by right side of the any of the relations

$$s_1 = \frac{(t_M - t_m)^2}{4d_0}, \quad s_2 = \frac{(t_M + t_m)^2}{4d_0},$$

(see (82)) we get relation (84b).

Thus, the equation in s given by (84a) has the solutions s_1 and s_2. These solutions can be also written as

$$s_{1,2} = \frac{u\hat{u} + R_0^2}{u + \hat{u}} \mp \sqrt{\left(\frac{u\hat{u} + R_0^2}{u + \hat{u}}\right)^2 - R_0^2}$$

and it is easily seen that $s_1 s_2 = R_0^2$.

Also, if u and $\hat{u}$ in (84b) are interchanged, then

$$u = \frac{2R_0 s_i - \left(R_0^2 + s_i^2\right) \hat{u}}{-2s_i \hat{u} + R_0^2 + s_i^2} = \frac{-2R_0^2 d_0 + \left(R_0^2 + d_0^2 - r_0^2\right) \hat{u}}{2d_0 \hat{u} - \left(R_0^2 + d_0^2 - r_0^2\right)}, \quad i = 1, 2. \tag{85}$$

The above relations in u, $\hat{u}$, s_1, s_2 are very important since they open the way to the use of both of the characteristic points S_1 and S_2. The relation (84a) is connected with both of the characteristic points S_1 and S_2.

Theorem 24. *Let C_1 and C_2 be two nested circles such that*

R_0 = radius of C_1, r_0 = radius of C_2,

d_0 = distance between centers of C_1 and C_2.

Let xOy be a coordinate system with origin O at the center of C_1 and positive x-axis containing the center of C_2. Let $P(u, v)$ be any given point of C_1 and let $\hat{P}(\hat{u}, \hat{v})$ be a point of C_1 such that the chord $P\hat{P}$ of C_1 contains the characteristic point $S_1(s_1, 0)$, that is,

$$\hat{u} = \frac{-2R_0^2 d_0 + \left(R_0^2 + d_0^2 - r_0^2\right) u}{2d_0 u - \left(R_0^2 + d_0^2 - r_0^2\right)}, \quad \hat{v}^2 = R_0^2 - \hat{u}^2.$$

Then the point $Q(\hat{u}, -\hat{v})$ of C_1 has the property that the chord PQ of C_1 contains the characteristic point $S_2(s_2, 0)$ (see Figure 9).

Proof. The condition that the line through the points P and Q contains characteristic point S_2 can be written as

$$-v = \frac{v + \hat{v}}{u - \hat{u}}(s_2 - u)$$

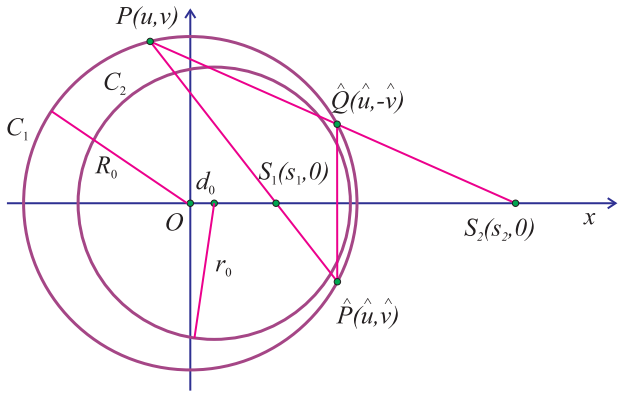

Figure 9. Geometrical interpretation of the points P, $\hat{P}$, S_1 and the points P, Q S_2.

or

$$-\frac{v}{\hat{v}} = \frac{u - s_2}{\hat{u} - s_2}. \tag{86a}$$

The condition that the line through the points P and $\hat{P}$ contains point S_1 is given by

$$\frac{v}{\hat{v}} = \frac{u - s_1}{\hat{u} - s_1}. \tag{86b}$$

Thus, the condition that the line through P and $\hat{P}$ contains the characteristic point S_1 and the line through P and Q contains the characteristic point S_2 is given by

$$\left(\frac{v}{\hat{v}}\right)^2 = \left(\frac{u - s}{\hat{u} - s}\right)^2, \tag{87}$$

where $s = s_1$ in the first case and $s = s_2$ in the second case. We make use of the relations

$$v^2 = R_0^2 - u^2, \quad \hat{v}^2 = R_0^2 - \hat{u}^2, \quad \hat{u} = \frac{-2R_0^2 d_0 + \left(R_0^2 + d_0^2 - r_0^2\right) u}{2d_0 u - \left(R_0^2 + d_0^2 - r_0^2\right)}$$

which hold for any u such that the point $P(u, v)$ belongs to the circle C_1. Using computer algebra we get the following equation in s:

$$\begin{aligned}
&d_0^4 R_0^2 su - d_0^4 su^3 - d_0^3 R_0^4 s - d_0^3 R_0^4 u - d_0^3 R_0^2 s^2 u + d_0^3 R_0^2 u^3 + d_0^3 s^2 u^3 + d_0^3 su^4 \\
&- 2d_0^2 r_0^2 R_0^2 su + 2d_0^2 r_0^2 su^3 + d_0^2 R_0^6 + d_0^2 R_0^4 s^2 + 2d_0^2 R_0^4 su - 2d_0^2 R_0^2 su^3 - d_0^2 R_0^2 u^4 \\
&- d_0^2 s^2 u^4 + d_0 r_0^2 R_0^4 s + d_0 r_0^2 R_0^4 u + d_0 r_0^2 R_0^2 s^2 u - d_0 r_0^2 R_0^2 u^3 - d_0 r_0^2 s^2 u^3 - d_0 r_0^2 su^4 \\
&- d_0 R_0^6 s - d_0 R_0^6 u - d_0 R_0^4 s^2 u + d_0 R_0^4 u^3 + d_0 R_0^2 s^2 u^3 + d_0 R_0^2 su^4 + r_0^4 R_0^2 su \\
&- r_0^4 su^3 - 2r_0^2 R_0^4 su + 2r_0^2 R_0^2 su^3 + R_0^6 su - R_0^4 su^3 = 0
\end{aligned}$$

whose roots are

$$s_1 = \frac{R_0^2 + d_0^2 - r_0^2 - \sqrt{(R_0^2 + d_0^2 - r_0^2)^2 - 4R_0^2 d_0^2}}{2d_0},$$
$$s_2 = \frac{R_0^2 + d_0^2 - r_0^2 + \sqrt{(R_0^2 + d_0^2 - r_0^2)^2 - 4R_0^2 d_0^2}}{2d_0}.$$

□

Corollary 25. *The equation in s given by* (84) *is the same as the equation given by* (87)*. Each of them has only the solutions s_1 and s_2.*

Corollary 26. *Let $n \geq 4$ be an even integer with Fuss' relation $F_n(R_0, r_0, d_0) = 0$. There are two bicentric n-gons $A_1 \cdots A_n$ and $B_1 \cdots B_n$ with the following properties.*

($\mathbf{i}_1$) $A_1 = P(u, v)$, $B_{1+\frac{n}{2}} = Q(\hat{u}, -\hat{v})$.

($\mathbf{i}_2$) *For each $A_i(u_i, v_i),\ i = 1, \ldots, \frac{n}{2}$, there is $B_{i+\frac{n}{2}}\left(u_{i+\frac{n}{2}}, -v_{i+\frac{n}{2}}\right)$ such that the line through the points A_i and $B_{i+\frac{n}{2}}$ contains point S_2.*

($\mathbf{i}_3$) *For each $A_i(u_i, v_i),\ i = 1, \ldots, \frac{n}{2}$, there is $A_{i+\frac{n}{2}}\left(u_{i+\frac{n}{2}}, v_{i+\frac{n}{2}}\right)$ such that the chord $A_i A_{i+\frac{n}{2}}$ of C_1 contains point S_1.*

($\mathbf{i}_4$) *The point A_i and $B_i,\ i = 1, \ldots, \frac{n}{2}$, are symmetric about the x-axis.*

($\mathbf{i}_5$) *For each $i = 1, \ldots, \frac{n}{2}$,*

$$|A_i S_2| \left|A_{i+\frac{n}{2}} S_2\right| = s_2^2 - R_{)}^2,$$
$$|B_i S_2| \left|B_{i+\frac{n}{2}} S_2\right| = s_2^2 - R_{)}^2.$$

Proof. ($\mathbf{i}_2$): The proof easily follows from the equation of the line through the points A_i and $B_{i+\frac{n}{2}}$.

($\mathbf{i}_4$): From the Figure 9 can be easily seen that the chord $Q\hat{P}$ of C_1, that is, the chord $B_{1+\frac{n}{2}} A_{1+\frac{n}{2}}$, is perpendicular to the x-axes.

($\mathbf{i}_5$): The proof is in the same way as the proof that holds the relation (40). □

Here is an example. Using Example 4, where $n = 6$, can be easily found that the vertices of the hexagon $A_1 \cdots A_6$ (determined by given tangent lengths) are

$$A_1(3.58220619, 7.531948163), \qquad A_2(7.862976314, 2.781375164),$$
$$A_3(8.129674451, -1.863018422), \qquad A_4(4.920109639, -6.734609525),$$
$$A_5(-4.628245672, -6.938428231), \qquad A_6(-6.49623254, 5.230813236).$$

In this case is $\hat{A}_1 = A_4$, $\hat{A}_2 = A_5$, $\hat{A}_3 = A_6$, .

The vertices of the hexagon $B_1 \cdots B_6$ are such that if $A_i(u_i, v_i),\ i = 1, \ldots, 6$, then $B_i(u_i, -v_i),\ i = 1, \ldots, 6$.

In Example 4 it is shown that $t_M = 6.7677574552$, $t_m = 2.14242886$. Thus $s_1 = 4.288544701$, $s_2 = 16.22052397$. It is easy to verify the assertions ($\mathbf{i}_1$) – ($\mathbf{i}_5$). Also, the relations like those given by (84) and (85) can be verified.

Concluding Remark. The main result of the present paper refers to the given definition of characteristic points for two nested circles and their properties useful in research of bicentric polygons. Some old and difficult problems are solved. It seems that there are many problems concerning bicentric polygons for which the characteristic points can be very useful. In this connection we remark that the characteristic points can be also useful in research of bicentric $2n$-gons from the class $C_{2n}(R_i, r_i, d_i)$ which is obtained from the class $C_n(R_0, r_0, d_0)$ using function f_1 and f_2 given in Definition A. Some results from this area are given in Theorem 5, 6, 14. Also some results concerning functions f_1 and f_2 given in [7] are extended.

References

[1] A. Cayley, Development on the porisme of the in-and-circum-scribed polygon, *Philos. Mag.*, VII (1854) 339–345.

[2] N. Fuss, De quadrilateris quibus circulum tam inscribere quam cicumscribere licet, *Nova acta Academiae scientiarum imperialis Petropolitanae* X (1797) 103–125.

[3] N. Fuss, De poligonis simmetrice irregularibus calculo simul inscriptis et circumscripti, *Nova acta Academiae scientiarum imperialis Petropolitanae* XIII (1802) 168–189.

[4] J. V. Poncelet, *Traité des propriétés des figures*, t. I, Paris, 1865, first ed. in 1822.

[5] M. Radić, Certain relations obtained starting with three positive numbers and their use in investigation of bicentric polygons, *Math. a Pannon.*, 22 (2011) 49–72.

[6] M. Radić, Z. Kaliman, and V. Kadum, A condition that a tangential quadrilateral is also a chordal one, *Math. Commun.*, 12 (2007) 33–52.

[7] M. Radić, Functions of triples of positive real numbers and their use in study of bicentric polygons, *Beitr. Algebra Geom.*, 54 (2013) 709–736.

[8] M. Radić, About two characteristic points concerning two separated circles and their use in study of bicentric polygons, *J. Geom.*, 105 (2014), no. 3, 465-493.

Mirko Radić: Department of Mathematics, University of Rijeka, 51000 Rijeka, Radmile Matejčić 2, Croatia

E-mail address: poganj@pfri.hr

Forum Geometricorum
Volume 15 (2015) 159–164.

FORUM GEOM
ISSN 1534-1178

Do Dogs Play with Rulers and Compasses?

Li Zhou

Abstract. A dog runs at the speed of 1 and swims at the speed of $s < 1$. If the dog is at point A on the shoreline and tries to get to a ball in water at point B in the least time, what path should the dog take? In this article we discuss geometric solutions to this optimization problem and its variations.

1. Introduction

A dog runs at the speed of 1 and swims at the speed of $s < 1$. If the dog is at point A on the shoreline and tries to get to a ball in water at point B in the least time, what path should the dog take?

This problem and equivalent versions of it have been typical exercises in calculus textbooks for decades. But in [5] the author discovered that his dog Elvis seemed to follow instinctively the optimal path. Since then this problem has gone "viral" and several follow-up articles [1, 2, 4, 6, 7] have discussed variations and different perspectives for the dog.

In this article we give the dog a simple geometric perspective.

2. A ruler-compass solution

As in Figure 1(a), construct the circle Σ with diameter BD, where D is the foot of perpendicular from B onto the shoreline. Let $d = BD$ and construct point Q on Σ such that $DQ = sd$. This is useful because the dog runs the distance d in the same time as he swims the distance sd. If BQ intersects AD at a point E between A and D, then the dog should run from A to E and swim from E to B. How could the dog know for sure?

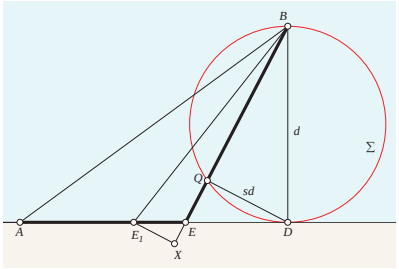

Figure 1(a). Construction of the optimal path AEB

Publication Date: June 18, 2015. Communicating Editor: Paul Yiu.

Take a different point E_1, as in Figure 1(a). Let X be the foot of perpendicular from E_1 onto BE. Note that $\triangle EE_1X \sim \triangle DBQ$, so the dog runs the distance E_1E in the same time as he swims the distance XE. But E_1B is a longer distance to swim than the distance XB. Therefore, the path AE_1B takes longer time than the path AEB (denoted by $AE_1B \succ AEB$ from now on). The proof remains valid if E_1 is taken on the other side of E.

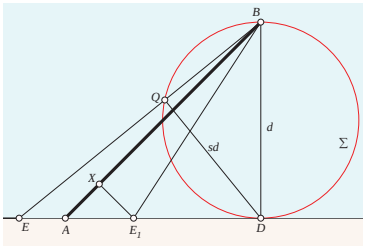

Figure 1(b). Proof that the optimal path is AB

If E falls beyond A, as in Figure 1(b), then the dog should directly swim from A to B. Indeed, take a different point E_1 between A and D. Let X be the foot of perpendicular from E_1 onto AB. Then the dog swims the distance AX in less time than he runs the distance AE_1, and XB is a shorter distance than E_1B to swim. Hence $AE_1B \succ AB$. Equivalently, $EE_1B \succ EAB$, which means that the time for the path EE_1B increases as E_1 moves away from E. Similarly, if E_1 is to the left of E, then the time for the path E_1EB decreases as E_1 moves towards E.

3. Snell's law

If A is further inland, as in Figure 2, then it is the well-known Snell's law that $s \cdot \sin\alpha = 1 \cdot \sin\beta$ at the optimal point E. The geometric proof that AEB takes the least time is similar.

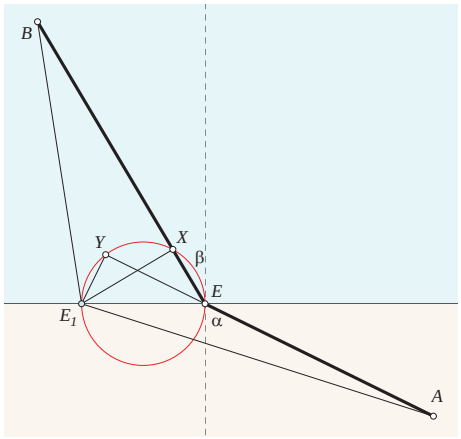

Figure 2. Proof of Snell's law

Take a different point E_1 from E. Let X and Y be the feet of perpendiculars from E_1 onto BE and AE respectively. Then

$$sEY = sE_1E \sin\alpha = E_1E \sin\beta = EX,$$

that is, the dog runs the distance EY in the same time as he swims the distance EX. But AE_1 is a longer distance than AY to run, and E_1B is a longer distance than XB to swim. Hence $AE_1B \succ AEB$. Following the references in [1] we learn that this is a rediscovery of Huygens's proof from 1678 [3]. So an old dog may not be taught new tricks, but an old dog may be motivated to rediscover old tricks. The location of the point E in this case requires the solution of a quartic equation, thus can not be constructed by ruler and compass. But [7] gives a geometric construction using the trammel of Archimedes.

4. Bifurcation

In [4], the authors discuss the following variation: what if the dog is originally at a point A also in water? Then the optimal path could be directly swimming from A to B or a SRS path: swimming to a point F on the shoreline, then running along the shoreline to another point E, and swimming from E to B. Now we give a simple geometric solution to this problem as well.

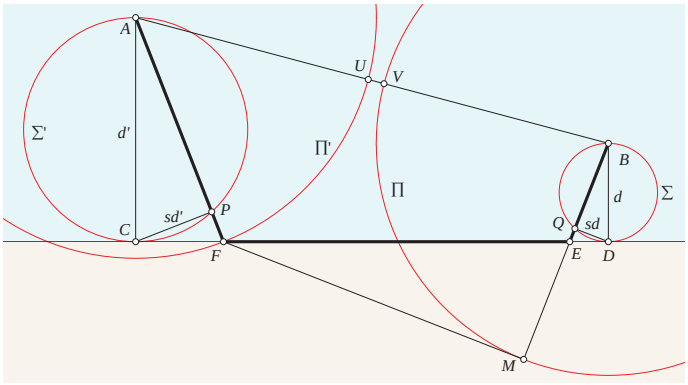

Figure 3(a). Constructing the optimal path $AFEB$

First, we construct points E and F on the shoreline as in §2. See Figure 3(a). Let M be the foot of perpendicular from F onto BE. Since $\triangle FEM \sim \triangle BDQ \sim \triangle ACP$, the dog runs the distance FE in the same time as he swims the distance ME. Now draw circles Π' and Π centered at A and B with radii AF and BM respectively. If Π and Π' are externally disjoint, as in Figure 3(a), then the SRS path $AFEB$ takes the same time as swimming from A to U and then from V to B, thus $AB \succ AFEB$. Also, it can be proved in the same way as in §2 that any other SRS paths will take longer time than $AFEB$.

On the other hand, if Π and Π' are not externally disjoint, as in Figure 3(b), then the argument above proves that the optimal path is directly swimming from A to B. The "bifurcation" mentioned in [4] occurs exactly when Π and Π' are externally

tangent to each other, in which case swimming from A to B takes exactly the same time as the SRS path $AFEB$.

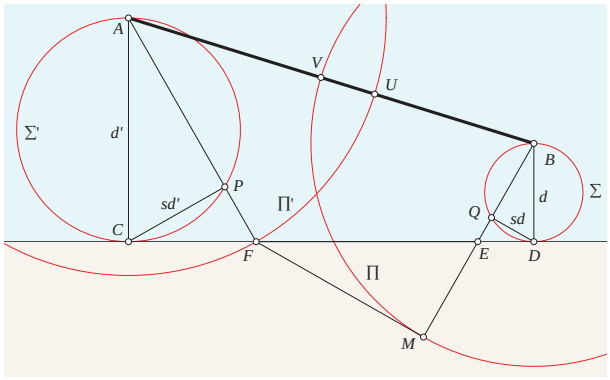

Figure 3(b). Proof that the optimal path is AB

5. Bended Shoreline

The discussions above naturally lead to the case where the shoreline is not straight. In the figures below, the shore consists of two lines l and m meeting at T. Points E and F are constructed as before, forming the optimal angle θ from B to the shorelines l and m. Note that E may not be between D and T, and F may not be between A and T, causing variations in the pictorial proofs.

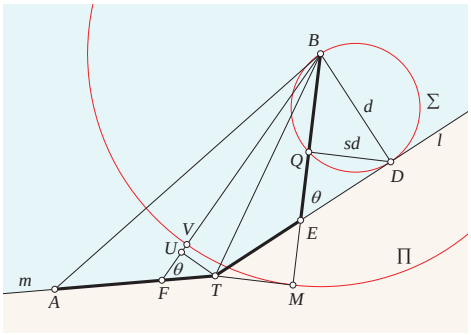

Figure 4(a). Proof that $ATEB$ is optimal, where M and U are feet of perpendiculars from T onto BE and BF

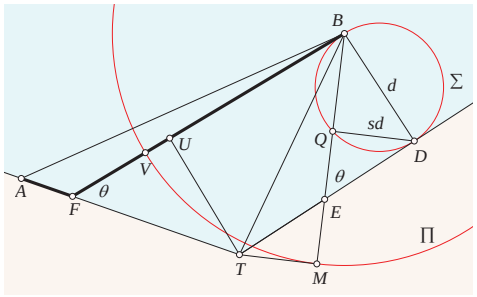

Figure 4(b). Proof that AFB is optimal

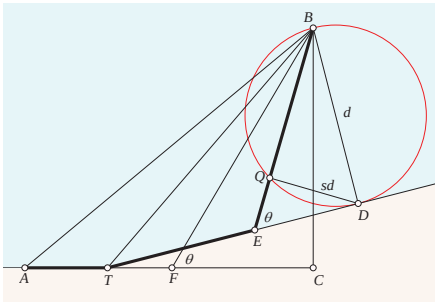

Figure 5. Proof that $ATEB$ is optimal

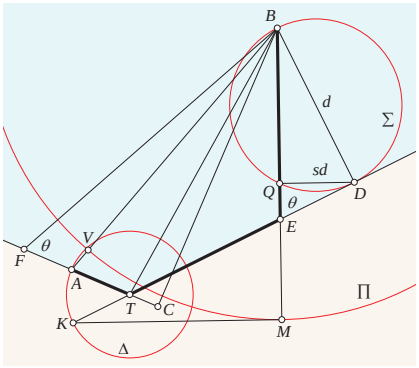

Figure 6(a). Proof that $ATEB$ is optimal, where M is the foot of perpendicular from K onto BE

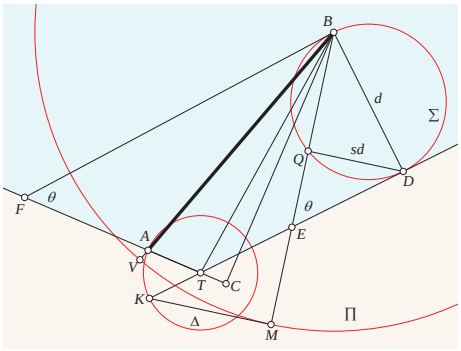

Figure 6(b). Proof that AB is optimal

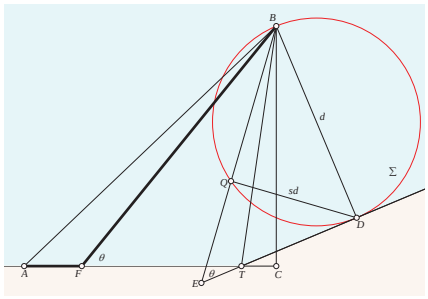

Figure 7. Proof that AFB is optimal

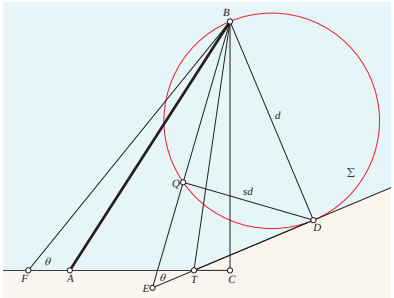

Figure 8. Proof that AB is optimal

To challenge the dog more, we can also move A into the water, as in Figure 9. Then the dog has to decide between AB, $AGFB$, $AHEB$, and $AGTEB$. The interested readers are invited to play with rulers and compasses, or with their dogs.

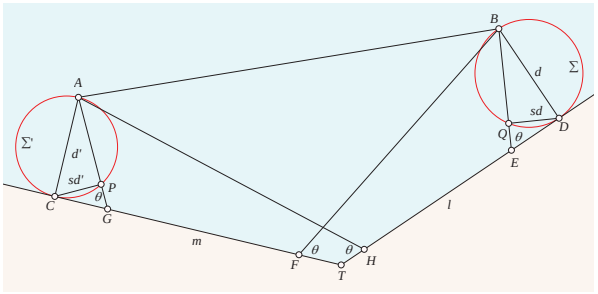

Figure 9. What is the optimal path?

Finally, we can also have more bends in the shoreline. The solutions and proofs are all the same, only with more overwhelming numbers of cases!

6. Dogs' Day-Dreams

Consider a lake Ω in the shape of a convex polygon. For any two points A and B in Ω (including the shoreline), define the dog-distance $\delta_s(A, B)$ to be the least time the dog (with running speed 1 and swimming speed $s < 1$) can get from A to B. Then all the geodesics can be constructed by ruler and compass. Fix a point A, what is the locus of points B such that there are more than one geodesics between A and B? Fix two points A and B, what is the shape of $\mathcal{N}_s(A) = \{X \in \Omega : \delta_s(A, X) < \delta_s(X, B)\}$? Perhaps dogs day-dream many more questions about the geometry of (Ω, δ_s).

Acknowledgments. I am very grateful to my friend and colleague Dr. David Rose whose talk at our Professional Development Day motivated me to discover the geometric solution in §2.

References

[1] M. Bolt and D. C. Isaksen, Dogs don't need calculus, *College Math. J.* **42** (2010), 10–16.
[2] L. Dickey, Do dogs know calculus of variations?, *College Math. J.* **37** (2006), 20–23.
[3] C. Huygens, *Treatise on Light*, translated by S. P. Thompson, Dover, New York, 1962.
[4] R. Minton and T. J. Pennings, Do dogs know bifurcations?, *College Math. J.* **38** (2007), 356–361.
[5] T. J. Pennings, Do dogs know calculus?, *College Math. J.* **34** (2003), 178–182.
[6] P. Perruchet and J. Gallego, Do dogs know related rates rather than optimization?, *College Math. J.* **37** (2006), 16–18.
[7] M. Schwartz, Do dogs know the trammel of Archimedes?, *College Math. J.* **42** (2011), 299–308.

Li Zhou: Department of Mathematics, Polk State College, Winter Haven, FL 33881 USA
E-mail address: lzhou@polk.edu

Forum Geometricorum
Volume 15 (2015) 165–172.

FORUM GEOM
ISSN 1534-1178

On a Flawed, 16th-Century Derivation of Brahmagupta's Formula for the Area of a Cyclic Quadrilateral

Eisso J. Atzema

Abstract. Around 1545, the Indian commentator Gaṇeśa suggested an interesting, but ultimately flawed, derivation of Brahmagupta's formula for the area of a cyclic quadrilateral in terms of its sides. In this paper we show that Gaṇeśa's approach is actually valid and that his proof is easily fixed. We will also investigate to what extent his idea can be generalized to arbitrary (convex) quadrilaterals.

1. Introduction

In the early 6th century, the Indian mathematician Brahmagupta suggested that the area $ABCD$ of a cyclic quadrilateral with vertices A, B, C, D and a, b, c, d the lengths of the sides AB, BC, CD, DA is given by the formula

$$ABCD = \sqrt{(s-a)(s-b)(s-c)(s-d)}.$$

where $s = (a+b+c+d)/2$. Proofs for Brahmagupta's claim were given by al-Shannī (10th century), Jyeṣṭhadeva (16th century) and others.[1] Although rather different in the details, all of these proofs follow a similar approach. A different type of proof was suggested by Jyeṣṭhadeva's contemporary Gaṇeśa.[2]

Gaṇeśa's "proof" can be found in his commentary on the *Līlāvati* of Bhāskara II. According to Gaṇeśa himself, this commentary was composed in 1545 CE. In this note, we will pursue Gaṇeśa's line of reasoning and show how it can be modified to lead to the desired result.[3] Along the way, we will see that some of his ideas apply to any (convex) quadrilateral, albeit in a less elegant form than for the cyclic case. We start with the big idea.

Publication Date: June 23, 2015. Communicating Editor: Paul Yiu.

Most of the research for this paper was done while the author was on sabbatical leave at Utrecht University (The Netherlands). The author wishes to thank Prof. Dr. Jan Hogendijk and the Department of Mathematics for their hospitality.

[1]For more details on the history of Brahmagupta's formula, see [1].

[2]For biographical information on Gaṇeśa, see [3], p.320.

[3]The original text of the commentary seems to have been included in Āpate's standard edition of the *Līlāvati* (1937). We will mostly rely on [2].

2. Preliminaries

Before we proceed, we will quickly review (mostly without proof) a number of major results regarding quadrilaterals. We need a definition first.

Definition 1. *Let l be a line in the real projective plane. Then an involution on l is a projective transformation on l that is its own inverse.*

Any two distinct points that are images of one another under an involution are said to be conjugate points (under the involution). In addition, any involution has exactly two fixed points. i.e. points that are mapped onto themselves. Any involution is fully determined by the images of any two points on the line, i.e. by two pairs of conjugate points, its two fixed points, or one fixed point and one pair of conjugate points. One example of an involution on a line was first formulated by Girard Desargues in the 1630s.

Theorem 1 (Desargues)**.** *Let $ABCD$ be a quadrilateral in the projective plane and let l be an arbitrary line in the same plane not passing through either A, B, C, or D. Then the three pairs of points of intersection of l with the opposite sides AB and CD, with AD and BC, as well as with the diagonals AC and BD are such that each pair is a pair of conjugate points under the involution determined by the other two pairs of points.*

By the principle of duality, involution is well-defined for a pencil of lines as well. Obviously, the dual version of Theorem 1 provides an example of such an involution. Another example follows from the same theorem by choosing ℓ_∞, the line at infinity, for our line ℓ. In that case, one could say that the directions of the sides and diagonals of $ABCD$ form conjugate pairs under one and the same involution. If we think of the vectors $\overrightarrow{AB}$ and so on as all having their tail at a point O, this can be expressed by saying that the lines these vectors lie on are conjugate lines under one and the same involution on the pencil of lines through O.

Involutions on lines and pencils can also be defined by means of a conic section. We need a definition first.

Definition 2. *Let A_1 and A_2 be two points in the projective plane with a_1 and a_2 their polar lines with respect to a conic $\mathcal{C}$ in the same plane. Then A_1 and A_2 are said to be conjugate points with respect to $\mathcal{C}$ if and only if a_1 lies on A_2 (and therefore a_2 lies on A_1).*

From this definition, it follows immediately that for any point P on a line ℓ not tangent to $\mathcal{C}$, there is exactly one point P' on ℓ that P is conjugate with. Therefore, conjugation with respect to a given conic of the points of a line in the plane of the conic defines an involution. In fact, any involution can be defined as a conjugation of the points of a line with respect to a conic. A conic that is pertinent in the case of the involution on ℓ_∞ defined by a quadrilateral $ABCD$ per Theorem 1 is given by the following theorem.

Theorem 2 (Nine-point Conic)**.** *Let $ABCD$ be a quadrilateral in the affine plane with no parallel sides. Let $E = AC \cap BD$, $F = AD \cap BC$, $G = AB \cap DC$,*

while M_{AB} denotes the mid-point of the line segment AB and so on. Then, the nine-point conic of $ABCD$ is the unique conic passing through the nine points E, F, G, M_{AB},...,M_{CD}. In case $ABCD$ is convex or self-intersecting, its associated nine-point conic is a hyperbola. In case $ABCD$ is concave, its nine-point conic is an ellipse.

It is now easy to verify that the involution on ℓ_∞ defined by a quadrilateral $ABCD$ per Theorem 1 coincides with conjugation of the points of ℓ_∞ with respect to $\mathcal{H}$ of $ABCD$. Alternatively, we could define the involution of the directions of the sides as the conjugation with respect to $\mathcal{H}$ of the lines of the pencil centered at the center of $\mathcal{H}$. Consequently, we have the following result.

Theorem 3. *Let $ABCD$ be a convex quadrilateral in the affine plane with no parallel sides. Then, the fixed lines of the involution of directions of $ABCD$ are real and parallel to the asymptotes of $\mathcal{H}$.*

In other words, the directions of the asymptotes of $\mathcal{H}$ harmonically separate each of the pairs of directions of AB, CD and AC, BD and AD, BC. This immediately leads to the following observation.

Corollary 4. *Let $ABCD$ be a convex quadrilateral with the hyperbola $\mathcal{H}$ for its nine-point conic. Then, for each of the pairs of lines AB, CD and AC, BD and AD, BC, there is a parallelogram that has its sides parallel to the asymptotes of $\mathcal{H}$ and its diagonals parallel to the pair of lines.*

Proof. This follows immediately from the fact that the directions of the sides of a parallelogram separate the directions of the diagonals harmonically... □

We can make the preceding more specific for the case of the diagonals AC and BD, with $E = AC \cap BD$. Let X, X' and Y, Y' be points on AC and BD, respectively, such that XY and $X'Y'$ are conjugate under the aforesaid involution. Furthermore, let x, y, x', y' be the signed lengths of EX, EY, EX', EY'. Then, the ratios $x : y$ and $x' : y'$ can be associated with two points with coordinates $[x : y]$ and $[x' : y']$ on the canonical projective line. By construction, these points are conjugate under an involution on the projective line. Specifically, $[1 : 0]$ (representing AC) is paired with $[0 : 1]$ (representing BD). Furthermore, let e_A, e_C, f_B, and f_D be the lengths of EA, EC, FB, FD, respectively. Then, $[e_A : f_B]$ and $[e_A : f_D]$ are paired with $[e_C : f_D]$ and $[e_C : f_B]$, respectively. As any involution mapping $[x : y]$ to $[x' : y']$ is described by a relation of the form $Axx' + B(xy' + yx') + Cyy' = 0$, it follows that the involution above is described by the relation $e_A e_C yy' = f_B f_D xx'$. We can use this observation to prove the following theorem.

Theorem 5. *Let $ABCD$ be a convex quadrilateral with no parallel sides, with E and e_A, e_C, f_b, f_D defined as above, while e and f are the lengths of AC and BD, respectively. Furthermore, let A^* be on the ray from E through A, B^* on the ray from E through B, C^* on the ray from E through C and D^* on the ray from E through D be such that $A^*E/AC = C^*E/AC = \sqrt{e_A e_C}/e$ and $B^*E/BD = D^*E/BD = \sqrt{f_B f_D}/f$. Then, the two pairs of parallel sides of*

parallelogram $A^*B^*C^*D^*$ are parallel to the asymptotes of the nine-point conic $\mathcal{H}$ of $ABCD$.

Proof. Since the sides of $A^*B^*C^*D^*$ are in the directions of the fixed lines of the involution defined by the pairs of opposite sides of $ABCD$ it immediately follows that they are parallel to the asymptotes of $\mathcal{H}$. □

This concludes our preliminary section. We are now ready to prove our main result.

3. Constructing a pair of inscribed parallelograms

Let $ABCD$ be a convex quadrilateral with no parallel sides. Let the asymptotes of the nine-point conic $\mathcal{H}$ of $ABCD$ be the axes of an oblique coordinate system and denote the center of $\mathcal{H}$ by O. Furthermore, let $\bar{a}$, $\bar{b}$, $\bar{c}$, $\bar{d}$, $\bar{e}$, $\bar{f}$ denote the vectors $\overrightarrow{AB}$, $\overrightarrow{BC}$, $\overrightarrow{CD}$, $\overrightarrow{DA}$, $\overrightarrow{AC}$, $\overrightarrow{BD}$ (with a, b, c, d, e, f their lengths). Finally, let $\bar{p}$ and $\bar{q}$ denote the vectors $\overrightarrow{A^*B^*}$ and $\overrightarrow{B^*C^*}$ (with p and q their lengths). The following result now applies (See Figure 1).

Theorem 6. *For a quadrilateral $ABCD$ in the affine plane with no parallel sides, let A' be the unique point on AB such that $2\overrightarrow{AA'}$ is the sum of $\bar{a}$ and the oblique projection of $\bar{c}$ onto $\bar{a}$ in the direction of $\bar{p}$ and let B', C', D' be defined analogously. Similarly, let B'' be the unique point on AB such that $2\overrightarrow{AA'}$ is the sum of $\bar{a}$ and the oblique projection of $\bar{c}$ onto $\bar{a}$ in the direction of $\bar{q}$ with A'', C'', D'' analogously. Then, $A'B'C'D'$ is a parallelogram inscribed in $ABCD$ such that $\overrightarrow{A'B'}$ is the oblique projection of $\bar{e}$ onto $\bar{p}$ in the direction of $\bar{q}$, while $\overrightarrow{B'C'}$ is the oblique projection of $\bar{f}$ onto $\bar{q}$ in the direction of $\bar{p}$. Similarly, $A''B''C''D''$ is a parallelogram inscribed in $ABCD$ such that $\overrightarrow{A''B''}$ is the oblique projection of $\bar{f}$ onto $\bar{p}$ in the direction of $\bar{q}$, while $\overrightarrow{B'C'}$ is the oblique projection of $\bar{e}$ onto $\bar{q}$ in the direction of $\bar{p}$. Finally, the oriented areas of $A'B'C'D'$ and $A''B''C''D''$ are each equal to the oriented area of $ABCD$.*

Proof. Let $\bar{a} = a_1\bar{p} + a_2\bar{q}$, $\bar{c} = c_1\bar{p} + c_2\bar{q}$ and so on. By Corollary 4, $a_1c_2 = -a_2c_1$. Therefore, the projection of $\bar{c}$ onto $\bar{a}$ in the direction of $\bar{p}$ is given by $-c_1\bar{p} + c_2\bar{q}$. In other words, $\overrightarrow{AA'} = \frac{1}{2}((a_1 + c_1)\bar{p} + (a_2 - c_2)\bar{q})$ while $\overrightarrow{BA'} = \frac{1}{2}((-a_1 + c_1)\bar{p} + -(a_2 + c_2)\bar{q})$ with analogous expressions for $\overrightarrow{BB'}$ and $\overrightarrow{CB'}$ and so on. Now, note that $\bar{a} + \bar{b} + \bar{c} + \bar{d} = \bar{0}$ by construction. Therefore, $\overrightarrow{A'B'} = \overrightarrow{A'B} + \overrightarrow{BB'}$ equals $\frac{1}{2}((a_1 + b_1 - c_1 - d_1)\bar{p} + (a_2 + b_2 + c_2 + d_2)\bar{q}) = e_1\bar{p}$. Similarly, $\overrightarrow{B'C'} = f_2\bar{q}$, while $\overrightarrow{C'D'} = -\overrightarrow{A'B'}$ and $\overrightarrow{D'A'} = -\overrightarrow{B'C'}$. We conclude that $A'B'C'D'$ is a parallelogram which by construction is inscribed in $ABCD$ with its sides parallel to the asymptotes of $\mathcal{H}$. Finally, let $\bar{a} \times \bar{b}$ denote the oriented area of the parallelogram spanned by $\bar{a}$ and $\bar{b}$ and so on. Then, the oriented area of $ABCD$ equals $\frac{1}{2}(\bar{e} \times \bar{f}) = \frac{1}{2}(e_1\bar{p} + e_2\bar{q}) \times (f_1\bar{p} + f_2\bar{q}) = \frac{1}{2}(e_1f_2 - e_2f_1)(\bar{p} \times \bar{q})$. As $e_1f_2 = -e_2f_1$, the latter expression equals $e_1f_2(\bar{p} \times \bar{q}) = (e_1\bar{p}) \times (f_2\bar{q})$

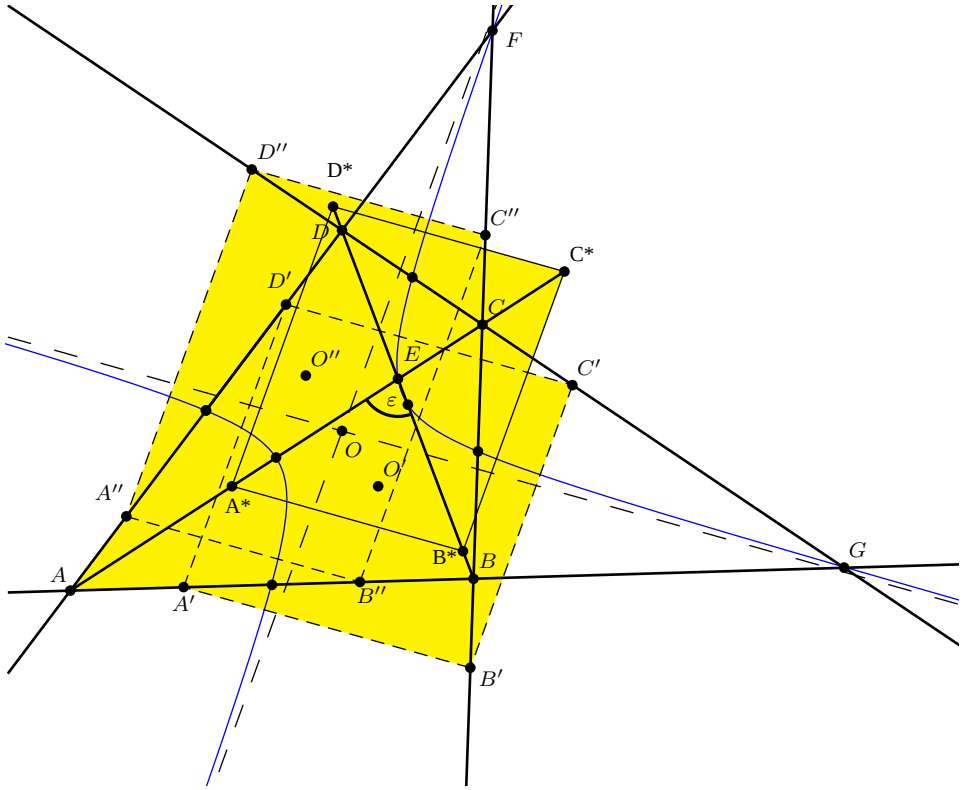

Figure 1. The two parallelograms inscribed in $ABCD$ with equal area to $ABCD$

or $\overrightarrow{A'B'} \times \overrightarrow{B'C'}$. This proves that the oriented area of $A'B'C'D'$ equals that of $ABCD$. The properties of $A''B''C''D''$ now follow similarly. □

If $ABCD$ does have parallel sides, i.e. if $ABCD$ is a trapezoid, the proof above does not apply. In this case, however, a slightly modified version can be fairly easily found and $A'B'C'D'$ and $A''B''C''D''$ end up being parallelograms with a pair of opposite sides on the parallel sides of $ABCD$.

The two parallelograms $A'B'C'D'$ and $A''B''C''D''$ are connected in various ways. Most notably, the centers O' and O'' of the two parallelograms are reflections of one another in the center O of the nine-point conic $\mathcal{H}$ of $ABCD$. Also, the line through the midpoints of A' and A'' and of C' and C'' is parallel to $\bar{e}$ and passes through O. Likewise, the line through the midpoints of B' and B'' and of D' and D'' is parallel to $\bar{f}$ and passes through O as well. Finally, the points of intersection $A'D' \cap D''C''$ and $C'B' \cap B''A''$ both lie on BD, while the points of intersection $D''A'' \cap A'B'$ and $B''C'' \cap C'D'$ both lie on AC. For the purposes of this paper, however, there is no need to investigate these properties any further.

4. Finding angles and sides

Our next task is to find expressions for the angles between the sides of $A'B'C'D'$ and $A''B''C''D''$ as well as for their lengths.

Theorem 7. *For $ABCD$ and $A^*B^*C^*D^*$ as defined above, let ϵ denote the signed angle from $\bar{e}$ to $\bar{f}$. Furthermore, let ζ be the signed angle from $\bar{p}$ to $\bar{q}$. Then*

$$\frac{\sin(\epsilon)}{\tan(\zeta)} = \frac{(f_B f_D - e_A e_C)}{2\sqrt{e_A e_C f_B f_D}}.$$

Proof. We have $pq\sin(\zeta) = \bar{p} \times \bar{q}$, which equals

$$(\frac{\sqrt{e_A e_C}}{e}\bar{e} - \frac{\sqrt{f_B f_D}}{f}\bar{f}) \times (\frac{\sqrt{e_A e_C}}{e}\bar{e} + \frac{\sqrt{f_B f_D}}{f}\bar{f}) = \frac{2\sqrt{e_A e_C f_B f_D}}{ef}\sin(\epsilon).$$

Similarly $pq\cos(\zeta) = \frac{e_A e_C - f_B f_D}{ef}$. The desired formula now immediately follows from these two equalities. □

As for the lengths of the sides of $A'B'C'D'$ and $A''B''C''D''$, let the lengths of the sides $A'B'$ and $B'C'$ be denoted by p' and q', while the lengths of the sides $A''B''$, $B''C''$ are denoted by p'' and q''. We now have the following relations.

Theorem 8. *Let $ABCD$ be a convex quadrilateral, with p, p', p'' and q, q', q'' defined as above. Then*

$$p' = \frac{ep}{2\sqrt{e_A e_C}},\ q' = \frac{fq}{2\sqrt{f_B f_D}} \text{ and } p'' = \frac{fp}{2\sqrt{f_B f_D}},\ q'' = \frac{eq}{2\sqrt{e_A e_C}}.$$

Proof. Both $\overrightarrow{A^*B^*}$ and $\overrightarrow{A'B'}$ are oblique projections onto $\bar{q}$ in the direction of $\bar{q}$ of parallel vectors. Therefore, the first relation follows from similarity. The other three relations are derived similarly. □

Corollary 9. *Let $ABCD$ be a convex quadrilateral, with p, p', p'' and q, q', q'' defined as above. Then*

$$p' = \frac{e}{2\sqrt{e_A e_C}}\sqrt{e_A e_C + f_B f_D - 2\sqrt{e_A e_C f_B f_D}\cos(\epsilon)},$$

$$q' = \frac{f}{2\sqrt{f_B f_D}}\sqrt{e_A e_C + f_B f_D + 2\sqrt{e_A e_C f_B f_D}\cos(\epsilon)},$$

$$p'' = \frac{f}{2\sqrt{f_B f_D}}\sqrt{e_A e_C + f_B f_D - 2\sqrt{e_A e_C f_B f_D}\cos(\epsilon)},$$

$$q'' = \frac{e}{2\sqrt{e_A e_C}}\sqrt{e_A e_C + f_B f_D + 2\sqrt{e_A e_C f_B f_D}\cos(\epsilon)},$$

where, as before, ϵ is the signed angle between $\bar{e}$ and $\bar{f}$.

Proof. This is a straightforward application of the Law of Cosines and Theorem 8. □

5. The case of the cyclic quadrilateral

For the general quadrilateral, the expressions above probably cannot be simplified. For the cyclic case, however, we have the following result.

Theorem 10. *Let $ABCD$ be a (convex) cyclic quadrilateral with no parallel sides, with p', q', p'', q'' defined as above. Then $A'B'C'D'$ and $A''B''C''D''$ are rectangles and*

$$p' = \sqrt{\frac{e}{f}(s-b)(s-d)}, \qquad q' = \sqrt{\frac{f}{e}(s-a)(s-c)}$$

and

$$p'' = \sqrt{\frac{f}{e}(s-b)(s-d)}, \qquad q'' = \sqrt{\frac{e}{f}(s-a)(s-c)},$$

where $s = \frac{1}{2}(a+b+c+d)$.

Proof. If $ABCD$ can be inscribed in a circle, then obviously $e_A e_C = f_B f_D$. Therefore, $1/\tan\zeta = 0$, by Corollary 7. In other words, the sides of $A'B'C'D'$ and $A''B''C''D''$ are at right angles. It also follows from Corollary 9 that $p' = \frac{e}{2}\sqrt{1-\cos\epsilon}$, while $q' = \frac{e}{2}\sqrt{1+\cos\epsilon}$. Next, note that for every quadrilateral $ABCD$, $2ef\cos\epsilon = b^2+d^2-a^2-c^2$ (Bretschneider's Formula, see [1]), while for any (convex) cyclic quadrilateral $ef = ac+bd$ (Ptolemy's Theorem). Elimination of ef and $\cos\epsilon$ and some straightforward algebraic manipulation now gives the desired result. □

Corollary 11. *Let $ABCD$ be a cyclic quadrilateral with no parallel sides. Then, its area $ABCD$ is given by the formula*

$$ABCD = \sqrt{(s-a)(s-b)(s-c)(s-d)}.$$

Proof. The statement immediately follows by combining Theorem 6 and Theorem 10. □

Again, the proof above does not apply to the only type of cyclic quadrilateral with parallel sides, i.e. the isosceles trapezoid. It is easily verified, however, that the statement of the theorem is true for this case as well. This concludes our derivation of the area formula for the cyclic quadrilateral as inspired by Gaṇeśa's flawed attempt to derive the same formula.

6. Conclusion

At this point, one might ask how all of this relates to Gaṇeśa's derivation. In light of the proofs of the results contained in this paper, it might seem highly unlikely that any 16th-century mathematical practitioner (regardless of the mathematical culture in which he was operating) would have been able to come up with a line of reasoning like ours. The answer is that Gaṇeśa did not either. It is true that essentially he gave the statement of Theorem 10 and used the argument of Corollary 11, implicitly assuming Theorem 6. But then, he only did so for the case of the cyclic quadrilaterals. Even for this more simple situation, however, Gaṇeśa's reasoning is hardly satisfactory. Thus, the construction of the points of the two

parallelograms $A'B'C'D'$ and $A''B''C''D''$ is a lot easier, as the asymptotes of the nine-point conic for a cyclic quadrilateral $ABCD$ are parallel to the angle bisectors of AEB. Therefore A' simply is the point on AB such that AA' has length $(a+c)/2$ and so on. This is exactly how Gaṇeśa constructs one of the two inscribed parallelograms $A'B'C'D'$ and $A''B''C''D''$, to then compute the area of the cyclic quadrilateral from the area of the inscribed parallelogram (which only requires tools and properties that were reasonably well-known to the mathematical culture in which Gaṇeśa operated). Of course, he still would have had to prove that his inscribed parallelogram is a rectangle and that the area of this rectangle equals that of $ABCD$. As it is, there is no proof of either in his work. At best, we could say that Gaṇeśa had the right intuition, but perhaps not the tools to fully back up his claims.

References

[1] E. J. Atzema, From Brahmagupta to Euler: On the formula for the area of a cyclic quadrilateral, *BSHM Bulletin: Journal of the British Society for the History of Mathematics*, 30 (2015) 20–34.

[2] M. G. Inamdar, An interesting proof of the formula for the area of a (cyclic) quadrilateral and a triangle given by the Sanskrit commentator Ganesh in about 1545 AD, *Nagpur University Journal*, 11 (1945) 36–42.

[3] K. Plofker, *Mathematics in India*, Princeton & Oxford, Princeton University Press, 2009.

Eisso J. Atzema: University of Maine, Orono, ME 04469 USA
E-mail address: atzema@math.umaine.edu

Forum Geometricorum
Volume 15 (2015) 173–176.

FORUM GEOM
ISSN 1534-1178

Another Construction of the Simson Lines Through a Given Point

Francisco Javier García Capitán

Abstract. We give a simple conic construction of the points on the circumcircle whose Simson line go through a given point.

The construction problem of the Simson lines through a given point has been solved elegantly by Jean Pierre Ehrmann in [1]. Given a point P in the plane of triangle ABC (with orthocenter H), the three points whose Simson lines pass through P are the intersections of the circumcircle and the *translation* by the vector $\mathbf{HP}$ of the rectangular circum-hyperbola through P. Ehrmann obtained this ingenious construction by applying remarkable results of Lalesco ([2]) on Simson lines. In this note we give another construction resulting from a simple-minded analysis.

We use barycentric coordinates with reference to triangle ABC. Let $P = (u : v : w)$. For an arbitrary point $M = (x : y : z)$, let B_0, C_0 be the pedals of M on the sidelines CA and AB respectively. When M lies on the circumcircle, B_0C_0 becomes the Simson line of M. Now, the line B_0C_0 contains the point P if and only if M lies on the conic Γ_a with equation

$$c^2(S_Au - S_Cw)y^2 + b^2(S_Au - S_Bv)z^2 + ((S^2 + 2S_A^2)u - S_{AB}v - S_{AC}w)yz$$
$$- b^2(c^2v + S_Aw)xz - c^2(b^2w + S_Av)xy = 0.$$

where S is, as usual, twice the area of triangle ABC.

Clearly, the conic Γ_a contains the vertex A. Proposition 1 exhibits five more points on the conic, which can be easily constructed; see Figure 1.

Proposition 1. *Let the perpendicular from P to AP^* intersect AC at M and AB at N.*
(a) *If the perpendicular from P to AB intersects CA at Y, then Y lies on Γ_a. In the same way, if the perpendicular from P to CA intersects AB at Z, then Z also lies on Γ_a.*
(b) *If the perpendicular to AQ at P intersects CA, AB at M, N, then the perpendiculars to CA, AB at M, N intersect at a point L on Γ_a.*

Publication Date: July 8, 2015. Communicating Editor: Paul Yiu.

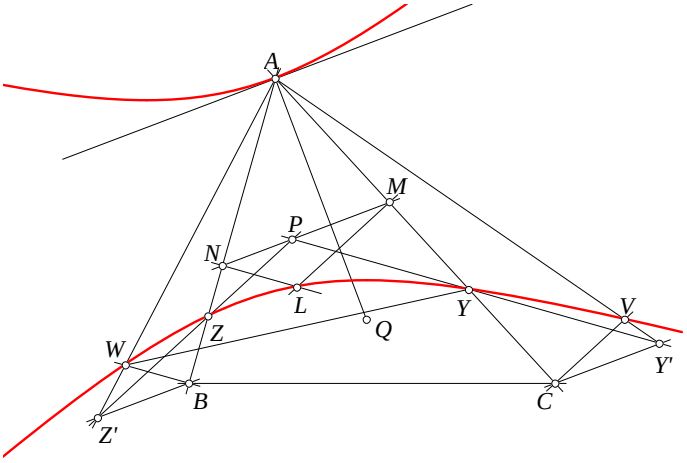

Figure 1.

(c) *If the perpendicular to AQ at C intersects PY at Y', then the perpendicular to CA at C intersects AY' at a point V on Γ_a. Likewise, if the perpendicular to AQ at B intersects PZ at Z', then the perpendicular to AB at B intersects AZ' at a point W on Γ_a.*

The conic Γ_a contains the infinite points of the altitudes through B and C. Therefore, it is a hyperbola. Proposition 2 gives a simple construction of the center of Γ_a, and hence its asymptotes (see Figure 2). Indeed, Γ_a goes through A and the normal at A is the A-cevian of the isogonal conjugate Q of P.

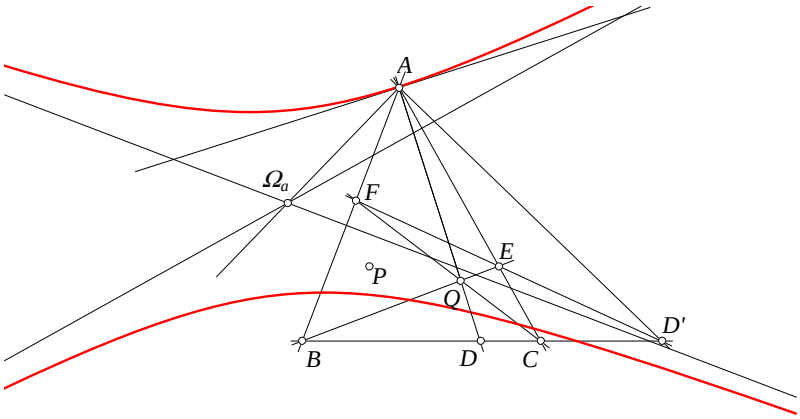

Figure 2.

Proposition 2. *If Ω_a is the center of Γ_a, the perpendicular to $A\Omega_a$ at A is the harmonic conjugate of AQ with respect to AB, AC. In other words, if DEF is the cevian triangle of Q, let $D' = DE \cap BC$ be the harmonic conjugate of D with respect to BC. Then AD' and $A\Omega_a$ are perpendicular.*

Clearly, apart from the vertex A, the common points of Γ_a and the circumcircle are the points whose Simson lines pass through the given point P. See Figure 3.

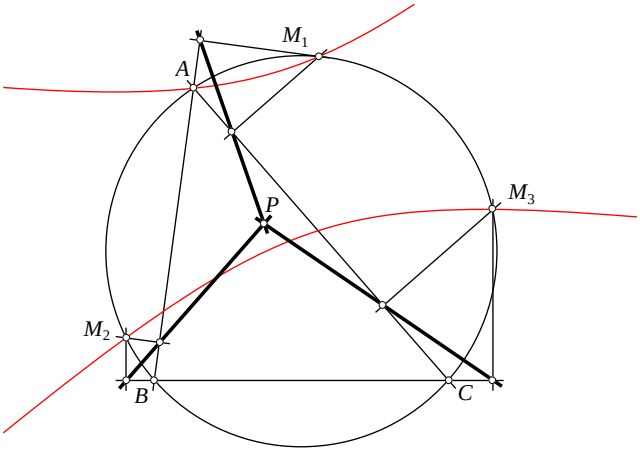

Figure 3.

Consider also the analogous hyperbolas Γ_b and Γ_c. Each of these also intersects the circumcircle at the same three points whose Simson lines pass through the given point P, as does Ehrmann's hyperbola, which has equation

$$u(S_B v - S_C w)\Gamma_a + v(S_C w - S_A u)\Gamma_b + w(S_A u - S_B v)\Gamma_c = 0.$$

Figure 4 shows the hyperbolas Γ_a, Γ_b, Γ_c, and Ehrmann's hyperbola h'.

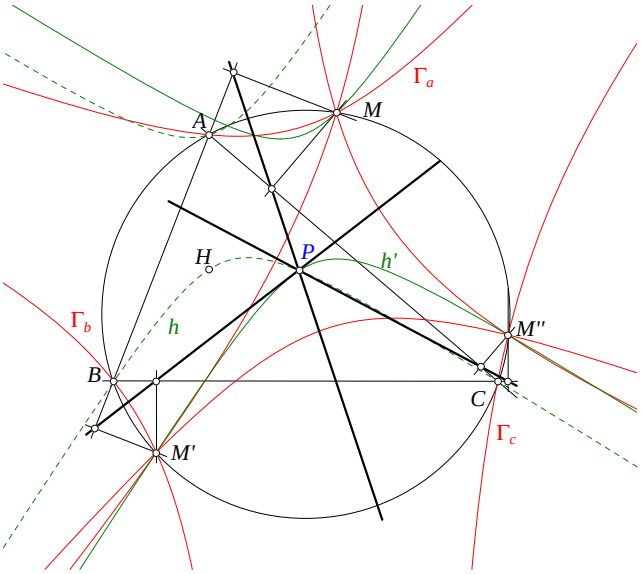

Figure 4.

We conclude this note with another construction of the center of Γ_a.

Let $A'B'C'$ be the cevian triangle of P and $A'' = B'C' \cap BC$, that is, A'' is the harmonic conjugate of A' with respect to B, C. If U is the midpoint of AP, let the parallel to AA'' intersect AB, AC at K, L. Then K and L are the orthogonal projections of Ω_a on CA and AB respectively. In other words, $\Omega_a K$ and $\Omega_a L$ are are the asymptotes of the hyperbola (see Figure 5).

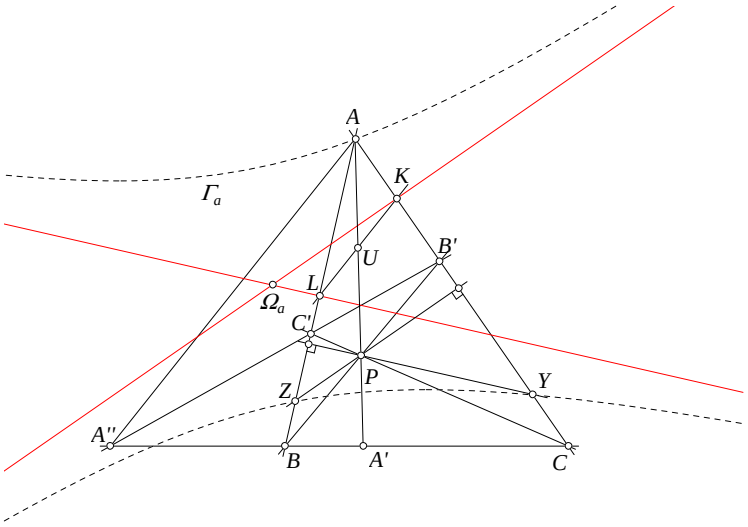

Figure 5.

References

[1] J.-P. Ehrmann, Some geometric constructions, *Forum Geom.*, 6 (2006) 327–334.
[2] T. Lalesco, *La geometrie du Triangle*, Paris Vuibert 1937; Jacques Gabay reprint 1987.

Francisco Javier García Capitán: Departamento de Matemáticas, I.E.S. Alvarez Cubero, Avda. Presidente Alcalá-Zamora, s/n, 14800 Priego de Córdoba, Córdoba, Spain

E-mail address: garciacapitan@gmail.com

Forum Geometricorum
Volume 15 (2015) 177–178.

FORUM GEOM
ISSN 1534-1178

Points on a Line that Maximize and Minimize the Ratio of the Distances to Two Given Points

Arie Bialostocki and Rob Ely

Abstract. Given a line ℓ and points B and C, we construct the two points on ℓ that maximize and minimize the ratio $\frac{XB}{XC}$ for X on ℓ.

In this note we solve a problem that generalizes the main result of [1]. Given triangle ABC with ℓ the line bisecting angle A, in [1] we asked to find the two points X_1 and X_2 that maximize and minimize $\frac{BX}{CX}$. It was proved that these two points are the incenter and excenter corresponding to angle A. It is worthwhile to notice that it is not difficult to prove a similar result where ℓ is the external bisector of A. In this case the two extremal points are the excenters which correspond to angles B and C. In this note we consider a more general problem where ℓ is an arbitrary line which does not contain the points B and C and find the two points X_1 and X_2 on ℓ which give the minimum and maximum of $\frac{BX}{CX}$.

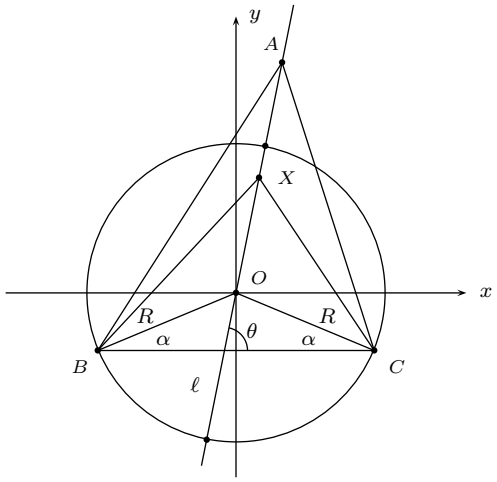

Figure 1

If ℓ is not perpendicular to BC, it intersects the perpendicular bisector of BC at a point O. Let R be the radius of the circle with center O and containing B and C. We make use of a Cartesian coordinate system with origin at O, and x-axis parallel to BC (see Figure 1). Thus, $B = R(-\cos\alpha, -\sin\alpha)$ and $C = R(\cos\alpha, -\sin\alpha)$, where $\alpha = \angle OBC = \angle OCB$.

Publication Date: July 15, 2015. Communicating Editor: Paul Yiu.

If the line ℓ makes an angle θ with the positive x-axis, then every point X on the line ℓ has coordinates $t(\cos\theta, \sin\theta)$ for some t. The ratio $\frac{BX}{CX}$ is a function of t. It is more convenient to consider

$$F(t) = \frac{BX^2}{CX^2} = \frac{t^2 + 2Rt\cos(\theta - \alpha) + R^2}{t^2 - 2Rt\cos(\theta + \alpha) + R^2}.$$

Differentiating with respect to t, we have

$$F'(t) = \frac{4\cos\theta\cos\alpha(R^2 - t^2)}{(t^2 - 2Rt\cos(\theta - \alpha) + R^2)^2}.$$

It is clear that $F'(t) = 0$ for $t = \pm R$. Therefore, F has two critical points which are on the circle, center O and containing B and C. In fact, $F(R) = \frac{1+\cos(\theta-\alpha)}{1-\cos(\theta+\alpha)}$ is maximum and $F(-R) = \frac{1-\cos(\theta-\alpha)}{1+\cos(\theta+\alpha)}$ is minimum.

Therefore, the points maximizing and minimizing the ratio $\frac{BX}{CX}$ are the intersections of ℓ and the circle through B and C, with center on ℓ.

If ℓ is the perpendicular through A to BC, then $\frac{BX}{CX}$ is a maximum (or minimum) at the intersection of ℓ and BC. It approaches 1 as X moves on ℓ away from BC.

Reference

[1] A. Bialostocki and D. Bialostocki, The incenter and an excenter as solutions to an extremal problem, *Forum Geom.*, 11 (2011) 9–12.

Arie Bialostocki: 458 Paradise Dr., Moscow, Idaho 83843, USA
E-mail address: arie.bialostocki@gmail.com

Rob Ely: Department of Mathematics, University of Idaho, Moscow, Idaho 83843, USA
E-mail address: ely@uidaho.edu

Forum Geometricorum
Volume 15 (2015) 179–183.

FORUM GEOM
ISSN 1534-1178

Reciprocal Jacobi Triangles and the McCay Cubic

Glenn T. Vickers

Abstract. Given a triangle and a set of three angles, the celebrated geometrical theorem of Jacobi produces a new triangle in perspective with the first. If this second triangle is related to the first by another set of three angles then these two triangles are said to be reciprocal Jacobi triangles. It is shown that the locus of the perspector is then the McCay cubic.

1. Jacobi Triangles.

With ABC being any triangle, construct the points P, Q, R so that

$$\angle RAB = \angle QAC = \alpha,\ \angle PBC = \angle RBA = \beta \text{ and } \angle QCA = \angle PCB = \gamma.$$

These points form a *Jacobi triangle* for ABC and Jacobi's theorem states that the lines $AP,\ BQ$ and CR are concurrent (at the point K), see Figure 1. To quote [5], this result 'was seemingly discovered by Carl Friedrich Andreas Jacobi (not to be confused with Carl Gustav Jacob Jacobi), and published in 1825 in Latin'.

Many proofs of this result are available, e.g. [4] and [1, pp. 55–56], but one is given here because some results from it will be needed later.

1.1. *A Proof of Jacobi's Theorem.* With reference to Figure 1, let the lines AP and BC meet at P'. The sine rule applied to triangles BPP' and CPP' gives

$$\frac{BP'}{P'C} = \frac{\sin\gamma}{\sin\beta}\frac{\sin\angle BPP'}{\sin\angle CPP'} \tag{1}$$

and applied to triangles ABP and ACP,

$$\frac{\sin\angle BPA}{\sin\angle CPA} = \frac{c}{b}\frac{\sin(B+\beta)}{\sin(C+\gamma)} = \frac{\sin\angle BPP'}{\sin\angle CPP'}. \tag{2}$$

Ceva's theorem now implies that AP, BQ, CR are concurrent at K, say.

Furthermore, (1) and (2) give

$$\frac{\cot C + \cot\gamma}{\cot B + \cot\beta} = \frac{BP'}{P'C} = \frac{\Delta BAP'}{\Delta CAP'} = \frac{\Delta BKP'}{\Delta CKP'} = \frac{\Delta ABK}{\Delta ACK},$$

and so the relative areal coordinates (x, y, z) of K may be chosen to be

$$(x, y, z) = \left(\frac{1}{\cot A + \cot\alpha},\ \frac{1}{\cot B + \cot\beta},\ \frac{1}{\cot C + \cot\gamma}\right).$$

Publication Date: August xx, 2015. Communicating Editor: Paul Yiu.

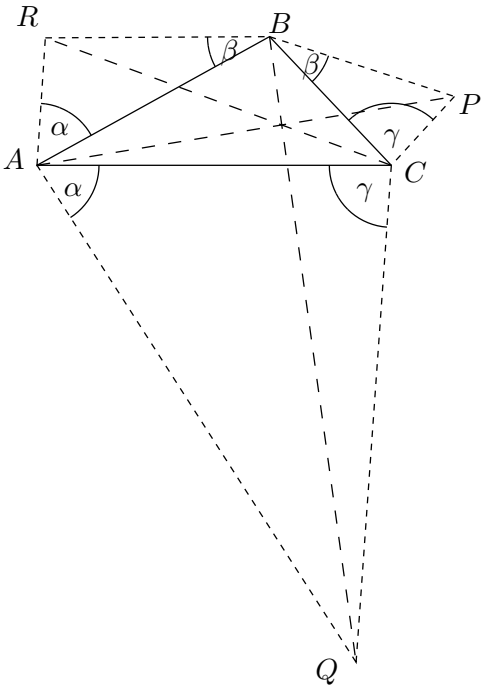

Figure 1. The points P, Q, R are constructed on a base triangle ABC with pairs of angles equal as shown. Jacobi's theorem states that AP, BQ, CR are concurrent and K will be used for the common point.

It can be seen that if $\alpha = \beta = \gamma$ then K lies on the rectangular hyperbola

$$yz(\cot B - \cot C) + zx(\cot C - \cot A) + xy(\cot A - \cot B) = 0$$

which is known as *Kiepert's hyperbola*.

2. Reciprocal Jacobi Triangles.

Given any triangle ABC and angles α, β, γ there is an associated Jacobi triangle PQR. Starting with triangle PQR and angles α', β', γ' another triangle may be constructed. If this third triangle coincides with the first then we say that ABC and PQR are *reciprocal Jacobi triangles*, see Figure 2. In this case, better notation is $A'B'C'$ rather than PQR (and A' may denote a point or an angle).

Theorem 1. *Let the triangle ABC and the angles α, β, γ in order produce the Jacobi triangle PQR and let the Jacobi triangle produced by this triangle with the angles α', β', γ' be the original triangle ABC. Then*

$$\frac{\sin(A + 2\alpha)}{\sin A} = \frac{\sin(B + 2\beta)}{\sin B} = \frac{\sin(C + 2\gamma)}{\sin C} \ (= \mu). \tag{3}$$

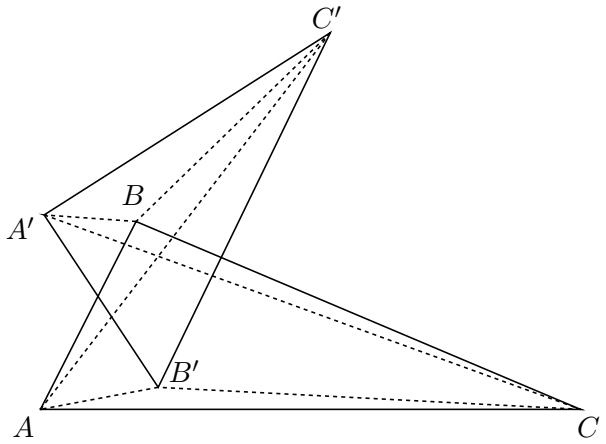

Figure 2. ABC and $A'B'C'$ are reciprocal Jacobi triangles. There are six pairs of equal angles, e.g. $\angle BAC' = \angle CAB'$. The lines AA', BB' and CC' are concurrent..

Proof. Since $\angle AQR = \beta'$ and $\angle ARQ = \gamma'$ we have

$$\left.\begin{array}{l}\beta'+\gamma'+2\alpha+A=\pi\\ \gamma'+\alpha'+2\beta+B=\pi\\ \alpha'+\beta'+2\gamma+C=\pi\end{array}\right\} \implies (\alpha'+\beta'+\gamma')+(\alpha+\beta+\gamma)=\pi \qquad (4)$$

giving

$$\left.\begin{array}{l}\alpha'=A+\alpha-\beta-\gamma\\ \beta'=B-\alpha+\beta-\gamma\\ \gamma'=C-\alpha-\beta+\gamma\end{array}\right\} \text{ and } \left.\begin{array}{l}A'=\pi-2A-2\alpha+\beta+\gamma\\ B'=\pi-2B+\alpha-2\beta+\gamma\\ C'=\pi-2C+\alpha+\beta-2\gamma\end{array}\right\}.$$

Hence $(A'+\alpha')+(A+\alpha)=\pi$ and so $AQPB$ is one of many cyclic quadrilaterals in the figure. It is now readily shown that

$$\begin{array}{ll}\angle APR=\angle ACR=\frac{\pi}{2}+\beta-\alpha-A, & \angle APQ=\angle ABQ=\frac{\pi}{2}+\gamma-\alpha-A;\\ \angle BQP=\angle BAP=\frac{\pi}{2}+\gamma-\beta-B, & \angle BQR=\angle BCR=\frac{\pi}{2}+\alpha-\beta-B;\\ \angle CRQ=\angle CBQ=\frac{\pi}{2}+\alpha-\gamma-C, & \angle CRP=\angle CAP=\frac{\pi}{2}+\beta-\gamma-C.\end{array}$$

Thus

$$\begin{aligned}\angle BPA &= \angle BPR+\angle RPA\\ &= \alpha'+(\tfrac{\pi}{2}+\beta-\alpha-A)\\ &= \tfrac{\pi}{2}-\gamma.\end{aligned}$$

Likewise $\angle CPA = \frac{\pi}{2}-\beta$ and so (2) gives

$$\frac{\cos\gamma}{\cos\beta}=\frac{\sin C}{\sin B}\frac{\sin(B+\beta)}{\sin(C+\gamma)}$$

$$\implies \quad \frac{\sin(C+\gamma)\cos\gamma}{\sin C}=\frac{\sin(B+\beta)\cos\beta}{\sin B}$$

$$\implies \quad \frac{\sin(C+2\gamma)}{\sin C}=\frac{\sin(B+2\beta)}{\sin B}$$

as required. □

Although not needed here, it is stated without proof that we also have

$$\frac{\tan\alpha'}{\tan\alpha} = \frac{\tan\beta'}{\tan\beta} = \frac{\tan\gamma'}{\tan\gamma}.$$

3. The Locus of K.

For a given triangle ABC, any value of μ gives a reciprocal triangle and so the point K is parametrized by μ. Figure 3 shows a typical result for its locus and it is this locus which is now investigated.

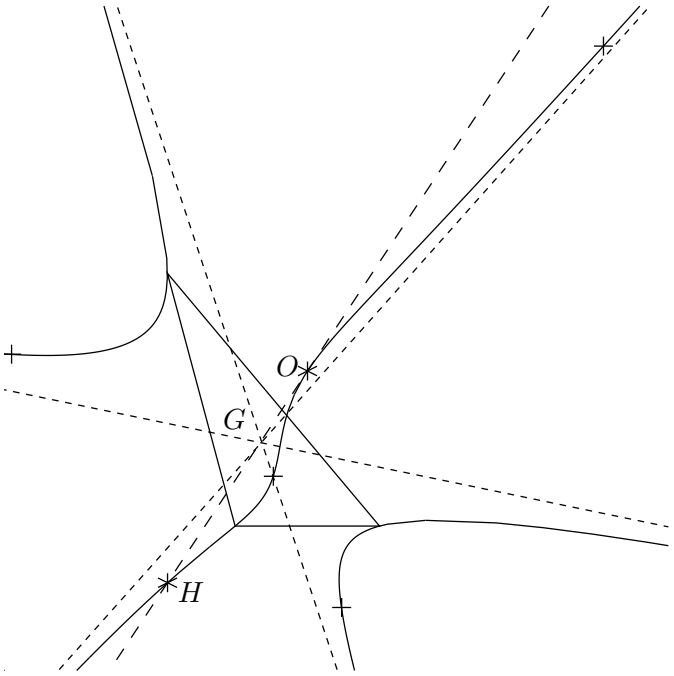

Figure 3. The locus of K (together with its asymptotes, shown as dotted lines) when α, β, γ are constrained by ABC having a reciprocal Jacobi triangle. The dashed line is the Euler line, O the circumcenter, G the centroid and H the orthocenter. Also shown (as crosses) are the incenter and ex-centers.

Using relative areal (a.k.a. barycentric) coordinates with ABC as the triangle of reference, it was shown in Section 1.1 that the coordinates of K (for any Jacobi triangle) are

$$\left(\frac{1}{\cot A + \cot\alpha}, \frac{1}{\cot B + \cot\beta}, \frac{1}{\cot C + \cot\gamma}\right).$$

Now

$$\mu = \frac{\sin(A+2\alpha)}{\sin A} = \cos 2\alpha + \cot A \sin 2\alpha \implies \cot A = \frac{\mu - \cos 2\alpha}{\sin 2\alpha}$$

and so

$$\cot A + \cot \alpha = \frac{\mu + 1}{\sin 2\alpha}.$$

Hence the coordinates of K (when there is a reciprocal Jacobi triangle) can be taken to be

$$(x, y, z) = (\sin 2\alpha, \sin 2\beta, \sin 2\gamma)$$

and it is easily seen that

$$\frac{x^2}{\sin^2 A} - 2\mu x \cot A + \mu^2 - 1 = 0,$$

from which it follows that the locus of K is

$$\frac{x^2}{\sin^2 A}(y \cot B - z \cot C) + \frac{y^2}{\sin^2 B}(z \cot C - x \cot A) + \frac{z^2}{\sin^2 C}(x \cot A - y \cot B) = 0,$$

or, equivalently,

$$a^2(-a^2 + b^2 + c^2)(c^2y^2 - b^2z^2)x + b^2(a^2 - b^2 + c^2)(a^2z^2 - c^2x^2)y + c^2(a^2 + b^2 - c^2)(b^2x^2 - a^2y^2)z = 0.$$

This cubic curve is known as the *McCay cubic* of ABC. Gibert's website [3], together with [2], gives a wealth of information regarding this and other cubic curves in triangle geometry.

References

[1] P. Baptist, *Die Entwicklung der Neueren Dreiecksgeometrie*, Wissenschaftsverlag, Mannheim/Leipzig/Wein/Zurich, 1992.

[2] J.-P. Ehrmann and B. Gibert, *Special Isocubics in the Triangle Plane*, 2015 edition, `http://bernard.gibert.pagesperso-orange.fr/files/isocubics.html`.

[3] B. Gibert, *Catalogue of Triangle Cubics*, `http://bernard.gibert.pagesperso-orange.fr/ctc.html`.

[4] G. Leversha, *The Geometry of the Triangle*, UKMT 2013.

[5] Y. Zhang and A. Bostan, Problem 11554, *Amer. Math. Monthly*, 118 (2011) 178; solutions, 119 (2012) 703–704.

Glenn T. Vickers: 5 The Fairway, Sheffield S10 4LX, United Kingdom

E-mail address: `glennmarilynvickers@gmail.com`

Forum Geometricorum
Volume 15 (2015) 185–190.

FORUM GEOM
ISSN 1534-1178

Pairs of Cocentroidal Inscribed and Circumscribed Triangles

Gotthard Weise

Abstract. Let Δ be a reference triangle and P a point not on the sidelines. We consider all inscribed and circumscribed triangles Δ' and Δ^* with centroid P and remarkable properties as well as relationships between them.

1. Notations

Let $\Delta = ABC$ an arbitrary positively oriented triangle with sidelines $a,\ b,\ c$, centroid G and area S. A point P in the plane of Δ is described by its standardized homogeneous barycentric coordinates u, v, w in reference to Δ with

$$u + v + w = 1. \tag{1}$$

For a triangle given by its vertices we use the matrix notation with vertex coordinates in the columns.

2. Inscribed triangles with centroid P

Given a fixed point $P = (u : v : w)$ not on the sidelines of Δ. The reflections of the medians of Δ in P intersect the respective sidelines at A'_0, B'_0 and C'_0. These points are the vertices of the inscribed (oriented) triangle Δ'_0 (see Figure 1)

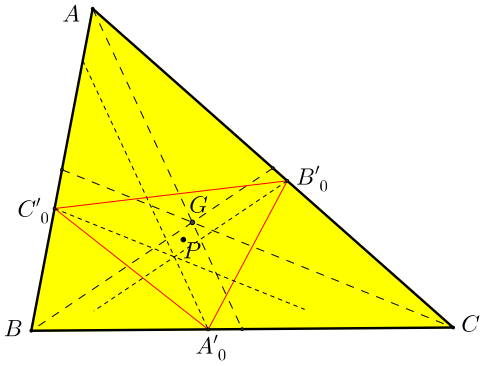

Figure 1.

with matrix notation

$$\Delta'_0 = (A'_0B'_0C'_0) = \frac{1}{2}\begin{pmatrix} 0 & 1-2(w-u) & 1+2(u-v) \\ 1+2(v-w) & 0 & 1-2(u-v) \\ 1-2(v-w) & 1+2(w-u) & 0 \end{pmatrix}. \tag{2}$$

Publication Date: September 15, 2015. Communicating Editor: Paul Yiu.

By introducing the abbreviations

$$\begin{aligned} p_0 &:= 2(v-w), \\ q_0 &:= 2(w-u), \\ r_0 &:= 2(u-v), \end{aligned} \tag{3}$$

the representation of Δ_0' is simplified to

$$\Delta_0' = (A_0'B_0'C_0') = \frac{1}{2}\begin{pmatrix} 0 & 1-q_0 & 1+r_0 \\ 1+p_0 & 0 & 1-r_0 \\ 1-p_0 & 1+q_0 & 0 \end{pmatrix}. \tag{4}$$

Proposition 1. *The centroid of Δ_0' is P.*

Proof. The row sums of (4) are barycentric coordinates of P. □

We know that Δ_0' is not the only inscribed triangle with centroid P, but there is an infinite family $\mathcal{D}' = \{\Delta'(t) |\ t \in \mathbb{R}\}$ of such *cocentroidal* triangles.

If A' is an arbitrary point on the sideline a, then the well-known construction of Δ' is the following: Let X be the point on the line $A'P$, so that P divides the line segment $A'X$ in the ratio $2:1$. Let Y be the reflection point of A in X. The parallel of c through Y cuts b at B'; the parallel of b through Y cuts c at C'.

Now we want to choose a parametric representation of Δ' with a simple geometrically relevant parameter t. Denote by S_a' the (oriented) area of the triangle $AA_0'A'$ (green in Figure 2).

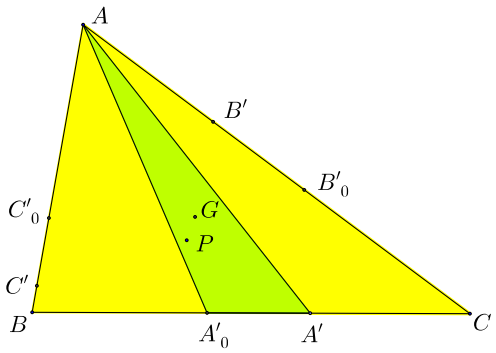

Figure 2.

According to (4) the second coordinate of A' is $\frac{1}{2}(1+p_0-2S_a')$, the third coordinate $\frac{1}{2}(1-p_0+2S_a')$. With

$$\begin{aligned} p &:= p_0 - 2t, \\ q &:= q_0 - 2t, \\ r &:= r_0 - 2t, \end{aligned} \tag{5}$$

and $t := S_a'$, we obtain $A' = \frac{1}{2}(0 : 1+p : 1-p)$. Define $B' := (1-q : 0 : 1+q)$ and $C' := (1+r : 1-r : 0)$. It is clear (see proof of Proposition 1) that the

triangles

$$\Delta'(t) = (A'B'C') = \frac{1}{2}\begin{pmatrix} 0 & 1-q & 1+r \\ 1+p & 0 & 1-r \\ 1-p & 1+q & 0 \end{pmatrix},\ t \in \mathbb{R} \tag{6}$$

have the centroid P and thus they constitute the family $\mathcal{D}'$.

Let us now calculate the area S' of Δ':

$$\begin{aligned} S' &= S \cdot \det \Delta' = \frac{S}{8}\left((1+p)(1+q)(1+r) + (1-p)(1-q)(1-r)\right) \\ &= \frac{S}{4}(1+pq+qr+rp). \end{aligned} \tag{7}$$

From (1), (3), (5) and the abbreviation

$$k := 1 - 2(u^2+v^2+w^2) \tag{8}$$

follows [1]

$$S' = \frac{3}{4} \cdot S \cdot (k + 4t^2) = S'_0 + 3S \cdot t^2. \tag{9}$$

This leads to

Proposition 2. *Among the triangles $\Delta'(t) \in \mathcal{D}'$, the triangle $\Delta'(0) = \Delta'_0$ has minimum area.*

A known special case is $P = G$: Δ'_0 is the medial triangle of Δ with $S'_0 = \frac{1}{4} \cdot S$.

3. Circumscribed triangles with centroid P

The above investigation of cocentroidal *inscribed* triangles Δ' with centroid P naturally suggests an investigation of *circumscribed* triangles Δ^* with the same centroid.

Let P_a, P_b, P_c be the traces of P. The line P_bP_c cuts the sideline a at P'_a. Denote the reflection point of P'_a in P by P^*_a and the line AP^*_a by a^*_0. The lines b^*_0, c^*_0 can be constructed similarly. These lines form a triangle Δ^*_0 with vertices A^*_0, B^*_0, C^*_0 (see Figure 3).

From this construction it is easy to calculate the standardized barycentric coordinates of the vertices of Δ^*_0:

$$\begin{aligned} \Delta^*_0 &= (A^*_0B^*_0C^*_0) \\ &= \frac{1}{k}\begin{pmatrix} -(1+q_0)(1-r_0)u & (1-r_0)(1-p_0)u & (1+p_0)(1+q_0)u \\ (1+q_0)(1+r_0)v & -(1+r_0)(1-p_0)v & (1-p_0)(1-q_0)v \\ (1-q_0)(1-r_0)w & (1+r_0)(1+p_0)w & -(1+p_0)(1-q_0)w \end{pmatrix}. \end{aligned} \tag{10}$$

Proposition 3. *P is the centroid of Δ^*_0.*

Proof. The row sums of (10) are barycentric coordinates of P. □

[1] k is zero, positive, or negative according as P lies on, inside or outside the Steiner in-ellipse.

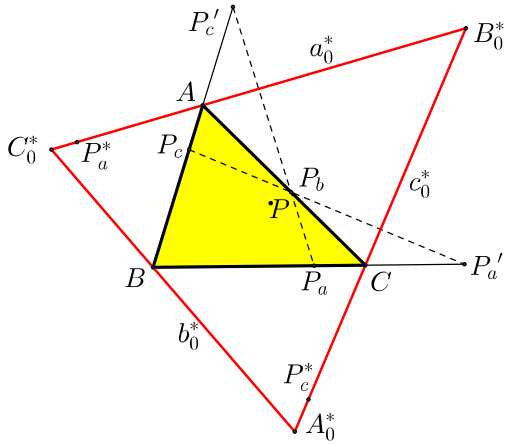

Figure 3.

In a similar fashion as in §2 (from (4) to (6)) we define from (10) for each $t \in \mathbb{R}$ the triangle

$$\begin{aligned}\Delta^*(t) = \ & (A^*B^*C^*) \\ = \ & \frac{1}{k+4t^2}\begin{pmatrix} -(1+q)(1-r)u & (1-r)(1-p)u & (1+p)(1+q)u \\ (1+q)(1+r)v & -(1+r)(1-p)v & (1-p)(1-q)v \\ (1-q)(1-r)w & (1+r)(1+p)w & -(1+p)(1-q)w \end{pmatrix}. \end{aligned} \tag{11}$$

It is not difficult to prove that $\Delta^*(t)$ is a circumscribed triangle with centroid P for all t. Thus the triangles $\Delta^*(t)$ constitute the family $\mathcal{D}^*$ of cocentroidal circumscribed triangles with centroid P.

3.1. *Construction of* Δ^*. Given a^* as an arbitrary line (sideline of $\Delta^*(t)$ for a certain t) through A, we are able to construct b^* and c^* :
Let T be the point on AP, so that P divides the line segment AT in the ratio $1:2$. Construct a_T^* the parallel to a^* through T, and a_B^*, a_C^* parallels to a^* through B, C respectively. The line TB cuts a_C^* at D_B, and TC cuts a_B^* at D_C. The intersection of D_BD_C with a is X. Then PX and a_T^* intersects at the required point A^*. The line A^*C cuts a^* at B^*, A^*B and a^* intersects at C^* (see Figure 4).

From (11) we determine the area S^* of Δ^*:

$$\begin{aligned} S^* &= \frac{S}{(k+4t^2)^3}uvw\left((1+p)(1+q)(1+r)+(1-p)(1-q)(1-r)\right)^2 \\ &= \frac{36\cdot uvw}{k+4t^2}S. \end{aligned} \tag{12}$$

From this follows for P inside the Steiner in-ellipse

Proposition 4. *Among the triangles $\Delta^*(t) \in \mathcal{D}^*$, the triangle $\Delta^*(0) = \Delta_0^*$ has maximum area.*

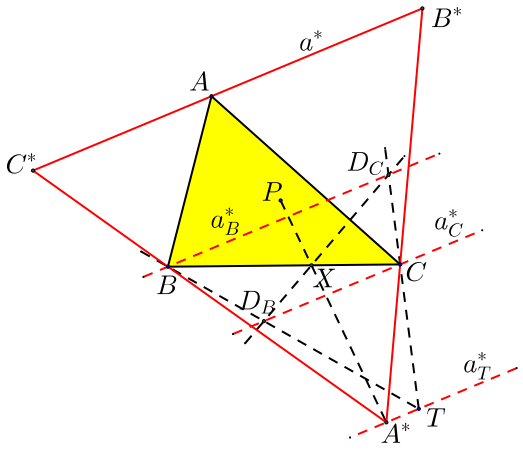

Figure 4.

Special case $P = G$: Δ_0^* is the antimedial (anticomlementary) triangle of Δ with $S_0^* = 4S$.

4. Cocentroidal pairs (Δ', Δ^*)

The structure of the coordinates of A_0^*, B_0^*, C_0^* shows that they are the barycentric products (symbol $*_b$) of P and the wedge (symbol $\wedge$) of two vertices of Δ_0', for instance

$$A_0^* = (B_0' \wedge C_0')^T *_b P,$$

similarly B_0^* and C_0' (see [1]). So it is clear that Δ_0^* is the *unary cofactor triangle* with respect to P of Δ_0'. We recall ([1], [2]) that the isoconjugate of a point $U = (l : m : n)$ with respect to pole $P = (u : v : w)$ is the point $U_P^\bullet = (\frac{u}{l} : \frac{v}{m} : \frac{w}{n})$. The unary cofactor triangle of triangle $T = T_1T_2T_3$ is the triangle $\mathbb{U}_P(T) =: X = X_1X_2X_3$ whose vertices X_i are the isoconjugates of the vertices of the line-polar triangle of the points $T_i = (\alpha_i : \beta_i : \gamma_i)$, that is

$$X_i = (T_{i+1} \wedge T_{i+2}) *_b P \tag{13}$$

(subscripts are taken modulo 3). In matrix notation,

$$\begin{aligned} \mathbb{U}_P(T) = \ & (X_1X_2X_3) \\ = \ & \begin{pmatrix} (\beta_2\gamma_3 - \beta_3\gamma_2)u & (\beta_3\gamma_1 - \beta_1\gamma_3)u & (\beta_1\gamma_2 - \beta_2\gamma_1)u \\ (\gamma_2\alpha_3 - \gamma_3\alpha_2)v & (\gamma_3\alpha_1 - \gamma_1\alpha_3)v & (\gamma_1\alpha_2 - \gamma_2\alpha_1)v \\ (\alpha_2\beta_3 - \alpha_3\beta_2)w & (\alpha_3\beta_1 - \alpha_1\beta_3)w & (\alpha_1\beta_2 - \alpha_2\beta_1)w \end{pmatrix}. \end{aligned} \tag{14}$$

This has the following simple properties.
(1) $\mathbb{U}_P(\mathbb{U}_P(T)) = T$.
(2) T is an inscribed triangle if and only if $\mathbb{U}_P(T)$ is a circumscribed triangle.
(3) If P is the centroid of T, then $\mathbb{U}_P(T)$ has the same centroid as T.

It is not difficult to see that the triangle (11) is the unary cofactor triangle with respect to P of triangle (6) with centroid P.

If we want to form "natural" pairs (Δ', Δ^*) of inscribed and circumscribed triangles with the same centroid P, then the obvious choice is $\Delta^* = \mathbb{U}_P(\Delta')$.

The elimination of t in (9) and (12) leads to:

Proposition 5. *The product $S'(t) \cdot S^*(t) = 27 \cdot uvw \cdot S^2$ is independent on t for all $t \in \mathbb{R}$.*

References

[1] P. L. Douillet, *Translation of the Kimberling's Glossary into Barycentrics*, www.douillet.info/~douillet/triangle/glossary/glossary.pdf.

[2] C. Kimberling, Triangle centers and central triangles, *Congressus Numerantium* 129 (1998) 1–295.

Gotthard Weise: Buchloer Str. 23, D-81475 München, Germany.
E-mail address: gotthard.weise@tele2.de

Forum Geometricorum
Volume 15 (2015) 191–201.

FORUM GEOM
ISSN 1534-1178

The Kariya Problem and Related Constructions

Paul Yiu

Abstract. Given a point Q other than the incenter I of a reference triangle, we give a simple conic construction of a homothety mapping I into Q so that the image of the intouch triangle is perspective with the reference triangle. This is a generalization of the Kariya theorem in the case $Q = I$ that the homothety can be arbitrary. The ratio of the homothety (the Kariya factor) is a unique nonzero finite number except when Q lies on the Feuerbach hyperbola or the line joining the incenter to the orthocenter of the reference triangle. For each nonzero real number t, we show that the locus of Q with Kariya factor t is a rectangular hyperbola. We give two simple constructions of this hyperbola.

1. The Kariya problem

This note presents several constructions related to the Kariya problem. Given a triangle $\mathbf{T} := ABC$ with incenter I, let the incircle be tangent to the sides BC, CA, AB at A_1, B_1, C_1 respectively. $A_1B_1C_1$ is the *intouch triangle* of ABC. For a real number t, let $I_a(t)$, $I_b(t)$, $I_c(t)$ be points on the lines IA_1, IB_1, IC_1 respectively, such that as vectors,

$$\mathbf{II_a}(\mathbf{t}) = t\mathbf{IA_1}, \qquad \mathbf{II_b}(\mathbf{t}) = t\mathbf{IB_1}, \qquad \mathbf{II_c}(\mathbf{t}) = t\mathbf{IC_1}.$$

Theorem (Kariya)**.** *For every real number t, the triangle $\mathbf{T}_I(t) := I_a(t)I_b(t)I_c(t)$ is perspective with $\mathbf{T}$ at a point on the Feuerbach hyperbola, the rectangular circum-hyperbola through I and H, the orthocenter of $\mathbf{T}$* (see Figure 1).

The Kariya problem studies the case when the incenter is replaced by an arbitrary point. We begin with a sign convention for distances along lines perpendicular to the sidelines of $\mathbf{T}$. For two points Y and Z on a line perpendicular to BC, the distance YZ is reckoned positive or negative according as the vector $\mathbf{YZ}$ is directly or oppositely parallel to $\mathbf{IA_1}$; similarly for points on lines perpendicular to CA and AB respectively. Given a point Q and a real number t, we denote by $Q_a(t)$, $Q_b(t)$, $Q_c(t)$ the unique points on the perpendiculars from Q to BC, CA, AB respectively with $QQ_a(t) = QQ_b(t) = QQ_c(t) = tr$, where r is the inradius of $\mathbf{T}$ (see Figure 2). In absolute barycentric coordinates,

$$Q_a(t) = Q+t(A_1-I), \qquad Q_b(t) = Q+t(B_1-I), \qquad Q_c(t) = Q+t(C_1-I).$$

Lemma 1. *Triangle $\mathbf{T}_Q(t)$ is homothetic to the intouch triangle $\mathbf{T}_I(1) = A_1B_1C_1$.*

Proof. Let T be the point dividing QI in the ratio $QT : TI = -t : 1$. It is clear that

$$TQ_a(t) : TA_1 = TQ_b(t) : TB_1 = TQ_c(t) : TC_1 = TQ : TI = t : 1.$$

Publication Date: October 7, 2015. Communicating Editor: Nikolaos Dergiades.

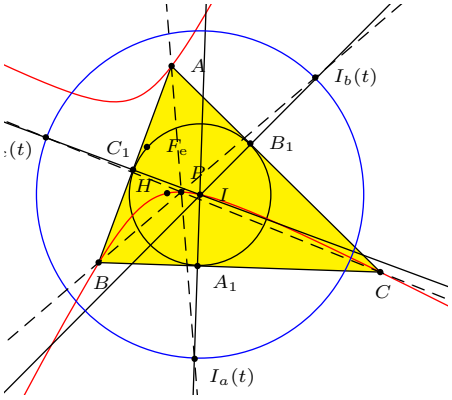

Figure 1

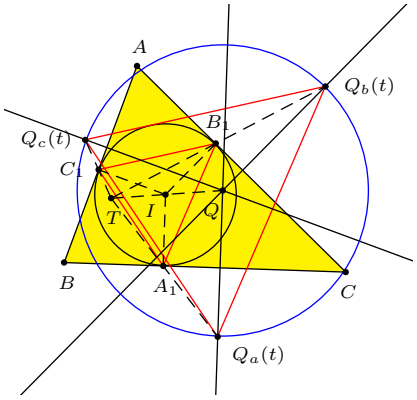

Figure 2

Triangle $\mathbf{T}_Q(t)$ is the image of the intouch triangle under the homothety $\mathsf{h}(T,t)$. □

For the orthocenter H, it is clear that for every real number t, $\mathbf{T}_H(t)$ is perspective with $\mathbf{T}$ at H. If $Q \neq H,\ I$, and $t \neq 0$, the triangle $\mathbf{T}_Q(t)$ is in general not perspective with $\mathbf{T}$. By the Kariya problem for Q, we mean the determination of t for which $\mathbf{T}_Q(t) := Q_a(t)Q_b(t)Q_c(t)$ and $\mathbf{T}$ are perspective, and the location of the corresponding perspector. Here are some simple examples. Trivially, one may take $t = 0$, in which case $\mathbf{T}_Q(0)$ degenerates into the point Q, and is perspective with $\mathbf{T}$ at Q. If we also allow $t = \infty$ and infinite points, then the perspector is the orthocenter H. If Q is the circumcenter O, the angle bisectors intersect the circumcircle at points lying on the perpendiculars from O to the sidelines. Thus, $\mathbf{T}_O\left(\frac{R}{r}\right)$ is perspective with $\mathbf{T}$ at the incenter I. On the other hand, it is well known that the excentral triangle has circumcenter at the reflection I' of I in O, and circumradius $2R$. This means that $\mathbf{T}_{I'}\left(\frac{2R}{r}\right)$ is perspective with $\mathbf{T}$, also at I.

2. Solution of the Kariya problem

For a given $Q \neq H,\ I$, if the triangles $\mathbf{T}_Q(t)$ and $\mathbf{T}$ are perspective, the location of the perspector is quite easy even without knowing the corresponding value of t (see Theorem 2 below). This is a simple application of Thébault's proof of Sondat's theorem on perspective orthologic triangles. We say that triangle XYZ is orthologic to triangle $X'Y'Z'$ if the perpendiculars from X, Y, Z to $Y'Z'$, $Z'X'$, $X'Y'$ respectively are concurrent (at a point which we call the orthology center from XYZ to $X'Y'Z'$). For nondegenerate triangles, XYZ is orthologic to $X'Y'Z'$ if and only if $X'Y'Z'$ is orthologic to XYZ. Therefore, there are two orthology centers.

Theorem (Sondat [5])**.** *If two nondegenerate orthologic triangles are also perspective, then the perspector and the orthology centers are collinear.*

In his proof of Sondat's theorem in [6], Thébault also found the following remarkable result which leads to an easy solution of the Kariya problem.

Theorem (Thébault [6])**.** *If ABC and $A'B'C'$ are perspective at P and orthologic at Q'*, i.e., the perpendiculars from A to $B'C'$, B to $C'A'$, and C to $A'B'$ intersect at Q', *then A, B, C, P, Q' lie on a rectangular hyperbola*.

For example, the Kiepert triangle $\mathcal{K}(\theta)$ is perspective with $\mathbf{T}$ at the Kiepert perspector $K(\theta)$. It is orthologic to $\mathbf{T}$ at the circumcenter O. By Thébault's theorem, the other orthology center Q' also lies on the Kiepert hyperbola. By Sondat's theorem, it is the second intersection with the line $OK(\theta)$. This is the Kiepert perspector $K\left(\frac{\pi}{2} - \theta\right)$.

Now for the Kariya problem for an arbitrary point Q, we naturally expect that the Feuerbach hyperbola plays a key role.

Theorem 2. *For $Q \neq H,\ I$, if $\mathbf{T}_Q(t)$ is perspective with $\mathbf{T}$, the perspector is the second intersection of the Feuerbach hyperbola of $\mathbf{T}$ with the line IQ.*

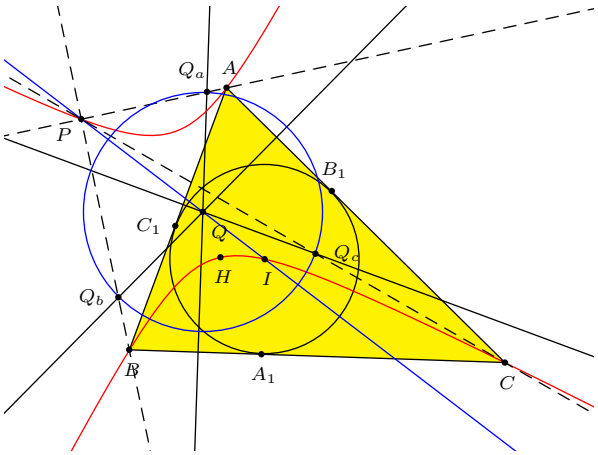

Figure 3.

Proof. Clearly, triangle $\mathbf{T}_Q(t)$ is orthologic to $\mathbf{T}$ at Q. Since $\mathbf{T}_Q(t)$ is homothetic to the intouch triangle (Lemma 1), the perpendiculars from A, B, C to the sidelines of $\mathbf{T}_Q(t)$ are concurrent at the incenter I (see Figure 2). By Sondat's theorem, if $\mathbf{T}_Q(t)$ is also perspective with $\mathbf{T}$, the perspector P must lie on the line IQ. Furthermore, by Thébault's theorem, A, B, C, P, I lie on a rectangular hyperbola. Now, the rectangular hyperbola through A, B, C, I must contain the orthocenter H, and is the Feuerbach hyperbola. It follows that P is the intersection (other than I) of the Feuerbach hyperbola and the line IQ (see Figure 3). □

If Q lies on the Feuerbach hyperbola, and if $\mathbf{T}_Q(t)$ is perspective with $\mathbf{T}$, the perspector must be Q, and the triangle degenerates to Q, corresponding to $t = 0$. On the other hand, if Q is a point on the line IH different from I and H, the second

intersection of IQ with the Feuerbach hyperbola is H. There is no finite value of t for which $\mathbf{T}_Q(t)$ is perspective with $\mathbf{T}$ at H.

Corollary 3. *For Q not on the Feuerbach hyperbola or the line IH, there is a unique nonzero $t = t(Q)$ for which $\mathbf{T}_Q(t)$ is perspective with $\mathbf{T}$.*

3. Kariya triangle $\mathbf{T}(Q)$ and the Kariya factor $t(Q)$

It follows from Corollary 3 that if Q is not on the Feuerbach hyperbola nor the line IH, then there is a unique triangle $\mathbf{T}(Q) = \mathbf{T}_Q(t(Q))$ perspective with $\mathbf{T}$ at a point $P(Q)$ on the Feuerbach hyperbola. We call $\mathbf{T}(Q)$ the Kariya triangle of Q, $t(Q)$ the Kariya factor of Q, and the circle, center Q, radius $t(Q)r$, the Kariya circle at Q.

The construction the $\mathbf{T}(Q)$ is now very easy; see Figure 3. First construct $P = P(Q)$ as the second intersection of the line IQ with the Feuerbach hyperbola. Then the intersections of AP, BP, CP with the perpendiculars from Q to the corresponding sidelines of $\mathbf{T}$ are the vertices Q_a, Q_b, Q_c of $\mathbf{T}(Q)$.

To determine the Kariya factor we work with homogeneous, and sometimes absolute, barycentric coordinates with reference to $\mathbf{T} = ABC$.

If Q has homogeneous coordinates $(u : v : w)$, the line IQ has equation

$$(cv - bw)x + (aw - cu)y + (bu - av)z = 0.$$

Apart from I, this line intersects the Feuerbach hyperbola

$$a(b-c)(b+c-a)yz + b(c-a)(c+a-b)zx + c(a-b)(a+b-c)xy = 0$$

at

$$P(Q) = \left(\frac{(b-c)(b+c-a)}{cv-bw} : \frac{(c-a)(c+a-b)}{aw-cu} : \frac{(a-b)(a+b-c)}{bu-cv} \right).$$

This is the perspector in Theorem 2 when $\mathbf{T}_Q(t)$ and $\mathbf{T}$ are perspective.

To find the corresponding $t(Q)$, we note that in absolute barycentric coordinates,

$$Q_a = \frac{(u,v,w)}{u+v+w} + t(Q)\left(\frac{(0, a+b-c, c+a-b)}{2a} - \frac{(a,b,c)}{a+b+c} \right).$$

This also lies on the line AP:

$$(a-b)(a+b-c)(aw-cu)y - (c-a)(c+a-b)(bu-av)z = 0.$$

Therefore,

$$\frac{\frac{v}{u+v+w} + t(Q)\left(\frac{a+b-c}{2a} - \frac{b}{a+b+c}\right)}{\frac{w}{u+v+w} + t(Q)\left(\frac{c+a-b}{2a} - \frac{c}{a+b+c}\right)} = \frac{(c-a)(c+a-b)(bu-av)}{(a-b)(a+b-c)(aw-cu)}.$$

From this,

$$t(Q) = \frac{2(a+b+c)\left(\sum_{\text{cyclic}} a(b-c)(b+c-a)vw\right)}{(u+v+w)\left(\sum_{\text{cyclic}}(b-c)(b+c-a)(b^2+c^2-a^2)u\right)}, \qquad (1)$$

provided that the denominator does not vanish.

Remarks. (1) The denominator $\sum_{\text{cyclic}}(b-c)(b+c-a)(b^2+c^2-a^2)u = 0$ if and only if Q lies on the line IH. In this case the perspector is H, and we shall put $t(Q) = \infty$.

(2) The numerator $\sum_{\text{cyclic}} a(b-c)(b+c-a)vw = 0$ if and only if Q lies on the Feuerbach hyperbola. In this case, we put $t(Q) = 0$.

4. Examples of Kariya factors

4.1. *The line IG.* The line IG intersects the Feuerbach hyperbola at the Nagel point N_{a}. The cevian AN_{a} contains the antipode of A_1' on the incircle. From this we conclude that for every point $Q \neq I$ on the line IN_{a}, $P(Q) = N_{\text{a}}$, and $t(Q) = -t$ if $N_{\text{a}}Q : QI = t : 1-t$. In particular, for the centroid G, $t(G) = -\frac{2}{3}$ (see Figure 4).

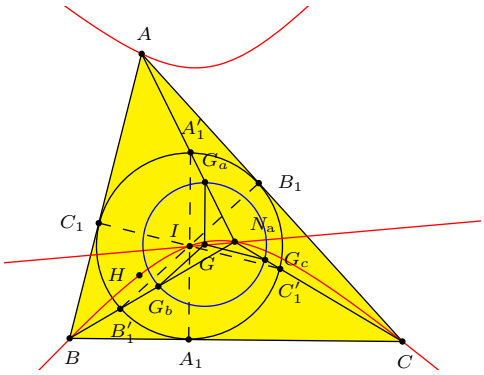

Figure 4

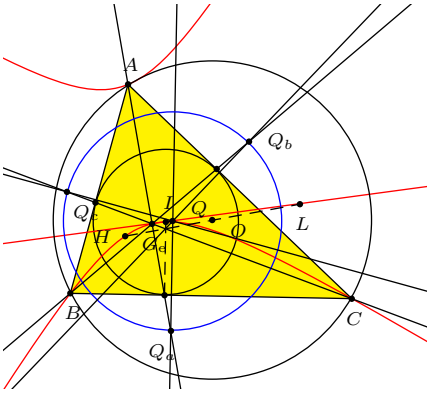

Figure 5

4.2. *The line joining I to the Gergonne point G_{e}.* Since the Gergonne point G_{e} lies on the Feuerbach hyperbola, for every point $Q \neq I$ on the line IG_{e}, $P(Q) = G_{\text{e}}$, and $t(Q) = t$ if $G_{\text{e}}Q : QI = t : 1-t$ (see Figure 5).

The line IG_{e} is called the Soddy line. It is well known that it contains the deLongchamps point L, the reflection of H in O ([7]), and $G_{\text{e}}L : LI = 4R+2r : -(4R+r)$. In this case, $t = \frac{4R+2r}{r}$. Therefore, the Gergonne cevians intersect the perpendiculars from L to the sidelines at points which are at equal distances $4R+2r$ from L. Note that $4R+2r$ is the sum of the radii of the incircle and the three excircles.

Remark. The coordinates of the points are quite simple:

$$\begin{aligned}
L_a &= (-a(a+b+c) : (b+c)(a+b-c) : (b+c)(c+a-b)),\\
L_b &= ((c+a)(a+b-c) : -b(a+b+c) : (c+a)(b+c-a)),\\
L_c &= ((a+b)(c+a-b) : (a+b)(b+c-a) : -c(a+b+c)).
\end{aligned}$$

The circle containing them has equation

$$a^2yz + b^2zx + c^2xy + (x+y+z)\left(\sum_{\text{cyclic}} (b+c)(2a+b+c)x\right) = 0.$$

4.3. *The line joining I to the Feuerbach center.* The Feuerbach center F_{e} is the point of tangency of the nine-point circle with the incircle. It is also the center of the Feuerbach hyperbola. The second intersection of the hyperbola with IF_{e} is the antipode of I, the triangle center

$$I^\dagger = \left(\frac{1}{a^2-b^2-c^2+bc} : \frac{1}{b^2-c^2-a^2+ca} : \frac{1}{c^2-a^2-b^2+ab}\right).$$

For $Q \neq I$ on the line IF_{e}, $P(Q) = I^\dagger$. [1]

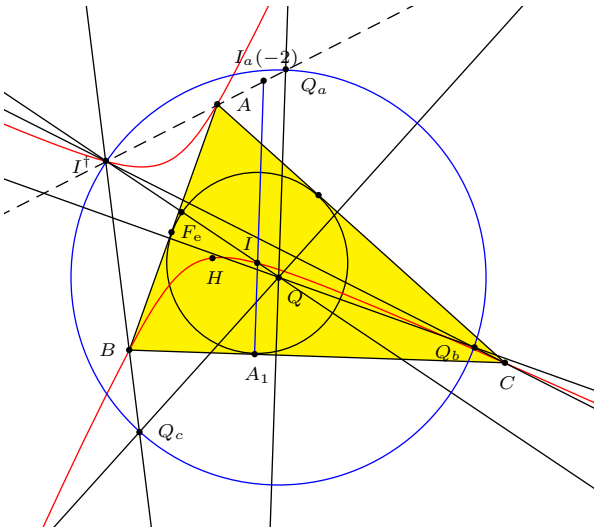

Figure 6.

Now, the lines $AI^\dagger$ and IA_1 intersect at

$$(3a^2 : c^2 - a^2 - b^2 + ab : b^2 - c^2 - a^2 + ca),$$

which divides IA_1 in the ratio $-2 : 3$. Therefore, this is the point $I_a(-2)$. Since $II^\dagger = 2r$, the circumcircle of $\mathbf{T}_I(-2)$ contains $I^\dagger$. More generally, for every point Q on the line IF_{e}, $t(Q) = -\frac{|QI^\dagger|}{r}$, and the circumcircle of $\mathbf{T}(Q)$ contains $I^\dagger$. In particular,

$$t(F_{\text{e}}) = -1, \qquad t(N) = -\frac{R+2r}{2r}$$

for the nine-point center N.

[1] $I^\dagger$ is the triangle center $X(80)$ in [3]; henceforth referred to as ETC. The notation adopted here indicates that it is the reflection conjugate of I. In the notations of §1, $I_a(2)$, $I_b(2)$, $I_c(2)$ are the reflections of I in the sidelines of $\mathbf{T}$. The circles $I_a(2)BC$, $I_b(2)CA$, and $I_c(2)AB$ are concurrent at $I^\dagger$.

4.4. *Two examples with* $t(Q) = -\frac{R}{r}$. We make some deduction from the fact that $\mathbf{HN}_{\mathrm{a}} = 2\mathbf{IO}$ ([2, Theorem 362]; see Figure 7).

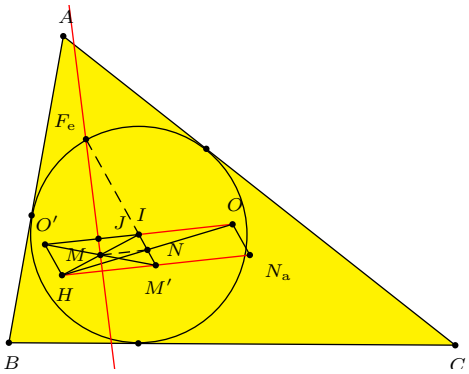

Figure 7.

(1) Consider the reflection O' of O in I. [2] Clearly, $P(O') = I$. Since $t(O) = \frac{R}{r}$, we have $t(O') = -\frac{R}{r}$. The Kariya circle at O' is congruent to the circumcircle of $\mathbf{T}$.
(2) Since N is the midpoint of OH, the midpoint of HN_{a} lies on the line IN. This midpoint is M'. [3] Note that this is the reflection of I in N, and $M'I^\dagger = 2NI^\dagger - II^\dagger = 2(\frac{R}{2} + r) - 2r = R$. Therefore, $P(M') = I^\dagger$, and $t(M') = -\frac{R}{r}$. The Kariya circle at M' is also congruent to the circumcircle of $\mathbf{T}$.

5. The hyperbola $\mathscr{H}(t)$ and its construction

For a given t, the locus of Q for which $t(Q) = t$ is the conic

$$\mathscr{H}(t): \qquad 2(a+b+c)\left(\sum_{\text{cyclic}} a(b-c)(b+c-a)yz\right) - t(x+y+z)\left(\sum_{\text{cyclic}} (b-c)(b+c-a)(b^2+c^2-a^2)x\right) = 0.$$

This is clear from (1). Note that this defines a pencil of conics $\mathscr{H}(t)$ homothetic to the Feuerbach hyperbola. Since the line

$$\sum_{\text{cyclic}} (b-c)(b+c-a)(b^2+c^2-a^2)x = 0$$

contains the incenter I and the orthocenter H, these are the common points of the rectangular hyperbolas $\mathscr{H}(t)$.

[2] O' is the triangle center $X(1482)$ in ETC.
[3] M' is the triangle center $X(355)$ in ETC.

5.1. *The line of centers.* The centers of these hyperbolas lie on a line, which clearly contains the Feuerbach center $F_{\rm e}$. To identify this line, it is enough to note that in §4.4, we have obtained $t(M') = t(O') = -\frac{R}{r}$. The four points I, M', H, O' are all on the hyperbola $\mathscr{H}\left(-\frac{R}{r}\right)$. Since they are also vertices of a parallelogram, the common midpoint of their diagonals is the center of the hyperbola. Therefore, the line of centers of $\mathscr{H}(t)$ is the line joining the Feuerbach center $F_{\rm e}$ to the midpoint M of IH; [4] see Figure 7.

Note that NM is parallel to OI. If OI intersects the line of centers $F_{\rm e}M$ at a point J, then $\frac{F_{\rm e}J}{F_{\rm e}M} = \frac{F_{\rm e}I}{F_{\rm e}N} = \frac{2r}{R}$. Since M is the center of $\mathscr{H}\left(-\frac{R}{r}\right)$, we conclude that J is the center of $\mathscr{H}(-2)$. [5]

Theorem 4. *Let J be the intersection of OI and the line joining the Feuerbach center to the midpoint M of IH. The center of the hyperbola $\mathscr{H}(t)$ is the point dividing $F_{\rm e}J$ in the ratio $-t : t+2$.*

This leads to a simple construction of the center of $\mathscr{H}(t)$. Let $F'_{\rm e}$ be the antipode of the Feuerbach center on the incircle. Then $F'_{\rm e}F_{\rm e} = 2r$. If K'_t is a point on the line $F_{\rm e}F'_{\rm e}$ such that $F_{\rm e}K'_t = tr$, the common radius of the Kariya circles, construct a parallel through K'_t to $F'_{\rm e}J$ to intersect the line of center at K_t. This intersection is the center of $\mathscr{H}(t)$.

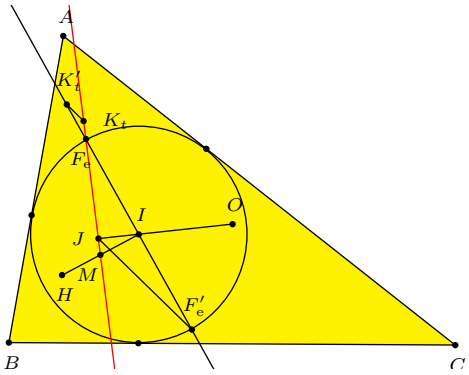

Figure 8.

5.2. *Construction of $\mathscr{H}(t)$.* Knowing the center of $\mathscr{H}(t)$, it is easy to construct the conic by choosing five distinct points on it. Two of them being I and H, their antipodes (reflections in K_t) contribute two more, provided $K_t \neq M$, the midpoint of IH. Since the hyperbola is rectangular, it also contains the orthocenter of the triangle formed by three of these points.

If $K_t = M$, the hyperbola is $\mathscr{H}\left(-\frac{R}{r}\right)$ containing I, M', H, O' (see Figure 7), and the orthocenter of any triangle formed by three of these points.

---

[4] M is the triangle center $X(946)$ in ETC.

[5] J is the triangle center $X(65)$ in ETC.

6. A simpler construction of $\mathscr{H}(t)$

Let A', B', C' as the second intersections of the Feuerbach hyperbola with the lines IA_1, IB_1, IC_1 respectively. Consider the point $A'_a(-t)$. We show that in Proposition 5 below that this lies on the hyperbola $\mathscr{H}(t)$. The same reasoning shows that $B'_b(-t)$ and $C'_c(-t)$ are also on the same hyperbola. This leads to a simpler construction of the hyperbola $\mathscr{H}(t)$ as the conic containing the five points I, H, $A'_a(-t)$, $B'_b(-t)$, $C'_c(-t)$ (see Figure 9).

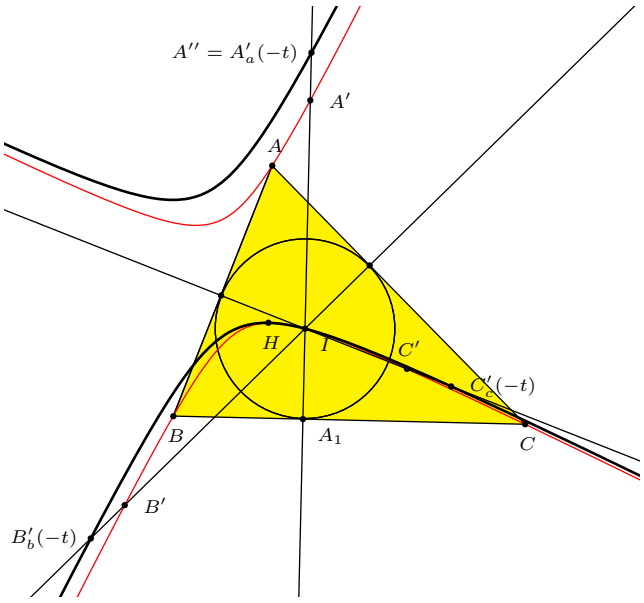

Figure 9.

Proposition 5. *The point $A'_a(-t)$ lies on the rectangular hyperbola $\mathscr{H}(t)$.*

Proof. The line IA_1 intersects the Feuerbach hyperbola at $A' := (a : c-a : b-a)$. For brevity, we denote $A'_a(-t)$ by A''. Clearly, $A''_a(t) = A'$. In absolute barycentric coordinates,

$$A'' = \frac{(a, c-a, b-a)}{b+c-a} - t\left(\frac{(0, a+b-c, c+a-b)}{2a} - \frac{(a,b,c)}{a+b+c}\right).$$

With this, we compute the coordinates of $A''_b(t)$.

$$\begin{aligned} A''_b(t) = {} & A'' + t\left(\frac{(a+b-c, 0, b+c-a)}{2b} - \frac{(a,b,c)}{a+b+c}\right) \\ = {} & \frac{(a, c-a, b-a)}{b+c-a} + t\left(\frac{(a+b-c, 0, b+c-a)}{2b} - \frac{(0, a+b-c, c+a-b)}{2a}\right). \end{aligned}$$

In homogeneous coordinates, this is

$$\begin{aligned} A_b''(t) = \ & (a(2ab + t(a+b-c)(b+c-a)) \\ & : b(2a(c-a) - t(a+b-c)(b+c-a)) \\ & : -(a-b)(2ab + t(a+b-c)(b+c-a))). \end{aligned}$$

From these homogeneous coordinates, it is easy to see that both A' and $A_b''(t)$ lie on the line $(a-b)x+az = 0$, which clearly passes through the vertex B. Similarly, $A_c''(t) = A'' + t\left(\frac{(c+a-b,b+c-a,0)}{2c} - \frac{(a,b,c)}{a+b+c}\right)$ is such that the line $A'A_c''(t)$ passes through the vertex C. It follows that $\mathbf{T}_{A''}(t)$ and ABC are perspective at A'. Since $A''A' = tr$, A'' lies on the hyperbola $\mathscr{H}(t)$. □

We conclude this paper with a remark on the triangle $A_a'(-t)B_b'(-t)C_c'(-t)$ (which is not a Kariya triangle). It is clearly orthologic to $\mathbf{T}$, with orthology center I. The other orthology center is the point

$$\left(\frac{a(b+c-a)}{2a+t(b+c-a)} : \frac{b(c+a-b)}{2b+t(c+a-b)} : \frac{c(a+b-c)}{2c+t(a+b-c)}\right)$$

on the Feuerbach hyperbola. This is the isogonal conjugate of the point dividing OI in the ratio $2R + rt : -2r$. On the other hand, this triangle is perspective with $\mathbf{T}$ only if $t = -\frac{2R}{r}$. In this case, the triangle is oppositely congruent to $\mathbf{T}$ at the midpoint M of IH. The orthology centers are I and H. The conic (rectangular hyperbola) through H, I, and its three vertices is the hyperbola $\mathscr{H}\left(-\frac{2R}{r}\right)$. For each point Q on this hyperbola, the Kariya circle has radius $-2R$. The perspector of the Kariya triangle Q is the intersection if the line IQ with the Feuerbach hyperbola, as we have established in Theorem 2.

Appendix A. Verification of Sondat-Thébault's theorem

If triangles ABC and XYZ are perspective at $P = (x : y : z)$ and the perpendiculars from X, Y, Z to the sidelines BC, CA, AB are concurrent at $Q = (u : v : w)$, the vertices X, Y, Z have homogeneous barycentric coordinates

$$\begin{aligned} X = \ & ((S_Bu + a^2w)y - (S_Cu + a^2v)z : \ (S_Bv - S_Cw)y : \ (S_Bv - S_Cw)z), \\ Y = \ & ((S_Cw - S_Au)x : \ (S_Cv + b^2u)z - (S_Av + b^2w)x : \ (S_Cw - S_Au)z), \\ Z = \ & ((S_Au - S_Bv)x : \ (S_Au - S_Bv)y : \ (S_Aw - c^2v)x - (S_Bu - c^2w)y). \end{aligned}$$

The perpendiculars from A to YZ, B to ZX, and C to XY are concurrent at the point

$$Q' = \left(\frac{S_By - S_Cz}{wy - vz} : \frac{S_Cz - S_Ax}{uz - wx} : \frac{S_Ax - S_By}{vx - uy}\right).$$

From these we deduce

(a) Sondat's theorem: P, Q, Q' are collinear; the line containing them is

$$(wy - vz)\mathbb{X} + (uz - wx)\mathbb{Y} + (vx - uy)\mathbb{Z} = 0;$$

(b) Thébault's theorem: the points P and Q' are on the circumconic

$$\frac{x(S_B y - S_C z)}{\mathbb{X}} + \frac{y(S_C z - S_A x)}{\mathbb{Y}} + \frac{z(S_A x - S_B y)}{\mathbb{Z}} = 0,$$

which is a rectangular hyperbola since it contains the orthocenter $\left(\frac{1}{S_A} : \frac{1}{S_B} : \frac{1}{S_C}\right)$.

References

[1] F. G.-M., *Exercices de Géométrie*, 6-th edition, 1920; Gabay reprint, 1991.

[2] R. A. Johnson, *Advanced Euclidean Geometry*, 1929; Dover reprint, 2007.

[3] C. Kimberling, *Encyclopedia of Triangle Centers*, available at http://faculty.evansville.edu/ck6/encyclopedia/ETC.html.

[4] S. N. Kiss and P. Yiu, The touchpoints triangles and the Feuerbach hyperbolas, *Forum Geom.*, 14 (2014) 63–86.

[5] P. Sondat and Sollerstinsky, Question 38, *L'intermédiaire des mathématiciens*, (1894) 10; solution, *ibid*, 94.

[6] V. Thébault, Perspective and orthologic triangles and tetrahedrons, *Amer. Math. Monthly*, 59 (1952) 24–28.

[7] A. Vandegehn, Soddy's circles and the de Longchamps point of a triangle, *Amer. Math. Monthly*, 71 (1964) 167–170.

Paul Yiu: Department of Mathematical Sciences, Florida Atlantic University, 777 Glades Road, Boca Raton, Florida 33431-0991, USA

E-mail address: yiu@fau.edu

Forum Geometricorum
Volume 15 (2015) 203–209.

FORUM GEOM
ISSN 1534-1178

Construction of Ajima Circles via Centers of Similitude

Nikolaos Dergiades

Abstract. We use the notion of the centers of similitude of two circles to give a simple construction of the Ajima circles tangent to two sides of a triangle and a circular arc through two vertices.

1. Ajima's theorem

Theorem 1 below is the solution of a famous Japanese temple geometry problem; it is sometimes referred to as a "hard but important Sangaku problem" (see, for example, [2]). It was mentioned in Fukagawa - Pedoe's *Japanse Temple Geometry* [4, Problem 2.2.8, pp. 28, 103]. A proof was given in Fukagawa - Rigby [5, pp. 17–18, 96–97], where the result is attributed to Naonobu Ajima (1732–1798).

Theorem 1 (Ajima)**.** *Given a triangle ABC and a circle $O'(R')$ passing through B and C and containing A in its interior, there is a circle $K_1(r_1)$ tangent to AB and AC, and the circle $O'(R')$ internally. If M and N are the midpoints of BC and the arc of the circle $O'(R')$ on the opposite side of A, then*

$$r_1 = r + \frac{2d(s-b)(s-c)}{as} = r\left(1 + \tan\frac{A}{2}\tan\frac{\varphi}{2}\right),$$

where a, b, c are the sidelengths of triangle ABC, and r, s its inradius and semiperimeter, $d = MN$, and $\frac{\varphi}{2} = \angle BCN$ (see Figure 1)*.*

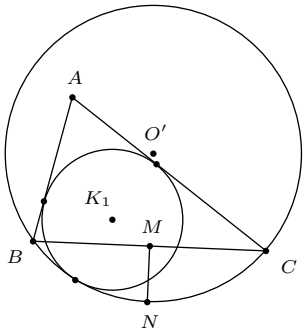

Figure 1

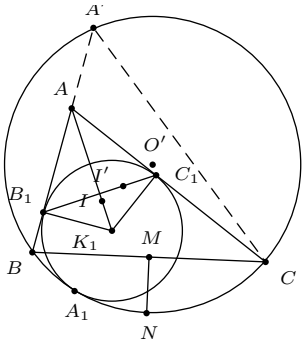

Figure 2

Publication Date: October 8, 2015. Communicating Editor: Paul Yiu.

Construction of the circle $K(r_1)$. Let the line BA meet the circle $O'(R')$ again at A', and I, I' be the incenters of triangles ABC and $A'BC$ respectively. By Sawayama's lemma [2], the perpendicular from I' to AI meets AB, AC at the contact points B_1, C_1 of the required circle with AB, AC, and the perpendicular from B_1 to AB meets the line AI at K, which is the center of the required circle. From this, the circle can be easily constructed (see Figure 2).

The circle (K_1) is inside the curvilinear triangle ABC. We can draw similarly a circle outside of the curvilinear triangle ABC a circle tangent externally to the arc (BC) of the circle and prove similarly the following, where r_a is the radius of the A-excircle of triangle ABC.

Theorem 2. *The circle that is tangent externally to the curvilinear triangle* ABC *has radius*

$$r_2 = r_a \left(1 + \tan\frac{A}{2}\tan\frac{\varphi}{2}\right).$$

The construction of this circle and the proof of Theorem 2 are similar to those in Theorem 1, except that the incenter I of triangle ABC is replaced by the excenter I_a (see Figure 4)

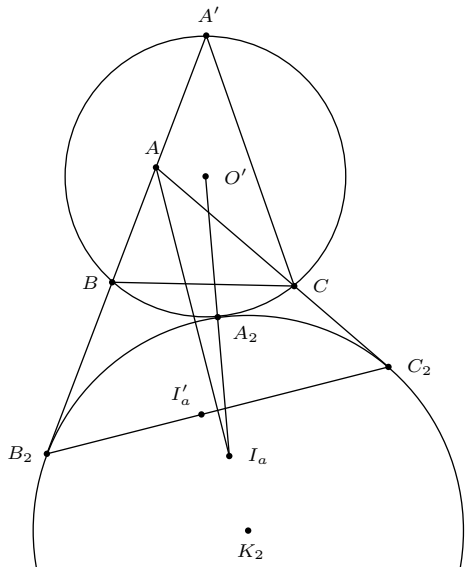

Figure 3

We call the circles (K_1) and (K_2) the internal and external Ajima circles, and the points of tangency A_1, A_2 the Ajima points for the curvilinear triangle ABC bounded by the circle (O').

We worked in Theorems 1 and 2 with angle φ positive, i.e., the mid point N of the arc (BC) and the vertex A are on opposite sides BC. If φ is negative, then we have similar results and constructions as shown in Figures 2(b) and 3(b). In Theorem 1 the internal tangency became external, and vice versa in Theorem 2.

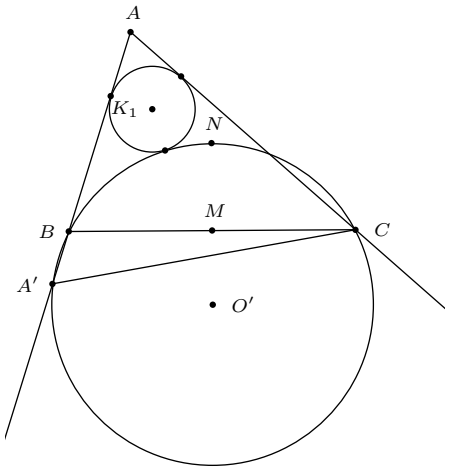

Figure 2(b)

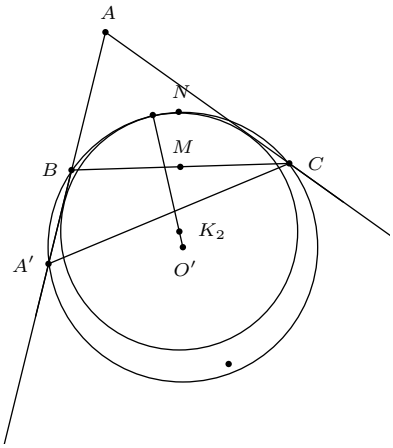

Figure 3(b)

2. Construction via centers of similitude

We present an alternative approach by making use of the notion of center of similitude of two circles. Two nonconcentric circles of unequal radii have two centers of similitude, one internal and the other external. We call these of type $+1$ and -1 respectively. We shall make use of the following d'Alembert theorem.

Theorem 3 (d'Alembert)**.** *Let (O_1), (O_2), (O_3) be three unequal circles with non-collinear centers. For $i = 1, 2, 3$, consider a center of similitude of (O_j) and (O_k), $j, k \neq i$, of type ε_i. The three centers of similitude are collinear if and only if $\varepsilon_1\varepsilon_2\varepsilon_3 = -1$.*

The proof is a simple application of Menelaus' theorem; see, for example, [3, §1260].

Let ABC be a triangle with incircle $I(r)$, and $O'(R')$ an arbitrary circle. Denote by S_ε the internal or external center of similitude of the two circles according as $\varepsilon = +1$ or -1., i.e.,

$$O'S_\varepsilon : \ S_\varepsilon I = R' : \varepsilon r.$$

For the curvilinear triangle ABC bounded by ABC with a circle (O') and the sides AB, AC of triangle ABC, we label an Ajima circle $(K_{\varepsilon a})$ and A_ε the point of tangency with the arc BC, for $\varepsilon = +1$ or -1 according as the tangency with (O') is external or internal. Note that A_ε is the ε center of similitude of the two circles.

The following proposition gives an easy construction of the circle by first locating the point of tangency A_ε.

Theorem 4. *For $\varepsilon = \pm 1$,*
(a) *A_ε is the intersection of the arc BC of (O') with the line AS_ε,*
(b) *$K_{\varepsilon a}$ is the intersection of the $O'A_\varepsilon$ with the bisector of angle A.*
(see Figure 4).

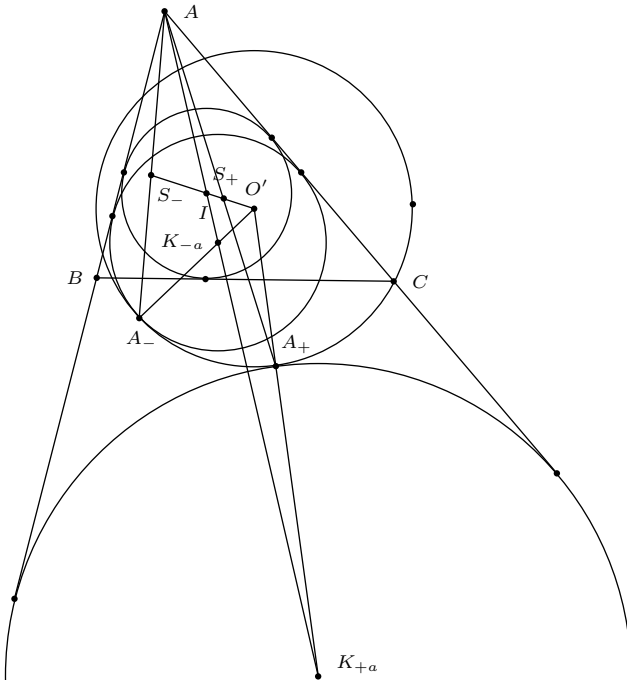

Figure 4.

Proof. We need only prove (a). Consider the three circles (I), (O') and $(K_{\varepsilon a})$. The vertex A is the external center of similitude of (I) and $(K_{\varepsilon a})$. $A_{\varepsilon a}$ is the ε center of similitude of (O') and $(K_{\varepsilon a}$. By d'Alembert theorem, the ε-center of similitude of (O') and (I) is collinear with A and A_ε. Therefore, A_ε lies on the line AS_ε.
(b) follows from (a) immediately. □

Now consider the intersections of the circle $O'(R')$ with the sidelines of triangle ABC. Let it intersect the halflines AC, AB at B_a, C_a, the halflines BA, BC at C_b, A_b, and the halflines CB, CA at A_c, B_c respectively (see Figure 5).

Corollary 5. *For $\varepsilon = \pm 1$, let A_ε be the point of tangency of the Ajima circle of the curvilinear triangle AB_aC_a in angle A, external or internal according as $\varepsilon = +1$ or -1; similarly define B_ε and C_ε. The triangles ABC and $A_\varepsilon B_\varepsilon C_\varepsilon$ are perspective at the center of similitude S_ε of (O') and the incircle of triangle ABC.*

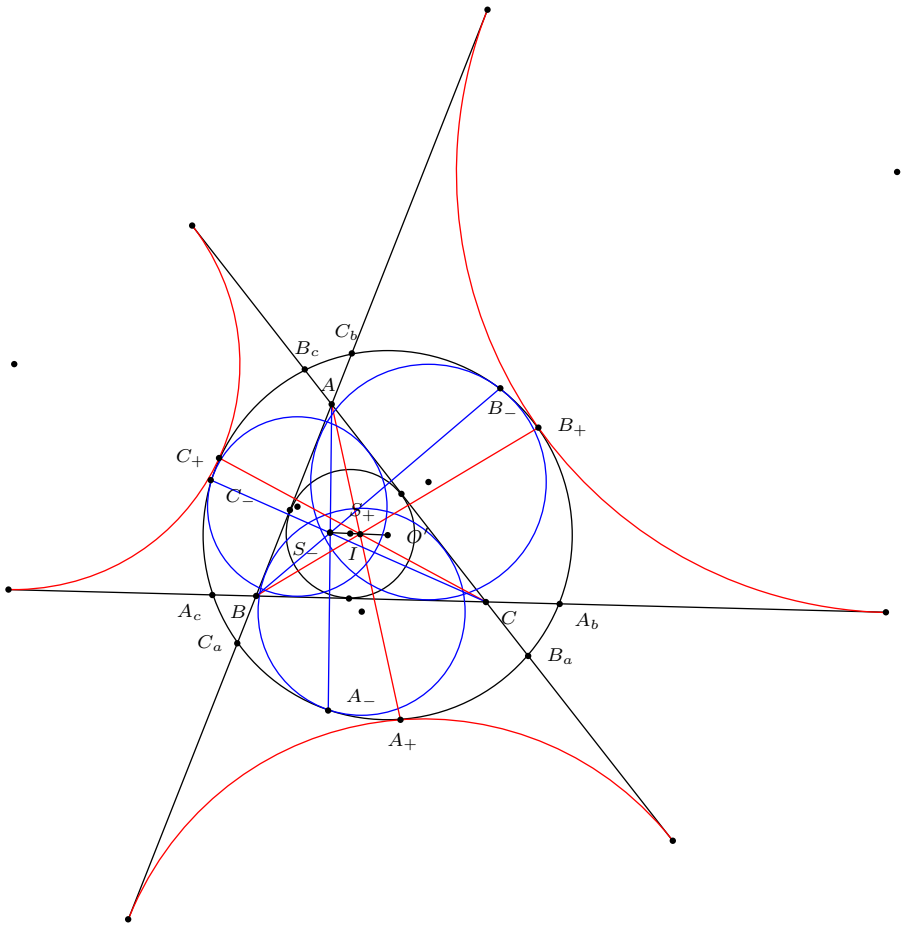

Figure 5.

3. Examples

3.1. *The circumcircle.* In this case the Ajima circles are the curvilinear excircles and curvilinear incircles. $S_+ = X(55)$ and $S_- = X(56)$ in ETC [7], the centers of similitude of the circumcircle and the incircle.

3.2. *The circumcircle of the anticomplementary triangle.* This has center H, the orthocenter, and radius $2R$. In this case, $S_+ = X(388)$ and $S_- = X(497)$.

3.3. *The Bevan circle.* This is the circumcircle of the excentral triangle, with center $X(40)$ and radius $2R$. In this case, $S_+ = X(1697)$ and $S_- = X(57)$.

3.4. *The nine-point circle.* The incircle is tangent internally (see Figure 6) to the nine-point circle with radius $\frac{R}{2}$ at the Feuerbach point $X(11)$, which is the external

center of similitude of incircle and nine-point circle. The internal center of similitude S_+ is the outer Feuerbach point $X(12)$. Also, the excircles are externally tangent to the nine-point circle at the points F_a, F_b, F_c respectively. Hence the incircle and the excircles are the Ajima circles for the nine-point circle. Hence the triangles ABC and $F_aF_bF_c$ are perspective at S_+. The lines AF_a, BF_b, CF_c meet the nine-point circle again at the points A_+, B_+, C_+ that are also Ajima points and for three other external Ajima circles for the nine-point circle. The lines $AF_{\rm e}$, $BF_{\rm e}$, $CF_{\rm e}$ meet again the nine-point circle at the points A_-, B_-, C_- that are also Ajima points for three internal Ajima circles for the nine-point circle.

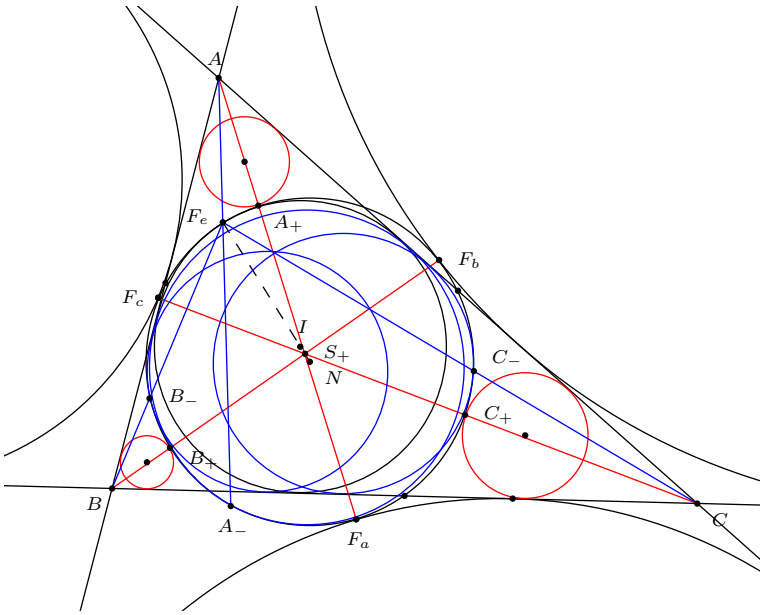

Figure 6.

3.5. *The Apollonius circle.* The Apollonius circle is tangent to the three excircles internally. It is the inversive image of the nine-point circle in the Spieker radical circle. Its center lies on the line joining the nine-point center to the Spieker center. Since the Apollonius circle is also a Tucker circle, its center is also on the Brocard axis. This is $X(970)$ (see [**?**, p.179]). The excircles are the internal Ajima circles. Therefore, $S_- = X(181)$. The other center of similitude S_+ is the harmonic conjugate of S_- with respect to I and $X(970)$. This is $X(1682)$. From this, the external Ajima circles can be constructed.

References

[1] J. L. Aymes, Sawayama and Thebault's theorem, *Forum Geom.*, 3 (2003) 225–229.
[2] A. Bogomolny, A hard but important Sangaku problem, `http://www.cut-the-knot.org/triangle/HardSangaku.shtml`.
[3] F. G.-M., *Exercices de Géométrie*, 6th ed., 1920; Gabay reprint, Paris, 1991.

[4] H. Fukagawa and D. Pedoe, *Japanese Temple Geometry Problems*, Charles Babbage Research Centre, Winnipeg, 1989.
[5] H. Fukagawa and J. F. Rigby, *Traditional Japanese Mathematics Problems of the 18th and 19th Centuries*, SCT Press, Singapore, 2002.
[6] D. Grinberg and P. Yiu, The Apollonius circle as a Tucker circle, *Forum Geom.*, 2 (2002) 175–182.
[7] C. Kimberling, *Encyclopedia of Triangle Centers*, available at `http://faculty.evansville.edu/ck6/encyclopedia/ETC.html`.

Nikolaos Dergiades: I. Zanna 27, Thessaloniki 54643, Greece
E-mail address: `ndergiades@yahoo.gr`

Forum Geometricorum
Volume 15 (2015) 211–228.

FORUM GEOM
ISSN 1534-1178

Circle Incidence Theorems

J. Chris Fisher, Eberhard M. Schröder, and Jan Stevens

Abstract. Larry Hoehn discovered a remarkable concurrence theorem about pentagrams. Draw circles through two consecutive vertices and the intersection points of the sides in between. Then the radical axes of each pair of consecutive circles are concurrent or parallel. In this note we prove a generalization to n-gons.

1. Introduction

Given a triangle, there are unexpected triples of lines that pass through one point; e.g, the three medians, altitudes, and angle bisectors are all concurrent. Larry Hoehn discovered a remarkable concurrence theorem about pentagons, illustrated in Figure 1, see [2]. In this note we prove a generalization to n-gons.

Let $A_1, \ldots, A_n$ be n points in the plane, no three on a line, and such that the lines $l_{i+1} = \langle A_i, A_{i+2}\rangle$ and $l_i = \langle A_{i-1}, A_{i+1}\rangle$ are not parallel, where we consider the indices modulo n. Let $B_{i,i+1}$ be the intersection point of l_i and l_{i+1}. Through the three points A_i, $B_{i,i+1}$ and A_{i+1} passes a unique circle $c_{i,i+1}$. Let g_i be the radical axis of the two consecutive circles $c_{i-1,i}$ and $c_{i,i+1}$.

Theorem 1 ([2])**.** *Given five points $A_1, \ldots, A_5$ in the plane the five radical axes $g_1, \ldots, g_5$, constructed as above are concurrent or parallel* (see Figure 1)*.*

We use the terminology that lines *lie in a pencil* if they are concurrent or parallel. For $n \geq 6$ the radical axes in general do not lie in a pencil. For $n = 6$ we show that it is necessary and sufficient that the six points $B_{i,i+1}$ lie on a conic. This is equivalent to the condition that the three lines $\langle A_i, A_{i+3}\rangle$ lie in a pencil. In fact, the initial six points have to be in a special position for just three consecutive axes to lie in a pencil: Fisher, Hoehn and Schröder showed that this condition implies that than the remaining three axes lie in the same pencil [3]. Our main result generalizes this to $n > 6$.

Theorem 2. *Let $A_1, \ldots, A_n$ be n points in the plane, no three on a line, and such that the lines $l_{i-1} = \langle A_{i-1}, A_{i+1}\rangle$ and $l_{i+1} = \langle A_i, A_{i+2}\rangle$ intersect in a point $B_{i,i+1}$ (indices considered modulo n). Let $c_{i,i+1}$ be the circle through A_i, $B_{i,i+1}$ and A_{i+1}, and let g_i be the radical axis of the circles $c_{i-1,i}$ and $c_{i,i+1}$.*

If the lines $g_1, g_2, \ldots, g_{n-3}$ lie in a pencil, then the remaining three radical axes g_{n-2}, g_{n-1} and g_n lie in the same pencil.

We prove the theorem under weaker assumptions and in a more general setting. As shown in [3], the theorem is a result in affine geometry: a radical axis g_i can be constructed by drawing parallel lines.

Publication Date: October 23, 2015. Communicating Editor: Paul Yiu.

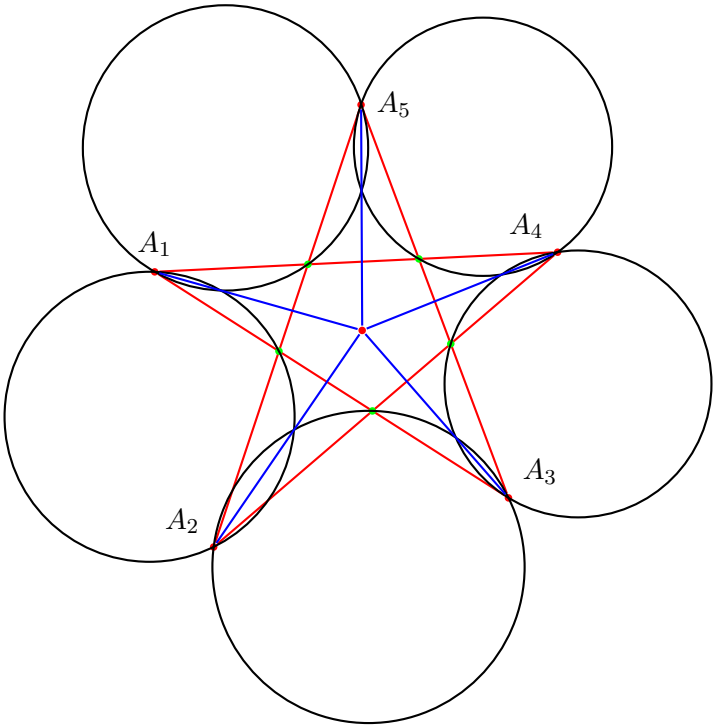

Figure 1. The 5-circle theorem

We can relax the condition that no three points lie on a line. In fact, the theorem continues to hold in certain limiting cases, if the elements of the construction are suitably reinterpreted. We make one case for $n = 5$ explicit for later use.

2. Preliminaries

We work in the affine plane $\mathbb{A}^2(k)$ over an arbitrary field k, which we view as embedded in $\mathbb{P}^2(k)$. All lines considered are projective lines. Two lines (different from the line at infinity) are parallel if their intersection point is a point at infinity. A general reference for this section is the book [1].

Definition. Let (P, Q) and (R, S) be two pairs of finite points on a line l; it is allowed that $P = Q$ or $R = S$, but neither R nor S may coincide with P or Q. Let $A \notin l$ be a finite point. Denote by l_P be the line through P that is parallel to the line $\langle A, R\rangle$ and take $l_S \parallel \langle A, Q\rangle$ through S. Set $B = l_P \cap l_S$. The line $g = \langle A, B\rangle$ is the *axis* of the configuration, see Figures 2 and 3.

The difference $P - Q$ of two points in the affine plane is a well defined vector in the associated vector space. For points P, Q, R, S on a line with $R \neq S$, the vector $P - Q$ is a scalar multiple of the vector $R - S$, so the ratio $\frac{P-Q}{R-S}$ is an element of the ground field k. We use the convention that $\frac{P-Q}{P-R} = 1$ if P lies at infinity and Q and R are distinct finite points.

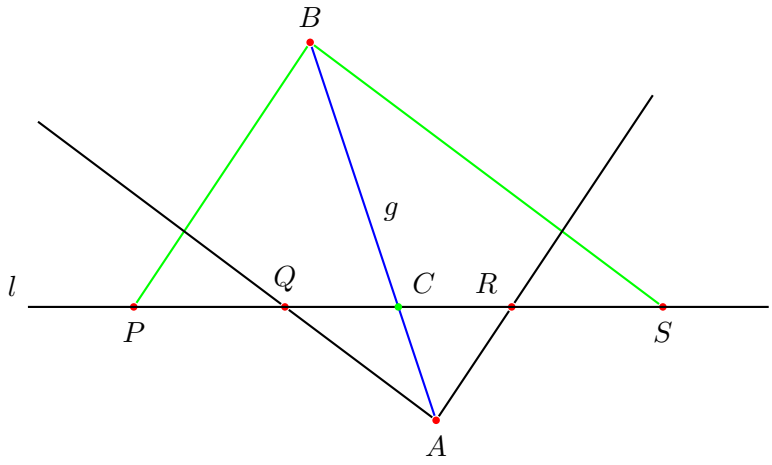

Figure 2. Construction of the axis

Lemma 3. *The intersection point $C = g \cap l$ is determined by the equivalent conditions*

$$\frac{C-Q}{C-R} = \frac{Q-S}{R-P},$$

which in case $P \neq Q$ is equivalent to

$$\frac{C-Q}{C-P} = \frac{R-Q}{R-P}\frac{S-Q}{S-P}$$

and to

$$\frac{C-S}{C-R} = \frac{Q-S}{Q-R}\frac{P-S}{P-R}$$

in case $R \neq S$.

Notation. We denote the point so determined by $C = [P, Q \mid R, S]$.

The lemma can be proved by direct computation. It also follows (if the four points P, Q, R and S are all distinct) from [3, Lemma 1] and its corollary, which

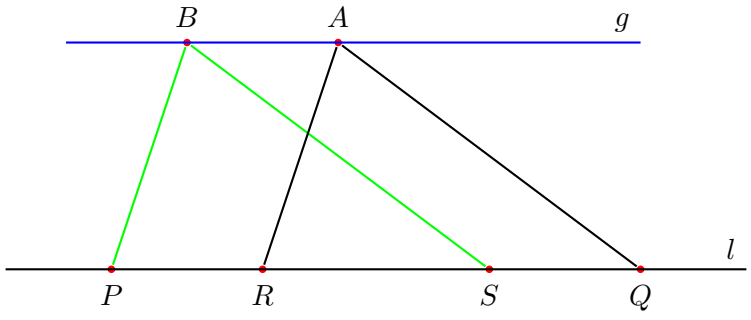

Figure 3. Axis parallel to the line

moreover establish that the above affine definition of the axis gives the radical axis of circles as in Figure 4, in the context of general affine metric planes.

Remark 1. For the euclidean plane these properties can easily be established with geometric arguments. To prove the lemma we use similarity of triangles in Figure 2, in case C is a finite point. We have that $\Delta BCP \sim \Delta ACR$ and $\Delta BCS \sim \Delta ACQ$. Therefore

$$\frac{C-P}{C-R} = \frac{C-B}{C-A} = \frac{C-S}{C-Q}\,.$$

It follows that

$$\frac{R-P}{C-R} = \frac{C-P}{C-R} - 1 = \frac{C-S}{C-Q} - 1 = \frac{Q-S}{C-Q}\,.$$

In the case that C lies at infinity (Figure 3) we have $R-P = B-A = Q-S$.

To find the axis as radical axis we add circles to the figure (see Figure 4).

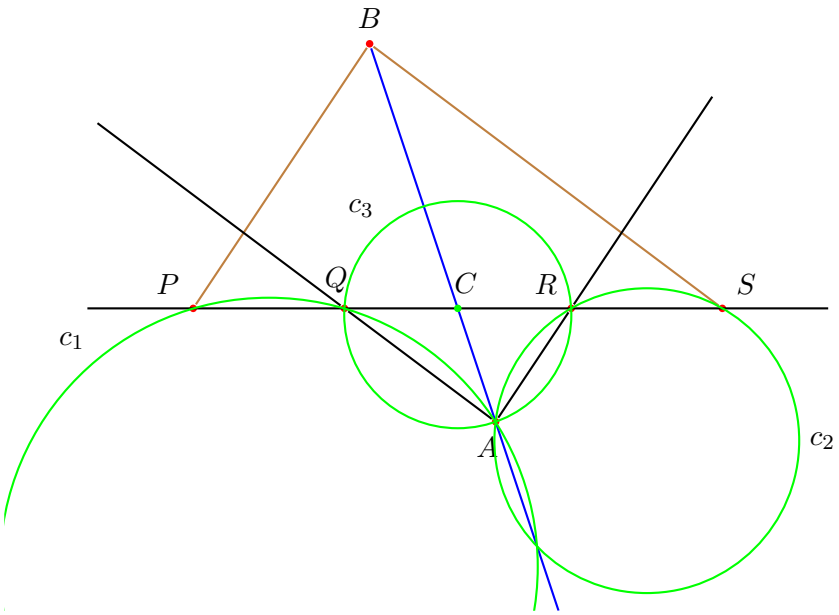

Figure 4

Let c_1 be the circle through A, P, Q and c_2 the circle through A, R, S. If $P = Q$, then c_1 is the circle through A which is tangent to the line l in the point $P = Q$; if $R = S$, the circle c_2 is tangent to l. Consider also the circle c_3 through A, Q and R. Then c_1 and c_3 intersect in A and Q, so the line $\langle A, Q\rangle$ is the radical axis of c_1 and c_3. The parallel line l_S is the locus of points for which the power with respect to c_1 has constant difference with the power with respect to c_3, the difference being $(S-P)\cdot(S-Q) - (S-Q)\cdot(S-R) = (S-Q)\cdot(R-P)$. The line l_P is the locus where the power with respect to c_2 differs from the power with respect to c_3 by the same quantity, as $(P-S)\cdot(P-R) - (P-R)\cdot(P-Q) = (P-R)\cdot(Q-S)$.

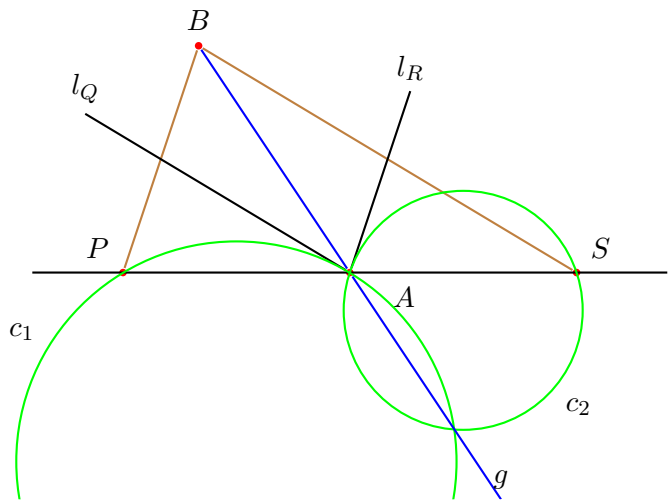

Figure 5

Therefore the intersection point $B = l_S \cap l_P$ lies on the radical axis of c_1 and c_2, so this radical axis is the axis $g = \langle A, B\rangle$.

In the situation of Figure 3 the center of the circle c_1 lies on the perpendicular bisector of PQ, which is also the perpendicular bisector of RS, on which the center of c_2 lies. Therefore the radical axis is parallel to l and B lies on it.

Lemma 4. *Given C and (R, S) on l, the map $\gamma\colon l \to l$, sending $X \in l$ to the point $\gamma(X)$, determined by $C = [X, \gamma(X) \mid R, S]$ is an involutive projectivity.*

Proof. To find $\gamma(X)$ we choose a point $A \notin l$ and draw the line l_X through X, parallel to $\langle R, A\rangle$ (see Figures 2 and 3, reading X and $\gamma(X)$ for P and Q). It intersects the line g in a point Y. Through Y we draw the line $l_S = \langle Y, S\rangle$. Then we draw a line m through A parallel to l_S and define $\gamma(X) = l \cap m$. This construction can be described as first projecting the line l from the point at infinity on the line $\langle A, R\rangle$ onto the line g, then projecting G from S onto the line l_∞ at infinity and finally projecting l_∞ onto l from A. This shows that the map γ is a projectivity.

That $\gamma^2 = \mathrm{id}$ can be seen from the formulas in Lemma 3 or by observing that γ interchanges R with S, and C with the point at infinity on the line l. □

Remark 2. Given the involution $\gamma\colon l \to l$ the point C is determined as the image of the point at infinity on the line l.

Remark 3. The point C on l is determined by the unordered pairs (P, Q) and (R, S), independent of the point A outside the line. We have emphasized the construction using a particular choice of points (Q and R) connected to A, as the construction with the points $A_1, \ldots, A_n$ naturally leads to this situation: the line $l = l_i$ is determined by the points points $P = A_{i-1}$ and $S = A_{i+1}$, while $Q = B_{i-1,i}$

and $R = B_{i,i+1}$ arise as intersection points of l with the lines $l_{i-1} = \langle A_{i-2}, A_i\rangle$ and $l_{i+1} = \langle A_i, A_{i+2}\rangle$. This extra structure makes it possible to define the axis if $A_i \in l_i$; in such a case there would be no involution on the line l_i.

Let A be a point on the line $l = \langle P, S\rangle$, different from P and S and let l_Q and l_R be two lines through A. Denote by B the intersection point of the line l_P through P, parallel to l_R and l_S through S, parallel to l_Q. We define the axis of this configuration as the line $\langle A, B\rangle$. In the case of the Euclidean plane it is the radical axis of the circle though P, tangent to l_Q in A, and the circle through S, tangent to l_R in A. The proof of Remark 1 extends to this situation, with the circle c_3 reduced to the point $A = Q = R$ (compare Figure 5 with Figure 4).

3. An n-axes theorem

We now formulate our main theorem.

Theorem 5. *Let $A_1, \ldots, A_n$ be a sequence of $n \geq 5$ distinct points in $\mathbb{A}^2(k)$, and define $l_i = \langle A_{i-1}, A_{i+1}\rangle$ (indices considered modulo n). Assume that*

(i) $A_i \notin l_{i-2}, l_i, l_{i+2}$,
(ii) $l_{i-1} \neq l_{i+1}$,
(iii) $l_i \nparallel l_{i+1}$,

and set $B_{i,i+1} = l_i \cap l_{i+1}$, $C_i = [A_{i-1}, B_{i-1,i} | B_{i,i+1}, A_{i+1}]$, and, finally, let $g_i = \langle A_i, C_i\rangle$ be the axis through A_i. If the $n-3$ axes $g_1, g_2, \ldots, g_{n-3}$ lie in a pencil, then the remaining three axes g_{n-2}, g_{n-1}, g_n lie in the same pencil.

As $A_i \in l_{i+1} = \langle A_i, A_{i+2}\rangle$ but $A_i \notin l_i$ by assumption (i), we have that $l_i \neq l_{i+1}$ and therefore assumption (iii) guarantees the existence of the point $B_{i,i+1}$ as a well-defined finite point.

By (i) and (ii) the points A_{i-1}, $B_{i-1,i}$, $B_{i,i+1}$ and A_{i+1} are four distinct points on the line l_i and A_i is a point outside, so that the axis g_i is defined. The condition $l_{i-1} \neq l_{i+1}$ means that A_{i-2}, A_i and A_{i+2} are not collinear. It is therefore equivalent to each of the conditions $A_{i-2} \notin l_{i+1}$ and $A_{i+2} \notin l_{i-1}$. Therefore the assumptions (i) and (ii) can be replaced by

(iv) $A_i \notin l_{i-3}, l_{i-2}, l_i, l_{i+2}, l_{i+3}$.

In particular this means that for $n \leq 6$, (i) and (ii) together are equivalent to the condition that no three points are collinear. Therefore the Theorem holds for $n = 5$ and $n = 6$ by the results of [3].

Definition. We call the common (finite or infinite) point of the pencil $\{g_i\}$ the *center* of the sequence $A_1, \ldots, A_n$.

4. A degenerate case of the 5-axes theorem

The 5-axes theorem states that for five points $A_1, \ldots, A_5$ in the plane, no three collinear, and $\langle A_{i-1}, A_{i+1}\rangle \nparallel \langle A_i, A_{i+2}\rangle$, the five axes $g_1, \ldots, g_5$ lie in a pencil. Motivated partly because they will be required later, but also because they are themselves of some interest, we study in this section some special and limiting cases. We first consider when the center is a point at infinity. More generally, we investigate the relationship of the center to the position of the initial five points.

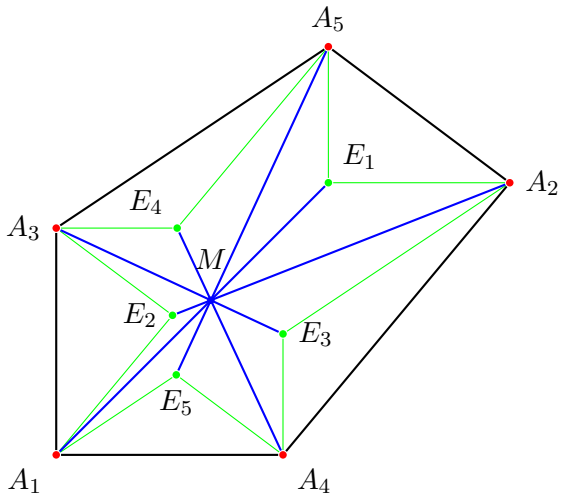

Figure 6

Theorem. *Consider four points A_1, A_2, A_3 and A_4 in an affine plane $\mathbb{A}^2(k)$, such that no three are collinear and such that $l_2 = \langle A_1, A_3\rangle$ is not parallel to $l_3 = \langle A_2, A_4\rangle$. A point A_5 in the plane, such that the assumptions of the 5-axes theorem are satisfied* (*i.e., A_5 does not lie on a line $\langle A_i, A_j\rangle$, while $l_i \nparallel l_{i+1}$ for all $i \neq 2$*) *determines a center M in the extended plane $\mathbb{P}^2(k)$. The correspondence $A_5 \mapsto M$ is the restriction of a projective transformation $\mathbb{P}^2(k) \to \mathbb{P}^2(k)$. In particular, the locus of points A_5 for which M is a point at infinity* (*i.e., for which the axes are parallel*) *is a line.*

Proof. This is a computation. We construct the axis g_i from the intersection point E_i of the line through A_{i-1}, parallel to $\langle A_i, B_{i,i+1}\rangle = \langle A_i, A_{i+2}\rangle$, with the parallel to $\langle A_i, B_{i,i-1}\rangle = \langle A_i, A_{i-2}\rangle$ through A_{i+1}, see Figure 6.

We use homogeneous coordinates and take $A_1 = (0 : 0 : 1)$, $A_3 = (0 : 1 : 1)$, $A_4 = (1 : 0 : 1)$, $A_2 = (a : b : c)$ and $A_5 = (x : y : z)$.

The point E_1 is easily seen to be $(cx : bz : cz)$. We compute $E_4 = (bx + (c - a)y + (a - c)z : bz : bz)$ and find M as the intersection of the axes $g_1 = \langle A_1, E_1\rangle$ and $g_4 = \langle A_4, E_4\rangle$. The result is

$$M = (cx : bz : (c - b)x + (a - c)y + (c - a + b)z) \ .$$

In particular, M is at infinity if and only if $(c-b)x+(a-c)y+(c-a+b)z = 0$, which is the equation of a line whose slope is $\frac{c-b}{c-a}$. □

Remark 4. With a little more effort one can compute all points E_i and check that M lies on all axes $g_i = \langle A_i, E_i\rangle$. This gives a computational proof of the five-axes theorem.

Our stipulation that the conditions of the five-axes theorem be satisfied was sufficient for defining the five axes. But the resulting formula for M makes sense under more general circumstances, indicating that the theorem also holds in degenerate

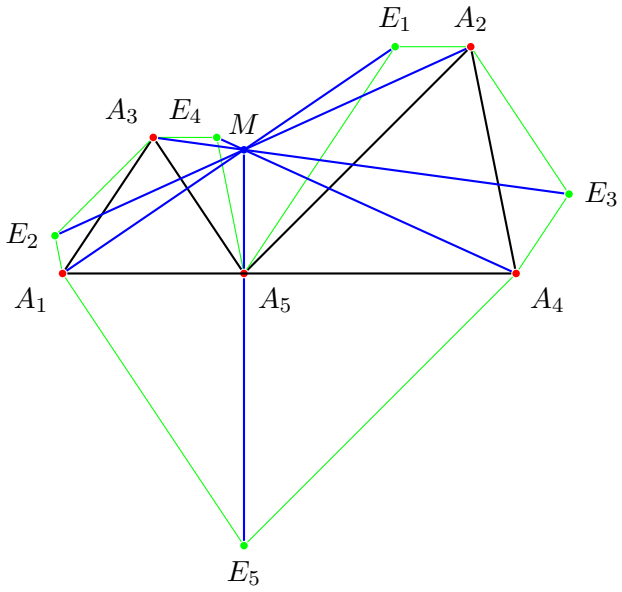

Figure 7. $A_5 \in l_5$

cases with a suitable definition of the axes. The point M fails to be determined only if $cx = bz = -bx + (a-c)(y-z) = 0$. When A_2 and A_5 are finite points ($c \neq 0$ and $z \neq 0$), this happens if either $A_2 = A_4$ and $A_5 \in \langle A_1, A_3\rangle$ or $A_5 = A_3$ and $A_5 \in \langle A_1, A_4\rangle$. If, say, A_5 lies at infinity ($z = 0$), then $A_5 = \langle A_1, A_3\rangle \cap \langle A_2, A_4\rangle$. Note that our coordinates are based on the assumption that A_1, A_3, A_4 form a triangle. In general we can say that the center is undefined when for some i, A_{i-1} coincides with A_{i+1} and the remaining three points are collinear, or when $\langle A_{i-1}, A_{i-3}\rangle \parallel \langle A_{i+1}, A_{i+3}\rangle$ with A_i being their intersection point at infinity, or when all five points are collinear. Moreover, if M is defined, but coincides with the point A_i, then the axis g_i is not defined.

We focus now on one degenerate case, which we need later, in which three consecutive points are collinear: $A_i \in l_i = \langle A_{i-1}, A_{i+1}\rangle$. We have that $A_i = l_{i-1} \cap l_{i+1} = l_{i-1} \cap l_i \cap l_{i+1}$, so $A_i = B_{i-1,i} = B_{i,i+1}$. In this case the axis g_i can be defined as in Remark 3.

Theorem 6. *Let five points A_1, A_2, A_3, A_4 and A_5 in the affine plane be given such that $A_5 \in \langle A_1, A_4\rangle$, but no other three points are collinear. Assume that $l_i = \langle A_{i-1}, A_{i+1}\rangle$ is not parallel to $l_{i+1} = \langle A_i, A_{i+2}\rangle$. Then the five axes g_1, g_2, g_3, g_4 and g_5 lie in a pencil.*

The computation, alluded to in Remark 4, also covers this degenerate case, illustrated in Figure 7. The geometric proof of the 5-circle theorem in [2, 3] can be extended to this situation to show that the four axes g_1, g_2, g_3 and g_4 lie in a pencil. If g_i is considered as radical axis of the circles $c_{i-1,i}$ and $c_{i,i+1}$, this suffices to conclude that all five radical axes lie in a pencil: if the center M is a finite point, then the fact that M lies on g_1, g_2, g_3 and g_4 implies that the power of M with

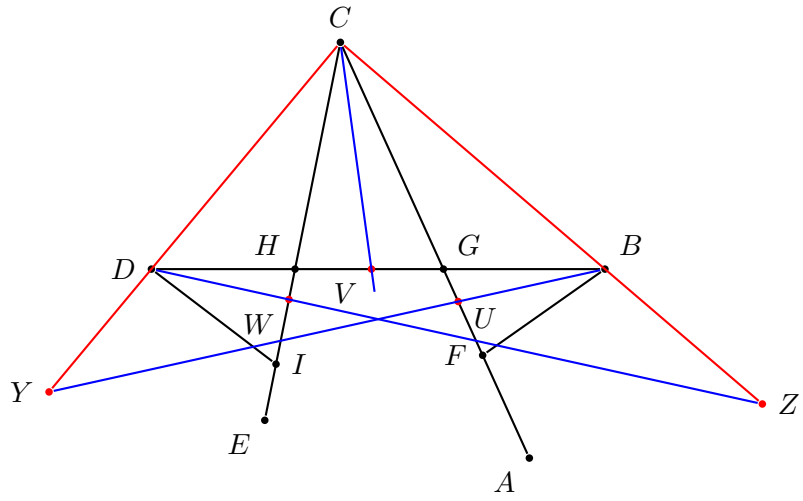

Figure 8

respect to $c_{5,1}$ is equal to the power with respect to $c_{1,2}$, equal to the power with respect to $c_{2,3}$, $c_{3,4}$ and $c_{4,5}$. As the power of M with respect to $c_{4,5}$ is equal to that that with respect to $c_{5,1}$, the point M lies on the radical axis g_5. If the center M is infinite, then the centers of all circles involved are collinear.

The main ingredient of the geometric proof is Lemma 2 of [2, 3], which we now recall.

Lemma 7. *Let A, C and E be three non collinear points in $\mathbb{A}^2(k)$, and let A, C, F, G be collinear, just as C, E, H, I and B, D, G, H (see Figure 8). Let $U = [A, F \mid C, G]$, $V = [H, D \mid B, G]$ and $W = [C, H \mid E, I]$. Then the lines $\langle B, U\rangle$, $\langle C, V\rangle$ and $\langle D, W\rangle$ lie in a pencil if and only if*

$$\frac{B-G}{B-H}\frac{E-H}{E-C}\frac{F-C}{F-G} = \frac{D-H}{D-G}\frac{A-G}{A-C}\frac{I-C}{I-H}\,. \tag{1}$$

Lemma 8. *The above lemma also holds if A and F coincide* (see Figure 9).

Proof. The proof follows [2, 3]. Let $Y = \langle B, U\rangle \cap \langle C, D\rangle$ and $Z = \langle D, W\rangle \cap \langle C, B\rangle$. By Ceva's theorem, applied to ΔBCD and its cevians $\langle B, Y\rangle$, $\langle C, V\rangle$ and $\langle D, Z\rangle$, the lines $\langle B, U\rangle$, $\langle C, V\rangle$ and $\langle D, W\rangle$ lie in a pencil if and only if

$$\frac{Y-C}{Y-D}\frac{V-D}{V-B}\frac{Z-B}{Z-C} = -1\,.$$

Menelaus' theorem first for ΔCDG and the points B, U and Y and then for ΔCBH and the points D, W and Z gives

$$\frac{Y-C}{Y-D} = \frac{U-C}{U-G}\frac{B-G}{B-D} \quad \text{and} \quad \frac{Z-B}{Z-C} = \frac{D-B}{D-H}\frac{W-H}{W-C}\,.$$

The condition $W = [C, H \mid E, I]$ gives by Lemma 3 that $\frac{W-C}{W-H} = \frac{E-C}{E-H}\frac{I-C}{I-H}$, while $V = [H, D|B, G]$ gives $\frac{V-D}{V-B} = \frac{D-G}{B-H}$ and finally $U = [C, G|A, A]$ implies

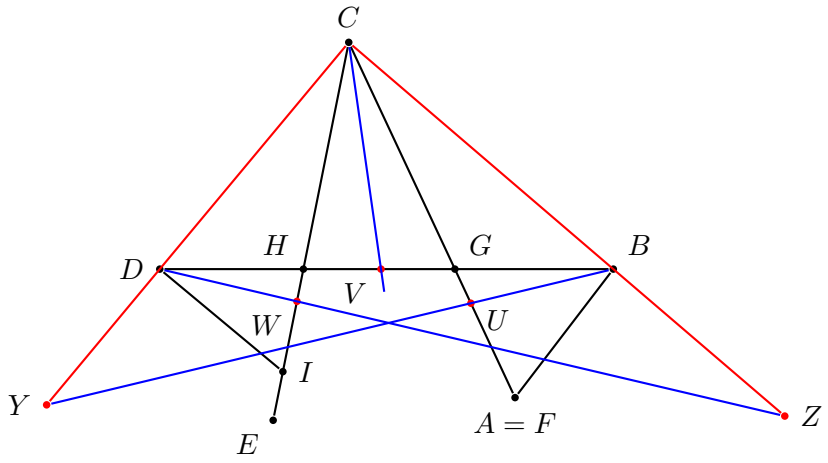

Figure 9

$\frac{U-G}{U-C} = (\frac{A-G}{A-C})^2$. Plugging these expression in in the equation and rearranging gives that $\langle B, U\rangle$, $\langle C, V\rangle$ and $\langle D, W\rangle$ lie in a pencil if and only if

$$\frac{A-C}{A-G}\frac{B-G}{B-H}\frac{E-H}{E-C} = \frac{A-G}{A-C}\frac{I-C}{I-H}\frac{D-H}{D-G}\ .$$

□

Proof that $g_1, \ldots, g_4$ lie in a pencil. In order to show that the lines g_1, g_2 and g_3 lie in a pencil, we verify the condition of Lemma 8 with $(B, C, D, E, A = F) = (A_1, A_2, A_3, A_4, A_5 = B_{5,1})$, $(G, H, I, U, V, W) = (B_{1,2}, B_{2,3}, B_{3,4}, C_1, C_2, C_3)$, where $C_i = l_i \cap g_i$. Both sides of the equation are equal to 1 by Menelaus' theorem applied to ΔCGH, on the left with the collinear points B, A and E, and on the right with D, I and A. Similarly one shows that g_2, g_3 and g_4 lie in a pencil. □

5. Six points

For six points the axes in general do not lie in a pencil.

Theorem 9. *Let six points $A_1, \ldots, A_6$, be given, no three collinear and such that the six points $B_{i,i+1} = \langle A_{i-1}, A_{i+1}\rangle \cap \langle A_i, A_{i+2}\rangle$ are finite. Then the following are equivalent:*

(1) the six axes $g_1, \ldots, g_6$, lie in a pencil
(2) for some i the axes g_{i-1}, g_i, g_{i+1} lie in a pencil,
(3) the main diagonals of the hexagon $A_1A_2A_3A_4A_5A_6$ lie in a pencil,
(4) the six points $B_{i,i+1}$ lie on a conic.

Proof. $(1) \implies (2) \implies (3) \implies (1)$:
We show that condition (3) is equivalent to g_{i-1}, g_i, g_{i+1} lying in a pencil for all i. But as the condition on the main diagonals does not single out three lines, it suffices to prove equivalence for one specific i, say $i = 3$.

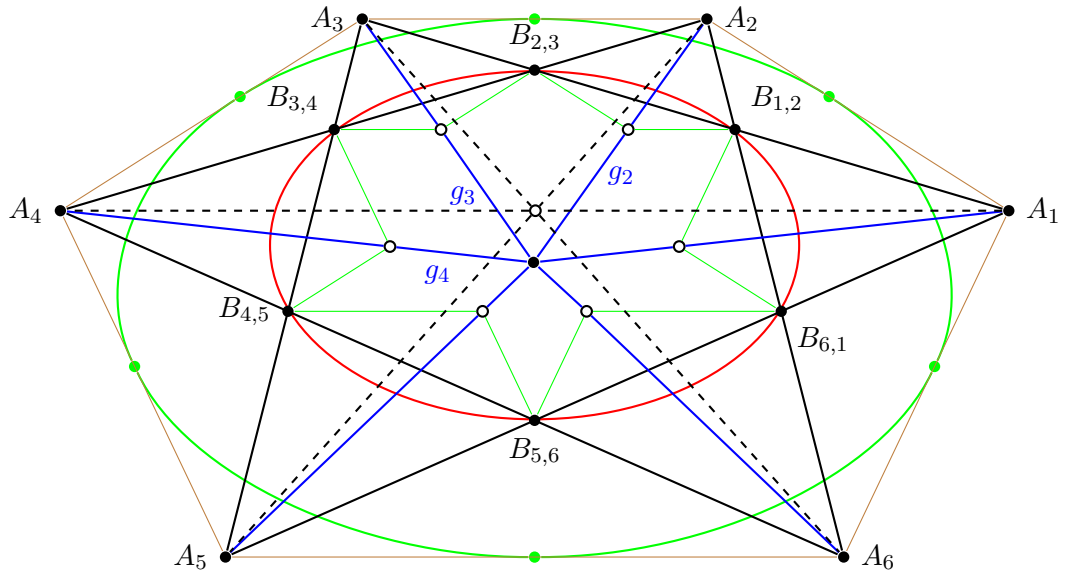

Figure 10

We take affine coordinates (x, y) with A_3 as origin, $A_2 = (0, 1)$, $A_4 = (1, 0)$, $A_1 = (a, b)$, $A_6 = (c, d)$ and $A_5 = (e, f)$. We compute $B_{2,3} = (\frac{a}{a+b}, \frac{b}{a+b})$, $B_{3,4} = (\frac{e}{e+f}, \frac{f}{e+f})$, $B_{1,2} = (\frac{ac}{bc-ad+a}, \frac{bc}{bc-ad+a})$ and $B_{4,5} = (\frac{ed}{ed-fc+f}, \frac{fd}{ed-fc+f})$. The condition (1) of Lemma 7 (with the labels $A, \ldots, I$ applied, in order, to A_1, $\ldots$, A_5, $B_{1,2}$, $B_{2,3}$, $B_{3,4}$, $B_{4,5}$) then becomes

$$\frac{a(e+f)}{(a+b)e} \cdot \frac{e+f-1}{e+f} \cdot \frac{c(a+b)}{(c+d-1)a} = \frac{f(a+b)}{(e+f)b} \cdot \frac{a+b-1}{a+b} \cdot \frac{d(e+f)}{f(c+d-1)} ,$$

which simplifies to

$$(e+f-1)cb = (a+b-1)de . \tag{2}$$

Here we used $a + b \neq 0$ (as $l_2 \nparallel l_3$), $e + f \neq 0$ and $a \neq 0$ (as $A_2 \notin l_2$), $f \neq 0$ and $c + d \neq 1$ (as $A_6 \notin l_3$).

The diagonal $\langle A_3, A_6\rangle$ has equation $dx - cy = 0$, the diagonal $\langle A_1, A_4\rangle$ is given by $bx + (1-a)y = b$ and $\langle A_2, A_5\rangle$ by $(1-f)x + ey = e$. The condition that these three diagonals lie in a pencil is given by the vanishing of the determinant

$$\Delta = \begin{vmatrix} b & 1-a & -b \\ 1-f & e & -e \\ d & -c & 0 \end{vmatrix} = \begin{vmatrix} 0 & 1-a-b & -b \\ 1-e-f & 0 & -e \\ d & -c & 0 \end{vmatrix} .$$

Computing this determinant with Sarrus' rule shows that $\Delta = 0$ if and only if equation (2) holds.

(3) $\iff$ (4):

The lines $\langle A_1, A_4\rangle$, $\langle A_2, A_5\rangle$ and $\langle A_3, A_6\rangle$ lie in a pencil if and only if the triangles $\Delta A_1A_3A_5$ and $\Delta A_4A_6A_2$ are perspective from a center which, by Desargues's theorem, holds if and only if they are perspective from an axis. Note that the line

$l_i = \langle A_{i-1}, A_{i+1}\rangle$ coincides with the line $\langle B_{i-1,i}, B_{i,i+1}\rangle$. Therefore the axis of perspectivity is also the Pascal line of the points $B_{i,i+1}$, whence these points lie on a conic if and only if the original three lines lie in a pencil. □

Remark 5. If $\operatorname{char} k \neq 2$ the hexagon $A_1A_2A_3A_4A_5A_6$ circumscribes a conic by Brianchon's theorem. This is not true in characteristic 2, as then all tangents to a conic pass through one point. Figure 10 illustrates the result in the euclidean plane. To make the conics clearly visible the axes g_i are constructed by drawing parallels through $B_{i-1,i}$ and $B_{i,i+1}$.

Remark 6. The above proof shows that under weaker conditions, the equivalence between the axes g_2, g_3 and g_4 lying in a pencil and the main diagonals lying in a pencil continues to hold. The condition (1) applied to $(A, B, C, D, E) = (A_1, A_2, A_3, A_4, A_5)$ does not involve the position of the point A_6. The proof, when written in homogeneous coordinates, therefore remains valid should A_6 lie at infinity ($l_1 \parallel l_5$), or should $A_6 \in l_2, l_4, l_6$. Also the degenerations $A_1 \in l_5$, $A_5 \in l_1$, $A_2 \in l_6$, $A_4 \in l_6$ or $l_5 \parallel l_6$, $l_1 \parallel l_6$ do not affect the conclusion.

6. The proof of the main result

We have now seen that Theorem 5 holds for extended versions of the cases $n = 5$ and $n = 6$. For $n \geq 7$ we find it convenient to assume that the axes $g_2, \ldots, g_{n-2}$ lie in a pencil.

The proof of Theorem 5 proceeds by induction on the number of vertices. The idea is the following. Suppose $A_1, \ldots, A_n$ are given with $g_2, \ldots, g_{n-2}$ in a pencil. Then we construct a sequence $A_1, A_2, A_{3,4}, A_5, \ldots, A_n$ of $n-1$ points by replacing A_3 and A_4 by the intersection $A_{3,4}$ of l_2 and l_5. For the new configuration the axes $g_2, g_{3,4}, g_5, \ldots, g_{n-2}$ lie in a pencil with the same center, and the induction hypothesis applies, provided the configuration satisfies the assumptions of the theorem. Sometimes this will not be the case, but we shall see that without loss of generality, one can replace the given configuration by one which does satisfy the assumptions.

Three consecutive axes g_{i-1}, g_i, g_{i+1} are determined by seven points A_{i-3}, A_{i-2}, A_{i-1}, A_i, A_{i+1}, A_{i+2} and A_{i+3}. Let D_i be the (possibly infinite) intersection point of $l_{i-2} = \langle A_{i-3}, A_{i-1}\rangle$ and $l_{i+2} = \langle A_{i+1}, A_{i+3}\rangle$. The point D_i exists as $l_{i-2} \neq l_{i+2}$, because $A_{i+1} \notin l_{i-2}$. The axes g_{i-1}, g_i, g_{i+1} are also the axes through A_{i-1}, A_i, A_{i+1} in the hexagon $D_iA_{i-2}A_{i-1}A_iA_{i+1}A_{i+2}$. This hexagon does not necessarily satisfy all the conditions (i), (ii), (iii), but by Remark 6 less is needed to conclude that the lines g_{i-1}, g_i, g_{i+1} lie in a pencil if and only if the lines $\langle A_{i-2}, A_{i+1}\rangle$, $\langle A_{i-1}, A_{i+2}\rangle$ and $\langle A_i, D_i\rangle$ lie in a pencil (see also Figure 11). Only the three conditions $l_{i+1} \neq \langle A_{i+2}, A_{i-2}\rangle$, $l_{i-1} \neq \langle A_{i+2}, A_{i-2}\rangle$ and $l_{i-2} \neq l_{i+2}$ are not directly covered by the properties of the original configuration and the allowable degenerations from the remark. We already showed that $l_{i-2} \neq l_{i+2}$. If $l_{i-1} = \langle A_{i+2}, A_{i-2}\rangle$, then A_{i-2}, A_i and A_{i+2} are collinear, which whould imply that $l_{i-1} = l_{i+1}$, contradicting the condition (ii) for the original configuration; for the same reason $l_{i+1} \neq \langle A_{i+2}, A_{i-2}\rangle$. So the condition to test is indeed that each triple of lines $\langle A_{i-2}, A_{i+1}\rangle$, $\langle A_{i-1}, A_{i+2}\rangle$ and $\langle A_i, D_i\rangle$ lies in a pencil.

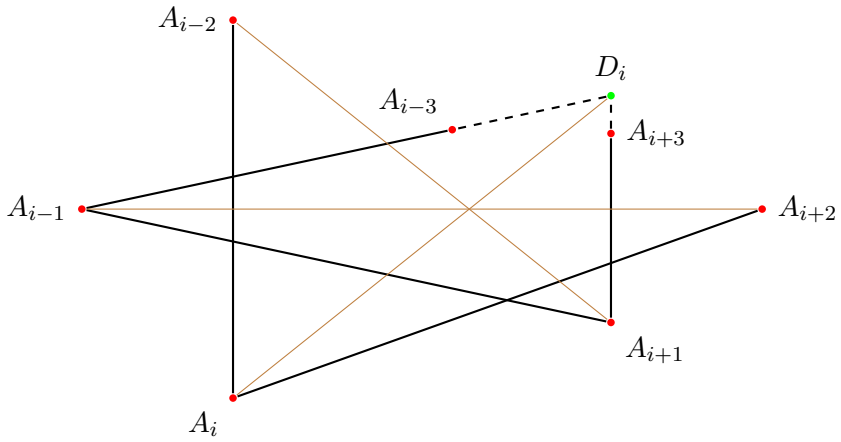

Figure 11

In the following lemma we consider a sequence of points $A_0, A_1, \ldots, A_6$, which may be part of a larger configuration. Because of the lemma's limited scope, we require only that the indices in the assumptions (i) – (iii) lie between 0 and 6.

Lemma 10. *Let A_0, A_1, …, A_5, A_6 be a sequence of distinct points satisfying the assumptions* (i) – (iii) *limited to indices between 0 and 6, such that the axes g_2, g_3 and g_4 lie in a pencil. Choose a point $A'_3 \in l_4$ with $A'_3 \neq B_{3,4}$ and $A'_3 \neq \langle A_1, A_2\rangle \cap l_4$. Let $P = \langle A_1, A_4\rangle \cap \langle A_2, A'_3\rangle$. Define the point $A'_2 \in l_1$ as $A'_2 = l_1 \cap \langle P, A_3\rangle$. Suppose that the sequence A_0, A_1, A'_2, A'_3, A_4, A_5, A_6 also satisfies the limited assumptions* (i) – (iii). *Denote the axes of this new configuration by g'_i. Then $g_4 = g'_4$ and the the axes g'_2, g'_3 and g'_4 lie in the same pencil as g_2, g_3 and g_4. If moreover one of the axes g_1, g'_1 is defined and also lies in the same pencil, then $g'_1 = g_1$.*

Proof. The construction is illustrated in Figure 12. We want to apply the 6-axes theorem (Theorem 9) to the points A_1, A_2, A_3, A_4, A'_3, A'_2. Therefore we check that they are distinct and satisfy assumptions (i) – (iii).

By construction $A'_2 = A_2$ if and only if $A'_3 = A_3$, but then there is nothing to prove. We therefore assume $A'_3 \neq A_3$. This also gives $l'_3 \neq l_3$ and $l'_2 \neq l_2$. We have that $A'_3 \in l_4$; as $A_2 \notin l_4$ and $A_4 \notin l_4$, $A'_3 \neq A_2$ and $A'_3 \neq A_4$; similarly for A'_2. The only other requirements that do not follow from the assumptions on A_0, A_1, A_2, A_3, A_4, A_5, A_6 and A_0, A_1, A'_2, A'_3, A_4, A_5, A_6, are $A_2 \notin l'_2$, $A'_2 \notin l_2$, $A_3 \notin l'_3$ and $A'_3 \notin l_3$.

If $A'_3 \in l_3$, then $A'_3 = B_{3,4}$. If $A_3 \in l'_3 = \langle A'_2, A_4\rangle$, then $A_4 \in \langle A'_2, A_3\rangle \cap \langle A_1, A_4\rangle = \{P\}$, which again implies the excluded case $B_{3,4} = A_2A_4 \cap A_3A_5 = A_2P \cap A_3A_5 = A'_3$.

The condition $A'_3 \neq \langle A_1, A_2\rangle \cap l_4$ gives $A_2 \notin \langle A_1, A'_3\rangle = l'_2$. If $A'_2 \in l_2 = \langle A_1, A_3\rangle$, then $P \in \langle A_1, A_3\rangle$. As also $P \in \langle A_1, A_4\rangle$ this implies that $P = A_1$ and again $A_2 \in \langle A_1, A'_3\rangle = l'_2$.

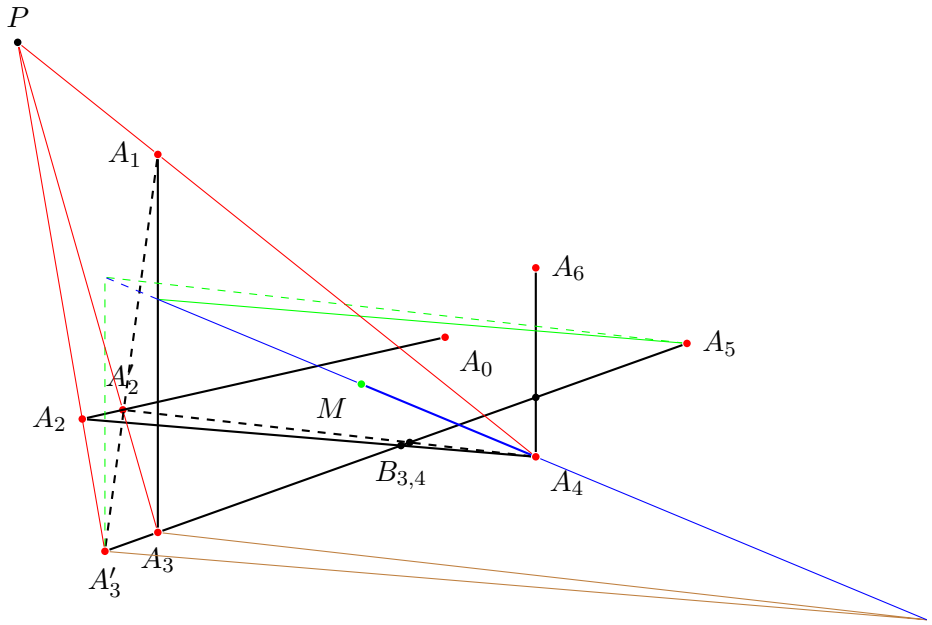

Figure 12

As $\langle A_1, A_4\rangle$, $\langle A_2, A_2'\rangle$ and $\langle A_3, A_2'\rangle$ lie in a pencil, the axes $\bar{g}_1$, $\bar{g}_2$, $\bar{g}_3$, $\bar{g}_4$, $\bar{g}_3'$ and $\bar{g}_2'$ of the hexagon $A_1A_2A_3A_4A_3'A_2'$ lie in a pencil. Because A_0, A_2 and A_2' are collinear and also A_5, A_3 and A_3', we have that $\bar{g}_2 = g_2$, $\bar{g}_3 = g_3$, $\bar{g}_2' = g_2'$ and $\bar{g}_3' = g_3'$.

As g_4 lies in the pencil of $g_2 = \bar{g}_2$ and $g_3 = \bar{g}_3$, the axis g_4 also coincides with $\bar{g}_4$. The axis g_4 is constructed as $\langle A_4, E_4\rangle$, with E_4 the intersection point of the parallel to $l_5 = \langle A_4, A_6\rangle$ through A_3 and the parallel to $l_3 = (A_4, A_2)$ through A_5. For $\bar{g}_4 = \langle A_4, \bar{E}_4\rangle$ one finds $\bar{E}_4$ as intersection point of the parallel to $\bar{l}_3 = l_3 = \langle A_4, A_2\rangle$ through A_3' and the parallel to $\bar{l}_3' = l_3' = \langle A_4, A_2'\rangle$ through A_3. For $g_4' = \langle A_4, E_4'\rangle$ one intersects the parallel to $l_5 = \langle A_4, A_6\rangle$ through A_3' with the parallel to $l_3' = (A_4, A_2')$ through A_5. By Pappus' theorem applied to the collinear points A_3, A_3' and A_5 and the points at infinity of the three lines l_3, l_3' and l_5 the points E_4, $\bar{E}_4$ and E_4' are collinear. As E_4 and $\bar{E}_4$ lie on $g_4 = \bar{g}_4$, the point E_4' also lies on it and therefore $g_4' = g_4$.

Furthermore, if g_1 lies in the pencil the same argument gives that $g_1' = g_1$. □

Remark 7. The requirement that the sequence A_0, A_1, A_2', A_3', A_4, A_5, A_6 also satisfy assumptions (i) – (iii) implies only finitely many forbidden positions for A_3'. Those can be made explicit. One finds that A_3' should not be equal to A_5, $\langle A_0, A_1\rangle \cap l_4$, $l_1 \cap l_4$, $l_5 \cap l_4$, $\langle A_1, A_4\rangle \cap l_4$ and also not equal to $l_4 \cap m_1$, where m_1 is the line through A_1, parallel to l_1. There will, of course, be a few more forbidden positions when the given points are part of a larger configuration. For A_2' one has corresponding forbidden positions. As one finds A_2' from A_3' by first projecting l_4

from A_2 onto the line $\langle A_1, A_4\rangle$ and then projecting from A_3 on the line l_1, those positions of A'_2 yield further forbidden positions of A'_3.

This covers all assumptions except $l_2 \nparallel l'_3$, $A'_2 \notin l'_2$ and $A'_3 \notin l'_3$. They involve the position of the point $B_{2,3}$: in the first case it lies at infinity, in the second $B_{2,3} = A'_2$ and finally $B_{2,3} = A'_3$. The point $B'_{2,3}$ is the intersection $\langle A_1, A'_3\rangle \cap \langle A_4, B'_{3,4}\rangle$ and as $(A'_3, B'_{3,4})$ is a pair of an involution on l_4 the point $B'_{2,3}$ moves on a (possibly degenerate) conic through A_1, A_4 and $B_{2,3}$, as A'_3 moves on l_4. The intersection of this conic with the line at infinity, l_1 and l_4 gives at most six forbidden positions for $B'_{2,3}$ and therefore for A'_3.

On the other hand, because we could, if needed, embed the given plane in a plane over a field extension we can assume without loss of generality that there are infinitely many allowable positions for A'_3 on l_4.

Proof of Theorem 5. Suppose distinct points $A_1, \ldots, A_n$ ($n \geq 7$) are given, satisfying the assumptions (i), (ii), (iii) and such that the $n-3$ lines $g_2, \ldots, g_{n-2}$ lie in a pencil. The lines l_2 and l_5 are not equal, as $A_4 \in l_5$, but $A_4 \notin l_2$.
Let

$$A_{3,4} = l_2 \cap l_5 \text{ (possibly at infinity)}, \quad l_{3,4} = \langle A_2, A_5\rangle,$$
$$B_3 = l_{6,4} \cap l_2 \text{ and } B_4 = l_{3,4} \cap l_5.$$

Consider the sequence of $n-1$ points A_1, A_2, $A_{3,4}$, A_5, …, A_n. Suppose first that $A_{3,4}$ is a finite point and that the sequence also satisfies the assumptions (i) – (iii), as in Figure 13.

The lines l_2 and l_5 occur both in the configuration of n points and of $n-1$ points, and also in the configuration formed by the five points A_2, A_3, A_4, A_5, $A_{3,4}$. Now $A_{3,4} \neq A_3$, as $A_{3,4} \in l_5$ but $A_3 \notin l_5$; similarly $A_{3,4} \neq A_4$.

We verify the conditions (i) – (iii) for the pentagon $A_2A_3A_4A_5A_{3,4}$. Most of them are conditions which also appear as conditions for A_1, A_2, $A_{3,4}$, A_5, …, A_n or A_1, A_2, A_3, A_4, …, A_n. For (i) we note that $A_3 \notin l_{3,4}$, as A_2, A_3 and A_5 are not collinear, because $A_2 \notin l_4$; likewise $A_4 \notin l_{3,4}$. Also $A_{3,4} \notin l_4$, for otherwise $A_{3,4} = l_2 \cap l_4 = A_3$, similarly $A_{3,4} \notin l_3$. For (ii) we have $l_{3,4} \neq l_4$ (and similarly $l_{3,4} \neq l_3$) because A_2, A_3 and A_5 are not collinear.

Therefore the 5-axes theorem applies to the configuration A_2, A_3, A_4, A_5, $A_{3,4}$. Its axes $\bar{g}_2$, $\bar{g}_3$, $\bar{g}_4$, $\bar{g}_5$ and $\bar{g}_{3,4}$ lie in a pencil. As $\bar{g}_3$ coincides with the axes g_3 of the configuration A_1, A_2, A_3, A_4, …, A_n, and likewise $\bar{g}_4 = g_4$, and g_2 and g_5 lie in a pencil with g_3 and g_4, we find that also $\bar{g}_2 = g_2$ and $\bar{g}_5 = g_5$. By the same argument as in the previous proof we conclude that g_5 is also the axis through A_5 in the configuration A_1, A_2, $A_{3,4}$, A_5, …, A_n, and a similar statement holds for g_2. The axes $\bar{g}_{3,4}$ is also the axis through $A_{3,4}$ in the configuartion of $n-1$ points. Therefore the $n-4$ axes g_2, $g_{3,4}$, g_5, …, g_{n-2} lie in a pencil and by the induction hypothesis the axes g_1, g_{n-1} and g_n lie in the same pencil, which is also the pencil of g_2, g_3, g_4, g_5, …, g_{n-2}.

If $A_{3,4}$ lies at infinity or coincides with one of the other points, or the configuration A_1, A_2, $A_{3,4}$, A_5, …, A_n does not satisfy the assumptions (i) – (iii), we use the construction of Lemma 10 to replace A_1, A_2, A_3, A_4, A_5, …, A_n by another

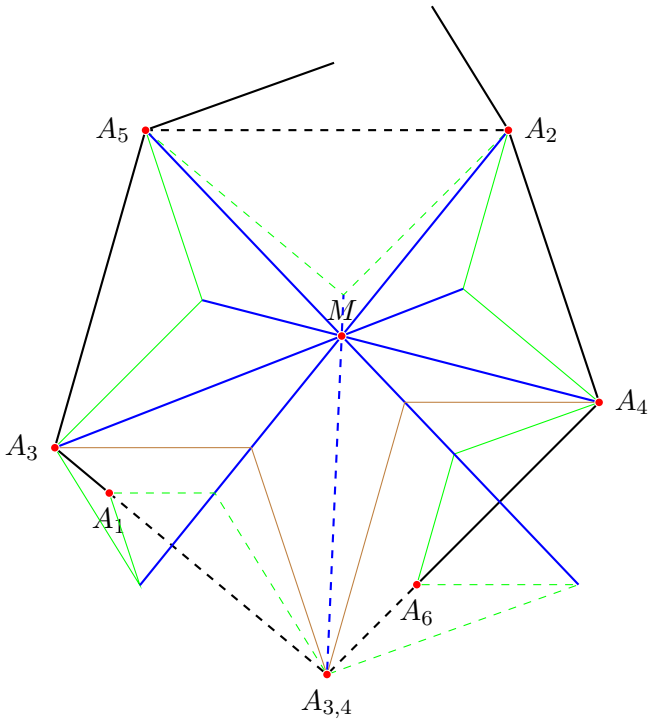

Figure 13

one $A'_1, \ldots, A'_n$ with the same center, such that A'_1, A'_2, $A'_{3,4}$, $A'_5, \ldots, A'_n$ does satisfy the assumptions. As mentioned earlier, the new sequence need not be defined over the field k; it suffices for the induction that it is defined over a field extension.

Some of the assumptions (i) – (iii) for the configuration A_1, A_2, $A_{3,4}$, $A_5, \ldots, A_n$ follow directly from the properties (i) – (iv) of the n points $A_1, \ldots, A_n$, but for the others we have to modify the given configuration. We do this step by step. At each step we maintain $n-2$ points from the previous step and move the other two in a way that corrects one specific shortcoming (it is here that we might have to make use of a field extension). We then relabel the points so that the resulting configuration is free of all previous shortcomings, yet has the same center.

We now list the conditions and discuss how to satisfy them. We treat the cases which are connected by the symmetry $A_n \mapsto A_{7-n}$ together, postponing $A_{3,4} \notin l_{3,4}$ to the end.

- $l_2 \nparallel l_5$.
  This condition implies that the point $A_{3,4} = l_2 \cap l_5$ is a finite point,
  as desired. As $l_2 \neq l_4$, $A_1 \notin l_4$. Moving A_3 on l_4 means that the line l_2 moves in the pencil of lines through A_1, whereas l_4 does not change. Therefore, if we were given $l_2 \parallel l_5$, we could make these lines intersecting by moving A_2 and A_3.

- $A_1 \neq A_{3,4}$ and $A_6 \neq A_{3,4}$.
  If $A_{3,4} = A_6$, then $l_2 = \langle A_1, A_3 \rangle$ intersects $l_5 = \langle A_4, A_6 \rangle$ in A_6. Moving A_3 on l_4 means that l_2 moves in the pencil of lines with center A_1. As $A_6 \neq A_1$, this means that $A_{3,4}$ moves. If $A_{3,4} = A_1$, we move instead A_4 on l_3.
- $A_{3,4} \neq A_j$ for $j = 7, \ldots, n$.
  If $A_j = l_2 \cap l_5$, we move l_2 in the pencil of lines through A_1.
- $A_1 \notin l_{3,4}$ and $A_6 \notin l_{3,4}$.
  If $A_1 \in l_{3,4}$, we move $l_{3,4}$ in the pencil through A_5 by moving A_2 on l_1.
- $A_{3,4} \notin l_1$ and $A_{3,4} \notin l_6$.
  Moving A_2 and A_3 means that $A_{3,4}$ moves on $l_5 \neq l_6$, while moving A_4 and A_5 makes $A_{3,4}$ to move on $l_2 \neq l_1$.
- $l_1 \neq l_{3,4}$ and $l_6 \neq l_{3,4}$.
  This first condition means that A_2, A_5 and A_n are not collinear, and the second that A_2, A_5 and A_7 are not collinear. For $n = 7$ these conditions coincide and are satisfied because $l_6 \neq l_1$. Let $n > 7$ and suppose $A_5 \in l_1$. Then $A_5 = l_1 \cap l_4$ ($l_1 \neq l_4$ as $A_2 \notin l_4$). We can move A_5 and A_6, moving A_5 on l_4 off l_1. If $A_2 \in l_6$, then moving A_5 on l_4 moves l_6 in the pencil of lines through A_7.
- $l_2 \neq l_5$.
  This holds as $A_3 \notin l_5$.
- $l_2 \nparallel l_{3,4}$ and $l_5 \nparallel l_{3,4}$.
  If $l_5 \parallel l_{3,4}$ we move A_2 and A_3, moving A_2 on l_1. As $A_5 \notin l_1$ by a previous step, this means that $l_{3,4}$ moves, whereas l_5 does not move. If $l_2 \nparallel l_{3,4}$ we move A_4 and A_5.

The last condition to be satisfied is $A_{3,4} \notin l_{3,4}$. If $A_{3,4} \in l_{3,4}$, then $l_{3,4}$, l_2 and l_5 are concurrent and $A_{3,4} = B_3 = B_4$. Now the conditions for the degenerate case of the 5-axes theorem (Theorem 6) are satisfied. We find that $\bar{g}_2$, $\bar{g}_3$, $\bar{g}_4$ and $\bar{g}_5$ lie in a pencil. We conclude that $\bar{g}_5 = g_5$ also in this case.

We compute the image of $A_{3,4}$ under the involution on l_5 determined by A_4, l_4 and g_5, both when $A_{3,4} \in l_{3,4}$ and $A_{3,4} \notin l_{3,4}$. According to the proof of Lemma 4 we have to intersect the line through $A_{3,4}$, parallel to l_4 with g_5 and connect the intersection point with A_4. Then we draw parallel to this last line a line through A_5. The construction of the axis $\bar{g}_5 = g_5$ shows that the line through A_4 is parallel to $\langle A_2, A_5 \rangle$. Therefore the image of $A_{3,4}$ is $B_4 = l_5 \cap \langle A_2, A_5 \rangle$.

If $A_{3,4} = B_4$, then it is a fixed point of the involution and by moving A_2 on l_1 and A_3 on l_4 we move $A_{3,4}$ on l_5, so that it is no longer a fixed point of the involution, and therefore $A_{3,4} \neq B_4$, giving $A_{3,4} \notin l_{3,4}$.

This shows that we can satisfy all assumptions. For the new configuration with the same center M we can conclude by the induction hypothesis that also g_1, g_n and g_{n-1} pass through M. This then also holds for the original configuration. □

References

[1] H. Eves, *A Survey of Geometry.* Boston etc: Allyn and Bacon Inc, revised ed., 1972

[2] J. C. Fisher, L. Hoehn and E. M. Schröder, A 5-circle incidence theorem, *Math. Mag.*, 87 (2014) 44–49.
[3] J. C. Fisher, L. Hoehn and E. M. Schröder, Zwei Kreistheoreme für affin-metrische Ebenen, *Mitt. Math. Ges. Hamburg*, 33 (2013) 167–180.

J. Chris Fisher: 2616 Edgehill Road, Cleveland Heights, Ohio 44106-2806, USA
E-mail address: fisher@math.uregina.ca

Eberhard M. Schröder: FB Mathematik der Universität, Bundesstrasse 55, D 20146 Hamburg, Germany
E-mail address: eberhard.schroeder@gmx.net

Jan Stevens: Mathematical Sciences, University of Gotheburg, Chalmers University of Technology, SE 412 96 Gothenburg, Sweden
E-mail address: stevens@chalmers.se

Forum Geometricorum
Volume 15 (2015) 229–242.

FORUM GEOM
ISSN 1534-1178

A Study of Risāla al-Watar wa'l Jaib ("The Treatise on the Chord and Sine")

Mohammad K. Azarian

Abstract. *Risāla al-watar wa'l jaib* is one of the three most significant mathematical achievements of the Iranian mathematician and astronomer Ghiyāth al-Dīn Jamshīd Mas'ūd al-Kāshī (also known as Jamshīd Kāshānī; died 1429) that deals chiefly with the calculation of sine and chord of one-third of an angle with known sine and chord. The original manuscript is lost. However, since the core of this treatise was about the calculation of $\sin 1^\circ$, several of al-Kāshī's colleagues and successors have written commentaries in Arabic as well as Persian regarding the determination of $\sin 1^\circ$ motivated by al-Kāshī's iteration method. Our discussion will be based on *Sharh-i Zaīj-i Ulugh Beg* ("Commentaries on Ulugh Beg's Astronomical Tables"), written in Persian by the Persian astronomer and mathematician Nizām al-Dīn 'Abd al-'Alī ibn Muhammad ibn Husain al-Bīrjandī (also known as 'Abd al-'Alī Bīrjandī; died 1528). There are two parts in the calculation of $\sin 1^\circ$. First, al-Kāshī applied Ptolemy's theorem to an inscribed quadrilateral to obtain his famous cubic equation, and then he invented an ingenious and quickly converging iteration algorithm to calculate $\sin 1^\circ$ to 17 correct decimal digits (ten correct sexagesimal places) as a root of his cubic equation. Al-Kāshī completed this treatise sometime between 1424 and 1427.

Publication Date: October 28, 2015. Communicating Editor: Paul Yiu.

This work was supported by a grant from the John H. Schroeder Faculty Development Fund at the University of Evansville. The author presented this paper in two parts at the joint annual meetings of the American Mathematical Society and Mathematical Association of America in January 2014 and January 2015.

1. Preliminaries

The three greatest mathematical achievements of al-Kāshī [1] [2] [3] are: *al-Risāla al-muhītīyya* ("The Treatise on the Circumference"), *Miftāh al-hisāb* ("The Key of Arithmetic"), and *Risāla al-watar wa'l jaib* ("The Treatise on the Chord and Sine"). Al-Kāshī completed these three treatises in 1424, 1427, and sometime between 1424 (827 A.H.L.) and 1427 (830 A.H.L.), respectively. Many other mathematical discoveries and contributions of al-Kāshī are in conjunction with his work on astronomy. We direct the reader to [17] for a discussion of al-Kāshī's life and his other contributions to mathematics. For English summaries of *Meftah al-hesab* [*Miftāh al-hisāb*] and *al-Risāla al-muhītīyya* the reader is referred to [16] and [10], respectively. Our goal in this paper is the study of *Risāla al-watar wa'l jaib*. Unfortunately, the original manuscript of *Risāla al-watar wa'l jaib* is lost and sadly, there is not even a single extant treatise with this title. According to al-Kāshī himself, the core of this treatise was about the calculation of sine and chord of one-third of an angle with known sine and chord. Because of the importance and the applicability of $\sin 1^\circ$, several of al-Kāshī's colleagues and successors, as well as other mathematicians and astronomers, have written commentaries in Arabic as well as Persian regarding *Risāla al-watar wa'l jaib* and the determination of $\sin 1^\circ$ based on al-Kāshī's iteration method [4] in his *Risāla al-watar wa'l jaib.* All of these commentaries on *Risāla al-watar wa'l jaib* were written after al-Kāshī's death, because in these manuscripts al-Kāshī's name was accompanied by the word *rahimullah*,

[1] During the years 622 A.D. to 1600 A.D. a wealth of mathematics was preserved and advanced under the Islamic civilization, mostly in the current middle east and its surrounding areas. Although almost all of these advances and discoveries were recorded in Arabic (the common language of mathematics and sciences of that era), a majority of the authors were not Arabs. For example, all six principals of this paper are non-Arabs: Ulugh Beg, al-Rūmī, al-Qūshjī, and Chelebī are Turkish, and both Al-Kāshī and al-Bīrjandī are Persians. This is the reason that in the Persian literature and even some modern literature al-Kāshī (al-Kāshānī), al-Bīrjandī, al-Rūmī, and al-Qūshjī, are referred to as Kāshī (Kāshānī), Bīrjandī, Rūmī, and Qūshjī, without the definite article *al-* (*the*) in front of their names which is indicative of an Arabic name.

[2] The start of the Islamic calendar is the year 622 A.D., when prophet Muhammad migrated from his hometown of Mecca to the city of Medina, both cities in the Arabian peninsula. Prophet Muhammad's migration is called *hijra*. Nowadays, there are two Islamic calendars in use. One is the lunar calendar and the other is the solar calendar. The lunar calendar is 354 or 355 days long, while the solar calendar is 365 days long (the same length as the Gregorian calendar). In this paper, a year followed by "A.H.L."(After Hijra Lunar) represents an Islamic lunar year.

[3] Ghiyāth al-Dīn Jamshīd Mas'ūd al-Kāshī (also known as Jamshīd Kāshānī) was one of the most renowned mathematicians and astronomers in Persian history, and one of the most fascinating medieval Muslim mathematicians in the world. Kāshānī was born in Kāshān, a city in the central part of Iran in the second half of the fourteenth century and died on the morning of Wednesday June 22, 1429 (Ramadan 19, 832 A.H.L.) outside of Samarqand (in current Uzbekistan) at the observatory he had helped to build and directed for ten years. He was a mathematician, astronomer, and a physician by training. To call him a polyhistor is not an overstatement.

[4] To find an approximation for the $\sin 1^\circ$ as a root of his famous cubic equation (6), al-Kāshī coined a very clever iterative technique. This ingenious original procedure today is known as *fixed point iteration*, which is a standard root-finding technique in present day numerical analysis courses!

meaning "May God be merciful to him", a phrase used to refer respectfully to a deceased person.

Based on the Arabic manuscripts many mathematicians and astronomers in the West have written an account and/or translation of the calculation of $\sin 1^\circ$ by al-Kāshī. However, our discussion in this paper will be based on *Sharh-i Zaīj-i Ulugh Beg* ("The Commentary on Ulugh Beg's Astronomical Tables") [5] [6] written in Persian by the Persian astronomer and mathematician 'Abd al-'Alī al-Bīrjandī [7] which has not been studied yet. Al-Bīrjandī included the calculation of $\sin 1^\circ$ in *Bāb-i Duvvum* (Second Chapter) of *Maqāleh-i Duvvum* (Second Book) of his *Sharh-i Zaīj-i Ulugh Beg.*

The calculation of $\sin 1^\circ$ with a high degree of accuracy was a serious challenge for all mathematicians and astronomers since the early days of trigonometry, including Ptolemy and Nasīr al-Dīn Tūsī. It is very intriguing that after al-Kāshī's death his colleagues started discussing and presenting the calculation of $\sin 1^\circ$ in the same manner as al-Kāshī himself. At the Samarqand Observatory, it was customary for astronomers and mathematicians to present and discuss their scientific work with their peers. Al-Kāshī proudly and explicitly states the authoring of *Risāla al-watar wa'l jaib* in the introduction of his *Miftāh al-hisāb*, dedicated to Ulugh Beg. Undoubtedly he must have presented his work to his colleagues, or at least they were aware of the content of *Risāla al-watar wa'l jaib.* So, is it possible that someone purposely misplaced al-Kāshī's manuscript? Or is it possible that someone copied the content and then destroyed the manuscript? These are yet

---

[5] Ulugh Beg Guragān (1394-1449), grandson of Tīmūr, not only was a known mathematician and astronomer, but he also was a Tīmūrid sultan (king). Although he is better known as Ulugh Beg (Great Ruler), his actual name was Mīrzā Mohammad Tāraghay bin Shāhrukh. He has been credited for building both Ulugh Beg's state-of-the-art observatory and Ulugh Beg's Madrasa (School) in Samarqand as well as transforming both cities of Samarqand and Bukhara (in current Uzbekistan) into major cultural and learning centers.

[6] *Zaīj-i Ulugh Beg* was co-authored in 1437 by Ulugh Beg and a team of three other prominent Muslim astronomers al-Kāshī, al-Rūmī, and al-Qūshjī, who were cooperating in many other scientific projects at Ulugh Beg's observatory in Samarqand. It contained the most accurate astronomical tables and the most comprehensive catalogue of stars at that time. It surpassed the work of all previous astronomers, including Ptolemy's *Almagest* and Nasīr al-Dīn Tūsī's *Zīj-i Īlkhānī.*

[7] Nizām al-Dīn 'Abd al-'Alī ibn Muhammad ibn Husain al-Bīrjandī (known as 'Abd al-'Alī Bīrjandī; died 1528) a student (and colleague) of both Jamshīd al-Kāshī and his cousin Mu'īn al-Dīn al-Kāshī, was a renowned 16th century Persian astronomer, mathematician, physicist, and logician, who lived in Birjand, the center city of Southern Khorāsān province in Iran. Like most people of that era there is no record of his date of birth. However, it is believed that he died sometime in 934 A.H.L. (ca. 1528). He is buried in a village on the outskirts of the city of Birjand calld *Wujd*. From an inspiring list of Bīrjandī's work in diverse areas, without exaggeration, one could label him a polymath. He wrote some of his work in his native language Persian. However, to make his work more accessible to a wider readership he wrote most of his work in Arabic. Although he was known for his numerous contributions in astronomy, he also wrote impressive treatises, commentaries, and books on mathematics, astrology, logic, cosmology, and agriculture. What is even more impressive are his commentaries in Arabic concerning the sacred book of Islām, the holy Qurān. The most well known of his work in the West is his *Sharh-i Zaīj-i Ulugh Beg*, which is the main source of our paper [4-7].

other indications in support of A. Qurbani's argument [24] that (*i*) al-Kāshī did indeed complete *Risāla al-watar wa'l jaib*, and (*ii*) both al-Rūmī and al-Bīrjandī had a copy of *Risāla al-watar wa'l jaib* in their possession. Qurbani [24] claims that *A Treatise on the Determination of the Sine of One Degree With True Precision, Determined by the Most Perfect of the Geometers, Jamshīd al-Qāsānī [al-Kāshānī] Edited and Revised in This Letter by Qādī-Zādeh al-Rūmī, the Author of the Commentary on Chaghmīnī* is actually the recreation of *Risāla al-watar wa'l jaib* by al-Rūmī. We note that this is exactly the title of the manuscript used by Rosenfeld and Hogendijk [27].

We need to keep in mind that at the time of al-Kāshı̄, trigonometry was a very important and essential tool that played a key role in the study and application of astronomy, astrology, navigation, surveying, geography, and more. The study of the aforementioned subjects required the establishment of trigonometric tables with the most accurate values of trigonometric functions. The value of $\sin 1^\circ$ was the foundation for the calculations of all of these tables, yet a more precise value of $\sin 1^\circ$ was particularly desirable. The calculation of a highly accurate value of $\sin 1^\circ$ has been a serious challenge for mathematicians and astronomers alike, since at least Ptolemy's era and his famous astronomical masterpiece *Almagest* (The Greatest). A more precise value of $\sin 1^\circ$ along with some basic known trigonometric formulas such as $\sin(\alpha \pm \beta) = \sin\alpha \cdot \cos\beta \pm \cos\alpha \cdot \sin\beta$, $\sin^2\alpha + \cos^2\alpha = 1$, $\sin\alpha = \cos(90^\circ - \alpha)$, double-angle, and half-angle formulas, would have enabled one to find $\sin n^\circ$ and $\sin(\frac{1}{2^n})^\circ$, for all integers n. Also, one could have used $\sin n^\circ$, $\sin(\frac{1}{2^n})^\circ$, and interpolation algorithm to find the sine of other smaller angles as well. So, who had the talent, the ambition, the insight, and the imagination to tackle such a seemingly impossible task? Who else, but arguably the second Ptolemy, Jamshīd Kāshānī [8] [9]! Al-Kāshī's calculation of $\sin 1^\circ$, and of course his calculation of π with stunning accuracy for his time, are truly energizing and inspiring.

2. Manuscripts containing commentaries on *Risāla al-watar wa'l jaib* or the determination of the sine of one degree

In this section we present a list of extant manuscripts that include the calculation of $\sin 1^\circ$ and/or contain commentaries and expositions on *Risāla al-watar wa'l jaib*. These manuscripts may not necessarily be written by the authors themselves,

[8] From the standard Euclidian constructions, the values of $\sin 72^\circ$ and $\sin 60^\circ$ and the sine of many other angles were known to al-Kāshī. Also, the half angle formulas and the expansions of $\sin(\alpha \pm \beta)$ were known to him as well. Therefore, he had many options for finding the value of $\sin 3^\circ$, including the expansion of $\sin(18^\circ - 15^\circ)$.

[9] Finding a value for $\sin 1^\circ$ from $\sin 3^\circ$ is as challenging as trisecting an arbitrary angle into three equal parts using only a compass and an unmarked straightedge. The three most famous unsolved Greek problems of antiquity in the history of mathematics were trisecting an angle, doubling a cube, and squaring a circle. Pierre Wantzel in 1836 used Galois theory to show that trisecting an arbitrary angle by using only a compass and an unmarked straightedge is impossible [22].

but rather by some known or anonymous scribes. Detailed arguments for the authenticity of attributions of these manuscripts can be found in the references. The author himself examined the manuscripts at Tehran University, Malek National Library and Museum, and the Central Library of the Āstāne Qudse Razawī, the three well known research libraries for medieval scientific documents in Iran, and he has a copy of most of these manuscripts in his possession.

The following eight manuscripts of *Risāla fī istikhrāj jaib daraja wāhida* ("Treatise on the Determination of the Sine of One Degree") written in Arabic are attributed to al-Rūmī[10] (also known as Rūmī):

1-2. Number 3536/1 and Number 3180/11 of Malek National Library and Museum, Tehran, Iran. We note that the first one is the first treatise in Majmū' (Collection) Number 3536 and the second is the last treatise in Majmū' (Collection) Number 3180.

3-4. Number 12235/6 and Number 12225/4 of Central Library of the Āstāne Qudse Razawī, Mashhad, Iran.

5. Number 76 of Kandilli Observatory, Istanbul, Turkey.

6. Number 751/3 of Library of Hüseyin Chelebī, Istanbul, Turkey.

7. Number 37 of Mustafā Fādil collection, National Library, Cairo, Egypt. Also, a handwritten copy of this manuscript exists in the Scientific Library of the Humboldt University, Berlin, Germany.

8. Number 1531 (1519) of Majlis (Parliament) Library, Tehran, Iran, which is believed to be an incomplete copy.

Al-Kāshī's ingenious iteration method for estimation of $\sin 1^\circ$ was also included in many other texts including the following Persian manuscripts:

1. *Dar bayān-i istikhrāj-i jaib-i yak daraja* ("On the Explanation of the Determination of the Sine of One Degree"). This manuscript is attributed to al-Rūmī, and among other places, a copy of this treatise exists in the German State Library, Berlin (Pertsch n° 339).

2. A handwritten manuscript with the title, *Sharh-i Zaīj-i Ulugh Beg* is attributed to al-Qūshjī[11] (also known as Qūshjī). This is Number 3420 of Malek National Library and Museum, Tehran, Iran. Although it is believed that this manuscript is extant, it has not been studied yet.

3. *Dastūr al-'amal wa tashīh al-jadwal* ("The Rules of the Operation and Correction of the Table"), handwritten by Mīrim Chelebī[12] himself and also referred to as *Sharh-i Zaīj-i Ulugh Beg*. The microfilm Number 2341 of Tehran University is a copy of this manuscript. Also, a copy of this manuscript exists (Number 848-9) at

[10]The Turkish astronomer and mathematician Salāh al-Dīn Mūsā Qādī zāde al-Rūmī (1360-1437) was Ulugh Beg's teacher and his scientific mentor.

[11]The Turkish astronomer, mathematician, and physicist Alā al-Dīn Alī ibn Mohammad al-Qūshjī (1403-1474) known as Alī al-Qūshjī was a disciple of Ulugh Beg. He was born in Samarqand, and after Ulugh Beg's death he went to Kermān in Iran to continue his work in astronomy.

[12]The Turkish astronomer Mīrim Chelebī (1450-1525) was the grandson of both al-Rūmī and al-Qūshjī.

Ahmet Hamdi Tanpinar Literature Museum and Library, Istanbul, Turkey. Rosenfeld and Hogendijk [27] believe that this manuscript is based on *Sharh-i Zaīj-i Ulugh Beg* by al-Qūshjī and *Dar bayān-i istikhrāj-i jaib-i yak daraja* by al-Rūmī.

4. *Sharh-i Zaīj-i Ulugh Beg* (also called *Sharh-i Zaīj-i Sultānī*), written by al-Bīrjandī. Copies of this manuscript exist at Tehran University [4, 5], Āstāne Qudse Razawī [6], and Majlis Library [7]. Manuscript Number 704 of the Tashkent Institute for Oriental Studies, Tashkent, Uzbekistan, is believed to be a copy of the section of the second book of al-Bīrjandī's commentaries on the determination of $\sin 1^\circ$ [27].

Also, the following manuscripts of *Risāla fī istikhrāj jaib daraja wāhida* are among those with anonymous authors. Rosenfeld and Hogendijk [27] and others have speculated that the author of each of the following manuscripts must be al-Rūmī, Ulugh Beg, al-Qūshjī, or al-Kāshī himself.

1. Number 791 of Majlis Library (Tabātabāī Collection), Tehran, Iran.

2. Number 555/1 of Ketābkhān-i Madrasa-i Āli Shaheed Motahharī (Library of Martyr Motahharī's College), Tehran, Iran.

3. Number 3109 of the general collection of Al-Zahiriyah Library, Damascus, Syria.

4. MS. Arab. e.93, Bodleian Library, Oxford University, Oxford, England.

We caution the reader that there still may be some manuscripts that include the calculation of $\sin 1^\circ$ or contain commentaries and expositions on *Risāla al-watar wa'l jaib* that we are not aware of, or which have not been studied yet. Also, we note that there may be copies of the above manuscripts with some minor comments in certain small libraries or private collections.

3. Modern Commentaries and Translations

As we discussed in the previous section the early commentaries on *Risāla al-watar wa'l jaib* were written in Arabic or Persian. However, because of the importance of the calculation of $\sin 1^\circ$, the commentaries on *Risāla al-watar wa'l jaib* has been translated and/or commented on by various historians of mathematics and astronomy into English, French, German, and Russian.

In 1954, A. Aaboe [1] presented a sketch of the calculation of $\sin 1^\circ$ in English from Chelebī's manuscript and included his own additional commentaries and insights. In 2000, A. Ahmedov and B. A. Rosenfeld [3] presented English commentaries along with a sketch of the calculation of $\sin 1^\circ$ based on an Arabic manuscript entitled *Risāla fī istikhrāj jaib daraja wāhida*, and they argued that the author of the Arabic manuscript that they used was Ulugh Beg. However, E. Calvo, who reviewed this paper for *Mathematical Reviews* [MR 1977597(2004d:01006)], attributed the manuscript to al-Rūmī. Also, in 2003, B. A. Rosenfeld and J. P. Hogendijk in [27] provided an English translation with commentaries of an anonymous [13] Arabic manuscript that they obtained from Tehran, but the title suggested

[13] Rosenfeld and Hogendijk speculated that the author of their manuscript could be al-Kāshī himself, al-Rūmī, Ulugh Beg, or al-Qūshjī. However, Rosenfeld argued strongly in favor of Ulugh Beg as the probable author of their manuscript.

that it must have been written in Turkey. The entire English title of this lithograph manuscript is *A Treatise on the Determination of the Sine of One Degree With True Precision, Determined by the Most Perfect of the Geometers, Jamshīd al-Qāsānī* [*al-Kāshānī*] *Edited and Revised in This Letter by Qādī-Zādeh al-Rūmī, the Author of the Commentary on Chaghmīnī.* They appended a facsimile of Tehran's lithograph edition to their paper. Finally, F. Riahi [25] presented al-Kāshānī's calculation of $\sin 1^\circ$ in decimal system without mentioning *Risāla al-watar wa'l jaib*. In this article, Riahi added his own insight as well as some intriguing historical commentaries.

The section regarding the calculation of $\sin 1^\circ$ of Chelebī's manuscript *Dastūr al-'amal wa tashīh al-jadwal* has been translated into French by L. A. Sédillot in 1853 [32, 33]. In 1854, the German Orientalist and mathematician F. Woepcke used Chelebī's manuscript and discussed al-Kāshī's method of calculation of $\sin 1^\circ$ in German, and incorrectly called it "Chelebī's method". Apparently Woepcke used infinite series in his discussion and this caused his calculations to be somewhat unclear [1]. Also, C. Schoy translated part of Chelebī's commentaries into German in 1922 [31].

In 1960, B. A. Rosenfeld and A. P. Youschkevitch translated the Arabic manuscript [9] into Russian along with a historical introduction and commentaries [29, 30]. The title of [9] suggests that the manuscript is that of al-Rūmī. Nonetheless, E. S. Kennedy, who reviewed this article for *Mathematical Reviews* [MR0132682-4 (24 #A2521a-c)] stated that the numerical solution that the authors presented for the calculation of $\sin 1^\circ$ was based on an iterative method by Jamshīd al-Kāshī.

4. Determination of Sine of One Degree

In this section we present the calculation of $\sin 1^\circ$ both in sexagesimal [14] as well as the decimal systems. Our calculation of $\sin 1^\circ$ will be based on the calculation of $\sin 1^\circ$ by al-Bīrjandī in his *Sharh-i Zaīj-i Ulugh Beg* [5]. Throughout the proof we use $crd\ \alpha$ to represent the chord of the central angle α. There are two parts in the calculation of $\sin 1^\circ$. First, al-Kāshī applied Ptolemy's theorem to an inscribed quadrilateral to obtain his famous cubic equation, and then he invented an ingenious and quickly converging iteration algorithm to calculate $\sin 1^\circ$ to 17 correct decimal digits (ten correct sexagesimal places) as a root of his cubic equation. It is remarkable that al-Kāshī used both geometry and algebra to approximate $\sin 1^\circ$, to any desired accuracy! Not only was this the most fascinating and creative method of approximation, but it was the most significant achievement in medieval algebra. This was also the most accurate approximation of sin 1° at that time. The best previous approximations, correct to four sexagesimal places, were obtained in the tenth century by two other Muslim scientists Abu'l-Wafā' al-Būzjānī (940-998)

[14] We recall that in sexagesimal system (base 60) the digits are separated by commas, and the integral and fractional parts by semicolon. For example, $1, 23, 4; 56, 17, 8$ in sexagesimal system is the following number in the decimal system

$$1 \cdot 60^2 + 23 \cdot 60^1 + 4 \cdot 60^0 + 56 \cdot 60^{-1} + 17 \cdot 60^{-2} + 8 \cdot 60^{-3}.$$

and Abu'l-Hasan ibn Yunus (c. 950-1009). Al-Kāshī's approximation of $\sin 1^\circ$ was not surpassed until 16th century by Taqī al-Dīn Muhammad al-Asadī (1526–1585).

4.1. *Sexagesimal calculation of the sine of one degree.* Our sexagesimal calculation of $\sin 1^\circ$ will be based on A. Qurbanī's calculation of $\sin 1^\circ$ in Persian [24], whose main source was al-Bīrjandī's *Sharh-i Zaīj-i Ulugh Beg* [4-7].

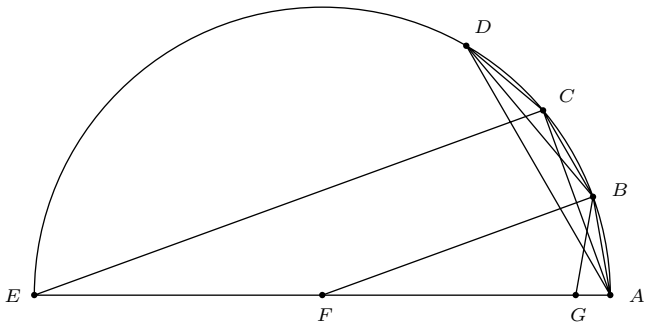

Figure 1

Al-Kāshī let A, B, C, D be points on a semicircle with center F and radius r (Figure 1) such that $AB = BC = CD = crd\ 2^\circ$. By Ptolemy's theorem [15],

$$AB \cdot CD + BC \cdot AD = AC \cdot BD.$$

Since $BD = AC$, al-Kāshī obtains

$$AB^2 + BC \cdot AD = AC^2. \tag{1}$$

Also, since $AB = BC = CD = crd\ 2^\circ$, implies that $AD = crd\ 6^\circ$, al-Kāshī multiplies $\sin 3^\circ$ by 2 to get the length of AD in sexagesimal system as [16]

$$AD = 2 \cdot 60 \cdot \sin 3^\circ = 6; 16, 49, 7, 59, 8, 56, 29, 40.$$

Next, he let

$$x = AB = BC = CD,$$

and uses (1) to obtain

$$x^2 + x(crd\ 6^\circ) = AC^2. \tag{2}$$

Al-Kāshī determines the point G on the diameter EA in a such a way that $EC = EG$. Then, from the similar isosceles triangles ABG and ABF, he gets

$$\frac{AB}{AG} = \frac{AF}{AB}, \text{ and hence } AG = \frac{AB^2}{r}.$$

[15] *If a quadrilateral is inscribed in a circle, then the product of the lengths of its diagonals is equal to the sum of the products of the lengths of the pairs of opposite sides.* We note that from Ptolemy's theorem many trigonometric identities can be obtained including the half angle and double angle identities as well as the identities $\sin(\alpha \pm \beta) = \sin\alpha \cdot \cos\beta \pm \cos\alpha \cdot \sin\beta$.

[16] It can easily be verified that if 2α is a central angle in a circle of radius r, then $crd(2\alpha) = 2r \sin\alpha$.

By assuming that the radius of the semicircle (Figure 1) is 60, he obtains

$$GE = AE - AG = 120 - \frac{AB^2}{60}. \tag{3}$$

From (3), the right triangle ACE, and the fact that $EC = EG$, al-Kāshī obtains

$$AC^2 = AE^2 - EC^2 = (120)^2 - \left(120 - \frac{AB^2}{60}\right)^2,$$

which is equivalent to

$$AC^2 = 4AB^2 - \left(\frac{AB^2}{60}\right)^2. \tag{4}$$

Again, from (2) and (4) he gets

$$x^2 + x(crd\ 6^\circ) = 4x^2 - \frac{x^4}{3600},$$

and he deduces that

$$crd\ 6^\circ = 3x - \frac{x^3}{3600}. \tag{5}$$

Finally, from (5) he obtains the famous al-Kāshī's cubic equation

$$x = \frac{x^3 + (60)^2 crd\ 6^\circ}{3(60)^2}.$$

He proceeds in solving his cubic equation to find an approximation for $\sin 1^o$, by first letting

$$a = (60)^2 crd\ 6^\circ = 6, 16, 49; 7, 59, 8, 56, 29, 40, \text{ and } b = 3(60)^2,$$

to obtain

$$x = \frac{a + x^3}{b}. \tag{6}$$

Al-Kāshī represents x in (6) as

$$x = s_1 + s_2 + s_3 + \cdots, \tag{7}$$

where s_i $(i = 1, 2, 3, 4, \cdots)$ are the sexagesimal digits of x. Since in a circle of radius 60, the values of $x = crd\ 2^\circ$ and x^3 are small, and hence the value of $\frac{x^3}{3 \cdot (60)^2}$ is even smaller, he safely let $x_1 \approx \frac{a}{b}$. In fact, he picks x_1 to be exactly the integer part of $\frac{a}{b}$ as follows

$$\begin{aligned} \frac{a}{b} &= \frac{6(60)^2 + 16(60) + 49 + 7(60)^{-1} + 59(60)^{-2} + \cdots + 40(60)^{-6}}{3(60)^2} \\ &= 2 + \frac{16(60) + 49 + 7(60)^{-1} + 59(60)^{-2} + \cdots + 40(60)^{-6}}{3(60)^2}. \end{aligned}$$

Hence, $x_1 = s_1 = 2$, which is the first sexagesimal digit of x. Now, he puts this value of s_1 in (7) and obtains

$$\begin{aligned} s_2 + s_3 + \cdots &= \frac{a + x_1^3}{b} - 2 = \frac{a - 2b + 2^3}{b} \\ &= \frac{6(60)^2 + 16(60) + 49 + \cdots + 40(60)^{-6} - 2 \cdot 3(60)^2 + 2^3}{3(60)^2} \\ &= \frac{16(60) + 49 + \cdots + 40(60)^{-6} + 2^3}{3(60)^2} \\ &= \frac{5}{60} + \frac{60 + 49 + \cdots + 40(60)^{-6} + 2^3}{3(60)^2}. \end{aligned}$$

Thus, $s_2 = \dfrac{5}{60}$, and hence $x_2 = 2 + \dfrac{5}{60}$. Similarly, from

$$s_3 + s_4 + \cdots = \frac{a + x_2^3}{b} - (s_1 + s_2) = \frac{a + (s_1 + s_2)^3 - b(s_1 + s_2)}{b},$$

al-Kāshī calculates $s_3 = \dfrac{39}{60^2}$, and consequently gets

$$x_3 = 2 + \frac{5}{60} + \frac{39}{60^2},$$

which is $2; 5, 39$ in the sexagesimal system. Al-Kāshī uses

$$x_{n+1} = \frac{a + x_n^3}{b},\ n \geqslant 3,$$

and continues his calculations as above to produce [17]

$$crd\ 2^\circ = 2; 5, 39, 26, 22, 29, 28, 32, 52, 33.$$

Next, he divides this value of $crd\ 2^\circ$ by 2, to achieve [18]

$$jaib\ 1^\circ = 1; 2, 49, 43, 11, 14, 44, 16, 26, 17,$$

which is correct to ten sexagesimal places. [19] Then, he divides the decimal value of the above result by 60, to find the value of $\sin 1^\circ$ in decimal system as

$$\sin 1^\circ = 0.017452406437283510 3712,$$

where the first 17 digits after the decimal point are correct.

---

[17] It is fascinating to note that each iteration produces one sexagesimal digit of the approximation of $crd\ 2^\circ$, and each iteration step requires only three simple operations; namely, cubing a number, an addition, and a division.

[18] Al-Kāshī used *jaib* (also spelled as *jayb*) of α to represent the sine of α in base 60. Therefore, $jaib\ 1^\circ = 60 \cdot \sin 1^\circ$.

[19] To find the value of $\sin 1^\circ$ in decimal system we convert

$$1; 2, 49, 43, 11, 14, 44, 16, 26, 17$$

from sexagesimal system to decimal system as follows

$$1 \cdot 60^0 + 2 \cdot 60^{-1} + 49 \cdot 60^{-2} + 43 \cdot 60^{-3} + \cdots + 26 \cdot 60^{-8} + 17 \cdot 60^{-9}.$$

4.2. *Decimal calculation of the sine of one degree.* As in §4.1, Al-Kāshī's calculation of $\sin 1^\circ$ was in sexagesimal system. However, since readers are more comfortable with the decimal system, in this section we present the calculation of $\sin 1^\circ$ in decimal system. Our decimal calculation will be based on al-Bīrjandī's *Sharh-i Zaīj-i Ulugh Beg* [5, 25].

Al-Kāshī let A, B, C, D be points on a semicircle with center F and radius r (Figure 1) such that $AB = BC = CD$. By Ptolemy's theorem,

$$AB \cdot CD + BC \cdot AD = AC \cdot BD.$$

Since $AB = CD = BC$ and $BD = AC$, he obtains

$$AB^2 + BC \cdot AD = AC^2. \tag{8}$$

Then al-Kāshī determines the point G on the diameter AE in a such a way that $EC = EG$. He observes that from the similar isosceles triangles ABG and ABF, he has $\dfrac{AB}{AG} = \dfrac{AF}{AB}$. Hence $AG = \dfrac{AB^2}{r}$, and thus

$$EG = 2r - AG = 2r - \frac{AB^2}{r}.$$

From the right triangle AEC, he gets

$$AC^2 = AE^2 - EC^2 = 4r^2 - EG^2, \tag{9}$$

and from (9), he deduces that

$$AC^2 = 4r^2 - (2r - \frac{AB^2}{r})^2 = 4AB^2 - \frac{AB^4}{r^2}. \tag{10}$$

Also, from (8) and (10) he obtains

$$AB^2 + AB \cdot AD = 4AB^2 - \frac{AB^4}{r^2},$$

and consequently he achieves

$$AD = 3AB - \frac{AB^3}{r^2}. \tag{11}$$

If $AB = crd\, 2\alpha$, then clearly $AD = crd\, 6\alpha$. From (11) and Footnote 16, al-Kāshī deduces [20] that

$$\sin 3\alpha = 3\sin\alpha - 4\sin^3\alpha. \tag{12}$$

Finally, he let $\alpha = 1^\circ$, $x = \sin 1^\circ$, and uses (12) to obtain

$$x = \frac{4}{3}x^3 + \frac{1}{3}\sin 3^\circ. \tag{13}$$

To find an approximation for $\sin 1^\circ$ as a root of (13) al-Kāshī proceeds as follows: Since $\sin 1^\circ$ is close to $\frac{1}{3}\sin 3^\circ = 0.0174453\cdots$, he let his initial estimate

[20] The discovery of the formula $\sin 3\alpha = 3\sin\alpha - 4\sin^3\alpha$ by al-Kāshī was a bonus for his quest in finding a highly accurate value of $\sin 1^\circ$. This formula was not known in the West until the sixteenth century when it was rediscovered by François Viète. As a second bonus, al-Kāshī invented an iterative method for solving cubic equations, yet his method was not discovered in the west until centuries later.

be $x_0 = 0.01$, and subsequent decimal estimations of the root to be of the form $x = 0.01d_1d_2d_3d_4\cdots$, where $0 \le d_i \le 9$. Al-Kāshī puts this initial estimate as well as the known value of $\frac{1}{3}\sin 3^\circ$ in (6) to get

$$0.01d_1d_2d_3d_4\cdots = \frac{4}{3}(0.01d_1d_2d_3d_4\cdots)^3 + \frac{1}{3}\sin 3^\circ, \tag{14}$$

and then he subtracts 0.01 from both sides to obtain

$$0.00d_1d_2d_3d_4\cdots = \frac{4}{3}(0.01d_1d_2d_3d_4\cdots)^3 + 0.0074453\cdots .$$

Now, the first nonzero digit in the above cubic term is in the sixth decimal place, and since the above equality must hold true digit by digit, he gets $d_1 = 7$, and hence, $x_1 = 0.017$. Next, he substitutes this value of d_1 in (14) and subtracts 0.017 from both sides to get

$$0.000d_2d_3d_4\cdots = \frac{4}{3}(0.017d_2d_3d_4\cdots)^3 + 0.0004453\cdots .$$

He applies the same argument as above and gets $d_2 = 4$, and thus $x_2 = 0.0174$. He continues his calculations in a similar fashion to get $d_3 = 5$, $d_4 = 2$, ..., and $d_{20} = 2$, and consequently, al-Kāshī achieves the approximation

$$0.01745240643728351037 12$$

for $\sin 1^\circ$, where the first 17 digits are correct[21].

References

[1] Asger Aaboe, *Al-Kashi's Iteration Method for the Determination of Sin* 1°, Scripta Mathematica, Vol.20, 1954, 24-29.

[2] Asger Aaboe, *Episodes from the Early History of Mathematics*, Random House, New York, 1964.

[3] A. Ahmedov and B. A. Rosenfeld,*The mathematical treatise of Ulugh Beg*, in: Science in Islamic Civilization, Istanbul: IRCICA, 2000, 143-150. MR1977597 (2004d:01006).

[4] Nizām al-Dīn 'Abd al-'Alī al-Bīrjandī, *Sharh-i Zaīj-i Ulugh Beg*, Tehran University library, manuscript number 2674 (in Persian), Tehran, Iran.

[5] Nizām al-Dīn 'Abd al-'Alī al-Bīrjandī, *Commentary on Ulugh Beg's Astronomical Tables*, Tehran University library, manuscript number 473 (in Persian), Tehran, Iran.

[6] Nizām al-Dīn 'Abd al-'Alī al-Bīrjandī, *Sharh-i Zaīj-i Ulugh Beg*, Number 14021 of the mathematics collection (in Persian) of the Central Library of the Āstān Qudse Razawī, Mashhad, Iran, 929 A.H.L.

[7] Nizām al-Dīn 'Abd al-'Alī al-Bīrjandī, *Sharh-i Zaīj-i Sultānī*, Majlis Library, manuscript number 2543 (in Persian), Tehran, Iran.

[8] Jamshīd al-Kāshī, *Miftāh al-hisāb, Risāla al-muhītīyya-Klyuch arifmetiki. Traktat ob okruzhnosti* (Arabic and Russian translation by B. A. Rosenfeld). Moscow: GITTL, 1956.

[9] Kazi-Zade al-Rumi, *Traite sur la determination du sinus d'un degre*, Istor.-Mat. Issled. Vol. 13 (1960), 539-552. MR0132683 (24 #A2521b).

[21] As in the case of sexagesimal calculations, it is intriguing to observe that again each iteration of this original iterative method provides at least one correct decimal digit of the approximation of $\sin 1^\circ$, and each step requires only a few simple operations.

[10] Mohammad K. Azarian, *Al-Risala al-Muhitiyya: A Summary*, Missouri Journal of Mathematical Sciences, Vol. 22, No. 2, 2010, 64-85. Mathematical Reviews, MR2675403 (2011e:01005). Zentralblatt MATH, Zbl 1204.01009.

[11] Mohammad K. Azarian, *The Introduction of al-Risāla al-Muhīṭiyya: An English Translation*, International Journal of Pure and Applied Mathematics, Vol. 57, No. 6, 2009, 903-914. Mathematical Reviews, MR2676249 (2011e:01004). Zentralblatt MATH, Zbl 1198.01003.

[12] Mohammad K. Azarian, *On the Fixed Points of a Function and the Fixed Points of its Composite Functions*, International Journal of Pure and Applied Mathematics, Vol. 46, No. 1, 2008, pp. 37-44. Mathematical Reviews, MR2433713 (2009c:65129), March 2009. Zentralblatt MATH, Zbl 1160.65015.

[13] Mohammad K. Azarian, *Fixed Points of a Quadratic Polynomial, Problem 841*, College Mathematics Journal, Vol. 38, No. 1, January 2007, p. 60. Solution published in Vol. 39, No. 1, January 2008, 66-67.

[14] Mohammad K. Azarian, *Forty-Five Nested Equilateral Triangles and* $\csc 1^\circ$, *Problem 813*, College Mathematics Journal, Vol. 36, No. 5, November 2005, 413-414. Solution published in Vol. 37 , No. 5, November 2006, 394-395.

[15] Mohammad K. Azarian, *Al-Kāshī's Fundamental Theorem*, International Journal of Pure and Applied Mathematics, Vol. 14, No. 4 (2004), 499–509. Mathematical Reviews, MR2072161 (2005b:01021). Zentralblatt MATH, Zbl 1059.01005.

[16] Mohammad K. Azarian, *Meftah al-hesab [Miftāh al-hisāb]: A Summary*, Missouri Journal of Mathematical Sciences, Vol. 12, No. 2 (2000), 75–95. Mathematical Reviews, *MR* 1 764 526, Zentralblatt MATH, Zbl 1036.01002.

[17] Mohammad K. Azarian, *A Summary of Mathematical Works of Ghiyāth ud-Dīn Jamshīd Kāshānī*, Journal of Recreational Mathematics, Vol. 29, No. 1 (1998), 32-42. Math Edu, ME 1999a.00015.

[18] John L. Berggren, *Episodes in the Mathematics of Medieval Islam*, Springer-Verlag, New York, New York, 1986.

[19] A. P. Guschkewitsch, *Jeschichte der mathematik im mittelalter*, Leipzig, 1964.

[20] Victor. J. Katz, *A History of Mathematics*, HarperCollins, New York, 1993.

[21] D. A. King, *A Survey of Scientific Manuscripts in the Egyptian National Library*, Winona Lake, Indiana, Eisenbrauns, 1986.

[22] Jesper Lützen, *Why was Wantzel overlooked for a century? The changing importance of an impossibility result*, Historia Math. 36 (2009), no. 4, 374-394.

[23] Claudius Ptolemy, *Almagest*, translated by G. J. Toomer. New York, Springer Verlag, 1984.

[24] Abu'l-Qāsim Qurbānī, *Kāshānī nāmeh* [A monograph on Ghiyāth al-Dīn Jamshīd Mas'ūd al-Kāshī], Tehran University Press, Tehran, Iran,1971(1350 A.H.S.). Revised edition 1989 (1368 A.H.S.).

[25] Farhad Riahi, *An Early Iterative Method for the Determination of sin* 1°, The College Mathematics Journal, Vol. 26, No. 1 (Jan., 1995), 16-21.

[26] Boris A. Rosenfeld and Ekmeleddin Ihsanoğlu, *Mathematicians, Astronomers, and Other Scholars of Islamic Civilization and Their Works* (7th-19th C.), Istanbul: IRCICA, 2003.

[27] Boris A. Rosenfeld and Jan P. Hogendijk, *A mathematical treatise written in the Samarqand observatory of Ulugh Beg*, Z. Gesch. Arab.-Islam. Wiss. 15 (2002/2003), 25-65. MR2024919 (2004k:01013).

[28] Boris A. Rosenfeld and Adolf P. Youschkevitch, *Ghiyath al-din Jamshid Masud al-Kashi (or al-Kashani)*, Dictionary of Scientific Biography, Vol. 7 (1981), 255-262.

[29] Boris A. Rosenfeld and Adolf P. Youschkevitch, *Le traite de Kazi-zade al-Rumi sur la determination du sinus d'un degre*, Istor.-Mat. Issled. Vol. 13 (1960), 533-538. MR0132682 (24 #A2521a).

[30] Boris A. Rosenfeld and Adolf P. Youschkevitch, *Notes au traite de Kazi-zade al-Rumi*, Istor.-Mat. Issled. Vol. 13 (1960), 552-556. MR0132684 (24 #A2521c).

[31] Carl Schoy, *Beitrage zur arabischen Trigonometrie*, ISIS, vol. V, 1922, 364-399.

[32] L. A. Sédillot, *De l'algegre chez les Arabes*, Journal asiatique, 5eme Serie, 2 (1853), 323-356.

[33] L. A. Sédillot, *Prolegomenes des tables astronomiques d Oloug-Beg*, traduction et commentaires, Paris, 1853, 77-83.
[34] Nathan Sidoli and Glen Van Brummelen, *From Alexandria, Through Baghdad, Surveys and Studies in the Ancient Greek and Medieval Islamic Mathematical Sciences in Honor of J. L. Berggren*, Springer-Verlag, 2014.
[35] Glen Van Brummelen, *Heavenly Mathematics, The Forgotten Art of Spherical Trigonometry*, Princeton University Press, 2013.
[36] Glen Van Brummelen, *The Mathematics of the Heavens and the Earth, The Early History of Trigonometry*, Princeton University Press, 2009.
[37] Glen Van Brummelen, *Jamshid al-Kāshī Calculating Genius*, Mathematics in School, September 1998, 40-44.
[38] Franz Woepcke, *Discution de deux methodes Arabes pour determiner une valeur approchee de sin 1*, Journal de math. pures et appliquees, tome 19, 1854, 153-176, 301-303.

Mohammad K. Azarian: Department of Mathematics, University of Evansville, 1800 Lincoln Avenue, Evansville, Indiana 47722, USA

E-mail address: azarian@evansville.edu

Forum Geometricorum
Volume 15 (2015) 243–251.

FORUM GEOM
ISSN 1534-1178

Topological Treatment of Platonic, Archimedean, and Related Polyhedra

Tom M. Apostol and Mamikon A. Mnatsakanian

Abstract. Platonic and Archimedean polyhedra and generalizations are treated in a unified manner by a method that focuses on topological properties of networks on a sphere rather than metric properties regarding lengths of edges or measurement of angles. This approach reveals new insights into the structure of these polyhedra.

1. Introduction and terminology

A Google search reveals that a large literature exists on five Platonic and thirteen Archimedean polyhedra. They are usually studied with the aid of Euler's classical formula

$$V + F = E + 2, \tag{1}$$

relating the number E of edges, the number F of faces, and the number V of vertices of any convex polyhedron, together with metric properties of regular polygonal planar faces. We treat Platonic and Archimedean polyhedra and their generalizations by a method that focuses on topological properties of networks rather than metric properties regarding lengths of edges or measurement of angles.

1.1. *General networks.* Consider V distinct points on the surface of a topological sphere, where $V \geq 2$. These are called *vertices*. An *edge* is any simple curve on the sphere joining two distinct vertices as end points and having no other vertices on it. A *V-network* is any configuration of nonintersecting edges joining V vertices. A *face* is a region on the sphere bounded by edges and vertices that contains no edges or vertices in its interior. We denote by E the number of edges, and by F the number of faces in the network.

When $V = 2$, a network can be formed by joining the two vertices by one curve, in which case $E = F = 1$. But the two vertices can also be joined by any number $E \geq 2$ of nonintersecting curves to form arbitrarily many networks with $E = F$.

1.2. *Triangular networks.* When each face is topologically equivalent to a triangle, as in the examples in Figure 1, the network is called a *triangular network*. Figure 1a shows a triangular network with 3 vertices, 3 edges, and 2 faces. The examples in Figures 1b and 1c have 4 vertices, 6 edges, and 4 faces.

Publication Date: October 28, 2015. Communicating Editor: Paul Yiu.

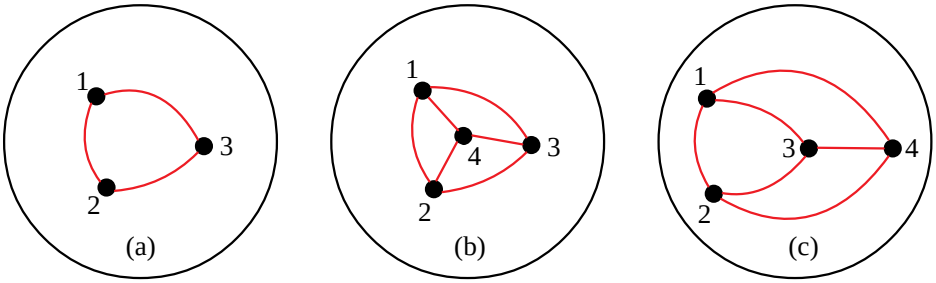

Figure 1. Triangular network with $V = 3$ in (a) and with $V = 4$ in (b) and (c).

2. Basic counting lemma for triangular networks

In a general network with $V = 2$, Euler's formula (1) implies that the number F of faces is always equal to the number E of edges, which can be arbitrary. Our first principal result is a Counting Lemma that gives explicit formulas expressing E and F in terms of V in any triangular network. The Counting Lemma can also be used to prove Euler's formula in a general network, and yields information for triangular networks not obtainable from Euler's formula alone. Therefore the Counting Lemma is a deeper result than Euler's formula.

Lemma 1 (Counting Lemma)**.** *In any triangular network with $V \geq 3$, the number of edges is $E = 3V - 6$, and the number of faces is $F = 2V - 4$.*

Proof. We shall prove both formulas by induction on V. When $V = 3$, we label the vertices as 1, 2, 3 as in Figure 1a. The number of edges joining them is 3, and the number of faces is 2, so $3V-6 = 3$ and $2V-4 = 2$ when $V = 3$, which agrees with the lemma. Now consider four vertices 1, 2, 3, 4. The first 3 are vertices of a triangle. Vertex 4 is either inside this triangle, as in Figure 1b, or outside as in Figure 1c, because it cannot be on one of its edges. Three edges are required to join vertex 4 to the other three vertices, giving a total of 6 edges and 4 faces, so $3V - 6 = 6$ and $2V - 4 = 4$ when $V = 4$, which agrees with the lemma.

Now assume the lemma is true for some fixed number of vertices $k \geq 3$ and consider a $(k + 1)$-triangular network joining vertices labeled $1, 2, ..., k + 1$. If we remove vertex $k + 1$ we are left with a new k-network that is no longer triangular. In the original $(k + 1)$-network, vertex $k + 1$ was connected to a certain number of vertices, say p, where $p \geq 3$, so the new k-network has p fewer edges than the $(k + 1)$-triangular network. However, this new network can be triangulated by adding $p - 3$ diagonal edges from one vertex to $p - 3$ vertices. This new triangulated network has k vertices so, by the induction hypothesis it has $3k - 6$ edges and $2k - 4$ faces, which gives three less than the number of edges and two less than the number of faces in the original $(k + 1)$-triangular network. So these latter numbers are $(3k - 6) + 3 = 3(k + 1) - 6$, and $(2k - 4) + 2 = 2(k + 1) - 4$, as required. This completes the proof by induction. □

For any triangular network, the Counting Lemma gives $V+F = 3V-4 = E+2$, which is Euler's theorem in (1). But it is well known (see [1, p. 239]) that if Euler's

formula holds for a triangular network then it also holds for a general network. Therefore, the Counting Lemma implies Euler's theorem for a general network.

The formula $E = 3V - 6$ is known (see [3, p. 240], where it is deduced from Euler's formula and the "handshake lemma"). Our analysis yields both $E = 3V-6$ and the companion result $F = 2V - 4$ without invoking Euler's formula.

2.1. *Triangulated networks realized as polyhedra inscribed in a convex sphere.* Given a triangulated network with $V \geq 3$, we can replace each edge by a line segment to form a configuration in 3-space that we call a *triangulated polyhedron*, inscribed in a convex sphere.

When $V = 3$ the configuration consists of a triangle with its vertices on the sphere. The Counting Lemma gives $E = 3$ and $F = 2$, and we regard this as a degenerate triangular prism of altitude zero, with two overlapping triangular faces.

When $V = 4$, the Counting Lemma gives $F = 4$ and $E = 6$; the triangulated polyhedron becomes a *tetrahedron* (inscribed in a sphere) with four triangular faces and six edges, as suggested by Figures 1b and 1c.

When $V = 6$, the Counting Lemma gives $F = 8$ and $E = 12$; the polyhedron can be realized as an *octahedron*, with eight triangular faces and twelve edges.

When $V = 12$, the Counting Lemma gives $F = 20$ and $E = 30$; the polyhedron can be realized as an *icosahedron*, with twenty triangular faces and thirty edges.

The tetrahedron, octahedron and icosahedron are three of the classical Platonic solids. The degenerate prism is not counted among the Platonic solids.

2.2. *Application to triangulated Platonic networks.* In any network, each edge connects two vertices. We divide each edge into two pieces, that we call *branches*, with one endpoint of each branch being a vertex of the network. By the Counting Lemma, every V-triangular network contains $6V - 12$ branches.

We define a *triangulated Platonic network* to be any triangulated network having the same number of branches at each vertex. Let's find those values of V for which triangulated Platonic networks exist. In such a network, the total number of branches is $6V - 12$, so the number of branches at each vertex is$(6V - 12)/V = 6 - 12/V$. Hence a triangulated Platonic network exists if, and only if, the ratio $12/V$ is an integer less than 6. Thus V must be a divisor of 12, so the possible values of $V \geq 3$ are 3, 4, 6, and 12. In other words, there are exactly four triangulated Platonic networks. They can be realized as polyhedra inscribed in a convex sphere. These are the degenerate triangular prism with 2 faces, and the three Platonic solids mentioned earlier: tetrahedron, octahedron, and icosahedron, with respective number of faces 4, 8, and 20. The cube, with 8 vertices, 12 edges, and 6 faces is also called a Platonic polyhedron, but it is not triangulated because its faces are squares. Another Platonic polyhedron, not triangulated, is the dodecahedron, with 12 pentagonal faces, 30 edges, and 20 vertices. The cube and dodecahedron will be treated in the next section.

3. General uniform networks

A general uniform network is one in which there may be two or more different types of polygonal faces around each vertex, say n_3 triangles, n_4 quadrilaterals, n_5 pentagons, etc. The term *uniform* means that the same configuration occurs at each vertex. The number of polygonal faces around each vertex is $n_3 + n_4 + n_5 + \cdots$. Thus if there are e branches meeting at each vertex we have

$$e = n_3 + n_4 + n_5 + \cdots . \tag{2}$$

Because e branches meet at each vertex, the number E of edges is given by

$$E = \frac{e}{2}V. \tag{3}$$

Solve for F in Euler's theorem (1) and use (3) to obtain

$$F = \frac{e-2}{2}V + 2. \tag{4}$$

This basic relation holds in every general uniform network.

We call the network *Platonic* if only one of the n_k is nonzero. For example, if n_3 is the only nonzero n_k the network is a triangulated Platonic network, all of which we have found earlier. Next we determine all general uniform Platonic networks. Note that our definition of *Platonic* makes no reference to lengths of edges or regularity of faces.

3.1. *k-gonal Platonic networks.* Assume that each face in a Platonic network is a k-gon, where $k \geq 3$. Each face has k edges, and each edge belongs to two faces, hence the total number of edges E is $k/2$ times F, the number of faces, so using (3) we have:

$$F = \frac{2}{k}E = \frac{e}{k}V. \tag{5}$$

Using this in (4) and solving for V we obtain

$$V = \frac{4k}{2k + e(2-k)}. \tag{6}$$

This is an explicit formula for the number V of vertices in a k-gonal Platonic network in which e branches meet at each vertex. By letting k take successive values $3, 4, 5, \ldots$ we can determine all uniform Platonic networks.

For example, when $k = 3$, (6) becomes $V = 12/(6 - e)$, hence $6 - e$ must be a divisor of 12. The possible values of e are 3, 4, and 5, which yield, respectively, $V = 4$, $V = 6$, and $V = 12$. The corresponding regular polyhedra are the tetrahedron, octahedron, and icosahedron, found earlier as triangulated polyhedra.

When $k = 4$, (6) gives $V = 8/(4-e)$, which becomes $V = 8$ when $e = 3$. The corresponding regular polyhedron is the cube.

When $k = 5$, (6) gives $V = 20/(10-3e)$, which becomes $V = 20$ when $e = 3$. The corresponding polyhedron is the dodecahedron.

When $k = 6$, (6) gives $V = 6/(3-e)$. The smallest value of e is 3, which gives an infinite number of vertices. This is not a network, but is equivalent to a hexagonal tiling of the plane.

3.2. *Heptagonal networks and beyond.* For a heptagonal network we have $k = 7$, and (6) becomes $V = 28/(14 - 5e)$, a negative number if $e \geq 3$, so no such network exists. Generally, no network exists in which every face is k-gonal with $k \geq 7$.

Thus, without using metric properties regarding lengths of edges or measurement of angles, we have shown that there are exactly five nondegenerate Platonic polyhedra: *three triangulated*, the tetrahedron, octahedron, and icosahedron, illustrated in Figure 2 as networks in (a), (c), and (e), and *two nontriangulated*, the cube and dodecahedron, shown as networks in (b)and (d).

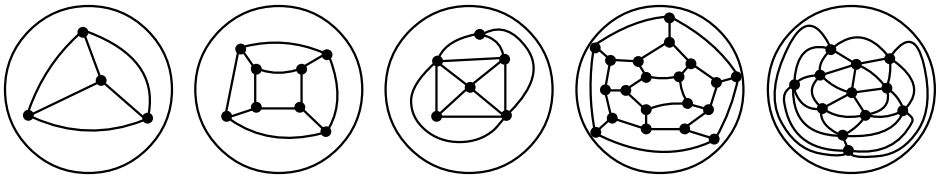

(a) tetrahedron (b) cube (c) octahedron (d) dodecahedron (e) icosahedron

Figure 2. Five Platonic networks, corresponding to tetrahedron ($V = 4$), cube ($V = 8$), octahedron ($V = 6$), dodecahedron ($V = 20$), and icosahedron ($V = 12$).

3.3. *Archimedean networks.* We shall define an Archimedean network to be a uniform network in which two or more types of polygons meet at each vertex with the same orientation. In other words, all vertices have topologically equivalent configurations of edges and faces. We shall list various examples of such networks by referring to the basic relation (4).

3.4. *Prismatic Archimedean networks and their antiprisms.* These are special configurations that can be realized as prismatic polyhedrons as shown in the top row of Figure 3. Below them are solids called *antiprisms*. In the first example, $e = 2$ at

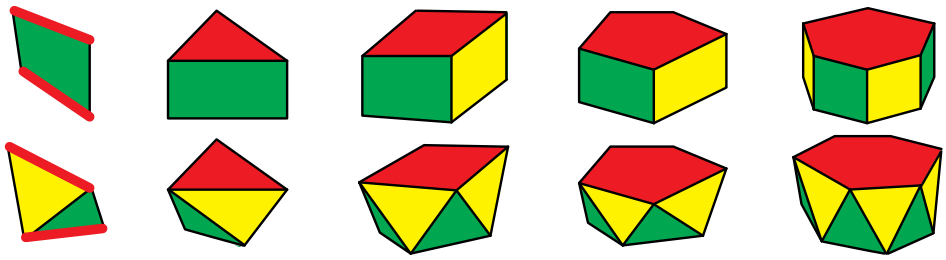

Figure 3. Examples of solids formed from prismatic Archimedean networks. Directly below them are antiprisms with $V + 2$ faces.

each vertex of the (degenerate) prism, while $e = 3$ at each vertex of its antiprism (a tetrahedron). In the remaining examples, $e = 3$, with one k-gon and two quadrilaterals meeting at each vertex. This can be realized as a prismatic polyhedron inscribed in a convex sphere, with two k-gonal bases and k lateral quadrilateral

faces. So $F = 2 + k$ and (4) becomes $V = 2k$, an even number. Since k can take any positive integer value, there are infinitely many such polyhedra. In these examples, each prismatic solid has $V/2$ lateral quadrilateral faces; the antiprism below it has V lateral triangular faces, making a total of $V + 2$ faces for the antiprism, with $e = 4$ at each vertex. Thus, each prismatic Archimedean network can be realized as a solid with an even number V of vertices and $V/2$ lateral quadrilateral faces. For such a prismatic solid, there is always an antiprism with V vertices, V lateral triangular faces and two congruent polygonal bases, for a total of $V + 2$ faces.

3.5. *Duals to triangulated networks.* Given a general network with V vertices, E edges, and F faces, we can form a *dual network* by choosing a point interior to each face of the given network and using it as a vertex of the dual network. The dual network now contains F vertices. For example, the network in Figure 1a has 2 faces, so its dual has two vertices that can be connected by three edges to form a nontriangular network with 3 faces. The dual of that network, in turn, has 3 vertices and is topologically equivalent to the original triangular network in Figure 1a. The triangular networks in Figures 1b and 1c are duals of one another. The duals of Archimedean solids are called Catalan solids.

When we take $e = 3$ in (4) we find

$$V = 2F - 4. \tag{7}$$

Comparing this with the formula $F = 2V - 4$ in the fundamental counting lemma for triangular networks, we see that F and V have been interchanged, so the network obtained by taking $e = 3$ in (4) is the dual of a triangulated network.

In particular, the dual of a prismatic Archimedean network is a triangular network. For example, the dual of a prismatic polyhedron with two k-gonal bases and k rectangular faces is formed by taking a pyramid with a k-gonal base and k triangular faces and joining it to its mirror image along the common base. The dual has $2k$ triangular faces and $2 + k$ vertices. When $k = 3$ this is a hexahedron formed by joining two tetrahedra along their common base. When $k = 4$ this is an octahedron formed by joining two square-based pyramids along their common base.

Thus, we have determined all Archimedean networks with $e = 3$. They are duals of triangular networks. They correspond to the following values in (2):

$n_k = 1, n_4 = 2$, $k = 3, 4, ...$ (A family of prismatic networks not considered by Archimedes.)

The following networks yield 7 of the polyhedra considered by Archimedes.

$n_3 = 1, n_6 = 2$,
$n_3 = 1, n_8 = 2$,
$n_3 = 1, n_{10} = 2$,
$n_4 = 1, n_6 = 2$,
$n_5 = 1, n_6 = 2$,
$n_4 = 1, n_6 = 1, n_8 = 1$,
$n_4 = 1, n_6 = 1, n_{10} = 1$.

3.6. *Archimedean networks with* $e = 4$. When $e = 4$, (3) and (4) become $E = 2V$ and $F = V + 2$. The smallest V that yields a network is $V = 6$ with $E = 12$ and $F = 8$. The corresponding polyhedra are the octahedron with 8 triangular faces, and the antiprism with two triangular bases.

The Archimedean networks with $e = 4$ correspond to the following values in (2), which include 4 of the polyhedra considered by Archimedes:

$n_3 = 1, n_4 = 3$;
$n_3 = 2, n_4 = 2$;
$n_3 = 2, n_5 = 2$;
$n_3 = 1, n_4 = 2, n_5 = 1$;

There are actually two polyhedra corresponding to $n_3 = 1, n_4 = 3$, only one of which was considered by Archimedes. This Archimedean solid, shown in Figure 4a, consists of three parts: two congruent caps shown in Figure 4b, together with

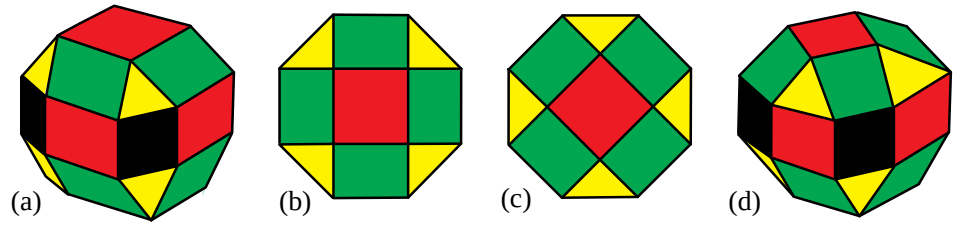

Figure 4. (a) Archimedean solid consisting of three parts. (b) Top and bottom caps of (a). (c) Top cap rotated 45 degrees. (d) Fourteenth Archimedean solid.

an intermediate zone consisting of eight adjacent squares joining the outer edges of the two caps. If one cap, say the top, is rotated by 45 degrees as indicated in Figure 4c, we obtain a new solid with $n_3 = 1, n_4 = 3$, shown in Figure 4d. This new solid, sometimes called the fourteenth Archimedean solid, was apparently known to Kepler, and independently rediscovered by Sommerfeld, Miller, and Ashkinuze. Specific references are given in [2] .

Figure 5 shows the networks corresponding to the two solids in Figure 4a and 4d.

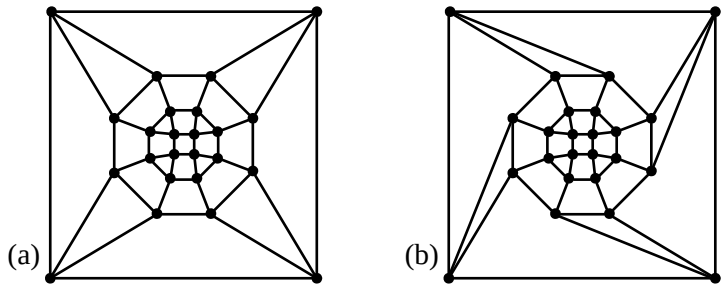

Figure 5. Networks: (a) Archimedean solid in Figure 4a; (b) Modified solid in Figure 4d.

We also have a family of antiprisms (not considered by Archimedes) corresponding to the following values in (2): $n_3 = 2, n_k = 2, k = 3, 4, ...$

3.7. *Archimedean networks with* $e = 5$. When $e = 5$, (3) and (4) becomes $E = 5V/2$ and $F = 3V/2 + 2$. Networks exist when $V = 24$ with $E = 60$ and $F = 38$, and when $V = 60$ with $E = 150$ and $F = 92$.

It can be shown that there are no Archimedean networks with $e > 5$, so those listed above form a complete list. They include the 13 solids considered by Archimedes, the additional one in Figure 4d, and two infinite families of prisms and antiprisms not treated by Archimedes.

4. Summary of results

4.1. *Triangular networks.* A *triangular network* is one in which each face is topologically equivalent to a triangle.

Counting Lemma. *In any triangular network with* $V \geq 3$, *the number of edges is* $E = 3V - 6$, *and the number of faces is* $F = 2V - 4$.

A *triangulated Platonic network* is any triangulated network having the same number of branches at each vertex. There are exactly four triangulated Platonic networks. When realized as polyhedra, they are the degenerate triangular prism with 2 faces, and the three Platonic solids, *tetrahedron*, *octahedron*, and *icosahedron*.

4.2. *General uniform networks.* In a general uniform network there are at least two types of faces around each vertex, say n_3 triangles, n_4 quadrilaterals, n_5 pentagons, etc. If e branches meet at each vertex, then

$$e = n_3 + n_4 + n_5 + \cdots ,$$

and F is related to V by Equation (4):

$$F = \frac{e-2}{2}V + 2.$$

We call the network *Platonic* if only one of the n_k is nonzero.

4.3. *k-gonal Platonic networks.* When each face in a Platonic network is a k-gon, where $k \geq 3$, the number of vertices is given by Eq. (6):

$$V = \frac{4k}{2k + e(2-k)}, \quad k = 3, 4, 5, ...$$

When $k = 3$, the possible values of e are 3, 4, 5, and the corresponding regular polyhedra are the tetrahedron, octahedron, and icosahedron, found earlier as triangulated polyhedra.

When $e = 3$, the corresponding regular polyhedron is the *cube* if $k = 4$, and the *dodecahedron* if $k = 5$. If $k = 6$, the value $e = 3$ gives an infinite number of vertices. This is not a network, but is equivalent to a hexagonal tiling of the plane.

4.4. *Archimedean networks.* We define an Archimedean network to be a uniform network in which two or more types of polygons meet at each vertex with the same orientation. Various examples of such networks are obtained from relation (4). When $e = 3$, (4) becomes $V = 2F - 4$.

4.5. *Prismatic Archimedean networks and their antiprisms.* The special configuration in which $e = 3$, with one k-gon and two quadrilaterals meeting at each vertex can be realized as a prismatic polyhedron inscribed in a convex sphere, with two k-gonal bases and k rectangular faces. So $F = 2+k$ and (4) becomes $V = 2k$, giving infinitely many such polyhedra. When $k = 4$ and the rectangular faces are squares, the corresponding prismatic polyhedron is a cube. Each prismatic Archimedean polyhedron has an even number V of vertices and $V/2$ rectangular faces. For each such solid, there is an antiprism with V vertices, V lateral triangular faces and two congruent polygonal bases, for a total of $V + 2$ faces.

4.6. *Dual networks.* Given a general network with V vertices, E edges, and F faces, the *dual network* has F and V interchanged. The dual of a prismatic Archimedean network is a triangular network. We have determined all Archimedean networks with $e = 3$. Relation (4) shows they are duals of triangular networks.

References

[1] R. Courant and H. Robbins, *What is Mathematics?*, 2nd Edition, revised by I. Stewart, Oxford University Press, New York, Oxford, 1996.

[2] B. Grunbaum, An enduring error, *Elemente der Mathematik*, 64 (2009) 89–101.

[3] R. A. Wilson, *Graphs, Colouring and the Four-Color Theorem*, Oxford University Press, New York,Oxford, 2002.

Tom M. Apostol: California Institute of Technology, 253-37 Caltech, Pasadena, California 91125 USA

E-mail address: apostol@caltech.edu

Mamikon A. Mnatsakanian: California Institute of Technology, 253-37 Caltech, Pasadena, California 91125 USA

E-mail address: mamikon@caltech.edu

Forum Geometricorum
Volume 15 (2015) 253–261.

FORUM GEOM
ISSN 1534-1178

Transforming Tripolar into Barycentric Coordinates

Albrecht Hess

Abstract. A simple construction is presented to find a point with given tripolar coordinates, i.e. the ratios of its distances to the points A, B, C of a reference triangle. This construction leads to a very nice transformation formula for tripolar into barycentric coordinates, that simplifies considerably an already existing transformation formula in Kimberling's *Encyclopedia of Triangle Centers*. The necessary and sufficient conditions for the constructibility are encoded in a triangle whose side lengths are products of the side lengths of ABC with the tripolar coordinates. Formulas for the area of this triangle are presented showing the role of inversion in this construction. As applications, one-line proofs for the formula of the pedal triangle area and the factorization of the dual of the circumcircle are given as well as simplifications of some formulas from ETC.

1. Introduction

When thinking about tripolar coordinates and looking for an idea how to transform results of [7] into the barycentric calculus, I was taken aback by the complicated transformation formulas from tripolar into barycentric coordinates I detected in the entry $X(5002)$ in [9]. Combining the techniques of inversion and of gluing similar figures, that played separate roles in my former FG articles, I found a simple construction leading to nice formulas.

2. Visual proof of Ptolemy's inequality

Gluing similar copies of ABD to CD and of BCD to AD leads to Ptolemy's inequality $\frac{bd}{f} \leq e + \frac{ac}{f}$ or

$$BC \cdot DA \leq AC \cdot DB + AB \cdot DC. \tag{1}$$

See Figure 1 and [3; p. 241, formula (49)], [5, pp. 42-43], [12, pp. 29ff].

This method is very likely behind the impressive calculations of Bretschneider [3]. In Figure 1 in [15], it leads to a short and visual proof of the maximum area property for cyclic quadrilaterals.

3. Existence of a point with given ratios of tripolar coordinates

Ptolemy's inequality (1) encodes the necessary condition for the existence of points D with given tripolar coordinates (see [1], [2], [6, pp. 6–10], [11]), i.e., the distances to the vertices A, B, C of a reference triangle have given ratios. Bottema

Publication Date: November 3, 2015. Communicating Editor: Paul Yiu.

The author would like to thank Michel Bataille and Peter J. C. Moses for their constructive comments of the first drafts of this article and especially Paul Yiu for his suggestion that I apply my results to some triangle centers.

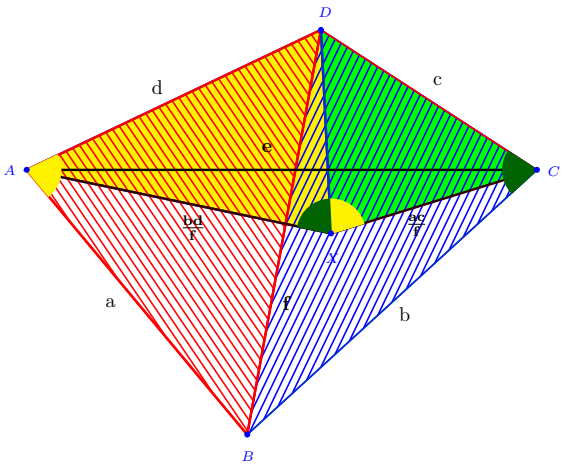

Figure 1

poses this problem in [1, Section 8.2] and proves analytically the following theorem by considering the intersections of Apollonian circles.

Theorem 1. *Given a triangle ABC and three positive numbers p, q, r. There exists (one or two) points D for which the ratios of its distances to A, B, C, are given by $DA : DB : DC = p : q : r$ if and only if we can draw a triangle, possibly degenerated, with sides $BC \cdot p$, $CA \cdot q$, $AB \cdot r$.*

A pure constructive proof, that the triangle inequalities $BC \cdot p \leq AC \cdot q + AB \cdot r$ etc. are equivalent to the existence of a point D for which $DA : DB : DC = p : q : r$, is based on the above mentioned gluing method.

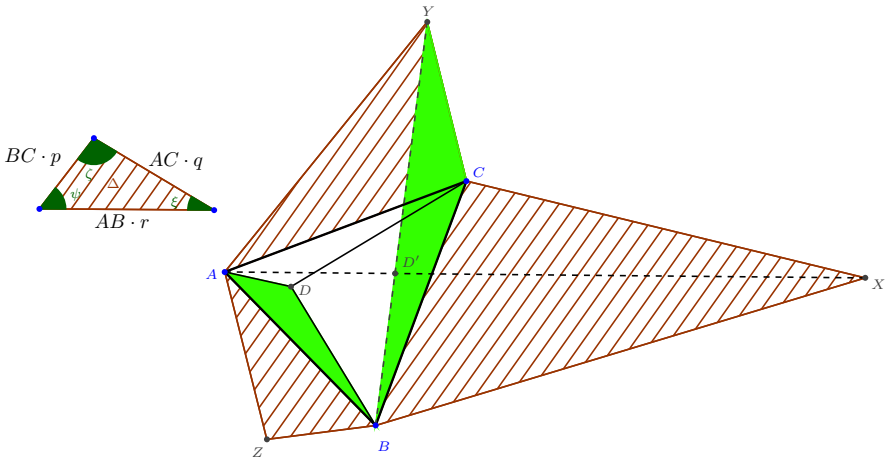

Figure 2

Proof. The necessity of the triangle inequalities, i.e. Ptolemy's inequalities, for the existence of D is obvious. To prove the sufficiency, assume first that Ptolemy's

inequalities are satisfied strictly. Glue a similar copy CAY of the triangle Δ with side lengths $BC \cdot p$, $AC \cdot q$, $AB \cdot r$ to AC as in Figure 2 above. A rotation around B followed by a dilation moves triangle YBC onto a triangle ABD, transforming YB onto AB. A rotation around B followed by a dilation moves triangle YAB onto a triangle BCD, transforming YB onto BC. The images of C, respectively A, both called D, though a priori different, are indeed identical, because the angles of the rotated triangles at B sum up to $\angle ABC$, and the distances of the images of C, respectively A, to B are $a \cdot \frac{c}{YB} = c \cdot \frac{a}{YB}$. Hence, these images must coincide at a point D, which satisfies $DA : DB : DC = p : q : r$ since $DA : DB = \frac{ap}{q} : a = p : q$, and $DC : DB = \frac{cr}{q} : c = r : q$. □

That there are in general two solutions $D_{\pm}$ to this problem becomes clear by the construction based on the Apollonius circles $XA : XB = p : q$, $XB : XC = q : r$, $XC : XA = r : p$. Two of these circles have in general two points of intersection that lie automatically on the third circle. This second solution can be obtained by gluing a similar copy of the nondegenerate triangle Δ onto the other side of AC and proceeding as above.

If Δ degenerates, suppose, for example, that $AB \cdot r + BC \cdot p = AC \cdot q$, the points A, B, C and D are concyclic by Ptolemy's theorem. The points X, Y, Z are on the sides of the triangle. In this example, Y is located in the interior of the segment AC, X and Z are on the extensions of BC and AB. AX, BY and CZ are parallel and meet at infinity, illustrating the fact that the isogonal conjugacy transforms points at infinity into points on the circumcircle, see [8; p.154, Theorem 234]. Figure 3 depicts this situation and serves also as a visual proof of Ptolemy's equation: $\frac{AB \cdot CD}{BD} + \frac{BC \cdot AD}{BD} = AC$.

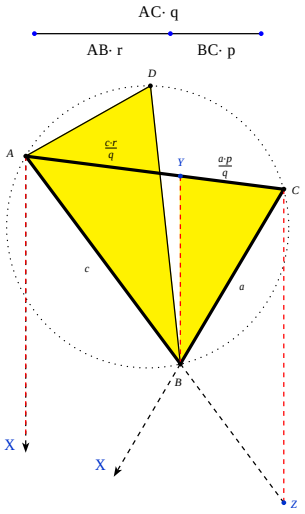

Figure 3

At the end of the next section we will have a look at the relationship between this construction and the inversion in the circumcircle k of ABC. In particular,

we will see that $D_\pm$ are inverted into each other. This explains the number of solutions: two in the case of nondegenerate Δ, except for $p = q = r = 1$, with the circumcenter as the unique solution, and one in the case of degenerate Δ.

4. Transforming tripolar into barycentric coordinates

If we glue similar copies ABZ, BCX, CAY of the triangle Δ outward, respectively inward, to all sides of the original triangle we see that the two solution $D_\pm$ to Bottema's problem are the isogonal conjugates ([8, pp. 153-157]) of the intersections $D'_\pm$ of AX, BY and CZ; see Figure 2. That these lines are concurrent can easily be seen by drawing the circumcircles of ABZ, BCX, CAY, and showing that these circles meet at one point which, by angle chasing, is the intersection of AX, BY and CZ (see [13, Theorem 4.2]). Another proof is by barycentric calculus as in [16; §3.5.2].

This construction is well known in a particular case, namely, the definition of the isodynamic points as isogonal conjugates of the Fermat points. In this case, p, q, r are the reciprocals $\frac{1}{a}$, $\frac{1}{b}$, $\frac{1}{c}$ of the side lengths and triangle Δ and its copies ABZ, BCX, CAY are equilateral. See [1, §23.2], [4, p. 303], [8, p. 295ff], and, as a curiosity, [13, p. 138], where the author decrees: "There may well be an existing name for D and E [the isodynamic points], but we shall call them the Napoleon points."

Let ξ, ψ, ζ be the angles of the triangle Δ, see Figure 2. By Conway's formula ([16, §3.4.2]), with $S_\theta = S\cdot\cot\theta$, $S = 2T_{ABC}$, and $2S_A = 2bc\cos\alpha = b^2+c^2-a^2$ etc., the barycentric coordinates of X, Y, Z are $X(-a^2 : S_C \pm S_\zeta : S_B \pm S_\psi)$, $Y(S_C \pm S_\zeta : -b^2 : S_A \pm S_\xi)$, $Z(S_B \pm S_\psi : S_A \pm S_\xi : -c^2)$.

Hence, the lines AX, BY, CZ intersect at $D'_\pm((S_A \pm S_\xi)^{-1} : (S_B \pm S_\psi)^{-1} : (S_C \pm S_\zeta)^{-1})$. Since the points $D_\pm$ with tripolar coordinates $(p : q : r)$ are isogonal conjugates of $D'_\pm$, we have just proved

Theorem 2. *The barycentric coordinates of the points D_ε, $\varepsilon = \pm 1$, with tripolar coordinates $(p : q : r)$ are*

$$(a^2(S_A + \varepsilon S_\xi) :\ b^2(S_B + \varepsilon S_\psi) :\ c^2(S_C + \varepsilon S_\zeta)). \tag{2}$$

The only place where I could find an expression for the barycentric coordinates $(x : y : z)$ of the points with given ratios $(p : q : r)$ of its distances from A, B, C is in the entry $X(5002)$ in ETC [9]:

$$\begin{aligned} x &= a^2S_A + k^2(-a^2p^2 + S_Cq^2 + S_Br^2),\\ y &= b^2S_B + k^2(S_C^2p^2 - b^2q^2 + S_Ar^2),\\ z &= c^2S_C + k^2(S_Bp^2 + S_Aq^2 - c^2r^2) \end{aligned} \tag{3}$$

for

$$k^2 = \frac{a^2p^2S_A + b^2q^2S_B + c^2r^2S_C + 2SS_\Delta}{a^2(p^2-q^2)(p^2-r^2) + b^2(q^2-r^2)(q^2-p^2) + c^2(r^2-p^2)(r^2-q^2)}.$$

where S_Δ is twice the area of the triangle with sides ap, bq and cr. A similar formula is derived in [4, p. 304], from Stewart's theorem, for $k = 1$ and the

distances p, q, r, (and not only their ratios) of the point with barycentric coordinates $(x : y : z)$ from A, B, C. Casey calls this result Lucas's Theorem, probably referring to [10, p. 133]. But beware, there are printing errors.

Likewise, formula (2) can be written as

$$D_{\pm}\ (a^2(\cot A \pm \cot \xi) :\ b^2(\cot B \pm \cot \psi) :\ c^2(\cot C \pm \cot \zeta)), \tag{4}$$

$$D_{\pm}\ \left(a^2\left(\frac{b^2+c^2-a^2}{2S} \pm \frac{(bq)^2+(cr)^2-(ap)^2}{2S_\Delta}\right) : \cdots : \cdots\right), \tag{5}$$

with $2S = \sqrt{(a+b+c)(-a+b+c)(a-b+c)(a+b-c)}$ and a similar expression with ap, bq, cr replacing a, b, c for $2S_\Delta$. These formulas are by far more transparent than those in (3). They will be applied in §7 to simplify the barycentric coordinate formulas of some triangle centers from [9]. In §5, formula (11), we will see that the ratio $\frac{S_\Delta}{S}$ is, up to a factor, just the power of $D_\pm$ with respect to the circumcircle k of ABC.

Let's see what happens if the triangle Δ degenerates. Calculating barycentric coordinates according to (2) and (3) fails, but by multiplying (4) by $2S_\Delta$, we can write the remaining unique point as

$$D\ \left(a^2(b^2q^2+c^2r^2-a^2p^2) :\ \cdots :\ \cdots\right). \tag{6}$$

Supposing again $AB \cdot r + BC \cdot p = AC \cdot q$ or $ap = bq - cr$, simplifies to $D\left(\frac{a}{p} : -\frac{b}{q} : \frac{c}{r}\right)$.

Theorem 3. *A point $D\ \left(\frac{a}{p} : -\frac{b}{q} : \frac{c}{r}\right)$, $p, q, r > 0$, is on the circumcircle k of the triangle ABC if and only if $ap + cr = bq$. In this case, $(DA : DB : DC) = (p : q : r)$.*

Proof. The "if" part being dealt with just before, we are left with the "only if" part that can be shown by putting $D\left(\frac{a}{p} : -\frac{b}{q} : \frac{c}{r}\right)$ into the circumcircle equation $k(x, y, z) = a^2yz + b^2zx + c^2xy = 0$. □

The easiest way to get the tangent equation to k at D is to write it as

$$k_x\left(\frac{a}{p} : -\frac{b}{q} : \frac{c}{r}\right)x + k_y\left(\frac{a}{p} : -\frac{b}{q} : \frac{c}{r}\right)y + k_z\left(\frac{a}{p} : -\frac{b}{q} : \frac{c}{r}\right)z = 0$$

and to simplify using $ap + cr = bq$. We obtain $p^2x + q^2y + r^2z = 0$.

We summarize the last calculations in Theorem 4 that can be used to get very short and nice solutions of tangency problems, e.g. the proof of Feuerbach's theorem.

Theorem 4. *A line $p^2x + q^2y + r^2z = 0$, $p, q, r \geq 0$, in barycentric coordinates $(x : y : z)$ is tangent to the circumcircle k of a reference triangle ABC if and only if*

$$(-ap + bq + cr)(ap - bq + cr)(ap + bq - cr) = 0. \tag{7}$$

Observe that a line $ux+vy+wz=0$ with coefficients u, v, w of different signs can never be tangent to k since it contains interior points of ABC. This result in its genuinely geometric form is Theorem 117 of [8, p. 89].

Theorem 5. *Let p, q, r be the tangent lengths from A, B, C to a circle K. Then K is tangent to the circumcircle k of ABC if and only if* (7) *is satisfied.*

Just observe that for tangent circles their radical axis, i.e. the zero set of the difference of their barycentric equations, is tangent to both and that the barycentric equations for k and K are related by

$$K(x,y,z)=k(x,y,z)-(x+y+z)(p^2x+q^2y+r^2z)=0,$$

see [16, Proposition 7.2.3].

With the appearance of $(-ap+bq+cr)(ap-bq+cr)(ap+bq-cr)$ in Theorem 4, it is tempting to put (p^2,q^2,r^2) into the equation

$$k^*(u,v,w)=a^4u^2+b^4v^2+c^4w^2-2a^2b^2uv-2b^2c^2vw-2c^2a^2wu=0$$

for the coefficients of the tangent lines $ux+vy+wz=0$ to k, i. e. the equation of the dual conic of k. It is barely a surprise that S_Δ appears in this factorization of the dual equation of k:

$$k^*(p^2,q^2,r^2)=4S_\Delta^2=(ap+bq+cr)(-ap+bq+cr)(ap-bq+cr)(ap+bq-cr). \tag{8}$$

What is the relation of all this with the inversion? The Apollonius circle $XA:XB=p:q$ occurring in the construction of the solutions of $DA:DB:DC=p:q:r$ belongs to the pencil with limit points A and B, since it intersects the line AB harmonically or, by an analytical argument, since its equation $q^2|X-A|^2-p^2|X-B|^2=0$ is a linear combination of the point-circles A and B. Therefore, this circle is orthogonal to any circle through the limit points A and B, in particular to the circumcircle k. This being so also for the circles $XB:XC=q:r$ and $XC:XA=r:p$, these Apollonius circles, left invariant by an inversion with respect to k, will therefore intersect in points $D_\pm$, which are images of each other in this inversion.

Moreover, the involvement of inversion in this problem will become clear, if we compare the area

$$T_\Delta=\frac{1}{4}\sqrt{(ap+bq+cr)(-ap+bq+cr)(ap-bq+cr)(ap+bq-cr)}$$

of the triangle Δ with sides $ap=a\cdot DA$, $bq=b\cdot DB$, $cr=c\cdot DC$, (p, q, r being now the distances from a point D to the vertices of ABC, and not only their ratios) with the area T of ABC. Bretschneider ([3, p. 241]) calls T_Δ the excentric area ("excentrische Fläche") of the quadrilateral $ABCD$. It expresses, as a numerical value for Ptolemy's theorem, the extent of the deviation of the quadrilateral from being cyclic. Using inversion, a nice formula connecting the areas of ABC and Δ will be derived in the next section.

5. Excentric area of a quadrilateral

Let us apply an inversion with respect to a circle $\kappa(D,\ \rho)$ to the triangle ABC with sides $a = BC$, $b = CA$, $c = AB$, circumcircle $k(O, R)$ and area T. The image is a triangle $A'B'C'$ with sides $a' = B'C'$, $b' = C'A'$, $c' = A'B'$, circumcircle $k'(O', R')$ and area T'.

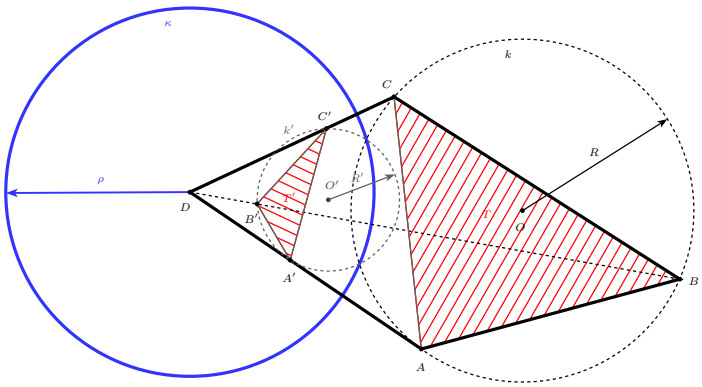

Figure 4

The side lengths transform according to

$$a' = \frac{\rho^2}{DB \cdot DC} \cdot a, \quad b' = \frac{\rho^2}{DC \cdot DA} \cdot b, \quad c' = \frac{\rho^2}{DA \cdot DB} \cdot c.$$

This leads to

$$T' = \frac{a'b'c'}{4R'} = \frac{\rho^6}{DA^2 \cdot DB^2 \cdot DC^2} \cdot \frac{abc}{4R'} \tag{9}$$

for the area T'. Inserting $R' = \frac{\rho^2}{|DO^2 - R^2|^2} \cdot R = \frac{\rho^2}{|P(D,k)|} R$ with $P(D, k) = DO^2 - R^2$, power of D with respect to k, into (9), we obtain

$$T' = \frac{\rho^4 |P(D, k)|}{DA^2 \cdot DB^2 \cdot DC^2} \cdot T_{ABC}. \tag{10}$$

Incidentally, from the triangle inequalities of $A'B'C'$ we again get Ptolemy's inequalities (1), but now by inversion.

From the similarity of Δ and $A'B'C'$ we obtain a formula for the ratio $\frac{T_\Delta}{T}$:

$$T_\Delta = \left(\frac{DA \cdot DB \cdot DC}{\rho^2} \right)^2 T' = |P(D, k)| T. \tag{11}$$

This is a nice expression of the fact that the vanishing of T_Δ is equivalent to the cyclicity of $ABCD$.

6. The Area of the Pedal triangle

As an application of (11) we derive a formula for the area of the pedal triangle PQR of a point D (for pedal triangles see [5, pp. 22ff] or [8, pp. 135ff]). Triangle

PQR is similar to triangle Δ with side lengths $a \cdot DA$, $b \cdot DB$, $c \cdot DC$. This follows from $QR = DA \sin A = \frac{a}{2R} \cdot DA$. Hence by (11)

$$T_{PQR} = \frac{1}{4R^2} \cdot T_\Delta = \frac{|P(D,k)|}{4R^2} \cdot T_{ABC}.$$

For another proof see [8, p.139, Theorem 198].

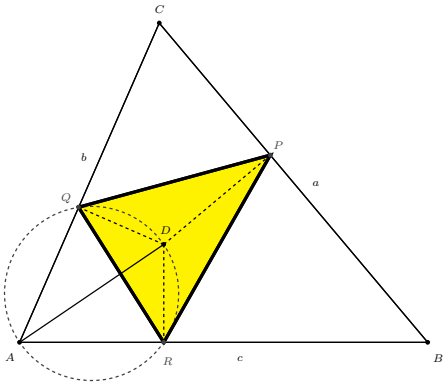

Figure 5

This formula captures the essence of the theorem about the Simson line [5, p.41, Theorem 2.51], [8, p.137, Theorem 192] that P, Q and R are collinear if and only if D is on the circumcircle of ABC.

7. Simplifications of barycentric coordinate formulas for some triangle centers

The possible simplifications, based on an application of formula (5), apply to any triangle center for which we have nice formulas for the ratios of its distances to the vertices of the triangle. As a sign change in (5) means inversion in the circumcircle, this is also a nice tool to invert triangle centers as can be seen in the following example.

For the orthocenter $D = X(4)$ we have $AD = \frac{aS_A}{S}$ etc. As tripolar coordinates of the orthocentre we take $(p : q : r) = (aS_A : bS_B : cS_C)$. From $ap + bq + cr = 2S^2$, etc. we get

$$2S_\Delta = \sqrt{(ap+bq+cr)(-ap+bq+cr)(ap-bq+cr)(ap+bq-cr)} = 4SS_AS_BS_C.$$

Similarly, $(bq)^2 + (cr)^2 - (ap)^2 = 2S_BS_C(S^2 - S_A^2)$. From (5) follows for the barycentrics of $X(4)$

$$x = a^2\left(\frac{S_A}{S} + \frac{(bq)^2+(cr)^2-(ap)^2}{2S_\Delta}\right) = \frac{a^2b^2c^2}{2S}\cdot\frac{1}{S_A} = \frac{a^2b^2c^2}{2S^2}\tan A \sim \tan A.$$

The barycentrics of X(186), the inverse of X(4) in the circumcircle, are given by the minus sign:

$$x = a^2\left(\frac{S_A}{S} - \frac{(bq)^2+(cr)^2-(ap)^2}{2S_\Delta}\right) = \frac{1}{2S}\cdot a^2 \cdot \frac{3S_A^2 - S^2}{S_A} \sim a^2 \cdot \frac{3S_A^2 - S^2}{S_A}.$$

We apply the formula (5) to get simpler barycentrics $(h(A,B,C) : h(B,C,A) : h(C,A,B))$ of the Walsmith point $X(5000)$ and its inverse $X(5001)$ in the circumcircle, see [9]. For this point, its distances to A, B, C have ratios $(p : q : r)$ with $p^2 = S_A$, $q^2 = S_B$, $r^2 = S_C$. Factorizing S_Δ we get the expression $h(A,B,C) = a^2(S_A\sqrt{S_AS_BS_CS_\omega} \pm SS_BS_C)$.

Applying to the first Walsmith-Moses point $X(5002)$ and its inverse $X(5003)$, the simplifications with $p = a$, $q = b$, $r = c$ lead to

$$h(A,B,C) = a^2(2S_A\sqrt{S_AS_BS_CS_\omega} \pm S(S_\omega S_A - S_BS_C)).$$

Finally, for the second Walsmith-Moses point $X(5004)$ and its inverse $X(5005)$, with $p^2 = b^2 + c^2$, $q^2 = c^2 + a^2$, $r^2 = a^2 + b^2$, we get the formula

$$h(A,B,C) = a^2S_A\sqrt{2S_\omega} \pm Sabc.$$

References

[1] O. Bottema, *Topics in Elementary Geometry*, Springer, 2008.

[2] O. Bottema, On the distances of a point to the vertices of a triangle, *Crux Math.*, 10 (1984) 242–246.

[3] C. A. Bretschneider, Untersuchung der trigonometrischen Relationen des geradlinigen Viereckes, *Archiv der Math.*, 2 (1842) 225–261, available at: `http://books.google.de/books?id=aNcLAAAAYAAJ`

[4] J. Casey, *A Treatise on the Analytical Geometry of the Point, Line, Circle and Conic Sections*, Dublin, London, 1893, available at: `https://archive.org/details/atreatiseonanal05casegoog`

[5] H. S. M. Coxeter and S. L. Greitzer, *Geometry Revisited*, Washington, MAA, 1967.

[6] L. Euler, De symptomatibus quatuor punctorum in eodem plano sitorum, *Acta Acad. Sci. Imperialis Petropolitinae* 6, (1786) 3–18, available at MAA's Euler Archive: `https://math.dartmouth.edu/~euler/docs/originals/E601.pdf`

[7] A. P. Hatzipolakis, F. M. van Lamoen, B. Wolk, and P. Yiu, Concurrency of four Euler lines, *Forum Geom.*, 1 (2001) 59–68.

[8] R. A. Johnson, *Advanced Euclidean Geometry*, Dover reprint, 2007.

[9] C. Kimberling, *Encyclopedia of Triangle Centers*, available at: `http://faculty.evansville.edu/ck6/encyclopedia/ETCPart4.html`

[10] E. Lucas, Sur les coordonnées tripolaires, *Mathesis*, 9 (1889) 129–134; 173–181, available at: `http://resolver.sub.uni-goettingen.de/purl?PPN599218835_0009`

[11] A. Poulain, Des coordonnées tripolaires, *Journal de Mathématiques Spéciales*, ser. 3, 3 (1889) 3–10, 51–55, 130–134, 155–159, 171–172.

[12] C. Ptolemy, *Almagest*, Book 1, Chapter 9; Greek with French translation: `http://gallica.bnf.fr/ark:/12148/bpt6k64767c`

[13] J. F. Rigby, Napoleon revisited, *Journal of Geometry*, 33 (1988) 129–146.

[14] K. G. C. von Staudt, Über einige geometrische Sätze, *Journal für die reine und angewandte Mathematik*, 57 (1860) 88–89.

[15] A. Varverakis, A maximal property of cyclic quadrilaterals, *Forum Geom.*, 5 (2005) 63–64.

[16] P. Yiu, *Introduction to the Geometry of the Triangle*, Florida Atlantic University Lecture Notes, 2001; with corrections, 2013, available at `http://math.fau.edu/Yiu/Geometry.html`

Albrecht Hess: Deutsche Schule Madrid, Calle Monastesio Guadelupe 7, 28049 Madrid, Spain
E-mail address: `albrecht.hess@gmail.com`

Forum Geometricorum
Volume 15 (2015) 263–265.

FORUM GEOM
ISSN 1534-1178

A Simple Dynamic Localization of the Gravitational Center of a Triangle

Grégoire Nicollier

Abstract. We describe the gravitational center of a triangle as the common point of three ellipses and give a one-line proof of its existence and uniqueness.

We consider a nondegenerate triangle ABC of constant area mass density with sides $AB = c$, $BC = a$, and $CA = b$. A point mass of the triangle plane is at a *gravitational center* of the triangle when the force of gravity exerted by the triangle on the point mass is zero (with $1/r$ potential). As shown in [1], the gravitational centers are the inner points of the triangle whose distances r_A, r_B, and r_C from the vertices fulfill

$$\left(\frac{r_A + r_B + c}{r_A + r_B - c}\right)^{1/c} = \left(\frac{r_B + r_C + a}{r_B + r_C - a}\right)^{1/a} = \left(\frac{r_C + r_A + b}{r_C + r_A - b}\right)^{1/b} \tag{1}$$

and there is exactly one such point, labeled $X(5626)$ in [3].

The gravitational center can be localized very easily as follows. Construct with a dynamic geometry software an ellipse $\mathcal{E}_c$ of foci A and B with some ratio

$$\frac{\text{major axis}}{c} = \frac{1}{\text{eccentricity}} =: \tan\theta_c, \quad \frac{\pi}{4} < \theta_c < \frac{\pi}{2}. \tag{2}$$

Permuting vertices and sides cyclically, construct ellipses $\mathcal{E}_a$ and $\mathcal{E}_b$ similarly, but let θ_a and θ_b depend on θ_c and on the ratio a/c or b/c by setting

$$\theta_{\text{side}} = \frac{3\pi}{4} - \arctan\left(\tan^{\text{side}/c}\left(\frac{3\pi}{4} - \theta_c\right)\right), \quad \text{side} = a,\, b. \tag{3}$$

(Relation (3) between θ_{side} and θ_c is then true when "side" and c are replaced with any elements of $\{a,\, b,\, c\}$.) Vary θ_c by moving the corresponding slider (Figure 1) until the three ellipses share a common point inside the triangle: this is the gravitational center.

Proof. Consider a point P at some distance r_A from A and r_B from B (and not on the triangle's boundary). Draw the ellipse $\mathcal{E}_c$ of foci A and B through P, with major axis μ. The quotient on the left of (1) is by (2)

Publication Date: November 13, 2015. Communicating Editor: Paul Yiu.

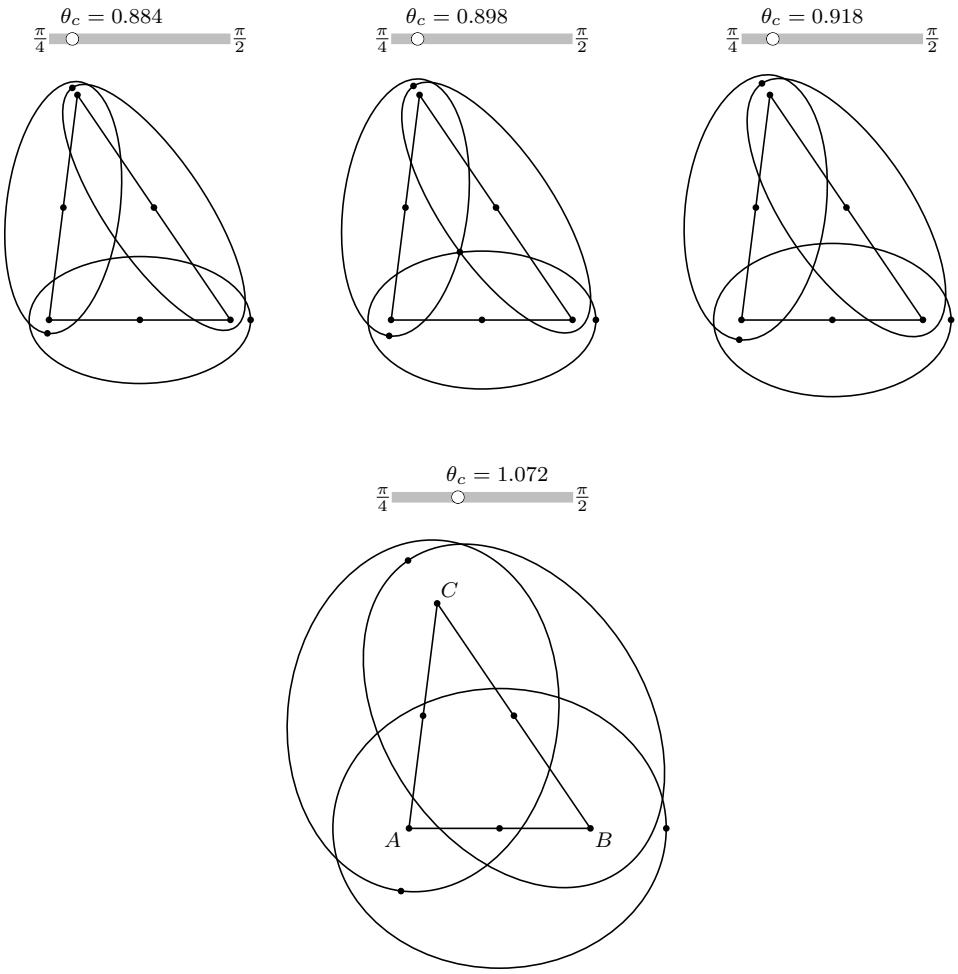

Figure 1. Triangle with sides $a : b : c = 6 : 5 : 4$

$$\frac{r_A + r_B + c}{r_A + r_B - c} = \frac{\frac{\mu}{c} + 1}{\frac{\mu}{c} - 1} = \tan\left(\frac{3\pi}{4} - \theta_c\right). \tag{4}$$

For the same point P, the other quotients of (1) without exponents are as in (4) $\tan\left(\frac{3\pi}{4} - \theta_a\right)$ and $\tan\left(\frac{3\pi}{4} - \theta_b\right)$ for some θ_a and θ_b between $\pi/4$ and $\pi/2$. The logarithmic version of (1) characterizes the gravitational center by

$$\frac{1}{a}\log\tan\left(\frac{3\pi}{4} - \theta_a\right) = \frac{1}{b}\log\tan\left(\frac{3\pi}{4} - \theta_b\right) = \frac{1}{c}\log\tan\left(\frac{3\pi}{4} - \theta_c\right). \quad \square$$

One sees at once that θ_a and θ_b given by (3) increase with θ_c and have the same range $(\pi/4, \pi/2)$ as θ_c. For values of the θs near $\pi/4$, the ellipses surround a gap inside the triangle (Figure 1); for values of the θs near $\pi/2$, the three ellipse

interiors have a common overlap. It is immediate that the transition gap/overlap takes place at the solution of (1), *i.e.*, at the gravitational center, which lies in every gap and every overlap. It is also clear from Figure 1 that the three ellipses share a common point *inside* the triangle for a *unique* θ_c: this proves the existence and uniqueness of the gravitational center. (We conjecture that (1) never has a solution outside the triangle.)

Remark. As the three ellipses share pairwise a focus, the three pairwise common chords are concurrent (if existing) [4, 2], but the concurrency point varies with θ_c.

References

[1] H. Abraham and V. Kovač, From electrostatic potentials to yet another triangle center, *Forum Geom.*, 15 (2015) 73–89.

[2] I. Bogdanov, Two theorems on the focus-sharing ellipses: a three-dimensional view, *J. Classical Geom.*, 1 (2012) 1–5.

[3] C. K. Kimberling, *Encyclopedia of Triangle Centers*, `http://faculty.evansville.edu/ck6/encyclopedia/ETC.html`

[4] E. Neville, A focus-sharing set of three conics, *Math. Gazette*, 20 (1936) 182–183.

Grégoire Nicollier: University of Applied Sciences of Western Switzerland, Route du Rawyl 47, CH–1950 Sion, Switzerland

E-mail address: `gregoire.nicollier@hevs.ch`

Forum Geometricorum
Volume 15 (2015) 267–273.

FORUM GEOM
ISSN 1534-1178

Some Theorems on Polygons with One-line Spectral Proofs

Grégoire Nicollier

Abstract. We use discrete Fourier transforms and convolution products to give one-line proofs of some theorems about planar polygons. We illustrate the method by computing the perspectors of a pair of concentric equilateral triangles constructed from a hexagon and leave the proofs of Napoleon's theorem, the Barlotti theorem, the Petr–Douglas–Neumann theorem, and other theorems as an exercise.

1. Introduction

The Fourier decomposition of a planar (or nonplanar [4]) polygon and circulant matrices have been used for a long time in the study of polygon transformations with a circulant structure (see [6] for a list of references). The replacement of circulant matrices with convolution products simplifies the approach [6, 7] and allows one-line proofs of many theorems about polygons: Napoleon's theorem, the Barlotti theorem, and the Petr–Douglas–Neumann theorem are such examples (Section 7). Sections 3–5 provide a short but self-contained overview of the necessary theory (see [6, 7] for more details). As an application we determine in Section 6 the perspectors of the pair of triangular Fourier components of a planar hexagon and find so an elegant and enlightening solution to a problem treated in [3]. In preparation for the hexagon problem we begin our exposition by expressing the perspectors of two concentric equilateral triangles.

2. Perspectors of two concentric equilateral triangles

By a theorem attributed to D. Barbilian (1930), but which is older, two concentric equilateral triangles are triply perspective [9] (with a short proof in trilinears), [5], [2, p. 71], [8, pp. 91–92]. We prove this result by giving an explicit formula for the perspectors (Figure 1).

Theorem 1. (1) *Two equilateral triangles centered at the origin of the complex plane with vertices* 1 *and* v, $|v| \neq 1$, *respectively, have the perspectors*

$$p_k = \frac{v^2 - \overline{v}}{1 - |v|^2}\,\omega^k = p_0\,\omega^k, \quad k = 0,\, 1,\, 2, \quad \textit{where} \quad \omega = e^{i2\pi/3}. \tag{1}$$

Publication Date: November 13, 2015. Communicating Editor: Paul Yiu.

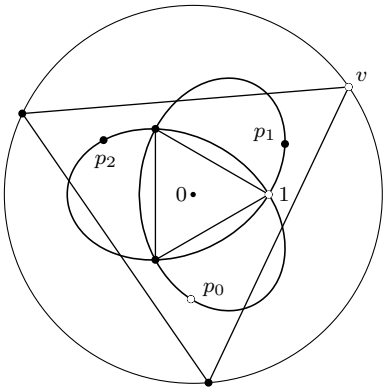

Figure 1. Common locus of the three perspectors for $|v| = 2.5$

The position of p_k on the line of the corresponding vertices ω^ℓ and $v\omega^{-\ell-k}$ is given by the real quotient

$$\frac{p_k - \omega^\ell}{v\omega^{-\ell-k} - \omega^\ell} = \frac{1 + 2\,\mathrm{Re}\left(v\omega^{\ell-k}\right)}{1 - |v|^2}, \quad \ell = 0,\, 1,\, 2. \tag{2}$$

When one triangle has its vertices on the sidelines of the other, the perspectors p_k are the vertices of the second triangle.

(2) *If $v \notin \{1, \omega, \overline{\omega}\}$ lies on the unit circle, the successive perspectors p_k are the points at infinity of the lines through 1 and $v\omega^{-k}$ obtained from one another by a rotation of $2\pi/3$ about 1.*

(3) *The origin is a further perspector when $\arg v$ is an integer multiple of $\pi/3$.*

Proof. Plug formula (1) into formula (2) and verify directly. □

If v lies neither on the unit circle nor on a sideline of the triangle $(1, \omega, \overline{\omega})$, the map $v \mapsto p_0 = \left(v^2 - \overline{v}\right)/\left(1 - |v|^2\right)$ is an involution whose fixed points z form the circle $|z + 1| = 1$ without ω and $\overline{\omega}$. If in addition the triangle $(v, v\omega, v\overline{\omega})$ has no vertex on this circle, *i.e.*, if 1 is not on its sidelines, the (different) triangles $(1, \omega, \overline{\omega})$, $(v, v\omega, v\overline{\omega})$, and (p_0, p_1, p_2) form a triad: each of them is perspector triangle of the others.

3. Spectral decomposition of a planar polygon

For an integer $n \geq 2$, an n-gon P in the complex plane is the sequence $P = (z_k)_{k=0}^{n-1}$ of its vertices in order representing the closed polygonal line

$$z_0 \to z_1 \to \cdots \to z_{n-1} \to z_0$$

starting at z_0. The vertices are indexed modulo n. We set $\zeta = e^{i2\pi/n}$ and use the Fourier basis of $\mathbf{C}^n$ (Figure 2) constituted by the standard regular $\{n/k\}$-gons

$$F_k = \left(\zeta^{k\ell}\right)_{\ell=0}^{n-1}, \quad k = 0,\, 1, \ldots,\, n-1.$$

After the starting vertex 1, each vertex of F_k is the kth next nth root of unity. $F_0 = (1,\, 1, \ldots,\, 1)$ is a trivial polygon and the other basis polygons are centered

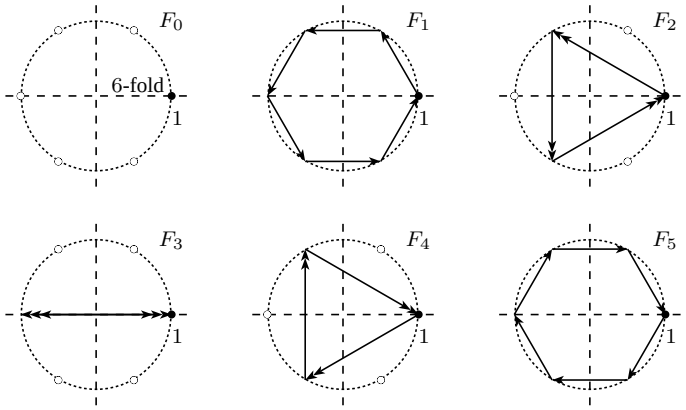

Figure 2. Fourier basis of $\mathbf{C}^6$

at the origin with $\overline{F_k} = F_{n-k}$. The Fourier basis is orthonormal with respect to the inner product of $\mathbf{C}^n$ given by

$$\langle P, Q\rangle = \left\langle (z_k)_{k=0}^{n-1}, (w_k)_{k=0}^{n-1}\right\rangle = \frac{1}{n}\sum_{k=0}^{n-1} z_k\overline{w_k}.$$

The *discrete Fourier transform* or *spectrum* of P is the polygon $\widehat{P} = (\hat{z}_k)_{k=0}^{n-1}$ given by the *spectral decomposition* of P in the Fourier basis:

$$P = \sum_{k=0}^{n-1} \hat{z}_k F_k \quad \text{with} \quad \hat{z}_k = \langle P, F_k\rangle\,, \quad k = 0, 1, \ldots, n-1,$$

where each nonzero $\hat{z}_k$ rotates and scales up or down the basis polygon about the origin. The trivial polygon $\hat{z}_0 F_0$ corresponds to the (vertex) centroid $\hat{z}_0$ of P.

4. Convolution filters

We consider a *filter* $\Phi_\Gamma\colon \mathbf{C}^n \to \mathbf{C}^n$ given by the cyclic convolution $*$ with a fixed polygon $\Gamma = (c_0,\, c_1, \ldots,\, c_{n-1})$: the kth entry of $\Phi_\Gamma(P) = P * \Gamma = \Gamma * P$ is

$$\sum_{\ell_1+\ell_2=k\,(\mathrm{mod}\ n)} z_{\ell_1} c_{\ell_2} = \sum_{\ell=0}^{n-1} z_\ell c_{k-\ell}, \quad k = 0,\, 1, \ldots,\, n-1.$$

A circulant linear transformation of a polygon in the complex plane that is given by the coefficients $(a_k)_{k=0}^{n-1}$ of the circulant linear combination of the vertices is simply the convolution of the initial polygon with the polygon $(a_0, a_{n-1}, a_{n-2}, \ldots, a_1)$ obtained from $(a_0, a_1, \ldots, a_{n-1})$ by going the other way around. The operator $*$ is commutative, associative and bilinear.

Since $F_k * F_\ell = \begin{cases} nF_k & (k=\ell) \\ (0,0,\ldots,0) & (k\neq\ell) \end{cases}$, one has

$$\Phi_\Gamma(P) = P*\Gamma = \left(\sum_{k=0}^{n-1} \hat{z}_k F_k\right) * \left(\sum_{\ell=0}^{n-1} \hat{c}_\ell F_\ell\right) = \sum_{k=0}^{n-1} n\hat{c}_k\hat{z}_k F_k,$$

i.e.,

$$\widehat{P*\Gamma} = n\widehat{P}\cdot\widehat{\Gamma},$$

where $\cdot$ is the entrywise product: the Fourier basis is a basis of eigenvectors of the convolution Φ_Γ with eigenvalues $n\hat{c}_k$ (geometrically clear!). $\Phi_\Gamma(P)$ and P always have the same centroid if and only if $\sum_{k=0}^{n-1} c_k = 1$, which means $\hat{c}_0 = 1/n$; the centroid is always translated to the origin if and only if $\hat{c}_0 = 0$.

5. Ears and diagonals

A *Kiepert n-gon* consists of the apices of similar triangular ears that are erected in order on the sides of the initial polygon $P = (z_k)_{k=0}^{n-1}$ (beginning with the side $z_0 \to z_1$) and that are directly similar to the normalized triangle $(0,1,a) \in \mathbf{C}^3$ with apex a: the apex of the ear for the side $z_0 \to z_1$ is defined as $z_1 + a(z_0 - z_1)$; it is a right-hand ear if $\operatorname{Im} a > 0$. The corresponding Kiepert polygon is thus given by the centroid-preserving convolution of P with

$$K(a) = (a, 0, \ldots, 0, 1-a).$$

An *ℓ-diagonal midpoint n-gon* consists of the midpoints of the diagonals $z_k \to z_{k+\ell}$ taken in order over the initial polygon $P = (z_k)_{k=0}^{n-1}$. As its first vertex is $(z_0 + z_\ell)/2$, the ℓ-diagonal midpoint n-gon is given by the centroid-preserving convolution of P with

$$M_\ell = \frac{1}{2}(\underset{\substack{\text{position}\\ \uparrow\\ 0}}{1}, 0, \ldots, 0, \underset{\substack{\uparrow\\ n-\ell}}{1}, 0, \ldots, \underset{\substack{\uparrow\\ n-1}}{0}).$$

We will only use the fact that these transformations are convolution products since they are circulant linear maps. We need neither the explicit convolving polygon nor its spectrum.

6. Filtered hexagons

Theorem 2. *Erect right-hand equilateral triangles on the sides of a planar hexagon. The midpoints of the opposite ear centers are the vertices of an equilateral triangle T. Left-hand ears lead to an equilateral triangle T' centered, as T, at the vertex centroid of the hexagon.*

Proof. For the hexagon

$$H = (z_k)_{k=0}^{5} = \sum_{k=0}^{5} \hat{z}_k F_k$$

the triangle T corresponding to right-hand ears is simply

$$T = H * K(a_{\pi/6}) * M_3 \quad \text{with} \quad a_{\pi/6} = \tfrac{1}{\sqrt{3}} e^{i\pi/6}.$$

The convolution with $K(a_{\pi/6})$ erects right-hand isosceles ears with base angles $\pi/6$. The following facts are geometrically immediate (Figure 2): F_1, F_3, and F_5 are filtered out by the diagonal midpoint construction, whereas F_0 and F_2 are left unchanged. F_4 is deleted by the ear erection, F_0 is left unchanged, and F_2 is rotated by $\pi/3$. By linearity, associativity, and commutativity of the convolution product, T is thus the (doubly covered) equilateral triangle

$$T = \hat{z}_0 F_0 + \eta \hat{z}_2 F_2 \quad \text{for} \quad \eta = e^{i\pi/3}$$

with the same centroid as the hexagon (T collapses to the centroid if H is F_2-free). Left-hand ears lead to

$$T' = \hat{z}_0 F_0 + \overline{\eta} \hat{z}_4 F_4. \qquad \square$$

Notice that the components $T_1 = \hat{z}_0 F_0 + \hat{z}_2 F_2$ and $T_1' = \hat{z}_0 F_0 + \hat{z}_4 F_4$ of the hexagon can be retrieved from T and T', respectively: T and T_1 form a regular hexagram, as do T' and T_1' as well as the perspector triangles of T, T' and T_1, T_1'. Since

$$\hat{z}_2 = \frac{1}{6}\left(z_0 + z_3 + \overline{\omega}(z_1 + z_4) + \omega(z_2 + z_5)\right) \quad \text{and}$$
$$\hat{z}_4 = \frac{1}{6}\left(z_0 + z_3 + \omega(z_1 + z_4) + \overline{\omega}(z_2 + z_5)\right) \quad \text{for} \quad \omega = e^{i2\pi/3},$$

$(\hat{z}_0, \hat{z}_2, \hat{z}_4)$ is the spectrum of the triangle $(w_k)_{k=0}^{2} = \frac{1}{2}(z_k + z_{k+3})_{k=0}^{2}$ formed by the first lap of $H * M_3$ and depends thus only (and bijectively) on the midpoints of the opposite vertices of H. These midpoints are collinear if and only if $\hat{z}_2$ and $\hat{z}_4$ have the same modulus [7]. Otherwise, the perspector p_0 of T and T' is by Theorem 1

$$p_0 = \hat{z}_0 + \frac{v^2 - \overline{v}}{1 - |v|^2} \overline{\eta} \hat{z}_4 \quad \text{for} \quad v = \omega \hat{z}_2 / \hat{z}_4, \tag{3}$$

$\omega \hat{z}_2 / \hat{z}_4$ being the quotient of the vertices $\eta \hat{z}_2$ of $T - \hat{z}_0 F_0$ and $\overline{\eta} \hat{z}_4$ of $T' - \hat{z}_0 F_0$. After transformation, formula (3) leads to the following result.

Theorem 3. *Consider a hexagon $(z_k)_{k=0}^{5}$ for which the midpoints*

$$w_k = \frac{z_k + z_{k+3}}{2}, \quad k = 0,\ 1,\ 2,$$

of the opposite vertices are not collinear. The equilateral triangles T and T' from Theorem 2 *have then the perspectors*

$$p_k = \hat{z}_0 + \frac{\hat{z}_2^2 \overline{\hat{z}_4} - \overline{\hat{z}_2} \hat{z}_4^2}{|\hat{z}_2|^2 - |\hat{z}_4|^2} \omega^k, \quad k = 0,\ 1,\ 2, \quad \textit{where} \quad \omega = e^{i2\pi/3},$$

and p_0 can be written as

$$p_0 = \frac{\sum_{\text{cyclic}} |w_0|^2 (w_1 - w_2)}{\sum_{\text{cyclic}} \overline{w_0}(w_1 - w_2)}. \tag{4}$$

(Formula (4) corrects the corresponding formula of [3].)

7. Other theorems with one-line spectral proofs

The following examples also have one-line spectral proofs, which are – with two exceptions – left to the reader as an exercise!

7.1. *Equilaterality.* A triangle (z_0, z_1, z_2) is positively oriented and equilateral (or trivial) if and only if

$$\hat{z}_2 = z_0 + \omega z_1 + \overline{\omega} z_2 = 0.$$

Negatively oriented equilateral triangles correspond to $\hat{z}_1 = 0$.

7.2. *Napoleon's theorem.* The centers of right-hand equilateral triangles erected on the sides of a triangle are the vertices of an equilateral (or trivial) triangle. The same is true for left-hand ears.

7.3. *The Barlotti theorem.* An n-gon in the complex plane is an affine image of F_k, $k \neq 0$, *i.e.*, of the form $aF_0 + bF_k + cF_{n-k}$, if and only if the centers of scaled copies of F_k erected on the sides are the vertices of a scaled copy of F_k.

7.4. *Side midpoint quadrilateral.* The side midpoints of a (planar) quadrilateral are the vertices of a parallelogram.

7.5. *The Petr–Douglas–Neumann theorem.* Start from a planar n-gon and replace it with the polygon whose vertices are the centers of scaled copies of some F_k, $k \neq 0$, erected on the sides. Repeat the operation on the actual polygon with another F_k until all integers $k \in [1,\, n-1]$ have been used. The result is the vertex centroid of the initial polygon.

Proof. The F_k-step erases (only) F_{n-k}. □

Remark. The F_k-step, $k \neq 0$, transforms obviously affine images of F_k into (possibly trivial) scaled copies of F_k and no other planar n-gon into an affine image of F_k: thus polygons becoming regular after more than one F_k-step do not exist – although they are explicitly described in [1] for $k = 1$!

7.6. *A theorem à la van Aubel.* The midpoints of the diagonals of a planar quadrilateral Q and the midpoints of the opposite centers of right-hand squares erected on the sides of Q form a square. The same is true for left-hand squares.

Proof. The midpoint step erases F_1 and F_3 without changing F_2. The half-square ear step turns F_2 by $\pi/2$. □

7.7. *Generalized van Aubel's theorem.* Erect right-hand squares on the sides of a planar octagon and take the quadrilateral Q whose vertices are the midpoints of the opposite square centers: Q has congruent and perpendicular diagonals and remains unchanged if one permutes the two transformations. The same is true for left-hand squares.

7.8. *Generalized Thébault's theorem.* Replace a planar octagon with the octagon of the side midpoints, erect right-hand squares on the sides of this midpoint octagon and take the quadrilateral Q whose vertices are the midpoints of the opposite square centers: Q is a square that remains unchanged for any order of the three transformations. The same is true for left-hand squares.

Remark. The transformation

$$\Phi\colon P = (z_k)_{k=0}^{n-1} \mapsto (az_k + z_{k+1} + z_{k-1})_{k=0}^{n-1}$$

multiplies the basis polygons F_ℓ and $\overline{F_\ell}$ by $a + 2\cos(2\ell\pi/n)$, and $\Phi/(a+2)$ is centroid-preserving if $a \neq -2$. The choice $a = -2\cos(2\ell_0\pi/n)$, $\ell_0 \neq 0$, erases thus exactly F_{ℓ_0} and $F_{n-\ell_0}$. To delete $F_{n-\ell_0}$ only, perform the F_{ℓ_0}-step of the Petr–Douglas–Neumann theorem.

7.9. *Filtered pentagon.* If ϕ is the golden ratio and $a = \phi$ or $1 - \phi$, the pentagon $P = (az_k + z_{k+1} + z_{k-1})_{k=0}^{4}$ obtained from $(z_k)_{k=0}^{4}$ is affinely regular and has thus a circumellipse. Unless its vertices are collinear, P is convex for $a = \phi$ and a pentagram for $a = 1 - \phi$.

References

[1] T. Andreescu, V. Georgiev, and O. Mushkarov, Napoleon polygons, *Amer. Math. Monthly*, 122 (2015) 24–29; correction, *ibid*, 844.

[2] D. Barbilian, *Opera Didactică, Vol. 1, Geometrie elementară*, Editura Tehnică, Bucharest, 1968.

[3] O. T. Dao, Equilateral triangles and Kiepert perspectors in complex numbers, *Forum Geom.*, 15 (2015) 105–114.

[4] G. Darboux, Sur un problème de géométrie élémentaire, *Bull. Sci. Math. Astr. 2^e Sér.*, 2 (1878) 298–304. `http://archive.numdam.org/ARCHIVE/BSMA/BSMA_1878_2_2_1/BSMA_1878_2_2_1_298_1/BSMA_1878_2_2_1_298_1.pdf`

[5] F. Morley, On the geometry whose element is the 3-point of a plane, *Trans. Am. Math. Soc.*, 5 (1904) 467–476.

[6] G. Nicollier, Convolution filters for polygons and the Petr–Douglas–Neumann theorem, *Beitr. Algebra Geom.*, 54 (2013) 701–708.

[7] G. Nicollier, Convolution filters for triangles, *Forum Geom.*, 13 (2013) 61–85.

[8] F. Smarandache and I. Pătraşcu, *The Geometry of Homological Triangles*, The Education Publisher, Columbus (Ohio), 2012.

[9] F. A. Third, Triangles triply in perspective, *Edinb. M. S. Proc.*, 19 (1901) 10–22.

Grégoire Nicollier: University of Applied Sciences of Western Switzerland, Route du Rawyl 47, CH–1950 Sion, Switzerland

E-mail address: `gregoire.nicollier@hevs.ch`

Forum Geometricorum
Volume 15 (2015) 275–280.

FORUM GEOM
ISSN 1534-1178

Some Remarks on a Sangaku from Chiba

Paris Pamfilos

Abstract. In this article we present solutions of a Sangaku problem and related generalizations avoiding excessive calculations.

1. A Sangaku from the Chiba prefecture

A basic reference on the traditional Japanese mathematics (wasan) and the collection of Sangaku tablets is the book by Fukagawa and Rothmann [1]. See also the short account by Rothman in the *Scientific American* [3]. An alternative solution to the problem at hand can be found in the article by Unger [4]. The solution proposed here, for the Sangaku from Chiba, is completely described by the next figure. In this τ represents the semi-perimeter of triangle ABC, a, b, c denote the

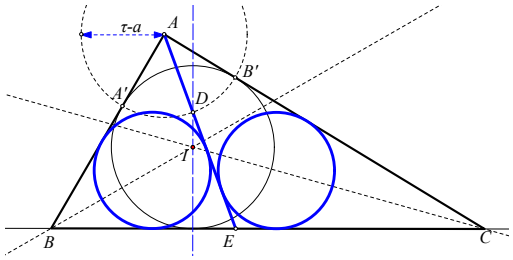

Figure 1. Sangaku at Chiba

lengths of the triangle sides, and I the incenter of the triangle. The content and the construction of the figure is described by the next theorem.

Theorem 1. *Let D denote the inner intersection point of the circle $A(\tau - a)$ with the orthogonal from to BC from I. Then the cevian AD divides the triangle in two subtriangles with equal incircles.*

Our proof, to be analyzed below, gives also as a byproduct the result described by the next figure, in which the basic triangle is divided in more than two subtriangles with equal incircles. Its content is described by the next well known theorem.

Theorem 2. *If a triangle ABC is divided by cevians through A in subtriangles $\{t_1, \dots, t_n\}$ with equal incircles. Then the triangles $s_i = t_i + t_{i+1}$, build by taking together two successive subtriangles, have also equal incircles.*

The handling of incircles in arbitrary divisions of a triangle in subtriangles, through cevians from A, is greatly facilitated by the following simple theorem.

Publication Date: December 9, 2015. Communicating Editor: Paul Yiu.

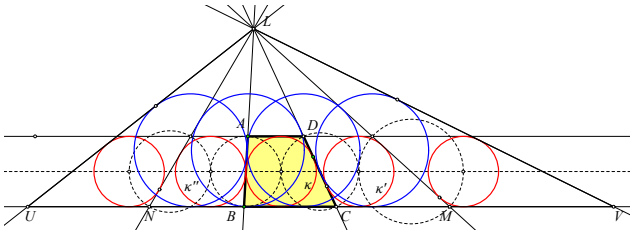

Figure 2. More equal circles inside the triangle

Theorem 3. *Let the cevian AD divide the triangle ABC in two subtriangles with corresponding incircle radii r_1, r_2, and r be the inradius of ABC. Let also R_1, R_2 be the corresponding excircles opposite to A and R be the excircle radius of ABC. Then*

$$\frac{r}{R} = \frac{r_1}{R_1} \cdot \frac{r_2}{R_2}.$$

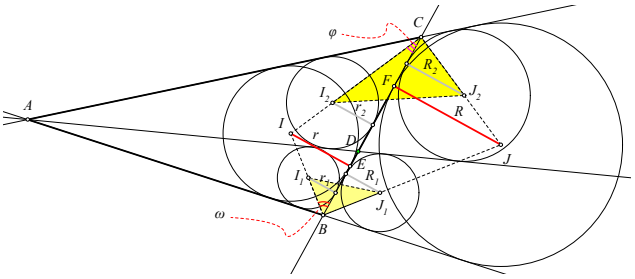

Figure 3. A basic relation for the subtriangles

Denoting by τ_1, τ_2 the corresponding semi-perimeters of the subtriangles and by a_1, a_2 the corresponding sides opposite to A ($a_1 + a_2 = a$), the preceding relation is equivalent to

$$\frac{\tau - a}{\tau} = \frac{\tau_1 - a_1}{\tau_1} \cdot \frac{\tau_2 - a_2}{\tau_2} \quad \Leftrightarrow \quad \left(1 - \frac{a}{\tau}\right) = \left(1 - \frac{a_1}{\tau_1}\right) \cdot \left(1 - \frac{a_1}{\tau_2}\right).$$

This is easily seen by projecting the centers of the circles involved onto the sides AB, AC. Later, using the area ε of ABC and the formulas $\varepsilon = r \cdot \tau = \frac{a \cdot h}{2}$, where h is the altitude from A, transforms to the well-known formula ([2])

$$\left(1 - \frac{2r}{h}\right) = \left(1 - \frac{2r_1}{h}\right) \cdot \left(1 - \frac{2r_2}{h}\right).$$

This formula, in turn, applied inductively to the case of a subdivision of n subtriangles with equal incircles ($r_1 = \cdots = r_n = r'$), leads to the equation for r'

$$\left(1 - \frac{2r}{h}\right) = \left(1 - \frac{2r'}{h}\right)^n,$$

which allows the construction of divisions in arbitrary many subtriangles with equal incircles.

2. The proofs

Let us start with the proof of the last theorem, which results immediately if we express everything in terms of the angles of the triangle $\omega = \alpha/2, \phi = \beta/2$ (See Figure 3) and note that the triangles I_1BJ_1 and I_2CJ_2 are rightangled and similar. Later follows by considering their circumcircles, which both pass through D. Thus, we have

$$\frac{r_1}{R_1} = \frac{|I_1B|\sin(\omega)}{|J_1B|\cos(\omega)}, \quad \frac{r_2}{R_2} = \frac{|I_2C|\sin(\phi)}{|J_2C|\cos(\phi)}$$
$$\Rightarrow \frac{r_1}{R_1}\cdot\frac{r_2}{R_2} = \frac{|I_1B|}{|J_1B|}\cdot\frac{|I_2C|}{|J_2C|}\tan(\omega)\tan(\phi) = \tan(\omega)\tan(\phi).$$

Last equality follows from the similarity of triangles I_1BJ_1 and I_2CJ_2. The last expression, on the other side, equals

$$\tan(\omega)\tan(\phi) = \frac{r}{|BE|}\cdot\frac{|FC|}{R} = \frac{|FC|}{|BE|}\cdot\frac{r}{R} = \frac{r}{R},$$

since $|BE| = |FC|$. This completes the proof of the last theorem.

The proofs of the other two theorems could be deduced by a calculation based on Theorem 3, but we prefer here to proceed by a geometric argument, which seems to be interesting for its own. In this we start with a basic configuration consisting of a circumscriptible trapezium $ABCD$, with incircle $\kappa(O)$. In this we extend the parallel sides to the same semi-plane of a non-parallel side and construct a circle

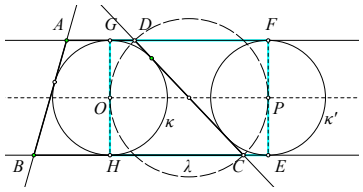

Figure 4. A side-circle of the trapezium

$\kappa'(P)$ equal to κ and tangent to the three sides of the trapezium (See Figure 4). We call such a circle a *side-circle* of the trapezium. There is, of course, also another side-circle, associated to the other non-parallel side of the trapezium. There is a simple observation leading to a quick construction of the side-circle, based on the following lemma, whose proof is trivial.

Lemma 4. *The side-circle $\kappa'(P)$ is a translation of $\kappa(O)$ parallel to BC at distance equal to $|CD|$.*

As a consequence, the circle λ with diameter OP has also CD as diameter (See Figure 4). Drawing the tangent to κ' from the intersection point $L = (AB, CD)$ of the non-parallel sides of the trapezium we obtain a new triangle LBM, which we call *side-triangle* of the trapezium (see Figure 5). A key fact in our proof is the following consequence.

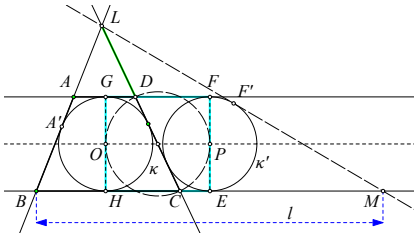

Figure 5. A side-triangle LBM of the trapezium

Lemma 5. *If τ denotes the semi-perimeter of the side-triangle LBM and $l = |BM|$, then $|LD| = \tau - l$.*

This is a consequence of the trivially verifiable relation

$$\begin{aligned}\tau &= \frac{|LA'| + |LF'|}{2} + |BH| + \frac{|HE|}{2} + |EM| \\ &= |LD| + \frac{|DC|}{2} + |BH| + \frac{|HE|}{2} + |EM| \\ &= |LD| + l.\end{aligned}$$

Here A', F' denote, respectively, the tangent points of LB, LM with the circles κ and κ'.

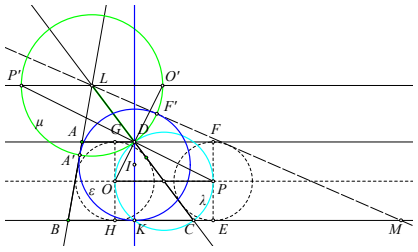

Figure 6. The incircle of the side-triangle

As a consequence of the lemma, the incircle ε of the side-triangle LBM touches the sides LB, LM correspondingly at points A', F', where the circle $\mu(L, |LD|)$ intersects these sides. Besides μ is tangent to circle λ at D. Consequently, the second intersection points O', P' of circle μ, respectively, with lines DO, DP define a diameter $O'P'$, which is parallel to OP. The location of the incenter I of the side-triangle is controlled by the following lemma (See Figure 6).

Lemma 6. *The incenter I of the side-triangle LBM is on the orthogonal to the parallels of the trapezium $ABCD$, passing through point D.*

The proof of the theorem follows from the following two lemmata.

Lemma 7. *Given two intersecting lines IB, IM and two points O', P' in general position, we draw parallels OP to $O'P'$ with $O \in IB$ and $P \in IM$. Then the locus of intersection points $J = (PP', OO')$ is a line passing through I.*

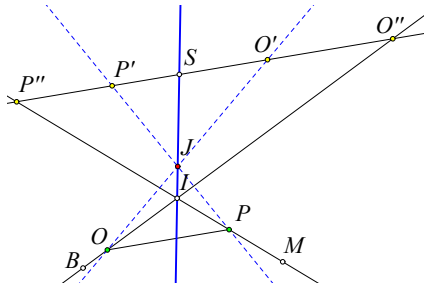

Figure 7. The locus of J

The proof follows trivially by considering the intersection points O'', P'' of line $O'P'$, respectively with lines IB, IM and noticing that the intersection point $S = (O'P', IJ)$ is fixed on $O'P'$ (See Figure 7), since it satisfies the relation

$$\frac{SP''}{SO''} = \frac{SP'}{SO'}.$$

To apply the lemma in our case, we consider, for the moment, the points O, P

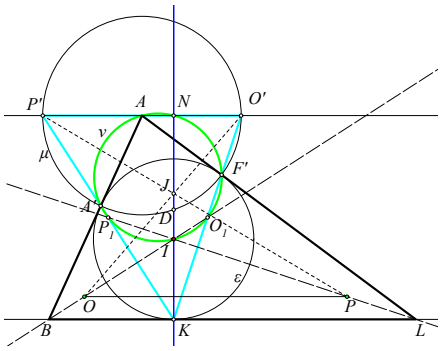

Figure 8. Applying the lemma

being variable on the bisectors of the triangle's angles at B and L, such that OP is parallel to $O'P'$ (See Figure 8). When the variable points O, P obtain, respectively, the position of the centers of circles κ, κ', we know, from our remarks above, that the corresponding locus-point J obtains the position of D. Hence the line-locus coincides with line ID, where I is the incenter of LBM. By the similarity of the triangles $O'AF'$ and $F'LK$, where $K = (O'F', BL)$, follows that $F'LK$ is isosceles and K is the contact point of the incircle with BL. The theorem follows by showing that K is a locus-point, obtained when O, P take, respectively the positions $O_1 = (BI, O'K), P_1 = (LI, P'K)$. This, in turn, is trivially implied by the following lemma.

Lemma 8. *The six points A, A', P_1, I, O_1 and F' are on the same circle ν, with diameter AI.*

In fact, since A', F' are contact points of the incircle, they view AI under a right angle. That O_1 is on this circle follows by measuring the angle IO_1K, which is seen to be equal to half the angle at A, hence quadrilateral $IAF'O_1$ is cyclic. Analogous is the proof for P_1. This completes the proof of the lemma and also the proof of Theorem 1.

As for Theorem 2, its proof results immediately from the following lemma.

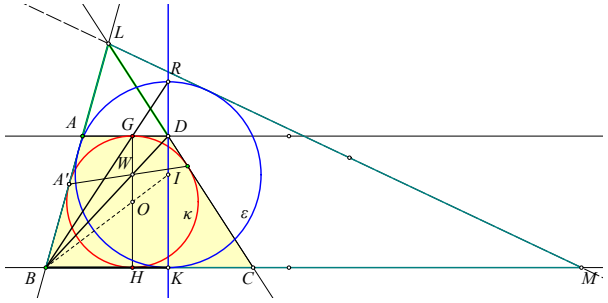

Figure 9. Relation of the incircles

Lemma 9. *The two side-triangles constructed on either non-parallel sides of the circumscriptible quadrilateral $ABCD$ have incircles of equal radii.*

In fact, the homothety centered at B and mapping the incircle κ of the trapezium to the incircle ε of the side-triangle (See Figure 9) maps the diameter GH of κ to the corresponding diameter RK of ε and their ratio can be read on GH and is equal to $\frac{|GH|}{|WH|}$. Since this is independent of the particular non-parallel side, the proof follows at once.

References

[1] H. Fukagawa and T. Rothman, *Sacred Mathematics*, Princeton University Press, Princeton, 2008.
[2] G. Huvent, *Sangaku*, Dunod, Paris, 2008.
[3] T. Rothman. Japanese Temple Geometry, *Scientific American*, 1998, 5:84–91.
[4] M. Unger. A collection of 30 Sangaku Problems, Internet Publication, 2014.

Paris Pamfilos: University of Crete, Greece
E-mail address: pamfilos@math.uoc.gr